# SISSA

**Scuola
Internazionale
Superiore di
Studi Avanzati**

Physics Area - Ph.D. course in
Astroparticle Physics

Ph.D. Thesis

# Magnetic Monopoles in Cosmic Magnetic Fields: Acceleration and Constraints

Candidate:
Daniele Perri

Supervisor:
Prof. Takeshi Kobayashi

Academic Year 2023-24

SISSA

# Abstract

Magnetic monopoles are intriguing hypothetical particles and inevitable predictions of theories of Grand Unification. They should be produced during phase transitions in the early universe, but also mechanisms like the Schwinger effect in strong magnetic fields could contribute to the monopole number density. In this thesis, we demonstrate the importance of the studies on the physics of magnetic monopoles in cosmic environments. In particular, we show how understanding the interplay between the monopoles and cosmic magnetic fields is crucial for the search of monopoles of astrophysical origin.

We provide a comprehensive analysis of the acceleration of magnetic monopoles in intergalactic magnetic fields and galactic magnetic fields. We demonstrate that monopoles with intermediate to low masses can be accelerated to relativistic velocities. This can significantly affect direct and indirect searches for magnetic monopoles. Concerning indirect searches, we show that the Parker bounds on the survival of galactic magnetic fields are modified in the presence of intergalactic fields. We also find that a cosmic population of monopoles can produce significant backreaction on the intergalactic fields. In the case of direct searches, experimental constraints on the monopole flux are often expressed in terms of the monopole velocity. From the study of the monopole acceleration, we obtain a speed-mass-abundance relation for the monopoles that might be detected by the terrestrial detectors. With this relation, we revisit for the first time the current bounds on the monopole flux from terrestrial experiments in terms of the monopole mass, providing a recipe for future works. We also show that by improving their constraints such experiments will soon be sensible to values of the monopole flux where the monopole velocity is influenced by the physics of magnetic fields in intergalactic voids.

We also present a comprehensive study of Parker-type bounds on magnetic monopoles with arbitrarily magnetic charges, including minicharged monopoles and magnetic black holes. In particular, we provide new bounds on the cosmic abundance of magnetic monopoles based on the survival of primordial magnetic fields during the reheating and radiation-dominated epochs. The new bounds can be stronger than the conventional Parker bound from galactic magnetic fields, as well as bounds from direct searches. We find that monopoles with different magnetic charges are best constrained by different astrophysical systems: while monopoles with a Dirac charge are tightly constrained by seed galactic magnetic fields, minicharged monopoles are strongly constrained by primordial magnetic fields, and magnetic black holes by the density of dark matter. We also assess the viability of the various types of monopoles as dark matter, by studying whether they can cluster with galaxies hosting magnetic fields. Finally, we apply our primordial bounds to monopoles produced by the primordial magnetic fields themselves through the Schwinger effect and derive additional conditions for the survival of the primordial fields.

This Ph.D. thesis is based on the works [1, 2, 3, 4], as well as on some preliminary results, carried out during the Ph.D. program in Astroparticle Physics at SISSA.

# Contents

# Chapter 1

# Introduction

Magnetic monopoles have long been a topic of intense study since Dirac showed in 1931 that their existence is consistent with quantum electrodynamics [5]. This discovery was followed by 't Hooft [6] and Polyakov [7] who found in the '70s classical soliton solutions of the classical field equation that correspond to monopoles. Such solitonic monopoles are an inevitable prediction of theories of grand unification and can be produced during phase transitions in the early universe [8, 9, 10]. Magnetic monopoles would then exist as cosmic relics in the present time, since the magnetic charge is conserved. The mass of solitonic monopoles is tied to the symmetry breaking scale, which depends on the details of the theory and thus can vary over many orders of magnitude. In particular, the breaking of the GUT symmetry would lead to supermassive monopoles at $m \gtrsim 10^{16}$ GeV. Such magnetic monopoles would retain the velocity distribution of particles in the galaxy at $\beta = 10^{-3}$, which approximately corresponds to the virial velocity of the Milky Way and to the proper motion of the Milky Way in the CMB rest frame [11]. Theories predicting later phase transitions could have generated intermediate mass monopoles, that could be easily accelerated to relativistic velocities by cosmic magnetic fields. Magnetic monopoles can also be produced in the presence of strong magnetic fields through the magnetic dual of the Schwinger effect [12, 13, 14]. Although magnetic monopoles have not been detected so far, the search for monopoles continues to be an active field of research with a potential to unlock new insights into the nature of our universe.

Magnetic monopoles would not only make the Maxwell equations symmetric between electricity and magnetism, but also be related to the observed quantization of the electric charge. The existence of magnetic monopoles implies in fact the quantization of the electric charge via the Dirac quantization condition [5] as $eg = 2\pi n$, $n \in \mathbb{Z}$. Due to this condition, experimental searches over the years have focused mainly on monopoles with a charge $g \sim 2\pi/e$. However, several theoretical works have recently considered monopoles possessing a wide range of charges. Minicharged monopoles with $g \ll 2\pi/e$ can be realized by having a physical Dirac string. Such configurations can arise, for instance, from a kinetic mixing between the Standard Model photon and a dark massive photon, in which case the monopole's charge under the visible magnetic fields is proportional to the mixing parameter [15, 16, 17, 18, 19, 20]. Going to very large masses, magnetically charged black holes can be seen as giant monopoles with small charge-to-mass ratio. The

phenomenology of black holes with magnetic charge has recently been discussed in [21, 22, 23, 24, 25, 26, 27, 28]. Such black holes are interesting as they cannot Hawking evaporate beyond extremality, leading to the possibility for primordial black holes with very small masses to survive until today. Both minicharged monopoles and magnetic black holes have also been considered interesting candidates for dark matter.

The flux of magnetic monopoles has been constrained in the past decades by a series of terrestrial experiments. The first attempts to direct search for magnetic monopoles mainly relied on the detection of an induced electric current in superconducting rings [29]. However, more recently the most promising mechanism of monopole detection is based on the energy released into calorimeters from the interactions of a monopole crossing a target, either man-made or natural (like the Earth atmosphere, oceans or polar ice) [30, 31, 32, 33, 34, 35, 36]. A subclass of GUT monopoles can catalyze nucleon decay, and searches based on this process have been performed, resulting in even stronger constraints [37, 38, 39, 40]; however, whether monopole catalysis occurs or not depends on the details of the model. Moreover, search for monopole pairs produced by the Schwinger effect in the presence of strong magnetic fields has been carried on by the MoEDAL collaboration [41, 42], and later by ATLAS [43].[1] It is extremely difficult to apply these methods for direct search to minicharged monopoles because of the sensitivity of the detectors and the selection algorithms used in the experiments. For magnetic black holes, their very large masses combined with the constraint from the critical density of the universe restrict their flux on Earth to be extremely tiny; hence, they are also minimally constrained by direct searches. We should also note that, although a subclass of minicharged monopoles can catalyze nucleon decay, whether monopole catalysis occurs depends on the details of the model. Thus, the possibility of deriving indirect bounds from astrophysical observations is even more compelling for monopoles possessing charges that are very different from the Dirac charge.

The relic abundance of magnetic monopoles is constrained by the requirement that they do not exceed the critical density of the universe [8, 46, 47]. However, even stronger constraints can be obtained from the magnetic fields present in the universe. The idea behind this is that magnetic fields lose energy by accelerating monopoles, hence requiring their survival imposes an upper bound on the monopole abundance. This was first proposed by Parker, who derived an upper bound on the monopole flux inside our Galaxy from the survival of the Galactic magnetic fields [48, 49, 50]. This limit, known as the Parker bound, was later extended to the survival of the seed magnetic field of our Galaxy [51], as well as magnetic fields in galactic clusters [52]. In the literature, Parker bounds based on Galactic magnetic fields have been derived under the assumption that monopoles have a velocity of $v \sim 10^{-3}$, which corresponds to the virial velocity or the peculiar velocity of the Milky Way Galaxy [11]. However, the bounds strongly depend on the kinetic energy of the monopoles, and thus are significantly affected by processes that accelerate the monopoles before they enter the Galaxy. Intergalactic magnetic fields [53, 54, 55, 56], on the other hand, may

---

[1]Lower bounds on the monopole mass have been also obtained by analyzing this effect on the surface of magnetars [18, 44], in heavy-ion collisions at the LHC [42, 44], and in primordial magnetic fields [1, 45].

not directly yield Parker-type bounds. This is because the accelerated monopoles do not effectively dissipate their kinetic energy in the intergalactic voids, and thus can end up returning the energy to the magnetic field. However, if the intergalactic fields have a primordial origin, as suggested by various studies (see e.g. [57] for a review), the monopoles could have shorted out the magnetic fields in the early universe by transferring the magnetic energy into the cosmic plasma. Parker-type bounds from primordial magnetic fields have thus been derived based on the fields' survival during the radiation-dominated and the reheating epochs [1, 2, 58].

Cosmic magnetic fields have been observed in the universe on various scales, from planets and stars to galaxies, galaxy clusters, filaments, and beyond, while their origin still remains unknown. Magnetic fields of $B \sim 10^{-6}$ G [59] have been observed within spiral galaxies. We now have a lot of information on the structure of the GMFs. In particular, thanks to a combination of a large dataset of rotation measures (RMs) and polarization, Unger and Farrar [60] provided the latest model for the coherent GMFs with great precision. Intergalactic magnetic fields (IGMFs), which extend across the vast intergalactic voids between galaxies over cosmological scales, are of significant importance for cosmic populations of magnetic monopoles. IGMFs have not yet been detected, although we have very significant indirect evidences which support their existence. They have been for long only constrained by upper limits on the field amplitude, mainly from cosmological observations of the cosmic microwave background as $B \lesssim 10^{-9}$ G. At present, upper bounds on the field amplitude are set by several measurements. Among the most constraining and conservative survives the one based on CMB anisotropies [61]. However, in the past decade the existence of IGMFs has been suggested from gamma-ray experiments with the non-observation around blazars of extended halos or delayed emission formed by secondary photons [53, 54, 55, 56]. High-energy (TeV) extragalactic gamma rays from the blazar sources should be reprocessed to lower-energy (GeV) gamma rays due to cascading processes in the intergalactic space: $\gamma\gamma \rightarrow e^+e^- \rightarrow \gamma$+showers [62, 63]. A recent conservative lower bound was set by the MAGIC collaboration [56] and less conservative bounds were set with *Fermi*-LAT [64]. Present and future observations on $\gamma-$ray reprocessing from Gamma Ray Burst (GRBs) could also probe IGMF strengths at a competitive level [65, 66]. These studies set lower limits on the IGMF strength of $B \gtrsim 10^{-15}$ G, if the correlation length $\lambda$ is of Mpc scale or larger. If $\lambda$ is much smaller than a Mpc, the lower limit further improves as $\lambda^{-1/2}$.[2] Finally, strong lower bounds on the magnetic field coherence length come from the decay of magnetic fields due to magnetic diffusion [69]. See e.g. [63, 70] for reviews on IGMFs.

The existence of intergalactic magnetic fields in intergalactic voids gives a strong indication that the fields have their origin in primordial magnetic fields produced in the early universe. Regarding the origin of the primordial magnetic fields, a class of scenarios that have been extensively studied invokes an explicit breaking of the Weyl invariance of the gauge field action, to excite magnetic fields during cosmic inflation [71, 72] or in the subsequent epoch dominated by an oscillating

---

[2]Explanations of the blazar observations that do not invoke IGMFs have also been proposed, see e.g. [67, 68].

inflaton [73].[3] A generic feature of these scenarios is that the magnetic fields are generated while the universe is cold because after reheating completes the universe turns into a good conductor and the magnetic flux freezes in. Hence the interplay between primordial magnetic fields and monopoles may well have been important from times prior to radiation domination.

The starting point of this thesis is the very simple observation that magnetic monopoles are accelerated by the magnetic fields in the universe, at different scales and times. Although based on very simple physics, the relationship between monopoles and cosmic magnetic fields presents many interesting aspects that can be used to improve our understanding of the characteristics of magnetic monopoles. In the following, we review the main results of this thesis, which will be addressed in detail in the following chapters.

In light of the observational results, in this study we analyze the acceleration of magnetic monopoles in IGMFs and GMFs, which represent the main contributions to the monopole velocity on cosmic scales, in a simplified model. Although IGMFs are extremely weak compared with Galactic fields, they contribute significantly to the monopole velocity by the large coherence length of the fields, accelerating the monopoles in homogeneous fields along cosmological distances. We demonstrate that IGMFs can easily accelerate the monopoles to relativistic velocities. [4] Moreover, we show that the backreaction of the monopoles on the IGMFs can drastically affect the acceleration process and must be taken into account for an accurate calculation of the monopole velocity. As an application of our study of the monopole acceleration in GMFs, we present a detailed derivation of Galactic Parker bounds for arbitrarily charged monopoles (including magnetic black holes). We also derive conditions for monopoles to be able to cluster with galaxies hosting magnetic fields, based on which we examine whether the various types of monopoles can provide viable dark matter candidates, being clustering a necessary condition. On the other hand, studying monopole acceleration in IGMFs, we show how Galactic Parker bounds are modified by taking into account the acceleration effects in the extra-galactic space. In particular, we find that the bounds from the survival of seed Galactic magnetic fields can be significantly relaxed in the presence of IGMFs within the observational limits.

Adopting our new calculation of monopole acceleration in cosmic magneic fields, we also recompute the most constraining experimental bounds on magnetic monopoles as a function of the monopole mass. Experimental bounds are mostly computed as a function of the monopole velocity at the detectors, because of the dependence of the energy loss in the medium to the velocity of the particles. However, the relevant information for testing theories of magnetic monopoles is the monopole flux in terms of the monopole mass, which is directly related to the fundamental parameters of the theory. The consistent framework of acceleration of magnetic monopoles in cosmic magnetic fields that we describe in this work allows us to relate the monopole mass to the velocity at the Earth surface. Analyzing the characteristics of each detector and taking into account the effects of the energy loss of the monopoles while crossing

---

[3]Cosmological phase transitions can also give rise to primordial magnetic fields [74, 75].

[4]See also the earlier works [76, 77, 78] which discussed relativistic monopoles from Galactic/intergalactic fields.

the Earth, we can relate the monopole velocity at the Earth surface to the velocity at the detectors, and then recast the experimental bounds in terms of the monopole mass.

As we have already mentioned, the process of monopole acceleration extracts energy from the fields. The energy that the monopoles extract from the primordial magnetic field is transferred to the primordial plasma through scattering processes with relativistic charged particles of the plasma [10]. With a monopole number density large enough, this can cause the disappearance of the field. Thus, from the survival of primordial magnetic fields until today, bounds similar to the Parker bound for galactic magnetic fields can be derived. Such bounds from the primordial magnetic fields during the radiation-dominated epoch were first considered by [58]. In this work, we present a comprehensive study of the Parker limit from primordial magnetic fields. We generalize the analysis of [58] to arbitrarily charged monopoles and evaluate the effects of monopole acceleration in primordial magnetic fields throughout the post-inflation universe, starting from the reheating epoch when the universe is dominated by an oscillating inflaton. We show that, depending on the early cosmological history, the survival of primordial magnetic fields during reheating imposes bounds on the monopole abundance that are more stringent than the Parker limit from Galactic magnetic fields and the bound presented in [58]. We also present a comprehensive study of primordial Parker-type bounds on the flux of magnetic monopoles with arbitrary charge, including minicharged monopoles and magnetically charged black holes. After deriving the flux bounds based on the survival of galactic magnetic fields, seed magnetic fields, and primordial magnetic fields, we clarify the range of applicability of each bound along the way and we compare the results. We find that, depending on the type of monopoles, the strongest bound arise from different astrophysical systems. In particular, we show that while seed galactic magnetic fields impose tight bounds on monopoles with a Dirac charge, minicharged monopoles are strongly constrained by primordial magnetic fields, and magnetic black holes by comparison with the dark matter density.

Although the magnetic fields in the universe today are rather weak, if they have a primordial origin, in the early universe they could have been extremely strong. Such strong magnetic fields can themselves produce monopole-antimonopole pairs through the magnetic dual of the Schwinger effect [12, 13, 14], even in the absence of any initial monopole population. Even superheavy monopoles can thus be produced in primordial magnetic fields [45]. The pair production in turn depletes energy from the magnetic fields, which, along with the subsequent acceleration of the produced monopoles, induce a self-screening of the fields. Hence, we also apply our generic bounds from the acceleration of monopoles in the primordial plasma to such pair-produced monopoles, in order to obtain the most conservative condition for the survival of primordial magnetic fields. The bound we derive is comparable to those obtained in [45] from considerations of the magnetic field screening by the Schwinger process, and the overproduction of monopoles.

This work is organized as follows. In Chapter 2 we review the theory of magnetic monopoles. In particular, we present some of the models of magnetic monopoles, the effective description of their interaction with matter, and the most relevant mechanisms of monopole production. In Chapter 3 we analyze monopole acceleration in the late universe, both in IGMFs and Galactic magnetic fields. We also study the

effect of backreaction on the IGMFs from monopole acceleration. In Chapter 4 we derive the Parker bound for the survival of galactic magnetic fields for arbitrarily charged monopoles. We also describe how the Galactic Parker bounds are affected by acceleration in IGMFs. In Chapter 5 we show how it is possible to recast terrestrial experiments on magnetic monopoles in terms of the monopole mass for a given scenario of cosmic acceleration. In Chapter 6 we describe the motion of arbitrarily charged magnetic monopoles in the early universe and in the presence of primordial magnetic fields. In Chapter 7 we apply the results for monopole acceleration in the early universe to a condition for the survival of primordial magnetic fields, getting new bounds on the average cosmic abundance of monopoles. In Chapter 8 we describe the process of Schwinger pair production of magnetic monopoles in the early universe and we derive conditions for the survival of the fields after the process of production and acceleration of the monopoles. In Chapter 9 we describe a solution to the monopole problem alternative to the standard inflationary paradigm, which involves the production of the monopoles in the early universe as global monopoles. We then conclude in Chapter 10.

Throughout this work we use Heaviside-Lorentz units, with $c = \hbar = k_B = 1$, and use $M_{\text{Pl}}$ to denote the reduced Planck mass $(8\pi G)^{-1/2}$. We use Greek letters for spacetime indices and Latin letters when we mean only the three spatial components. We choose the metric tensor signature $(+ - - -)$. We denote the monopole's mass by $m$, and the amplitude of the magnetic charge by $g$. The fundamental Dirac charge of a magnetic monopole is written as $g_{\text{D}} = 2\pi/e \approx 21$. Our analysis can be applied to both elementary and solitonic monopoles.

# Chapter 2

# Monopoles: theory, interaction, production

In 1873, Maxwell proposed the fundamental dynamical equations describing the theory framework of Electromagnetism, which is the Gauge Unified theory of Electricity and Magnetism. However, these equations are not symmetric under the exchange of electric and magnetic fields. This asymmetry is a direct consequence of the absence of magnetic charges: for some reason, in nature only isolated electric charges are permitted. As one can imagine, the scientific community could not be satisfied with some "a priori" motivation for the absence of magnetic charges. The "symmetrization" of the Maxwell's equations under an "electric–magnetic duality" has therefore intrigued and captivated physicists as early as the late 19th Century.

Pierre Curie was the first to propose in 1894 the existence of a magnetic charge and hence a magnetic current with the purpose of symmetrizing Maxwell's equations. Shortly after, Henri Poincaré used the expression for the force of a magnetic pole at rest in the presence of a moving electric charge to explain the Birkeland experiment in 1896, which observed the focusing of cathodic beams in a Crook's tube in the presence of a magnet. The field of a stationary isolated magnetic pole carrying "magnetic charge" $g$ corresponds to that of a magnetic monopole with that magnetic charge

$$\mathbf{B}_{\mathrm{mono}} = g\frac{\mathbf{r}}{r^3}. \tag{2.1}$$

For an electron with mass m, electric charge e, and position vector $\mathbf{r}$, in the presence of a magnetic field generated by a stationary magnetic pole carrying magnetic charge g, the nonrelativistic Lorentz force law implies an acceleration

$$\frac{d^2\mathbf{r}}{dt^2} = \frac{eg}{mc}\frac{1}{r^3}\frac{d\mathbf{r}}{dt} \times \mathbf{r}, \tag{2.2}$$

where c is the speed of light in vacuum. The solution for the electron's trajectory $\mathbf{r}(t)$ corresponds to conical geodesics, thereby explaining the focusing effect observed in the Birkeland experiment.

Later, Thomson [79] showed in 1904 that the total classical angular momentum of the electron in the presence of a magnetic field pole is

$$\mathbf{L} = m\mathbf{r} \times \frac{d\mathbf{r}}{dt} - \frac{eg}{c}\frac{\mathbf{r}}{r}. \tag{2.3}$$

The final term on the right comes from the interaction of the electron with the magnetic field pole, computed from the volume integral of the Poynting vector

$$\mathbf{L}_{eg} = \frac{1}{4\pi c} \int d^3 r' \left( \mathbf{r}' \times (\mathbf{E} \times \mathbf{B}_{\mathrm{mono}}) \right) = -\frac{g}{4\pi c} \int d^3 r' \frac{\mathbf{r}'}{r'} \left( \nabla' \cdot \mathbf{E} \right) = -\frac{eg}{c} \frac{\mathbf{r}}{r}. \quad (2.4)$$

Here $\mathbf{E}$ represents the electric field of the classical point-like electric charge of the electron, which vanish at infinity, and we applied Maxwell's equations to write $\nabla' \cdot \mathbf{E} = 4\pi e \delta^{(3)}(\mathbf{r} - \mathbf{r}')$.

It is interesting to note that by invoking the standard quantization rule for the angular momentum of the electromagnetic field part, $|\mathbf{L}_{eg}|$ must take integer or half-integer values, and therefore

$$\frac{eg}{c} = \frac{n}{2} \cdot 4\pi\hbar, \quad n \in \mathbb{Z}. \quad (2.5)$$

This is essentially already the Dirac quantization condition of the monopole charge, derived by Dirac over two decades later in a coherent quantum theory for magnetic monopoles and which we will describe in the next section.

## 2.1 Models of magnetic monopoles

We now review the most important models of magnetic monopoles proposed over the years. We start with the first model proposed by Dirac and then move to the more recent 't Hooft-Polyakov magnetic monopole. We will then briefly review the more exotic model of the Calabi-Yau monopoles, as representative of the monopoles that arise in compactified space-time geometries. For further details, see, for example, [10, 47, 80, 81].

### 2.1.1 Dirac monopoles

Electric charges are always detected as integer multiples of the electron charge, indicating a fundamental property of nature that demands explanation. In 1931, Dirac [5] proposed that the existence of magnetic monopoles could provide a theoretical motivation for the quantization of the electric charge.

In Dirac's theory, the magnetic monopole is located at one end of a semi-infinite one-dimensional solenoid that carries the magnetic flux. Such solenoid is usually called the "Dirac string". The magnetic field at the end of the solenoid resembles that of a point-source for the magnetic field. In Dirac's theory the magnetic monopole is considered a new fundamental particle, and the Dirac string is therefore not physical. This implies that no experiment should be able to detect the solenoid, and therefore the quantum wave function $\psi(\mathbf{r})$ of the electron in the static magnetic field of a monopole must be single-valued when it surrounds it.

Consider now an experiment of electron interference to detect the solenoid. The experiment yields no result (that is, $\psi(\mathbf{r})$ is single valued) if the phase acquired by the electron wave function when transported along a closed path around the solenoid is trivial. Suppose now to have a point monopole with a magnetic charge $g$ at the origin, producing the radial magnetic field $B_{\mathrm{mono}} = g/r^2$. Let us also assume conventionally that the solenoid extends along the positive z semi-axis. Dirac

assigned to the magnetic field pole the singular electromagnetic potential $\mathbf{A}$ defined as

$$\nabla \times \mathbf{A} = \mathbf{B}_{\text{mono}} = g\frac{\mathbf{r}}{r^3}. \tag{2.6}$$

In spherical coordinates and a suitable gauge, the only non-zero component of the vector potential is

$$A_\phi = g(1 - cos\theta), \tag{2.7}$$

where the $A_\phi$ is defined as $\mathbf{A} \cdot d\mathbf{r} = A_\phi d\phi$. When encircling the Dirac string in a closed loop $l$, at constant distances $r$ far from magnetic monopole, the electron's wave function acquires a phase change as

$$\psi(\mathbf{r}) \rightarrow \psi(\mathbf{r}) \exp\left(ie \oint_l \mathbf{A} \cdot d\mathbf{x}\right). \tag{2.8}$$

Therefore, the electron interference experiment does not detect the solenoid if

$$e \oint_l \mathbf{A} \cdot d\mathbf{x} = eg = 2\pi n, \quad n \in \mathbb{Z}, \tag{2.9}$$

which from the expression in Eq. (2.7) leads to the Dirac quantization condition of Eq. (2.5) (with $\hbar = c = 1$).

According to the quantization condition, all magnetic charges must be integer multiples of the Dirac charge $g_D = 2\pi/e$. We can reverse this argument as follows. Assume there is a magnetic monopole with magnetic charge $g_D$. Hence, a particle with electric charge $Q$ (and zero magnetic charge) can consistently exist only if $\exp\left(i2\pi nQg_D\right) = 1$, which means $Q$ must be a multiple integer of $2\pi/g_D$. Hence, the existence of even only one magnetic monopole implies the quantization of the electric charge.

The nonlocal Dirac string singularity, though invisible due to the Dirac quantization condition, significantly affects the formulation of effective field theories for magnetic monopoles. To avoid the use of Dirac strings, Cabibbo and Ferrari [82], Salam [83], and Zwanziger [84] developed a two-potential framework for classical field theories of magnetic monopoles, where the first potential corresponds to the standard photon, while the second one accounts for the magnetic potential of the magnetic monopoles. In particular, Salam suggested that 'photons' corresponding to the second potential should have different charge conjugation and parity properties compared to the conventional photon. On the other hand, in Zwanziger's approach, to ensure that the physical degrees of freedom match those of the observed electromagnetic photon, additional conditions are imposed on these two potentials.

### 2.1.2 'T Hooft-Polyakov monopoles

A completely different interpretation of magnetic monopoles, based on modern gauge theories, was independently proposed in 1974 by 't Hooft and Polyakov [6, 7]. They showed for the first time that magnetic monopoles can arise from non-trivial topologies of the vacuum manifold in simply connected symmetry groups spontaneously broken by a Higgs mechanism. In their theories, the monopole corresponds to a classical soliton solution of the equation of motion of a given Lagrangian. This solution is commonly known as the 't Hooft-Polyakov monopole.

The most simple theory that presents the monopole solution is the Georgi-Glashow $SU(2)$ gauge theory model, wherein a spontaneous symmetry breaking $SU(2) \to U(1)$ is achieved through an adjoint Higgs triplet field. We now describe the monopole solution of the model. The fields of the theory are a scalar triplet $\phi^a(t, \mathbf{x})$ and a gauge field $A^a_\mu(t, \mathbf{x})$, with $a = 1, 2, 3$ an $SU(2)$ index. The Lagrangian density is

$$\frac{\mathcal{L}}{\sqrt{-g}} = -\frac{1}{4} F^a_{\mu\nu} F^{a\mu\nu} + \frac{1}{2}(D_\mu \phi^a)(D^\mu \phi^a) - \frac{1}{4}\lambda(\phi^a \phi^a - v^2)^2. \qquad (2.10)$$

Here $v$ is the vacuum expectation value of the theory and $\lambda$ ($> 0$) is the self-coupling of the scalar. The field tensor $F^a_{\mu\nu}$ is defined as

$$F^a_{\mu\nu} = \partial_\mu A^a_\nu - \partial_\nu A^a_\mu + \tilde{g}\epsilon^{abc} A^b_\mu A^c_\nu, \qquad (2.11)$$

where $\epsilon^{abc}$ stands for the antisymmetric Levi-Civita symbol and $\tilde{g}$ is the charge of the scalar under the gauge field. The covariant derivative $D_\mu \phi^a$ is defined as

$$D_\mu \phi^a = \partial_\mu \phi^a + \tilde{g}\epsilon^{abc} A^b_\mu \phi^c. \qquad (2.12)$$

From the Lagrangian, we obtain the equations of motion for the gauge field and the scalar

$$D_\mu F^{a\mu\nu} = \tilde{g}\epsilon^{abc} \left(D^\nu \phi^b\right) \phi^c, \qquad (2.13)$$

$$D_\mu D^\mu \phi^a = -\lambda \left(\phi^b \phi^b\right) \phi^a + \lambda v^2 \phi^a. \qquad (2.14)$$

We now choose the gauge condition $A^a_0(\mathbf{x}) = 0$ and we search for static solutions of the equations of motion. We start from the spherically symmetric ansatz

$$\phi^a(\mathbf{x}) = \delta_{ia} v h(r) \frac{x^i}{r}, \quad A^a_i(\vec{x}) = \epsilon_{aij} \left(1 - K(r)\right) \frac{x^j}{\tilde{g}r^2}, \qquad (2.15)$$

with $i, j = 1, 2, 3$ and $r = |\mathbf{x}|$. This is the ansatz for the so-called "hedgehog solution", which characterizes the monopole structure. We want our solution to recover at spatial infinity the standard conditions for the vacuum space in the broken phase and for the potential to correspond at that for a point source of the magnetic field, while at the origin we require regularity of the solution. Notice also that the asymptotic behavior for $r \to \infty$ of the magnetic field must be given by:

$$\mathbf{B}(\mathbf{r}) \sim \frac{2\pi}{\tilde{g}} \frac{\mathbf{r}}{r^3}, \qquad (2.16)$$

which corresponds to the magnetic field of a point source. Therefore, we ask for the asymptotic behaviours

$$h(r) \to 1, \quad K(r) \to 0 \quad \text{when} \quad r \to \infty, \qquad (2.17)$$

and

$$h(0) = 0, \quad K(0) = 1. \qquad (2.18)$$
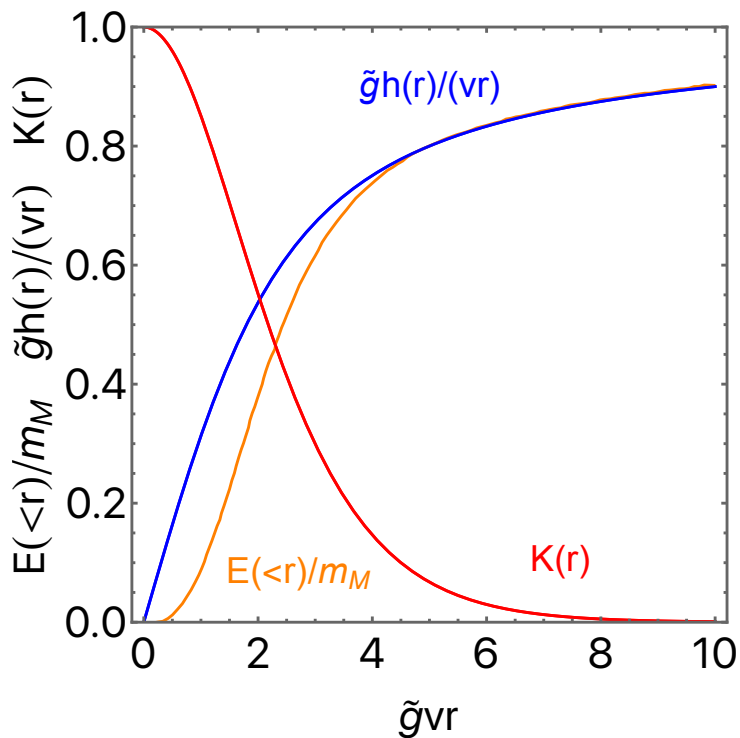
**Figure 2.1** Radial profiles for the Higgs field $\phi^a$ (blue curve), the gauge field $A_i^a$ (red curve) (as in Eq. (2.15)), and the energy contained in a sphere with radius $r$ (orange curve) (as in Eq. (2.20)), as a function of the distance $r$ from the monopole center, in the Georgi-Glashow model and in the Prasad-Sommerfeld limit $\lambda/\tilde{g}^2 \to 0$ (see Eq. (2.19)).

It has been shown [85] that for this simple model an analytic solution can be derived in the Prasad-Sommerfeld limit $\lambda/\tilde{g}^2 \to 0$. This is the explicit result:

$$\phi^a = (\tilde{g}vr \coth(\tilde{g}vr) - 1) \frac{x^a}{\tilde{g}r}, \quad A_i^a = \epsilon_{aij} \left(1 - \frac{\tilde{g}vr}{\sinh(\tilde{g}vr)}\right) \frac{x^j}{\tilde{g}r^2}. \tag{2.19}$$

One of the most important properties of the 't Hooft-Polyakov model is that their total energy (the rest mass, in flat spacetime) remains finite. The energy of a static monopole in flat spacetime is obtained by integrating the $T_t^t$ component of the monopole stress-energy tensor and is given by

$$E = \frac{1}{2} \int d^3x \left[\mathbf{B}^a \cdot \mathbf{B}^a + \mathbf{D}\phi^a \cdot \mathbf{D}\phi^a + \frac{1}{2}\lambda(\phi^a\phi^a - v^2)^2\right]. \tag{2.20}$$

One can show that the configuration for which the static energy is minimized corresponds to the monopole mass

$$m \sim \frac{4\pi}{\tilde{g}^2} m_{\mathrm{V}}, \tag{2.21}$$

where $m_{\mathrm{V}} = \tilde{g}v$ is the mass of the vector boson.

In Figure 2.1 we show the solution in the Prasad-Sommerfeld limit for the Higgs field $\phi^a$, the gauge field $A_i^a$ as in Eq. (2.19) and the energy contained in a sphere

with radius $r$, as a function of the distance from the monopole center, calculated from Eq. (2.20).

One might wonder under which conditions a monopole solution exists for a given lagrangian and a specific pattern of spontaneous symmetry breaking. Such conditions must be derived from the underlying topological structure of the theory. Let us consider an arbitrary gauge field theory with a gauge group $G$ that is spontaneously broken into a subgroup $H$. The order parameter for the breaking of the symmetry is a multiplet of scalar fields $\Phi$, which transforms under some representation of $G$. $H$ is the group that leaves the arbitrary chosen minimum $\Phi_0$ invariant. The manifold of the equivalent minima of the theory can be parametrized as the coset space,

$$G/H = \{\Phi : \Phi = \Omega\Phi_0, \ \Omega \in G\} . \tag{2.22}$$

We want to construct finite energy solutions of the classical field equations of the theory, and therefore we are interested in the field configurations where $\Phi$ approaches its minimum at spatial infinity. It is always possible for each finite-energy field configuration to associate a mapping from the two-dimensional sphere $S^2$ at spatial infinity into the vacuum manifold $G/H$. If this map cannot be continuously deformed to the trivial constant mapping that associates every point of $S^2$ to $\Phi_0$, the configuration represents a topological defect called "topological monopole". Mappings from $S^2$ into $G/H$ where the north pole of the sphere is mapped into $\Phi_0$ lie in homotopy classes, which present a natural group structure. This group is called $\Pi_2(G/H)$, the "second homotopy group" of $G/H$. Topological monopoles appear in the theory if $\Pi_2(G/H)$ is nontrivial, that is, it has more than only one element:

$$\Pi_2(G/H) \neq \{0\}. \tag{2.23}$$

We now discuss the properties of this group, explaining how those are related to the characteristics of magnetic monopoles in gauge theories.

First of all, $\Pi_2(G/H)$ is a discrete group, whose elements are the possible "topological charges" of the finite-energy field configuration. Topological charges are conserved, and the classical field theory has a topological conservation law. It is possible to show that the topological charge of the Georgie-Glashow model corresponds to the magnetic charge of the monopole solution, that is stabilized by the topological conservation law. This can be generalized to all the gauge theories that end up with a broken group phase containing electromagnetism. Secondly, it is possible to demonstrate the following important relation between the second homotopy group of the coset group and the first homotopy groups of the groups $G$ and $H$, assuming $G$ connected:

$$\Pi_2(G/H) \cong \Pi_1(H_0)/\Pi_1(G_0), \tag{2.24}$$

where we indicate with $G_0$ and $H_0$ the components of the groups $G$ and $H$ connected to the identity. In the case when $G$ is also simply connected, that is $\Pi_1(G_0) = \{0\}$, the condition for the existence of monopoles reduces to

$$\Pi_2(G/H) \cong \Pi_1(H_0). \tag{2.25}$$

Under this assumption, the presence of $U(1)$ symmetries in the group $H$ is a sufficient condition for the existence of the monopole solution because $\Pi_1(U(1)) \cong \mathbb{Z}$. In

particular, this is the case of the $SU(2)$ Georgie-Glashow model previously discussed, where one can now easily compute

$$\Pi_2(SU(2)/U(1)) \cong \mathbb{Z}, \tag{2.26}$$

where $\mathbb{Z}$ corresponds to the integer $n$ in the Dirac quantization condition. This means that the integer number labeling the elements of the second homotopy group corresponds to the magnetic charge of the monopole in Dirac units.

The symmetry group correctly describing the phenomenology of the real world is the non-compact group $SU(3)_c \otimes SU(2)_L \otimes U(1)_Y$ of the Glashow-Weinberg-Salam Standard Model. Unfortunately, according to the previous discussion, finite-energy monopoles are not expected in the framework of the electroweak symmetry breaking. However, once the Standard Model group is embedded in a larger compact group of some Grand Unified Theory (GUT), as $SU(5)$ or $SO(10)$, the existence of the monopoles is unavoidable. The estimate of their mass parallels that of the Georgi-Glashow model previously discussed, and hence the finite energy of the GUT monopole is given by Eq. (2.21), where now $\tilde{g}$ represents the GUT gauge group coupling, and $m_V$ is the vector boson mass of the spontaneously broken GUT theory, much heavier than the electroweak gauge bosons. Typically, scales of GUT theories lie in the range of $10^{14} - 10^{16}$ GeV. Hence, such monopoles are out of the production reach of current colliders, and one can only search for those produced from cosmic sources. However, the existence of magnetic monopoles in GUTs requires only that the $U(1)$ of electromagnetism is embedded in a larger compact group. Therefore, such a larger group can also result from a previous breaking of the GUT group. This may lead to significantly lighter monopoles than in a typical GUT $SU(5)$ theory. An example is provided by the following symmetry-breaking pattern of an initial $SO(10)$ GUT group:

$$SO(10) \longrightarrow SU(4) \otimes SU(2) \otimes SU(2) \longrightarrow SU(3)_c \otimes SU(2) \otimes U_Y(1). \tag{2.27}$$

The first phase transition might occur at GUT scales $10^{15}$ GeV, close to the inflationary scales, breaking the $SO(10)$ symmetry into the cross product group $SU(4) \otimes SU(2) \otimes SU(2)$. Hence, the second transition, where the $SU(4) \otimes SU(2) \otimes SU(2)$ group breaks into the Standard Model group, might occur at much lower scales, as $10^9$ GeV. In view of the mass relation in Eq. (2.21), one expects the resulting monopole mass to be of order $10^9$ GeV $\times \tilde{g}$, where $\tilde{g}$ is the coupling of the group in $SU(4) \otimes SU(2) \otimes SU(2)$ that is broken into the hypercharge $U(1)$ group. In this way, one obtains much lighter monopoles than the prediction of the original GUT models.

### 2.1.3 Kaluza-Klein monopoles

There are many exotic models that provide the existence of monopoles. Among them, those related to non-trivial geometries of compactified extra-dimensions are of particular interest for modern theories as string theories.

One very important example is the Kaluza-Klein monopole which arise in the Kaluza-Klein theories [86, 87, 88], which try to merge General Relativity with the other gauge forces by the implementation of additional space-time dimensions in the

theory. Indeed, the fundamental premise of Kaluza-Klein theories is that space-time is not just 4-dimensional, but rather (4+n)-dimensional. The $(4 + n)$ dimensional spacetime is then described by a metric where the n additional dimensions are spontaneously compactified into a compact manifold $N$ with radii close to the Planck length.

The classical vacuum solution of the Kaluza-Klein space-time is represented by the manifold $M^4 \times N$, which is the direct product of the four-dimensional Minkowski space $M^4$ and the compact manifold $N$. Any classical spherically symmetric field configuration that reaches the vacuum solution at spatial infinity therefore defines an N bundle [89] over a sphere. This bundle locally looks like the direct product $S^2 \times N$. However, if the N bundle over $S^2$ cannot be continuously deformed to the global direct product $S^2 \times N$, then also the field configuration cannot be continuously deformed to the vacuum solution and is classified as a topological soliton. We can correlate every $N$ bundle over $S^2$ with a loop in the isometry group H. The $N$ bundle over $S^2$ is topologically non-trivial only if the loops in $H$ have a non-trivial winding number. Consequently, all topological solitons possess a magnetic charges in the $H$ group.

The Kaluza-Klein monopole solution has been explicitly derived in the case of the original five-dimensional Kaluza-Klein theory, where $N$ is a circle and $H$ is the $U(1)$ of electromagnetism. Among the most interesting characteristics of these monopoles, we observe that monopole-antimonopole pairs have a different topology than the vacuum, and hence they cannot classically annihilate. Generally, it is expected that the five dimensional Kaluza-Klein monopole would approximately have the mass

$$m \sim \frac{\sqrt{8\pi}}{e} M_{\text{Pl}} \sim 5 \times 10^{19} \text{ GeV}. \tag{2.28}$$

## 2.2 Effective field theories and interaction with matter

A comprehensive quantum field theory of monopoles has not yet been fully developed, though several attempts have been made. The initial theoretic approaches for a local field theory utilized two electromagnetic potentials, one for the electric field and one for the magnetic field, but restricted to a single on-shell propagating degree of freedom through specific constraints. However, this approach was classic in the sense that it did not take into account second quantization. Although many formal approaches have been proposed over time, none of them have reached a suitable level for practical uses in discussing the interaction of monopoles with matter, which is important for monopole detection efforts. In particular, the results from collider physics obtained by the experiments of CMS, ATLAS, and MoEDAL [90, 91, 92] from photon fusion and Drell-Yan processes, although among the strongest lower bounds on the monopole mass, suffer from very strong theoretical uncertainties and are of not very practical use.[1]

Let us considering non-relativistic quantum scattering of a point particle with electric charge $e$ off a monopole with magnetic charge g, for small relative velocities v

---

[1]As we discuss later, the situation is different for the results obtained by MoEDAL [42] and ATLAS [43] from pair production in strong magnetic fields.
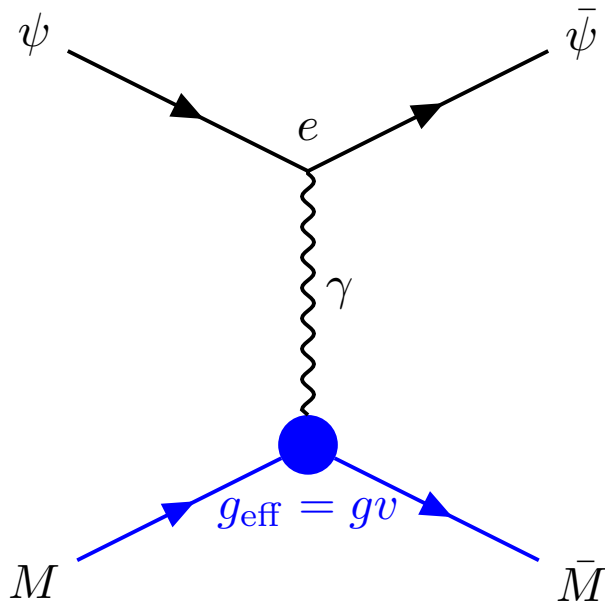
**Figure 2.2** Feynman diagram for a fermion ($\psi$, black line)-monopole (M, blue line) scattering with the exchange of a photon ($\gamma$, wavy line). The monopole vertex shows an effective interaction and is defined only for small monopole velocities.

of the scattered monopoles. It has been shown [93] that the differential cross section for small scattering angles is

$$\frac{d\sigma}{d\Omega} \simeq \left( \frac{eg}{2\mu v} \right)^2 \frac{1}{(\theta/2)^4}. \tag{2.29}$$

We note that once we define an effective velocity-dependent velocity for the monopoles,

$$g_{\text{eff}} \equiv gv, \tag{2.30}$$

this result corresponds to the Rutherford differential cross-section for non-relativistic electrically charged particles. It is therefore possible to describe the behavior of a magnetic monopole in matter considering such a "velocity-dependent" effective magnetic charge. Effective $U(1)$ gauge theories with the coupling in Eq. (2.30) have been proposed to search for magnetic monopoles at colliders. In particular, one can consider an effective $U(1)_{\text{em}} \otimes U(1)_{\text{dual}}$ gauge field theory for the coupling of monopoles and photons, where $U(1)_{\text{em}}$ represents the weakly coupled electromagnetic gauge group and $U(1)_{\text{dual}}$ represents a strongly coupled gauge group, which presents a velocity-dependent coupling. Unfortunately, the nonperturbative nature of the magnetic charge, as a result of the Dirac quantization, invalidates any attempt to use such an effective perturbative approach to interpret the data for relativistic monopoles. On the other hand, in virtue of the velocity-dependent magnetic coupling, such effective theories show a perturbative nature for small $v \ll 1$.

In Fig. 2.2 we show the Feynman diagram associated with a single-photon exchange during a fermion-monopole scattering in the discussed effective $U(1)_{\text{em}} \otimes U(1)_{\text{dual}}$. One can demonstrate that in this theory the effective charge of the

monopole is the one in Eq. 2.30, and therefore the diagram makes sense only for small monopole velocities. The effective description mentioned above can also describe the production of pairs of monopoles and antimonopoles from charged matter, by rotating the graph of Fig. 2.2 by 90° counterclockwise.

Finally, we must note that the interpretation of the magnetic charge as a velocity-dependent electric coupling is disputed, since at present there is no rigorous justification for its validity. Additionally, the fundamental effective field theory underlying monopoles production and/or scattering of matter is not yet fully understood. It has been also argued that because of the extended nature of the 't Hooft-Polyakov monopoles, with unknown inner structure, the cross-section for the production of extended topological objects is greatly suppressed by the finite size of the objects. This would completely invalidate attempts for the production of monopole-antimonopole pairs at colliders.

At the end of this section, we must cite an important physical effect of GUT monopoles interacting with matter, which defines some of the corresponding search strategies. This is the so-called Callan-Rubakov effect [37, 38] which asserts that in the presence of magnetic monopoles proton decay might be catalyzed, due to the induced baryon number non-conservation. Callan and Rubakov have shown that this effect is associated with dyonic excitations of the monopoles, resulting from the anomalous electric charge $Q = -e\theta$, which characterizes monopoles in CP-violating theories due to the vacuum misalignment angle $\theta$. Rubakov explained the effect highlighting that due to the axial anomaly, the monopole is not an eigenstate of chirality or baryon number, which permits large cross sections of baryon-number and chirality violative interactions in fermion-monopole scattering. Callan, on the other hand, pointed out the existence of baryon-number-violating boundary conditions when one regularizes the monopole solution with a finite core region and then allows the core size to approach zero. He argued that these boundary conditions reflect the complex physics inside the monopole core and result in unsuppressed baryon-number-violating cross sections for fermion-monopole scattering. Due to monopole-induced baryon-number-violating processes, proton decay can be enhanced in the presence of a GUT monopole. Protons moving with a relative velocity $v$ with respect to the monopole can decay with a cross section roughly $\sigma v \sim 10^{-27} \text{cm}^{-2}$, leading to a visible series of proton decays along the monopole's path. However, we underline that this is the property of only a subclass of the magnetic monopole models and cannot be applied generically.

## 2.3   Magnetic monopole production

Considering the very heavy mass of standard magnetic monopoles, even assuming their existence, it is really difficult to find efficient mechanisms of production. There are essentially three possible ways for the production of a significant amount of magnetic monopoles: production during phase transitions in the early universe, thermal production, and production via strong magnetic fields through the magnetic dual of the Schwinger effect. We now describe each of them in detail.

### 2.3.1   Production during phase transition in the early universe

'T Hooft-Polyakov magnetic monopoles are topologically stable, but they are not the minimum energy configurations. However, their production in cosmological phase transitions seems unavoidable. The process that describes the cosmological production is addressed as "Kibble mechanism" [94] and closely resembles the method for generating topological defects in standard laboratory phase transitions.

The Kibble mechanism relies on the fact that during a cosmological phase transition, any correlation length is invariably constrained by the particle horizon. The particle horizon represents the farthest distance over which a massless particle could have traveled since the Big Bang. This can be expressed as

$$d_H = a(t) \int_0^t \frac{dt'}{a(t')}, \tag{2.31}$$

where $a$ is the scale factor describing the time-dependent expansion of the Universe. If $a$ is proportional to $t^n$, with $n > 1$, then the horizon distance is given by $d_H = t/(1-n)$. The correlation length $\xi$ of the phase transition determines the furthest range over which the Higgs field remains correlated and depends on the specifics of the phase transition. This length changes with temperature, and is connected to the temperature-dependent Higgs mass as $\xi \sim M_H(T)^{-1} \sim T^{-1}$. However, the limited horizon distance in standard cosmology means that during the phase transition ($t = t_c$, $T = T_c$, where "c" stands for "critical"), the vacuum expectation value acquired by the Higgs field cannot correlate on scales larger than $d_H \sim H^{-1} \sim M_{\mathrm{Pl}}/T^2$. Hence, the particle horizon provides a strict upper limit for the correlation length and is the scale used in the Kibble mechanism to estimate the correlation length of the Higgs field.

Because of the finite correlation length of the Higgs field, if admitted by the theory, non-trivial vacuum configurations such as those for magnetic monopoles will necessarily be produced, with an approximated abundance of one per horizon volume. Hence, one can estimate the number density of the monopoles as $n_M \sim d_H^{-3} \sim T_c^6/M_{\mathrm{Pl}}^3$. Considering that the entropy density at temperature $T_c$ is $s \sim T_c^3$, the monopole-to-entropy ratio $n_M/s \sim (T_c/M_{\mathrm{Pl}})^3$. Assuming no significant monopole-antimonopole annihilation[2] or entropy production, this ratio stays constant and determines the current abundance of the monopole. For GUT monopoles we have $T_c \sim 10^{14}$ GeV and $m_M \sim 10^{16}$ GeV, and therefore the present monopole mass density results to be about $10^{11}$ times the critical density of the universe, which is clearly impossible. This is usually addressed as the "monopole problem". The monopole problem presents as optimal solution inflation, which should happen after the phase transition, exponentially diluting the initial monopole-to-entropy ratio.

We now compute more carefully the abundance of magnetic monopoles expected from the Kibble mechanism. Let us start with the scenario where the phase transition is either second order or weakly first order. According to standard cosmology, the age of the Universe when the phase transition occurs is approximately given by $t_c \sim 0.3 g_*^{-1/2} M_{\mathrm{Pl}}/T_c^2$. Taking as the correlation length $d_H \sim t_c$, we get the monopole-

---

[2]Preskill in [8] has shown that monopole-antimonopole annihilation is significant only if $n_M/s \gtrsim 10^{-10}$. In that case, the ratio is reduced by annihilation to $n_M/s \sim 10^{-10}$.

to-entropy ratio to be

$$\frac{n_M}{s} \sim 10^2 \left(\frac{T_c}{M_{\text{Pl}}}\right)^3 . \tag{2.32}$$

From this result, assuming adiabatic expansion since $T \sim T_c$, we compute the mass density in units of the critical density as

$$\Omega_M h^2 \sim 10^{11} \left(\frac{T_c}{10^{14} \text{ GeV}}\right)^3 \left(\frac{m_M}{10^{16} \text{ GeV}}\right) . \tag{2.33}$$

Therefore, considering that the magnetic monopole mass is of the order $m_M \sim 4\pi T_c/e$, the safety condition $\Omega_M < 1$ translates into the upper limit for the critical temperature of the phase transition, that is, $T_c \ll 10^{11}$ GeV if the transition does not happen before inflation. Based on the optimistic estimate provided for the correlation length in the Kibble mechanism, a phase transition at $T_c \sim 10^{11}$ GeV likely remains unsafe; should one develop an appealing unified model with $T_c = 10^{11}$ GeV, a more precise estimation of the correlation length would thus be necessary.

In the case of strongly first-order phase transitions, the estimate of the monopole abundance is slightly modified. In this case, the transition proceeds by bubble nucleation at the nucleation temperature $T_n \ll T_c$, when the nucleation rate becomes comparable to the Hubble rate $H$. Inside each bubble, the Higgs field is coherent; whereas, in distinct bubbles, it has no correlation. Consequently, it is expected that roughly one monopole forms per bubble. Specifically, as the Universe cools down to temperature $T_n$, bubbles start to form, expand, and quickly occupy all space. If $r_b$ represents the average bubble size during this phase, the expected monopole density is $n_M \sim r_b^{-3}$. Once the bubbles merge the Universe warms up again, and the entropy density becomes $s \sim g_* T_c^3$. Therefore, the monopole-to-entropy ratio becomes $n_M/s \sim (g_* r_b^3 T_c^3)^{-1}$. It has been shown in [95] that the bubble size can be approximately expressed as

$$r_b \sim \left(M_{\text{Pl}}/T_c^2\right) \left(\log\left(M_{\text{Pl}}^4/T_c^4\right)\right)^{-1} , \tag{2.34}$$

resulting in a relic monopole abundance of

$$\frac{n_M}{s} \sim \left[\left(\frac{T_c}{M_{\text{Pl}}}\right) \log\left(\frac{M_{\text{Pl}}^4}{T_c^4}\right)\right]^3 . \tag{2.35}$$

Therefore, with a first order phase transition the monopole problem is even worse.

Several potential solutions to the monopole problem have been proposed. Currently, as mentioned, the most compelling is the inflationary Universe model. The rapid expansion that comes with inflation allows a small, sub-horizon region of space, where the Higgs field is coherent, to extend across the entire observable Universe. Consequently, according to the Kibble mechanism, there is less than one monopole in the observable universe.

We cite also here two of the alternative solutions to the monopole problem present in the literature. The first one is that if there is no complete unification of the forces, for example, if $G = H \otimes U(1)$, or if the full symmetry of the GUT is not restored in the very early Universe (e.g., if the maximum temperature the Universe achieved was less than $T_c$), then the monopole problem would not arise because

monopoles would have never been produced. A second solution proposed in [96] is based on the unusual symmetry breaking pattern $SU(5) \rightarrow SU(3) \otimes SU(2) \otimes U(1) \rightarrow SU(3) \rightarrow SU(3) \otimes U(1)$. The monopoles are produced during the first phase transition, but between the second and the last phase transition, when the $U(1)$ of the electromagnetism is spontaneously broken, the Universe transitions to a superconducting state. Consequently, the magnetic flux confines into flux tubes, enhancing the annihilation rate of the monopoles and antimonopoles generated during the first transition. In this scenario, the final monopole density is approximately one per horizon volume by the conclusion of the superconducting phase, and therefore possibly smaller than in the standard scenario.

### 2.3.2   Thermal production in the early universe

There is another contribution to the production of magnetic monopoles in the early universe that is present even if the monopoles are not topological or if the Kibble mechanism can be avoided. This mechanism corresponds to the production of monopole-antimonopole pairs from the collisions of very energetic particles. This can be interpreted as thermal production of monopoles in the thermal plasma of the early universe. Thermal pair production leads to a relic monopole abundance of

$$\frac{n_M}{s} \sim 10^2 \left( \frac{m_M}{T_{\max}} \right)^3 \exp \left( -\frac{2m_M}{T_{\max}} \right), \tag{2.36}$$

with $T_{\max}$ the highest temperature reached after the spontaneous symmetry breaking [97]. Unfortunately, the amount of topological monopoles produced thermally is inherently small, since topological monopole configurations do not exist in the theory before the spontaneous symmetry breaking, that is for $T \gtrsim T_c$.

Considering that the monopoles possess a mass $m_M \sim 100 \, T_c$, in general we have $m_M/T_{\max} \lesssim 100$, which leads to a thermally produced monopole mass density today of $\Omega_M \lesssim 10^{-40}$, indicating a completely negligible amount of produced monopoles. However, the number density of the produced monopoles is highly sensitive to the ratio $m_M/T_{\max}$. So, even a change of a factor 3 or 5 can cause a significant shift in the expected production numbers. Moreover, in the case of non-topological monopoles, the temperature $T_{\max}$ might be much larger than the monopole mass. It is therefore plausible that thermal monopole production could result in a significant relic abundance of monopoles.

### 2.3.3   Pair production in strong magnetic fields

The last mechanism of monopole production that we describe here is based on non-perturbative monopole-antimonopole pair production in strong magnetic fields. This computation was first proposed by Schwinger in [12] for the pair production of electrically charged particles in an external electric field. Although the original computation invokes a weak coupling, and this is not the case for magnetic monopoles, the authors of [13, 14] were able to derive an expression for the vacuum decay rate due to monopole-antimonopole pair production in a static magnetic field through an

instanton method. They compute the rate of pair production as

$$\Gamma = \frac{(gB)^2}{(2\pi)^3} \exp\left[-\frac{\pi m^2}{gB} + \frac{g^2}{4}\right],\tag{2.37}$$

where B is the magnetic field strength, and in this formula we take the charge $g$ non-negative. This result holds for both Dirac point-like monopoles and 't Hooft-Polyakov extended objects, under the condition that the loop radius of the instanton solution $R = m/(gB)$ is much larger than the typical radius of a magnetic monopole $r = g^2/(4\pi m)$. We will discuss in detail the applicability of the formula in Chapter 8, so we skip here a more complete discussion of the result.

Differently from the perturbative Drell-Yan process of monopole pair production from electron-positron collision, the computation of the Schwinger production rate completely relies on non-perturbative techniques. Therefore, the computation is not affected by the large magnetic coupling of the monopoles to the photons, which causes a series of problems in defining a consistent effective field theory for the monopoles, as discussed in Section 2.2.

The expression for the pair production rate should be corrected by finite-temperature effects when the inverse of the thermal bath temperature is less than the instanton radius, $1/T < R$. These thermal corrections to the monopole production rate have been calculated in [98, 99]. Gravitational influences on monopole production are less explored, but it is generally expected that the production rate is affected when the curvature radius of spacetime is less than $R$. In a Friedmann–Robertson–Walker (FRW) universe, this is expressed as $1/H < R$, where H represents the Hubble expansion rate. These corrections would boost the pair production rate, potentially allowing production via sphalerons if the temperature and/or Hubble scale are sufficiently high.

The main contribution to the abundance of magnetic monopoles from pair production in strong magnetic fields would come from primordial magnetic fields [45], which could have been much stronger than known magnetic fields in the present universe. However, there have also been studies on monopole pair production in magnetars [44], and in heavy ion collisions at LHC [42, 43, 44], for small monopole mass.

# Chapter 3

# Monopole dynamics in the late universe

In this chapter we describe the acceleration of the magnetic monopoles in cosmic magnetic fields in the late universe. Magnetic monopoles are accelerated by magnetic fields through the magnetic force as in the equation of motion

$$m\frac{d}{dt}\left(\gamma\boldsymbol{v}\right)=g\mathbf{B},\qquad(3.1)$$

with $g$ the magnetic charge, $\mathbf{B}$ the magnetic field vector, $m$ the monopole mass, $\boldsymbol{v}$ the velocity of the monopoles and $\gamma=\left(1-v^2\right)^{-1/2}$. Cosmic magnetic fields accelerate the magnetic monopoles at different scales. We will show that, as a consequence of the acceleration, depending on the strength of the fields and the monopole mass, the population of cosmic magnetic monopoles can reach relativistic velocities.

In this analysis, we are interested in the velocity of the magnetic monopoles when they enter the Milky Way and when they approach the Earth or the terrestrial detectors. As we will discuss later, the incident velocity on the Milky Way is important for the Galactic Parker bounds, while the velocity at the Earth for direct search in terrestrial detectors.

For the computation of the incident velocity on the Milky Way, we must consider only acceleration in extra-galactic magnetic fields. Among the different extra-galactic contributions, we will consider acceleration from intergalactic magnetic fields (IGMFs) in cosmic voids, as we are interested in the average velocity of the cosmic population of MMs. There can be additional extragalactic magnetic fields, for instance fields in cosmic filaments, as well as fields transported by galactic winds (see, e.g. [100, 101, 102, 103, 104]). However, it is expected that such fields do not fill the entire universe [105], and thus can only affect the velocity of a small fraction of the cosmic MMs. Moreover, although weaker than the magnetic fields that surround the Milky Way, IGMFs accelerate magnetic monopoles over very long distances and therefore constitute the main extra-galactic contribution to the monopole velocity. Finally, the structure of the additional extra-galactic fields is not yet completely understood, while we search for conservative results. We hence exclude additional contributions from our analysis.

On the other hand, for the monopole velocity observed at the Earth it is also necessary to consider the acceleration in Galactic Magnetic Fields (GMFs), integrated

into a consistent framework together with IGMFs. This allows us to obtain a relation between the mass and the velocity of the monopoles. In the following chapter, we will use such a relation to recast velocity-dependent bounds into mass-dependent ones.

## 3.1   Acceleration in Galactic magnetic fields

From the analysis of the dataset of RMs and polarization of extra-galactic photons, we now have solid data-driven models for GMFs [60]. Observations provide GMFs with average amplitude $B_{\rm G} \sim 2 \times 10^{-6}$ G and coherence length $\lambda_{\rm G} \sim 1$ kpc. Currently, however, the motion of magnetic monopoles in the Milky Way has never been simulated numerically in realistic models of the GMFs, and this goes beyond the scope of this work. Hence, we will work in a simplified picture.

For this study, we introduce a method for the computation of monopole velocity given a certain framework of cosmic magnetic fields. Our results can be easily updated with different choice of magnetic fields scenarios. We estimate the energy gain of magnetic monopoles within the Milky Way modeling the GMFs as cells of uniform magnetic field $B_{\rm G}$ with size comparable to the coherence length of the fields $\lambda_{\rm G}$. Here we analyze the monopole acceleration as they pass through multiple cells.

The equation of motion of a monopole passing through the $N$th cell with uniform magnetic field $\boldsymbol{B}_N$ is

$$m\frac{d}{dt}(\gamma\boldsymbol{v}) = g\boldsymbol{B}_N. \tag{3.2}$$

Here $g$ denotes the amplitude of the magnetic charge, i.e. $g > 0$, and thus the monopole here has a positive charge. However, the following discussion can be applied to negatively charged monopoles by replacing $\boldsymbol{v} \to -\boldsymbol{v}$. By integrating the equation, one obtains the change in the monopole's Lorentz factor in the $N$th cell as,

$$\gamma_N^2 - \gamma_{N-1}^2 = \left(\frac{gB\tau_N}{m}\right)^2 + \frac{2g\boldsymbol{B}_N \cdot \boldsymbol{v}_{N-1}\gamma_{N-1}\tau_N}{m}. \tag{3.3}$$

Here $\tau_N$ denotes the time it takes for the monopole to pass through the $N$th cell, and $\gamma_N$ is the Lorentz factor when the monopole exits the $N$th cell and simultaneously enters the $(N + 1)$th cell; the same notation is used for the velocity $\boldsymbol{v}_N$. For $N = 1$, then $\gamma_{N-1}$ and $\boldsymbol{v}_{N-1}$ in the equation are replaced by the initial Lorentz factor $\gamma_i$ and velocity $\boldsymbol{v}_i$ upon entering the first cell.

We take all cells to have the same size $\lambda_{\rm G}$ and field strength, i.e. $B = |\boldsymbol{B}_N|$ for all $N$. Thus, the kinetic energy of a monopole changes within each cell by at most $\sim gB\lambda_{\rm G}$. If the kinetic energy is initially large such that $m(\gamma_i - 1) \gg gB\lambda_{\rm G}$, then the energy barely changes in the first cell. On the other hand if $m(\gamma_i - 1) \ll gB\lambda_{\rm G}$, the monopole is quickly accelerated so that upon exiting the first cell its energy reaches $m(\gamma_1 - 1) \simeq gB\lambda_{\rm G}$, and thereafter the energy does not change much within each cell. Hence independently of $\gamma_i$, we can write the crossing time for the second

cell onward as[1]

$$\tau_N \sim \frac{\lambda_{\mathrm{G}}}{v_{N-1}} \quad \text{for } N \geq 2. \tag{3.4}$$

Let us consider nonrelativistic monopoles for the moment. Then (3.3) at $N \geq 2$ can be rewritten using (3.4) as,

$$v_N^2 - v_{N-1}^2 = \frac{v_{\mathrm{mag}}^4}{4v_{N-1}^2} + v_{\mathrm{mag}}^2 \hat{\boldsymbol{B}}_N \cdot \hat{\boldsymbol{v}}_{N-1}. \tag{3.5}$$

Here a hat denotes a unit vector: $\hat{\boldsymbol{B}}_N \equiv \boldsymbol{B}_N/B$ and $\hat{\boldsymbol{v}}_N \equiv \boldsymbol{v}_N/v_N$. We also introduced

$$v_{\mathrm{mag}} \equiv \sqrt{\frac{2gB\lambda_{\mathrm{G}}}{m}}, \tag{3.6}$$

which corresponds to the velocity a monopole initially at rest obtains after passing through a single cell. From the discussions above (3.4) it follows that $v_1 \gtrsim v_{\mathrm{mag}}$ for general $v_i$.

Supposing for simplicity that the direction of the magnetic field is uncorrelated from one cell to the next, the second term in the right-hand side of (3.5) sources a random walk of $v^2$ in each cell. As we are interested in the mean behavior of the monopoles, let us ignore this term for now. Then we obtain a recurrence relation of the form[2]

$$\beta_N - \beta_{N-1} = \frac{1}{\beta_{N-1}}, \tag{3.7}$$

where $\beta_N \equiv 2v_N^2/v_{\mathrm{mag}}^2$. Since $\beta_1 \gtrsim 1$, this recurrence relation has an approximate solution,

$$\beta_N \simeq \sqrt{\beta_1^2 + 2(N-1)}. \tag{3.8}$$

Hence the exit velocity from the $N$th cell is obtained as

$$v_N^2 \simeq \sqrt{v_1^4 + \frac{N-1}{2}v_{\mathrm{mag}}^4}. \tag{3.9}$$

If $v_i \gtrsim v_{\mathrm{mag}}$, the discussions from (3.4) onward apply also to $N = 1$, then one can make the replacements $v_1 \to v_i$ and $N-1 \to N$ in the right-hand side of (3.9). On the other hand if $v_i \ll v_{\mathrm{mag}}$, then $v_1 \simeq v_{\mathrm{mag}}$ and (3.9) becomes $v_N^2 \simeq \sqrt{(N+1)/2}\,v_{\mathrm{mag}}^2$. In both cases, (3.9) can be rewritten at the order-of-magnitude level as

$$v_N^2 \sim \sqrt{v_i^4 + \frac{N}{2}v_{\mathrm{mag}}^4}. \tag{3.10}$$

---

[1]The exact value of $\tau_N$ also depends on the shape of the cell and the incident angle, however the expression (3.4) is good enough for our purpose of obtaining an order-of-magnitude estimate of the average energy gain.

[2]Here we are also roughly approximating the mean $\langle 1/v_{N-1}^2 \rangle$ by $1/\langle v_{N-1}^2 \rangle$.

In particular, the net change in the velocity squared in the limit of small and large $N$ takes the forms,

$$\Delta v_N^2 = v_N^2 - v_i^2 \sim \begin{cases} \dfrac{N}{4} \dfrac{v_{\mathrm{mag}}^4}{v_i^2} & \text{for } N \ll 8 \left( \dfrac{v_i}{v_{\mathrm{mag}}} \right)^4, \\[4mm] \sqrt{\dfrac{N}{2}}\, v_{\mathrm{mag}}^2 & \text{for } N \gg 8 \left( \dfrac{v_i}{v_{\mathrm{mag}}} \right)^4. \end{cases} \tag{3.11}$$

In the first line the acceleration is tiny such that $\Delta v_N \lesssim v_i$; this regime exists only if $v_i \gtrsim v_{\mathrm{mag}}$. Eventually, the monopole is accelerated as in the second line, where $\Delta v_N \gtrsim v_i$.

Let us discuss the second term in (3.5) which we have been ignoring. This sources a random walk behavior of $\Delta v^2$ in each cell with step size $\leq v_{\mathrm{mag}}^2$, which after $N$ cells yields a root-mean-square distance of order $\sqrt{N} v_{\mathrm{mag}}^2$. Now, consider $p$ number of monopoles with initial velocity $v_i$, each passing through $N$ cells in different parts of the galaxy. From the central limit theorem, the distribution of the average of $\Delta v_N^2$ with large enough $p$ is approximated by a normal distribution with mean (3.11) and standard deviation of

$$\sigma \sim \sqrt{\frac{N}{p}}\, v_{\mathrm{mag}}^2. \tag{3.12}$$

The expression (3.11) describes well the average behavior for the set of monopoles if it is much larger than $\sigma$. For this, the second line of (3.11) requires only $p \gg 1$, while the first line requires

$$pN \gg 16 \left( \frac{v_i}{v_{\mathrm{mag}}} \right)^4. \tag{3.13}$$

For relativistic monopoles ($v_N \simeq 1$), the mean recurrence relation becomes

$$\gamma_N^2 - \gamma_{N-1}^2 = \left( \frac{gB\lambda_{\mathrm{G}}}{m} \right)^2, \tag{3.14}$$

which yields

$$\gamma_N = \sqrt{\gamma_1^2 + (N-1) \left( \frac{gB\lambda_{\mathrm{G}}}{m} \right)^2}. \tag{3.15}$$

By following a similar analysis as for nonrelativistic monopoles, one arrives at results that match at the order-of-magnitude level with (3.11) and (3.13), with $v^2$ replaced by $2(\gamma - 1)$.

In summary, for both nonrelativistic and relativistic monopoles, the average energy gain after passing through $N$ cells takes the form

$$\Delta E_N = m(\gamma_N - \gamma_i) \sim \begin{cases} \dfrac{N}{4} \dfrac{(gB\lambda_{\mathrm{G}})^2}{m(\gamma_i - 1)} & \text{for } N \ll 8 \left( \dfrac{m(\gamma_i - 1)}{gB\lambda_{\mathrm{G}}} \right)^2, \\[4mm] \sqrt{\dfrac{N}{2}}\, gB\lambda_{\mathrm{G}} & \text{for } N \gg 8 \left( \dfrac{m(\gamma_i - 1)}{gB\lambda_{\mathrm{G}}} \right)^2. \end{cases} \tag{3.16}$$

For this to describe well the average behavior of a set of monopoles, the first line requires a sufficiently large number of monopoles $p$ such that

$$pN \gg 16 \left( \frac{m(\gamma_i - 1)}{gB\lambda_{\mathrm{G}}} \right)^2 , \tag{3.17}$$

while the second line requires only $p \gg 1$.

Let us now concentrate on magnetic monopoles that do not cluster with the Milky Way. If we define $R$ as the size of the magnetic region of the Galaxy, the unclustered monopoles pass through $N \sim R/\lambda_{\mathrm{G}}$ number of cells of uniform magnetic fields before reaching the Earth. Hence, in this case we can simply estimate the typical kinetic energy of a singly charged monopole accelerated in the Milky Way as

$$E_{\mathrm{k,G}} = m \left( \gamma_{\mathrm{G}} - 1 \right) \sim g_{\mathrm{D}} B_{\mathrm{G}} \lambda_{\mathrm{G}} \sqrt{N} \sim 10^{11} \text{ GeV}, \tag{3.18}$$

where in the last term we assume $B_{\mathrm{G}} = 10^{-6}$ G, $\lambda_{\mathrm{G}} = 1$ kpc , and $R \sim 10$ kpc.[3]

In Section 3.4, we will shown that the energy losses of magnetic monopoles due to interactions with the interstellar medium are negligible. Therefore, in this work, we ignore any dissipative energy loss for the monopoles. We also neglect any backreaction on the GMFs because the flux values for which the effect is non-negligible are excluded by the Galactic Parker bound [48, 49, 50], and not considered in this analysis.

## 3.2   Acceleration in intergalactic magnetic fields

IGMFs in cosmic voids are constrained by a large number of experiments (see [62, 63] for recent reviews). In particular, the amplitude of the IGMFs is constrained to be below $10^{-9}$ G from CMB observation [61, 106], and above $10^{-16}$ G from gamma-ray observatories [56, 64]. The coherence length is instead constrained to be larger than $\lambda_{\mathrm{I}} \gtrsim 10^{-5}$ Mpc from the combination of limits from early magnetic dissipation bounds [69] and from gamma-ray observatories.

In this section, we derive the velocity of magnetic monopoles after they have been accelerated in IGMFs for a Hubble time. We start by treating the IGMFs as a background. Then we discuss the backreaction of magnetic monopoles on the IGMFs, and evaluate the actual velocity that monopoles obtain in the intergalactic space.

### 3.2.1   Acceleration in an intergalactic magnetic field background

In a way similar to the galactic case, we model IGMFs with coherence length $\lambda_{\mathrm{I}}$ by dividing the universe into cells of uniform field, with each cell having a size $\lambda_{\mathrm{I}}$. We take the field strength in all cells to have the same value $B_{\mathrm{I}}$, and compute the monopole velocity after a Hubble time. We will ignore numerical factors of order unity.

---

[3]Magnetic monopoles that cross the Galaxy perpendicularly to the disk cross only 1-2 cells of uniform magnetic fields before exiting the Galaxy. In these cases, Eq. (3.18) overestimates the monopole kinetic energy by a factor $\sim \sqrt{R/\lambda_{\mathrm{G}}} \sim 3$. However, this does not affect our results significantly.

**First cell**

Let us consider all magnetic monopoles to be initially at rest at $t = 0$. They are then accelerated by a uniform field in the first cell as

$$m\gamma v = gB_\text{I}t, \tag{3.19}$$

where $\gamma = 1/\sqrt{1 - v^2}$. This can be used to compute the time it takes for the magnetic monopoles to travel a distance $\sim \lambda_\text{I}$ and exit the first cell as

$$\Delta t_1 \sim \max.\left\{\lambda_\text{I},\, \left(\frac{m\lambda_\text{I}}{gB_\text{I}}\right)^{1/2}\right\}. \tag{3.20}$$

The first term applies to magnetic monopoles that are accelerated to relativistic velocities within the first cell, while the second term is for monopoles that stay nonrelativistic.

**Second cell onward**

As the monopoles pass through multiple cells, they are deflected by the magnetic field in each cell. Assuming the directions of the field to be uncorrelated from one cell to the next, the average kinetic energy of each monopole grows with the number of cells crossed $N$ as

$$m(\gamma - 1) \sim gB_\text{I}\lambda_\text{I}N^{1/2}. \tag{3.21}$$

The detailed derivation is the same as that described in the previous section. In particular, the second line of Eq. (3.16) applies to our current case with a vanishing initial velocity. The number of cells each monopole crosses before becoming relativistic can be read off from (3.21) as,

$$N_\text{rel} \sim \left(\frac{m}{gB_\text{I}\lambda_\text{I}}\right)^2. \tag{3.22}$$

Using this, (3.21) can be rewritten as an expression for the product $\gamma v$ in the nonrelativistic and relativistic regimes as,

$$\gamma v \sim \begin{cases} \left(\dfrac{N}{N_\text{rel}}\right)^{1/4} & \text{for } N < N_\text{rel}, \\[2ex] \left(\dfrac{N}{N_\text{rel}}\right)^{1/2} & \text{for } N > N_\text{rel}. \end{cases} \tag{3.23}$$

If $m < gB_\text{I}\lambda_\text{I}$ (i.e. $N_\text{rel} < 1$), the monopoles become relativistic within the first cell and thus the second line in (3.23) holds for all $N$.

One sees from (3.23) that from the second cell onward, the monopole velocity does not change in each cell by more than an order-unity factor. Hence the crossing time for the $N$th cell can be estimated as

$$\Delta t_N \sim \frac{\lambda_\text{I}}{v}, \tag{3.24}$$

using the exit velocity $v$ from the $N$th cell as given in (3.23). For $2 \leq N < N_{\mathrm{rel}}$, the first line of (3.23) yields

$$\Delta t_N \sim \lambda_{\mathrm{I}} \left( \frac{N_{\mathrm{rel}}}{N} \right)^{1/4}. \tag{3.25}$$

At $N > N_{\mathrm{rel}}$, the monopole is relativistic and hence the crossing time becomes

$$\Delta t_N \sim \lambda_{\mathrm{I}}. \tag{3.26}$$

These expressions for the cell-crossing time can also be used for the first cell ($N = 1$), since (3.25) and (3.26) match respectively with the second and first terms in (3.20). By adding up (3.25) and (3.26) for all cells, and using the approximation $\sum_{n=1}^{N} n^{-1/4} \sim (4/3)N^{3/4}$, one can express the elapsed time in terms of the number of crossed cells as,

$$t = \sum_{n=1}^{N} \Delta t_n \sim \begin{cases} \lambda_{\mathrm{I}} N_{\mathrm{rel}}^{1/4} N^{3/4} & \text{for } N < N_{\mathrm{rel}}, \\ \lambda_{\mathrm{I}} N & \text{for } N > N_{\mathrm{rel}}. \end{cases} \tag{3.27}$$

One sees from this result that monopoles with $m > gB_{\mathrm{I}} \lambda_{\mathrm{I}}$ become relativistic after a time period of $t_{\mathrm{rel}} \sim \lambda_{\mathrm{I}} N_{\mathrm{rel}}$.

**Velocity after a Hubble time**

We are now ready to evaluate the velocity of monopoles that have been accelerated in an IGMF background. We consider the acceleration over a Hubble time $1/H_0$, and hence ignore cosmic expansion. In Appendix A we show that, even if the IGMF are remnants of primordial fields and the monopoles have been accelerated since the early universe, our estimate of the final monopole velocity is modified only by order-unity factors.

*Homogeneous IGMF.* If the magnetic coherence length is larger than the Hubble radius, $\lambda_{\mathrm{I}} > 1/H_0$, then the field is effectively homogeneous and the final value of $\gamma v$ is obtained by substituting $t = 1/H_0$ into (3.19). This yields

$$(\gamma v)_0 \sim \frac{gB_{\mathrm{I}}}{mH_0}. \tag{3.28}$$

*Inhomogeneous IGMF.* With sub-horizon coherence lengths, $\lambda_{\mathrm{I}} < 1/H_0$, the present-day velocity takes the forms,

$$(\gamma v)_0 \sim \begin{cases} \dfrac{gB_{\mathrm{I}}\lambda_I}{m} \dfrac{1}{(\lambda_{\mathrm{I}} H_0)^{1/2}} & \text{for } m < \dfrac{gB_{\mathrm{I}}\lambda_{\mathrm{I}}^{1/2}}{H_0^{1/2}}, \\[3mm] \left( \dfrac{gB_{\mathrm{I}}\lambda_{\mathrm{I}}}{m} \right)^{2/3} \dfrac{1}{(\lambda_I H_0)^{1/3}} & \text{for } \dfrac{gB_{\mathrm{I}}\lambda_{\mathrm{I}}^{1/2}}{H_0^{1/2}} < m < \dfrac{gB_{\mathrm{I}}}{\lambda_{\mathrm{I}} H_0^2}, \\[3mm] \dfrac{gB_{\mathrm{I}}}{mH_0} & \text{for } m > \dfrac{gB_{\mathrm{I}}}{\lambda_{\mathrm{I}} H_0^2}. \end{cases} \tag{3.29}$$

These can be understood as follows. Firstly, if the monopole mass is as large as $m > gB_{\mathrm{I}}/\lambda_{\mathrm{I}} H_0^2$, then one sees from (3.20) that $\Delta t_1 > 1/H_0$. The monopoles thus do not exit their first cells, and the final velocity is given by the same expression

as (3.28). Lighter monopoles, on the other hand, pass through multiple cells. However if $\Delta t_1 < 1/H_0 < \lambda_{\mathrm{I}} N_{\mathrm{rel}}$, then the monopoles on average stay nonrelativistic after a Hubble time. Hence the final velocity can be obtained by combining the first lines of (3.23) and (3.27) with $t = 1/H_0$; this yields the second line of (3.29). Finally, for even lighter monopoles satisfying $1/H_0 > \lambda_{\mathrm{I}} N_{\mathrm{rel}}$, the second lines of (3.23) and (3.27) yield the relativistic velocity in the first line of (3.29).

In the above discussions we have ignored the energy loss of magnetic monopoles due to interactions with the intergalactic medium and radiative emissions. In Section 3.4 we will show that these effects are actually negligible.

### 3.2.2 Backreaction on intergalactic magnetic fields

We have thus far treated the IGMFs as a background. However, magnetic monopoles extract energy from the IGMFs as they are accelerated, and hence the total kinetic energy of the monopoles cannot become larger than the initial energy of the IGMFs. We therefore have a constraint,

$$nm(\gamma - 1) < \frac{B_{\mathrm{I}}^2}{2}, \tag{3.30}$$

where $n$ is the average number density of magnetic monopoles in the universe. This sets the maximal Lorentz factor of the monopoles,

$$\gamma_{\max} - 1 = \frac{B_{\mathrm{I}}^2}{2nm}, \tag{3.31}$$

from which one can also obtain the maximal velocity $v_{\max}$.

If the velocity $v_0$ given in Eqs. (3.28) or (3.29) is much smaller than $v_{\max}$, the backreaction on the IGMFs is negligible. On the other hand if the monopole velocity approaches $v_{\max}$, then it implies that the energy of the IGMFs has been transferred to the monopoles. However, monopoles do not effectively dissipate the gained energy into the intergalactic medium as shown in Section 3.4, and thus they eventually return the energy to the IGMFs. This initiates an energy oscillation between the IGMFs and the population of magnetic monopoles [58], with the oscillation-averaged monopole velocity being of order $v_{\max}$. We expect the IGMF-magnetic monopole oscillation to avoid Landau damping; see Appendix B for discussions on this point.

The monopole velocity in the above two cases can collectively be written as

$$v_{\mathrm{CMB}} = \mathrm{min.}\left\{v_0, v_{\max}\right\}. \tag{3.32}$$

Here we used the subscript "CMB" to highlight that this is the monopole velocity with respect to the CMB rest frame. We also write the monopole flux in the CMB rest frame per area per time per solid angle[4] as $F_{\mathrm{CMB}} = nv_{\mathrm{CMB}}/4\pi$.

In the case where $v_0 > v_{\max}$, the expression (3.31) for the maximal velocity can be rewritten in terms of the flux as

$$\gamma_{\max} - 1 = \frac{B_{\mathrm{I}}^2 v_{\max}}{8\pi m F_{\mathrm{CMB}}}. \tag{3.33}$$

---

[4]This expression for the flux implicitly assumes the monopoles to be moving in random directions, which is not the case if the IGMF is homogeneous. However this is good enough for obtaining order-of-magnitude results.
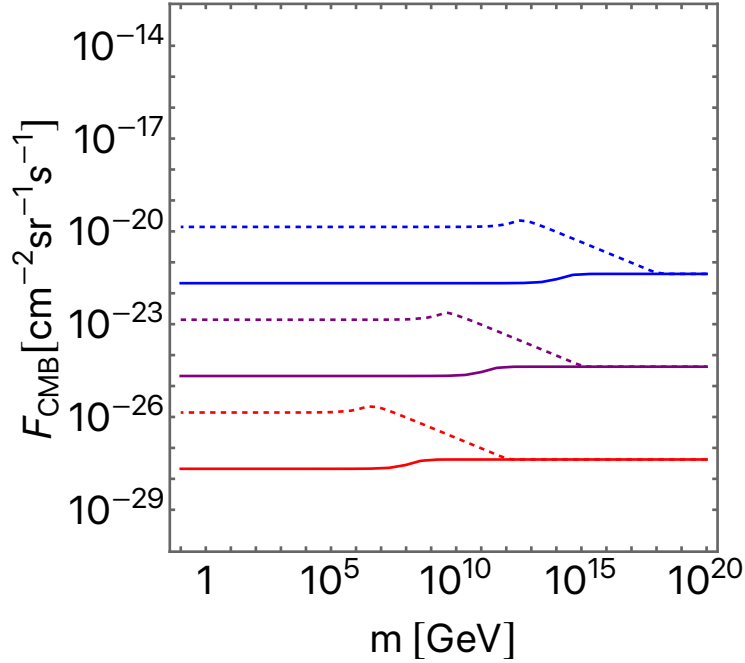
**Figure 3.1** Threshold value of the monopole flux beyond which the backreaction to the IGMFs becomes significant. The IGMF amplitude is varied as $B_I = 10^{-9}$ G (blue), $10^{-12}$ G (purple), $10^{-15}$ G (red), with the correlation length $\lambda_I > 1/H_0$ (solid) and $\lambda_I = 1$ Mpc (dashed). The monopole charge is fixed to $g = g_D$.

This can be solved in the nonrelativistic and ultrarelativistic limits to give the product $(\gamma v)_{\max}$ as,

$$(\gamma v)_{\max} \simeq \begin{cases} \dfrac{B_I^2}{4\pi m F_{CMB}} & \text{for } B_I^2 \ll 8\pi m F_{CMB}, \\[3mm] \dfrac{B_I^2}{8\pi m F_{CMB}} & \text{for } B_I^2 \gg 8\pi m F_{CMB}. \end{cases} \tag{3.34}$$

Notice that $v_{\max}$ is independent of the IGMF coherence length, while it depends on the monopole flux (or the density).

Writing the threshold value of the monopole flux beyond which the backreaction to the IGMFs becomes significant as $F_{BR}$, this can be obtained by solving $v_0 = v_{\max}$. For $\lambda_I > 1/H_0$, matching Eqs. (3.28) and (3.34) yields

$$F_{BR} \sim \frac{B_I H_0}{4\pi g}. \tag{3.35}$$

**(a)** $B_{\mathrm{I}} = 10^{-15}\,\mathrm{G}$, $\lambda_{\mathrm{I}} = 1\,\mathrm{Mpc}$.

**(b)** $B_{\mathrm{I}} = 10^{-15}\,G$, $\lambda_{\mathrm{I}} > 1/H_0$.

**(c)** $B_{\mathrm{I}} = 10^{-10}\,G$, $\lambda_{\mathrm{I}} = 1\,\mathrm{Mpc}$.

**(d)** $B_{\mathrm{I}} = 10^{-10}\,G$, $\lambda_{\mathrm{I}} > 1/H_0$.
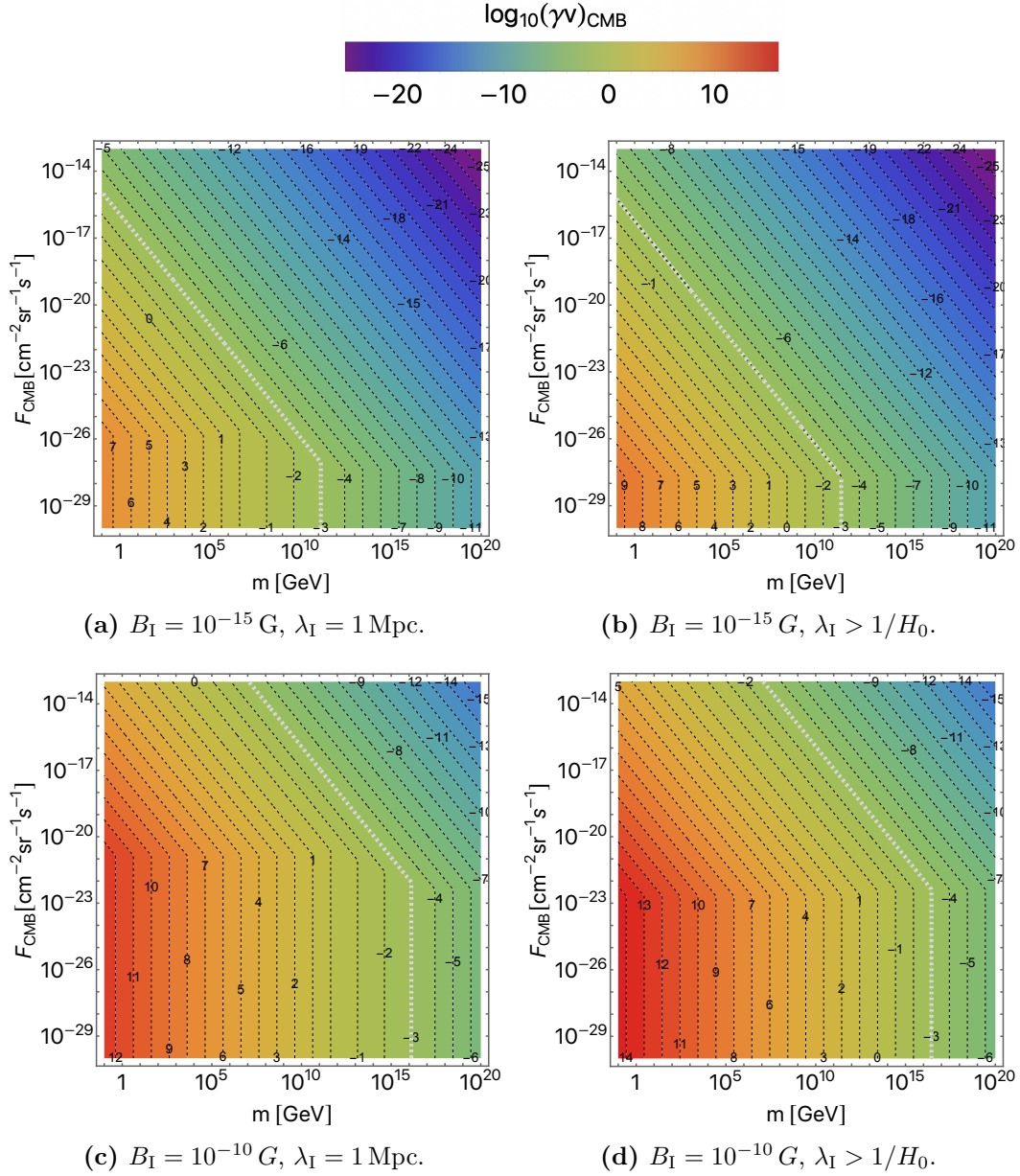
**Figure 3.2** Velocity of magnetic monopoles accelerated in IGMFs, in the CMB rest frame. The contours show $\log_{10}(\gamma v)_{\mathrm{CMB}}$. The monopole charge is fixed to $g = g_{\mathrm{D}}$, while the IGMF amplitude and coherence length are varied in each panel. Dashed gray lines highlight where $v_{\mathrm{CMB}} = 10^{-3}$.

For $\lambda_{\mathrm{I}} < 1/H_0$, Eqs. (3.29) and (3.34) give

$$
F_{\mathrm{BR}} \sim \begin{cases} \dfrac{B_{\mathrm{I}}}{4\pi g}\left(\dfrac{H_0}{\lambda_{\mathrm{I}}}\right)^{1/2} & \text{for } m < \dfrac{gB_{\mathrm{I}}\lambda_{\mathrm{I}}^{1/2}}{H_0^{1/2}}, \\[3mm] \dfrac{1}{4\pi}\left(\dfrac{B_{\mathrm{I}}^4 H_0}{g^2 m \lambda_{\mathrm{I}}}\right)^{1/3} & \text{for } \dfrac{gB_{\mathrm{I}}\lambda_{\mathrm{I}}^{1/2}}{H_0^{1/2}} < m < \dfrac{gB_{\mathrm{I}}}{\lambda_{\mathrm{I}}H_0^2}, \\[3mm] \dfrac{B_{\mathrm{I}}H_0}{4\pi g} & \text{for } m > \dfrac{gB_{\mathrm{I}}}{\lambda_{\mathrm{I}}H_0^2}. \end{cases} \tag{3.36}
$$
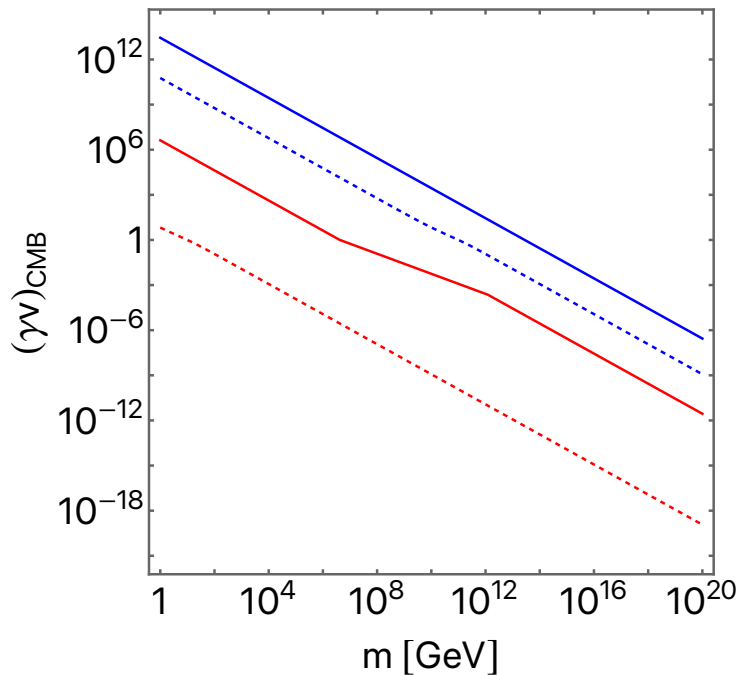
**Figure 3.3** monopole velocity in the CMB rest frame for fixed values of the monopole flux: $F_{\rm CMB} = 10^{-30}\,{\rm cm}^{-2}\,{\rm sr}^{-1}\,{\rm s}^{-1}$ (solid lines) and $10^{-20}\,{\rm cm}^{-2}\,{\rm sr}^{-1}\,{\rm s}^{-1}$ (dashed). The IGMF strength and coherence length are taken as $B_{\rm I} = 10^{-15}\,{\rm G}$ and $\lambda_{\rm I} = 1\,{\rm Mpc}$ for the red lines, while $B_{\rm I} = 10^{-10}\,{\rm G}$ and $\lambda_{\rm I} > 1/H_0$ for the blue lines. The monopole charge is fixed to $g = g_{\rm D}$.

We note that since the two expressions in (3.34) differ only by a factor 2, here we just used the first line to obtain order-of-magnitude estimates of $F_{\rm BR}$.

In Figure 3.1 we plot $F_{\rm BR}$ as a function of the monopole mass. The IGMF amplitude is varied as $B_{\rm I} = 10^{-9}\,{\rm G}$ (blue), $10^{-12}\,{\rm G}$ (purple), $10^{-15}\,{\rm G}$ (red), with the correlation length taken as $\lambda_{\rm I} > 1/H_0$ (solid lines) and $\lambda_{\rm I} = 1\,{\rm Mpc}$ (dashed lines). The solid and dashed lines with the same color join at large masses. The charge is fixed to $g = g_{\rm D}$. As one goes toward smaller masses each curve drops by a factor 2; this corresponds to the difference between the nonrelativistic and ultrarelativistic regimes as shown in Eq. (3.34). The displayed results match with the approximate expressions (3.35) and (3.36) up to order-unity factors. One sees that $F_{\rm BR}$ increases for larger $B_{\rm I}$, since the IGMF becomes more resilient to the backreaction from the monopoles. $F_{\rm BR}$ at small masses increases also for smaller $\lambda_{\rm I}$, since the monopole acceleration becomes less effective.

### 3.2.3 Summary of monopole acceleration in IGMFs

In Figure 3.2 we show the value of $(\gamma v)_{\rm CMB}$ in Eq. (3.32) as a function of the monopole mass and flux in the CMB rest frame. We display four combinations of the IGMF strength ($B_{\rm I} = 10^{-15}\,{\rm G}$ and $10^{-10}\,{\rm G}$) and correlation length ($\lambda_{\rm I} = 1\,{\rm Mpc}$ and $\lambda_{\rm I} > 1/H_0$). The monopole charge is fixed to $g = g_{\rm D}$. The values of $F_{\rm CMB}$ for which

the contour lines of $(\gamma v)_{\text{CMB}}$ are seen to bend correspond to the threshold $F_{\text{BR}}$, which we showed in Figure 3.1. In the lower regions of each plot where $F_{\text{CMB}} < F_{\text{BR}}$, the backreaction on the IGMFs is negligible and we have $v_{\text{CMB}} = v_0$, which is independent of the monopole density. On the other hand in the upper regions where $F_{\text{CMB}} > F_{\text{BR}}$, the backreaction is significant and $v_{\text{CMB}} = v_{\text{max}}$; here the monopole velocity depends on the flux but is independent of the IGMF coherence length, as shown in (3.34). The dashed gray line in the plot shows where $v_{\text{CMB}} = 10^{-3}$. This value is on the same order as the peculiar velocity of the Milky Way. We will comment in the following paragraphs why this value is important.

In Figure 3.3 we show $(\gamma v)_{\text{CMB}}$ as a function of the monopole mass for fixed values of the flux: $F_{\text{CMB}} = 10^{-30}\,\text{cm}^{-2}\,\text{sr}^{-1}\,\text{s}^{-1}$ (solid lines) and $10^{-20}\,\text{cm}^{-2}\,\text{sr}^{-1}\,\text{s}^{-1}$ (dashed). The IGMF strength and coherence length are taken as $B_{\text{I}} = 10^{-15}\,\text{G}$ and $\lambda_{\text{I}} = 1\,\text{Mpc}$ for the red lines, while $B_{\text{I}} = 10^{-10}\,\text{G}$ and $\lambda_{\text{I}} > 1/H_0$ for the blue lines. The flux on the solid lines satisfy $F_{\text{CMB}} < F_{\text{BR}}$, and thus the monopole velocity is set by $v_0$. On the other hand, the dashed lines have $F_{\text{CMB}} > F_{\text{BR}}$ and the monopoles move at $v_{\text{max}}$.

The above results show that, due to the acceleration in IGMFs, intermediate to low mass monopoles can become relativistic. This remains true even when taking into account the backreaction on the IGMFs, albeit with a reduction in the monopole velocity.

The peculiar velocity of the Milky Way Galaxy with respect to the CMB rest frame, $v_{\text{p}} \sim 10^{-3}$, sources a relative velocity between the cosmic magnetic monopoles and the Galaxy. However if the monopole velocity $v_{\text{CMB}}$ obtained in the IGMFs is even larger, this would dominate the relative velocity. Therefore, the monopole velocity in the rest frame of the Milky Way can be written as

$$v_{\text{I}} = \max. \{v_{\text{p}}, v_{\text{CMB}}\}. \tag{3.37}$$

We also denote the incident flux of monopoles on the Milky Way by $F_{\text{I}} = nv_{\text{I}}/4\pi$; this is equivalent to the monopole flux inside the Milky Way from the conservation of the number of magnetic monopoles. In Figure 3.2 we showed the combination of $m$ and $F_{\text{CMB}}$ for which $v_{\text{CMB}} \sim v_{\text{p}}$ by the dashed gray line. On the left of the gray line where $v_{\text{CMB}} > v_{\text{p}}$, the quantities $v_{\text{CMB}}$ and $F_{\text{CMB}}$ are identical to $v_{\text{I}}$ and $F_{\text{I}}$, respectively. On the other hand, on the right of the gray line where $v_{\text{CMB}} < v_{\text{p}}$, the monopole velocity in the Milky Way's rest frame becomes $v_{\text{p}}$. Therefore, contour plots of $(\gamma v)_{\text{I}}$ in the $m$-$F_{\text{I}}$ plane are the same as in Figure 3.2 except for that on the right of the gray dashed lines, $(\gamma v)_{\text{I}}$ is fixed to a constant value of $(\gamma v)_{\text{p}}$.

## 3.3 Comparison of the acceleration mechanisms

In this section we study the velocity of magnetic monopoles arriving on Earth, by focusing on monopoles that are not clustered with the Milky Way. Such unclustered monopoles are first accelerated in the IGMFs, then after entering the Milky Way they are further accelerated in the Galactic magnetic fields.

Considering the acceleration in both GMFs and IGMFs, the monopole velocity at the Earth is

$$(\gamma v)_{\text{E}} = \max \{(\gamma v)_{\text{I}}, (\gamma v)_{\text{G}}\}. \tag{3.38}$$

**(a)** $B_\mathrm{I} = 10^{-10}\,\mathrm{G}$.        **(b)** $B_\mathrm{I} = 10^{-15}\,\mathrm{G}$.
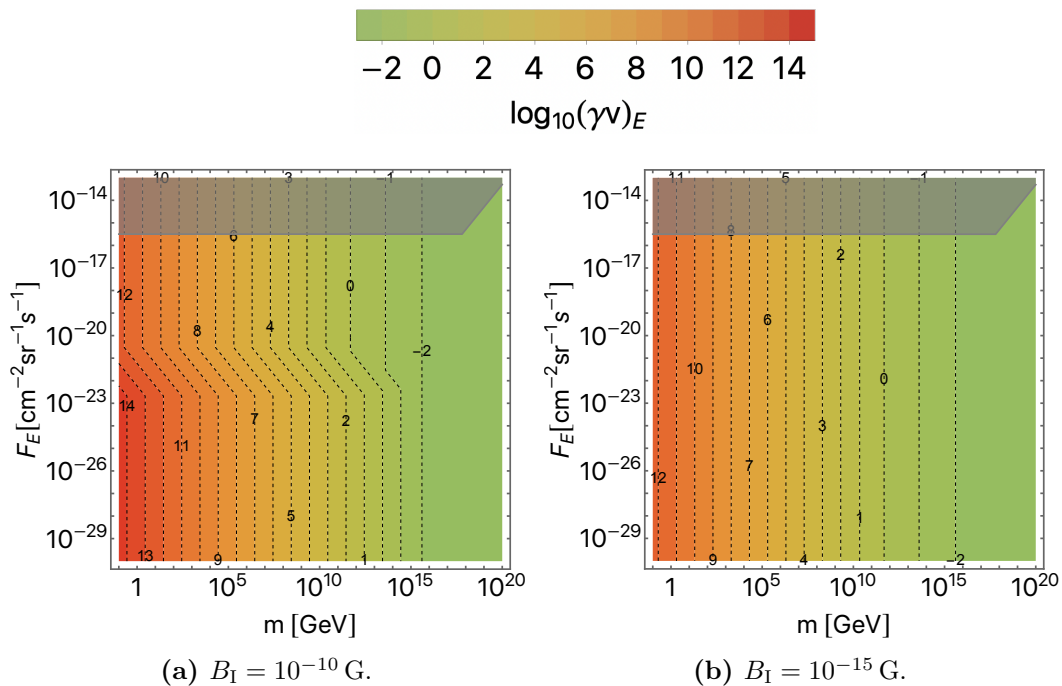
**Figure 3.4** monopole velocity on Earth evaluated by taking into account the acceleration in intergalactic and Galactic magnetic fields. The contours show $\log_{10}(\gamma v)_\mathrm{E}$. The parameters for the Galactic magnetic field are fixed to $B_\mathrm{G} = 10^{-6}\,\mathrm{G}$, $\lambda_\mathrm{G} = 1\,\mathrm{kpc}$, and $R = 10\,\mathrm{kpc}$. The IGMF is taken as homogeneous ($\lambda_\mathrm{I} > 1/H_0$), with the strength varied in each panel. The monopole charge is fixed to $g = g_\mathrm{D}$. The color scheme is the same as in Figure 3.2. The gray region is excluded by the Galactic Parker bound.

The dominance of one of either terms depends on the monopole mass and flux, and the characteristic of the considered IGMFs, as explained in the previous sections. In particular, the dependence on the monopole flux comes from the effect of back-reaction on IGMFs. We note that the velocity of the Earth with respect to the Milky Way is $\sim 10^{-3}$, which is comparable to the Milky Way's peculiar velocity $v_\mathrm{p}$. Since $v_\mathrm{E} \geq v_\mathrm{p}$ as is clear from Eq. (3.37), the monopole velocity in the rest frame of the Milky Way matches with that in the rest frame of Earth, at least at the order-of-magnitude level. Hence $v_\mathrm{E}$ can also be considered as the relative velocity between the monopoles and the Earth. For the same reason, and also because the flux of unclustered monopoles is conserved inside the Galaxy, the monopole flux incident on the Milky Way $F_\mathrm{I}$ is the same as that on Earth $F_\mathrm{E}$, i.e. $F_\mathrm{I} = F_\mathrm{E}$. We will use the expression in Eq. (3.38) in the following chapters to relate the monopole velocity at the Earth to the monopole mass.

In Figure 3.4 we show the values of $v_\mathrm{E}$ in Eq. (3.38) as a function of the monopole mass and flux on Earth. Here we assume a homogeneous IGMF with its amplitude varied as $B_\mathrm{I} = 10^{-10}\,\mathrm{G}$ (left) and $10^{-15}\,\mathrm{G}$ (right), while the parameters for the Galactic magnetic field are taken as $B_\mathrm{G} = 10^{-6}\,\mathrm{G}$, $\lambda_\mathrm{G} = 1\,\mathrm{kpc}$, and $R = 10\,\mathrm{kpc}$. The monopole charge is fixed to $g = g_\mathrm{D}$, and the color scheme follows that in Figure 3.2. The left plot exhibits a variety of behaviors of the monopole velocity. In the upper region, the acceleration by Galactic fields is dominant over that by IGMFs; here

the velocity is set by $v_{\mathrm{G}}$ and does not depend on the monopole flux. In the central region, the acceleration by IGMFs dominates with the monopoles' backreaction being significant; hence the velocity is given by $v_{\max}$. In the lower region, the acceleration by IGMFs dominates with negligible backreaction; the velocity is set by $v_0$ which is independent of the monopole flux. In the right part, the velocity is set by the peculiar velocity of the Milky Way, $v_{\mathrm{p}} \sim 10^{-3}$. On the other hand in the right plot with a weaker IGMF, the acceleration from Galactic fields completely dominates over that from IGMFs for all values of the monopole flux. From Eq. (3.18), the mass dependence of the velocity induced by the Galactic field can be read off as $(\gamma v)_{\mathrm{G}} \propto m^{-1}$ at small masses where $v_{\mathrm{G}} \simeq 1$, while $(\gamma v)_{\mathrm{G}} \propto m^{-1/2}$ at large masses where $v_{\mathrm{G}} \ll 1$; these behaviors are actually seen in the plots.

We note again that upon evaluating the acceleration in Eq. (3.18), we have ignored the backreaction of the magnetic monopoles on the Galactic fields. In reality, the monopole flux $F_{\mathrm{E}}$ ($= F_{\mathrm{I}}$) cannot exceed the Galactic Parker bound [48, 49, 50], otherwise the monopoles would short out the Galactic fields and contradict with observations. In the plots, the regions excluded by the Galactic Parker bound are shown in gray.

In Figure 3.5 we show the monopole velocity at the Earth of Eq. (3.38) as a function of the monopole mass for different values of the monopole flux. We consider four different benchmark scenarios for the IGMFs, assuming parameters within the experimental constraints. For the GMFs we consider $B_{\mathrm{G}} = 10^{-6}$ G, $\lambda_{\mathrm{G}} = 1\,\mathrm{kpc}$, and $R = 10\,\mathrm{kpc}$, and the monopole charge is fixed to $g = g_{\mathrm{D}}$. The monopole speed is limited from below by the peculiar velocity of the Milky Way, $v_{\mathrm{p}} \sim 10^{-3}$, which is the proper velocity of the Galaxy in the rest frame of the CMB. In Fig. 3.5a, we start showing an IGMF scenario for which the Galactic contribution to the monopole velocity is always dominant. By comparing Eqs. (3.18) and (3.37) in the relativistic case, the condition for the domination of the Galactic contribution can be expressed as

$$B_{\mathrm{I}} \lesssim 5 \times 10^{-11}\ \mathrm{G}\ \left( \frac{1\ \mathrm{Mpc}}{\min\left(\lambda_{\mathrm{I}}, 1/H_0\right)} \right)^{1/2}. \tag{3.39}$$

In this case, the mass-speed relation is set by the single relation displayed with a solid red line for all the possible monopole fluxes and monopoles are relativistic for masses smaller than $10^{12}$ GeV.

On the other hand, Figs. 3.5b, 3.5c and 3.5d show the cases of IGMFs close to the experimental upper limits of the magnetic field strength (Fig. 3.5d: $B_{\mathrm{I}} = 10^{-9}$ G, $\lambda_{\mathrm{I}} \gtrsim 1/H_0$; Fig. 3.5b: $B_{\mathrm{I}} = 10^{-10}$ G, $\lambda_{\mathrm{I}} \gtrsim 1/H_0$; Fig. 3.5c: $B_{\mathrm{I}} = 10^{-9}$ G, $\lambda_{\mathrm{I}} = 1$ Mpc). In these cases, once one fixes the parameters of the IGMFs, the question whether the most significant contribution to the monopole velocity comes from GMFs or IGMFs depends on both the mass and the flux of the magnetic monopoles. In general, the bottom red solid curve signals that the acceleration in GMFs is predominant, while any departure from that regime means that IGMF acceleration is the dominant contribution and is shown in blue curves. We now discuss each of the possible cases in details.

For monopole fluxes in the largest allowed limit ($F \gtrsim 10^{-18}\ \mathrm{cm}^{-2}\mathrm{sr}^{-1}\mathrm{s}^{-1}$ in panel 3.5b, 3.5c and $F \gtrsim 10^{-20}\ \mathrm{cm}^{-2}\mathrm{sr}^{-1}\mathrm{s}^{-1}$ in panel 3.5d), the monopole velocity receives the dominant contribution from the acceleration in GMFs. The correspondent

**(a)** $B_{\mathrm{I}} \lesssim 5 \times 10^{-11}\, G$
$\times \quad (1\, \mathrm{Mpc}/\min(\lambda_{\mathrm{I}}, 1/H_0))^{1/2}.$

**(b)** $B_{\mathrm{I}} = 10^{-10}\, G,\ \lambda_{\mathrm{I}} \gtrsim 1/H_0.$

**(c)** $B_{\mathrm{I}} = 10^{-9}\, G,\ \lambda_{\mathrm{I}} = 1\, \mathrm{Mpc}.$

**(d)** $B_{\mathrm{I}} = 10^{-9}\, G,\ \lambda_{\mathrm{I}} \gtrsim 1/H_0.$
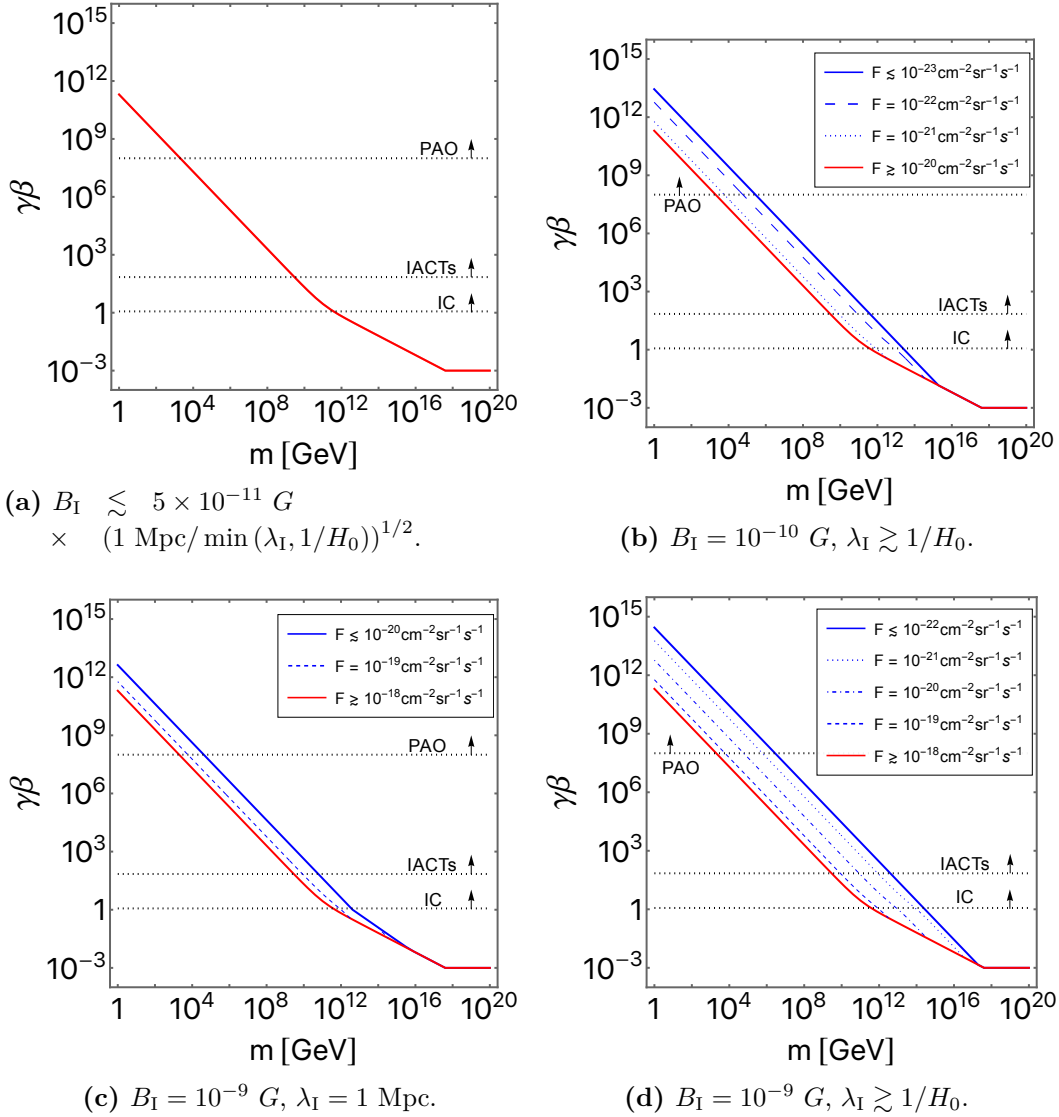
**Figure 3.5** monopole velocity on Earth as a function of the monopole mass evaluated by taking into account the acceleration in intergalactic and GMFs. The results are shown for different monopole fluxes, and the amplitude $B_{\mathrm{I}}$ and coherence length $\lambda_{\mathrm{I}}$ of IGMFs vary in each panel. The parameters for the Galactic magnetic field are fixed at $B_{\mathrm{G}} = 10^{-6}\, \mathrm{G}$, $\lambda_{\mathrm{G}} = 1\, \mathrm{kpc}$, and $R = 10\, \mathrm{kpc}$. The monopole charge is fixed to $g = g_{\mathrm{D}}$. We show in black dotted lines the thresholds of the IceCube (IC), IACT, and Auger (PAO) experiments for the detection of magnetic monopoles.

mass-velocity relation is given by the bottom red solid curve and is independent on the monopole flux and the characteristic of the IGMFs. In this case, monopoles move at relativistic velocities ($\gamma\beta \gtrsim 1$) for masses larger than $10^{12}$ GeV.

For smaller monopole fluxes ($F \lesssim 10^{-22}$ cm$^{-2}$sr$^{-1}$s$^{-1}$ in panel 3.5b, $F \lesssim 10^{-23}$ cm$^{-2}$sr$^{-1}$s$^{-1}$ in 3.5c, and $F \lesssim 10^{-20}$ cm$^{-2}$sr$^{-1}$s$^{-1}$ in panel 3.5d, the acceleration in IGMFs dominates over that in GMFs and there is no back-reaction

on the IGMFs. In this case, the mass-velocity relation is shown in the plots by the upper solid blue curve and is still independent on the monopole flux. In this case, magnetic monopoles move at relativistic velocities for masses smaller than a maximum mass in the interval $10^{13} - 10^{15}$ GeV, depending on the IGMFs.

For intermediate monopole fluxes between the two extreme cases discussed above, the dominant contribution to the monopole velocity can come from the acceleration in IGMFs, but the mass-velocity relation shows a flux dependence. This is because for monopole flux large enough the energy transferred from the fields to the monopoles is comparable with the total energy of the IGMFs and therefore backreaction on the fields is nonnegligible.

In Figure 3.5 we also show the speed thresholds for monopole observation of the detectors considered for this analysis. For monopole fluxes larger than $\sim 10^{-19}$ cm$^{-2}$sr$^{-1}$s$^{-1}$, the Galactic contribution to the velocity is always dominant over that from IGMFs, or at most comparable at the order of magnitude (solid red and dashed blue curves in the plots). For these values of the monopole flux, we will assume for the monopoles the kinetic energy in Eq. (3.18). As we discuss in Chapter 5, direct search limits constrain the monopole flux to values $\gtrsim 10^{-21}$ cm$^{-2}$sr$^{-1}$s$^{-1}$. For such fluxes, the intergalactic contribution is subdominant for amplitudes $B_{\mathrm{I}} < 10^{-9}$ G, or at most comparable at the order of magnitude (see Figures 3.5b and 3.5c). However, as shown in Figure 3.5d, in the extreme case of $B_{\mathrm{I}} = 10^{-9}$ G and $\lambda_{\mathrm{I}} \gtrsim 1/H_0$, intergalactic acceleration gives a significant contribution to the monopole velocity. Therefore, in this case, the experimental limits on the flux below $\sim 10^{-19}$ cm$^{-2}$sr$^{-1}$s$^{-1}$ should also take into account acceleration in IGMFs. We will discuss this in detail later.

We have demonstrated that the monopole velocity on Earth can be governed either by the acceleration in IGMFs, in Galactic fields, or by the Milky Way's peculiar velocity. Which of them dominates depends on a number of parameters, including the monopole flux, mass, and the relative strength of the intergalactic and Galactic fields.

## 3.4 Energy loss and radiative emission of monopoles

In this chapter we have ignored any dissipative energy loss for the monopoles. We now show that energy losses due to interactions with a nonrelativistic plasma and the interstellar medium are really negligible, as well as radiative emissions.

### 3.4.1 Energy loss of fast monopoles in a nonrelativistic plasma

A magnetic monopole traveling in a plasma loses its kinetic energy as it scatters off electrically charged particles. We evaluate the drag force experienced by the monopole by following the procedure outlined in Section 14.2 of [10]. However, here we consider the plasma to consist of nonrelativistic particles, and focus on cases where the monopole velocity is much larger than the velocities of the individual plasma particles in the rest frame of the plasma.

We start in the rest frame of a magnetic monopole with charge $g$. The magnetic field around the monopole is given by $\boldsymbol{B} = g\boldsymbol{r}/4\pi r^3$. (In this section $g$ is not

necessarily the charge amplitude and thus can be negative.) Hence the equation of motion of a particle with electric charge $q$, velocity $\boldsymbol{u}$, and momentum $\boldsymbol{p}$ is

$$\frac{d\boldsymbol{p}}{dt} = \frac{qg}{4\pi} \frac{\boldsymbol{u} \times \boldsymbol{r}}{r^3}. \tag{3.40}$$

Integrating this yields the total change in the momentum of the particle scattered by the monopole's magnetic field. Focusing on small-angle scatterings, and hence ignoring the effect of the magnetic field on the particle's trajectory, one obtains

$$\Delta p = \frac{|qg|}{4\pi} \int_{-\infty}^{\infty} dt \frac{u \sin \phi}{r^2} = \frac{|qg|}{2\pi b}, \tag{3.41}$$

where $\phi$ is the angle between $\boldsymbol{r}$ and $\boldsymbol{u}$, and $b$ is the impact parameter. Upon moving to the far right-hand side we used $\sin \phi = b/r$, and $r = \sqrt{(ut)^2 + b^2}$ with $t = 0$ corresponding to when the distance between the particle and the magnetic monopole is minimized. The scattering angle is $\theta = \Delta p/p$, with which the differential cross section is obtained as

$$\frac{d\sigma}{d\theta} = -2\pi b \frac{db}{d\theta} = \frac{(qg)^2}{2\pi p^2 \theta^3}. \tag{3.42}$$

We assume that in the rest frame of the plasma, the monopole velocity $\boldsymbol{v}$ has a much larger amplitude compared to the velocities of the individual plasma particles.[5] Then in the monopole rest frame, the particles can be considered to move with a universal velocity $\boldsymbol{u} = -\boldsymbol{v}$, and the scatterings with a collection of the particles induce the magnetic monopole to experience a force,

$$\begin{aligned} \boldsymbol{F} &= \gamma n_{\mathrm{p}} \int d\theta \frac{d\sigma}{d\theta} u \boldsymbol{p}(1 - \cos \theta) \\ &= \frac{C(qg)^2 n_{\mathrm{p}}}{4\pi m_{\mathrm{p}}} \frac{\boldsymbol{u}}{u}. \end{aligned} \tag{3.43}$$

Here $m_{\mathrm{p}}$ represents the mass of the plasma particles, and $n_{\mathrm{p}}$ is the particle number density in the plasma rest frame; note that in the monopole rest frame the number density is enhanced by the Lorentz factor $\gamma = 1/\sqrt{1 - v^2}$. The particle momentum is written as $\boldsymbol{p} = m_{\mathrm{p}} \gamma \boldsymbol{u}$, and we used that the average momentum transfer for a scattering with a small angle $\theta$ is $\boldsymbol{p}(1 - \cos \theta)$. Upon moving to the second line, we have written the integral over small angles as

$$C = 2 \int d\theta \frac{1 - \cos \theta}{\theta^3} \simeq \int \frac{d\theta}{\theta} = \ln \frac{\theta_{\max}}{\theta_{\min}}. \tag{3.44}$$

The upper limit of integration $\theta_{\max}$ can be set to unity as we are focusing on small-angle scatterings. The lower limit $\theta_{\min}$ arises from the fact that the above calculation based on single-particle scatterings breaks down if the impact parameter $b$ becomes larger than the mean free path of the particles in the plasma and/or the Debye length. Here we do not evaluate the detailed value of $\theta_{\min}$ since $\boldsymbol{F}$ is only logarithmically sensitive to it.

---

[5]A large relative velocity between the monopole and the plasma particles also supports the assumption of an unperturbed particle trajectory.

The expression for the drag force can be covariantized by noting that the force vector $\mathcal{F}^\mu$ should, in the monopole rest frame, have spatial components matching with (3.43), along with a vanishing time component since the monopole's energy does not change. These are satisfied by a force vector with the form,

$$\mathcal{F}^\mu = -\frac{C(qg)^2 n_{\mathrm{p}}}{4\pi m_{\mathrm{p}}} \frac{1}{v_{\mathrm{rel}}} \left\{ \frac{\mathrm{u}^\mu}{\mathrm{u}_\nu \mathrm{v}^\nu} + \mathrm{v}^\mu \right\}, \tag{3.45}$$

where we use $(-+++)$ for the metric signature, $\mathrm{v}^\mu$ is the four-velocity of the monopole, $\mathrm{u}^\mu$ is the four-velocity of the plasma, and $v_{\mathrm{rel}} = \sqrt{1-(\mathrm{u}_\nu \mathrm{v}^\nu)^{-2}}$ denotes the amplitude of the relative velocity between the monopole and the plasma (in the monopole rest frame, the spatial components of $\mathrm{u}^\mu$ reduce to $\gamma\boldsymbol{u}$, and $v_{\mathrm{rel}} = u$.)

The covariant equation of motion of a magnetic monopole with mass $m$ in electromagnetic fields is given by

$$m\mathrm{v}^\nu \nabla_\nu \mathrm{v}^\mu = g\tilde{F}^{\mu\nu}\mathrm{v}_\nu + \mathcal{F}^\mu, \tag{3.46}$$

with $\tilde{F}^{\mu\nu}$ being the dual electromagnetic field tensor. Taking a Minkowski metric and supposing that in the rest frame of the plasma there is only magnetic fields but no electric fields, then the equation of motion in the plasma rest frame reduces to

$$m\frac{d}{dt}(\gamma\boldsymbol{v}) = g\boldsymbol{B} - \frac{C(qg)^2 n_{\mathrm{p}}}{4\pi m_{\mathrm{p}}} \frac{\boldsymbol{v}}{v}. \tag{3.47}$$

Let us now compare the deceleration and acceleration terms in (3.47) in cosmic environments, by estimating their ratio:

$$\epsilon = \frac{1}{gB} \frac{C(qg)^2 n_{\mathrm{p}}}{4\pi m_{\mathrm{p}}}. \tag{3.48}$$

As particles with smaller masses yield a larger drag force, here we focus on free electrons (instead of protons). In the intergalactic space, using the electron density in the intergalactic medium (IGM) $n_e \sim 1\,\mathrm{m}^{-3}$, the IGMF lower limit $B_{\mathrm{I}} \sim 10^{-15}\,\mathrm{G}$, and further taking $g = g_{\mathrm{D}}$ and[6] $C \sim 1$, one finds $\epsilon \sim 10^{-10}$. In the Milky Way, considering instead the interstellar medium (ISM) with $n_e \sim 1\,\mathrm{cm}^{-3}$ and Galactic fields of $B_{\mathrm{G}} \sim 10^{-6}\,\mathrm{G}$ gives $\epsilon \sim 10^{-13}$. We thus see that both in the intergalactic space and the Milky Way, since the electron density is so small such that $n_e/m_e \ll B$, the acceleration of magnetic monopoles in the magnetic fields completely dominates over the deceleration by scattering free electrons.

Let us comment on effects that we have not taken into account. Firstly, the above calculation is based on classical single-particle scatterings. A quantum field theory computation may give rise to corrections to the scattering cross section, especially in the ultrarelativistic regime. We also note that the picture of single-particle scatterings breaks down at distances larger than the Debye length, where plasma effects become important. These have been studied in [107, 108] for slow monopoles, for which it was shown that the energy loss from plasma effects is typically not significantly larger than that from single-particle scatterings. Finally, we remark that magnetic

---

[6]Even if $C$ is larger by a few orders of magnitude, our main conclusion does not change.

monopoles can further loose energy through ionization of neutral particles, atomic excitations, bremsstrahlung, electron-pair production, and photonuclear interactions; the last two processes become particularly important in the ultrarelativistic regime. (See e.g. [78] for a study of various energy-loss processes for magnetic monopoles. In the next section we give a rough estimate of the interactions with neutral particles in the ISM, according to which they are negligible for a wide range of parameters.) It would be important to study all these effects, in particular in the ultrarelativistic regime. We leave this for future work.

### 3.4.2 Monopole energy loss in neutral interstellar medium

Here we provide a rough estimate of the energy loss from monopole's interactions with the interstellar medium and show that they are negligible.

Considering for simplicity a monopole moving more or less along a magnetic field line, its energy gain from the magnetic field per unit length is

$$\left(\frac{dE}{dx}\right)_{\text{mag}} \sim gB. \tag{3.49}$$

For instance for a charge $g = g_{\text{D}}$ and field strength $B = 10^{-6}\,\text{G}$, the energy gain is $(dE/dx)_{\text{mag}} \sim 10^{-2}\,\text{eV}\,\text{cm}^{-1}$.

Monopoles lose energy in the interstellar medium by ionization and atomic excitation of the constituent neutral particles. The energy loss can be evaluated from the Bethe–Bloch formula considering monopoles as particles with a velocity-dependent electric charge, $q = gv$ [109]. This gives, at the order-of-magnitude level,

$$-\left(\frac{dE}{dx}\right)_{\text{ion}} \sim \frac{e^2 g^2 n_{\text{m}}}{m_{\text{e}}}, \tag{3.50}$$

where $n_{\text{m}}$ is the number density of atoms in interstellar space and $m_{\text{e}}$ is the electron mass. Assuming $n_{\text{m}} = 1\,\text{cm}^{-3}$ [110] and $g = g_{\text{D}}$, the energy loss is $-(dE/dx)_{\text{ion}} \sim 10^{-14}\,\text{eV}\,\text{cm}^{-1}$, which is completely negligible with respect to the energy gain from the magnetic field. Other electromagnetic processes that induce energy loss of monopoles in matter include pair production and photonuclear interactions, however both contributions are subdominant compared to the ionization effect for $\gamma < 10^4$ [78]. There can also be energy loss through bremsstrahlung radiation in collisions; however this effect is inversely proportional to the monopole mass [78], so we expect it also to be subdominant.

We expect the main results of this section to be generic, however it would be important to analyze energy losses in more realistic models of the distribution of the interstellar medium, and also to perform a systematic study in the full parameter space. We leave these for the future.

### 3.4.3 Energy loss of fast monopoles through radiative emission

Here we estimate the energy loss of monopoles through the emission of electromagnetic radiation. Using the Liénard formula (i.e. relativistic version of the Larmor

formula), and exchanging the electric charge to magnetic, the energy loss per time of an accelerating monopole is

$$P \sim g^2 \gamma^6 \left\{ (\dot{\boldsymbol{v}})^2 - (\boldsymbol{v} \times \dot{\boldsymbol{v}})^2 \right\} = \frac{g^4 B^2}{m^2}, \tag{3.51}$$

where an overdot denotes a time-derivative. Upon moving to the far right-hand side, we have considered a magnetic monopole accelerating along a homogeneous magnetic field and dropped the cross product, and also used the equation of motion (3.47) without the drag force term. The ratio between the radiative energy loss, and energy gain per time from the acceleration in the magnetic field, $gBv$ (here we take $g > 0$), is thus

$$\delta \sim \frac{g^3 B}{m^2 v}. \tag{3.52}$$

For IGMFs of $B_{\mathrm{I}} = 10^{-15}$ G, relativistic ($v \sim 1$) monopoles with $g = g_{\mathrm{D}}$ give $\delta \sim 10^{-31} (1\,\mathrm{GeV}/m)^2$. For Galactic fields of $B_{\mathrm{G}} = 10^{-6}$ G, this becomes $\delta \sim 10^{-22} (1\,\mathrm{GeV}/m)^2$. In either case, radiative emissions are negligible for relativistic monopoles as long as the mass satisfies $m^2 \gg g^3 B$.

# Chapter 4

# Galactic Parker bounds for arbitrarily charged monopoles

Galactic Parker bounds are the most famous and important indirect bounds on the monopole flux in the Milky Way. They are based on the survival of the Galactic magnetic fields to the acceleration of the monopoles. In this chapter we first revisit the bounds, we generalize the results to arbitrarily charged monopoles (including magnetic black holes), we discuss conditions for the applicability of the bounds and, finally, we discuss how the bounds are modified by the acceleration of the monopoles in intergalactic magnetic fields.

## 4.1 Bounds from galactic magnetic fields

In this section, we revisit the Parker bounds on the monopole flux from galactic magnetic fields [48, 49] and seed fields [51]. We extend the previous computations to allow for the monopoles to carry arbitrarily magnetic charge, and we also clarify the range of applicability of the bounds.

Let us consider a generic galaxy hosting magnetic fields, that are amplified by dynamo action with a time scale $\tau_{\text{gen}}$. After the dynamo saturates, the magnetic field is assumed to stay nearly constant, and we represent the time period between saturation and today by $\tau_{\text{sat}}$. All cases with $\tau_{\text{sat}}$ being comparable to or smaller than $\tau_{\text{gen}}$ describe a similar situation where the fields have been growing until very recent times. Hence, without loss of generality we impose $\tau_{\text{sat}} \geq \tau_{\text{gen}}$.

Monopoles within a galaxy are accelerated by the magnetic fields. As explained in the previous section, we model the fields such that they exist in a region of size $R$, which is further divided into cells of uniform field. The size of each cell, i.e. the magnetic field's coherence length, is denoted by $\lambda_{\text{G}}$ ($< R$). We further assume that the field strength $B$ is the same in all cells, but the direction of the field is uncorrelated from one cell to the next. The average energy gain per monopole after

it has passed through $N$ uncorrelated cells is derived in Section 3.1 as

$$\Delta E_N \sim \begin{cases} \dfrac{N}{4}\dfrac{(gB\lambda_{\mathrm{G}})^2}{m(\gamma_i-1)} & \text{for } N \ll 8\left(\dfrac{m(\gamma_i-1)}{gB\lambda_{\mathrm{G}}}\right)^2, \\[2ex] \sqrt{\dfrac{N}{2}}\,gB\lambda_{\mathrm{G}} & \text{for } N \gg 8\left(\dfrac{m(\gamma_i-1)}{gB\lambda_{\mathrm{G}}}\right)^2. \end{cases} \tag{4.1}$$

where $\gamma_i$ is the initial Lorentz factor of the monopole upon entering the first cell.[1] In the first line the energy gain is smaller than the initial kinetic energy, i.e. $\Delta E_N < m(\gamma_i-1)$, while in the second line the monopole has been sufficiently accelerated such that $\Delta E_N > m(\gamma_i-1)$. If $m(\gamma_i-1) \ll gB\lambda_{\mathrm{G}}$, the energy gain is given by the second line from the first cell.

### 4.1.1 Do monopoles cluster with a galaxy?

If monopoles are bound in a galaxy, they would be moving with the virial velocity $v_{\mathrm{vir}}$ ($\ll 1$). However since the monopoles, on average, are constantly accelerated in galactic magnetic fields, they will eventually acquire a large enough velocity to escape from the galaxy. Considering that the escape velocity is not much larger than the virial velocity, let us estimate the time scale for the monopoles to escape from the galaxy as the time it takes for the monopoles' velocity to become larger than $v_{\mathrm{vir}}$ by a factor of order unity.

If $mv_{\mathrm{vir}}^2/2 \ll gB\lambda_{\mathrm{G}}$, then the monopole is accelerated to the escape velocity within a single cell. Then it suffices to consider a uniform magnetic field, in which the velocity varies as $\Delta \boldsymbol{v} = g\boldsymbol{B}\Delta t/m$ while the monopole is nonrelativistic. Hence we can estimate the escape time as

$$\tau_{\mathrm{esc}} \sim \frac{mv_{\mathrm{vir}}}{gB}. \tag{4.2}$$

On the other hand if $mv_{\mathrm{vir}}^2/2 \gg gB\lambda_{\mathrm{G}}$, the monopoles pass through multiple cells before reaching the escape velocity. The two limiting expressions in (4.1) represent the regimes where the monopole velocity has barely/significantly increased from its initial velocity. The escape velocity is acquired in between the two regimes, when the number of cells passed through is

$$N_{\mathrm{esc}} \sim 2\left(\frac{mv_{\mathrm{vir}}^2}{gB\lambda_{\mathrm{G}}}\right)^2. \tag{4.3}$$

Hence the escape time is

$$\tau_{\mathrm{esc}} \sim \frac{N_{\mathrm{esc}}\lambda_{\mathrm{G}}}{v_{\mathrm{vir}}} \sim \frac{2m^2 v_{\mathrm{vir}}^3}{g^2 B^2 \lambda_{\mathrm{G}}}. \tag{4.4}$$

---

[1]It would be very interesting to study more realistic models where the directions of magnetic fields are not completely random; this should realize a more efficient acceleration of monopoles and thus yield stronger flux bounds. The analysis here also neglects the effect of the galaxy's gravitational potential, as well as the possibility that the monopoles spend ample time in galactic regions without magnetic fields.

The escape time for both cases $mv_{\rm vir}^2/2 \ll gB\lambda_{\rm G}$ and $mv_{\rm vir}^2/2 \gg gB\lambda_{\rm G}$ can collectively be written as

$$
\begin{aligned}
\tau_{\rm esc} \sim {}& {\rm max.}\left\{ \frac{mv_{\rm vir}}{gB}, \frac{2m^2 v_{\rm vir}^3}{g^2 B^2 \lambda_{\rm G}} \right\} \\
\sim {}& {\rm max.}\Bigg\{ 10^7\,{\rm yr} \left( \frac{m}{10^{17}\,{\rm GeV}} \right) \left( \frac{g}{g_{\rm D}} \right)^{-1} \left( \frac{B}{10^{-6}\,{\rm G}} \right)^{-1} \left( \frac{v_{\rm vir}}{10^{-3}} \right), \\
& 10^7\,{\rm yr} \left( \frac{m}{10^{17}\,{\rm GeV}} \right)^2 \left( \frac{g}{g_{\rm D}} \right)^{-2} \left( \frac{B}{10^{-6}\,{\rm G}} \right)^{-2} \left( \frac{\lambda_{\rm G}}{1\,{\rm kpc}} \right)^{-1} \left( \frac{v_{\rm vir}}{10^{-3}} \right)^3 \Bigg\}.
\end{aligned}
\tag{4.5}
$$

The escape time decreases as $B$ is amplified, given that the other parameters do not change as much as $B$. Monopoles can thus stay clustered with a galaxy if the escape time is longer than the time elapsed since the magnetic field achieved its present-day strength $B_0$, i.e.,[2]

$$
\tau_{\rm esc}|_{B=B_0} > \tau_{\rm sat}.
\tag{4.6}
$$

Let us assume hereafter that the time scale of dynamo is comparable to or larger than the time it takes for a particle with virial velocity to cross the magnetic field region of the galaxy,

$$
\tau_{\rm gen} \gtrsim \frac{R}{v_{\rm vir}} \sim 10^7\,{\rm yr} \left( \frac{R}{10\,{\rm kpc}} \right) \left( \frac{v_{\rm vir}}{10^{-3}} \right)^{-1}.
\tag{4.7}
$$

From this it follows that $\tau_{\rm sat} > \lambda_{\rm G}/v_{\rm vir}$, indicating that monopoles that obtain the escape velocity within a single cell cannot stay clustered until today. Hence for monopoles to be clustered, $mv_{\rm vir}^2/2 \gg gB\lambda_{\rm G}$ is a necessary condition. An even stronger condition is obtained by substituting (4.4) into (4.6), which yields a lower bound on the mass of clustered monopoles as

$$
m \gtrsim 10^{18}\,{\rm GeV} \left( \frac{g}{g_{\rm D}} \right) \left( \frac{B_0}{10^{-6}\,{\rm G}} \right) \left( \frac{\lambda_{\rm G}}{1\,{\rm kpc}} \right)^{1/2} \left( \frac{\tau_{\rm sat}}{10^{10}\,{\rm yr}} \right)^{1/2} \left( \frac{v_{\rm vir}}{10^{-3}} \right)^{-3/2}.
\tag{4.8}
$$

Considering for instance the Milky Way, for which the typical parameters of the magnetic field and virial velocity are shown on the right-hand side as the reference values [59, 111, 112], monopoles with a Dirac charge can be clustered today only if their mass is larger than $10^{18}\,{\rm GeV}$.[3] Producing such ultraheavy monopoles in the postinflation universe presents a challenge for monopoles with charge $g \geq g_D$ to serve as dark matter. This is no longer the case for minicharged ($g \ll g_D$) monopoles, which can cluster with smaller masses.

---

[2]The derivation of $\tau_{\rm esc}$ uses the assumption of a constant $B$, which breaks down if $\tau_{\rm esc} > \tau_{\rm sat}$. In such cases the exact value of $\tau_{\rm esc}$ can be modified from (4.5), but we can still conclude that the monopoles can cluster with the galaxy. A similar discussion applies to the magnetic field dissipation time which we derive later.

[3]A similar bound can be obtained by requiring the gravitational acceleration of a monopole with virial velocity on a circular orbit at the radius of the galaxy ($v_{\rm vir}^2/r_{\rm g}$), to be larger than the magnetic acceleration ($gB_0/m$). This yields

$$
m \gtrsim 10^{18}\,{\rm GeV} \left( \frac{g}{g_{\rm D}} \right) \left( \frac{B_0}{10^{-6}\,{\rm G}} \right) \left( \frac{r_{\rm g}}{10\,{\rm kpc}} \right) \left( \frac{v_{\rm vir}}{10^{-3}} \right)^{-2}.
\tag{4.9}
$$

### 4.1.2 Backreaction from monopoles

We now derive bounds on the flux of monopoles inside galaxies by studying the backreaction from the monopoles on galactic magnetic fields.

**Unclustered monopoles**

We start by considering monopoles that are not trapped inside a galaxy but pass through it. The incident flux of such unclustered monopoles on a galaxy is equivalent to the flux inside the galaxy, from monopole number conservation.[4] Writing the flux per area per solid angle per time as $F$, and modeling the magnetic field region of the galaxy by a sphere with radius $R$, then the number of monopoles passing through the magnetic region per time is $4\pi^2 R^2 F$. (The extra power of $\pi$ is from integrating over the solid angle on one side of the surface of the magnetic region.) Each monopole crosses roughly $N = R/\lambda_\mathrm{G}$ cells as it traverses the magnetic region, and on average gains energy of $\Delta E_{N=R/\lambda_\mathrm{G}}$. In turn, the magnetic field loses energy at a rate,

$$\dot{E}_B \sim -4\pi^2 R^2 F \, \Delta E_{N=R/\lambda_\mathrm{G}}. \tag{4.10}$$

Comparing this with the total magnetic field energy, $E_B = (4\pi R^3/3)(B^2/2)$, the time scale for the magnetic field to be dissipated is computed as

$$\tau_\mathrm{dis} = \frac{E_B}{|\dot{E}_B|} \sim \max. \left\{ \frac{2m(\gamma_i - 1)}{3\pi g^2 F \lambda_\mathrm{G}}, \frac{B}{3\sqrt{2}\pi g F} \sqrt{\frac{R}{\lambda_\mathrm{G}}} \right\}, \tag{4.11}$$

where we substituted (4.1) into $\Delta E_{N=R/\lambda_\mathrm{G}}$. Here $\gamma_i$ is understood as the Lorentz factor of the monopoles with respect to the galaxy, upon galaxy entry, that is $\gamma_G$ of the previous chapter.

The backreaction from the monopoles has little effect on the magnetic field evolution if the field amplification by dynamo proceeds at a faster rate,

$$\tau_\mathrm{dis} > \tau_\mathrm{gen}. \tag{4.12}$$

This condition should hold throughout the galactic history for negligible backreaction,[5] and it translates into an upper bound on the monopole flux in the Milky Way,

$$F \lesssim \max. \left\{ 10^{-16} \, \mathrm{cm}^{-2} \mathrm{sec}^{-1} \mathrm{sr}^{-1} \left( \frac{m\,(\gamma_i - 1)}{10^{11}\,\mathrm{GeV}} \right) \left( \frac{g}{g_\mathrm{D}} \right)^{-2} \left( \frac{\lambda_\mathrm{G}}{1\,\mathrm{kpc}} \right)^{-1} \left( \frac{\tau_\mathrm{gen}}{10^8\,\mathrm{yr}} \right)^{-1} , \right.$$

$$\left. 10^{-16} \, \mathrm{cm}^{-2} \mathrm{sec}^{-1} \mathrm{sr}^{-1} \left( \frac{g}{g_\mathrm{D}} \right)^{-1} \left( \frac{B_\mathrm{G}}{10^{-6}\,\mathrm{G}} \right) \left( \frac{R}{\lambda_\mathrm{G}} \right)^{1/2} \left( \frac{\tau_\mathrm{gen}}{10^8\,\mathrm{yr}} \right)^{-1} \right\}. \tag{4.13}$$

---

[4]The velocity and number density upon entering the galaxy can each be different from those inside the galaxy, however their product remains constant. Here we do not consider initially unclustered monopoles becoming clustered, or vice versa. We also neglect monopole-antimonopole annihilation.

[5]This guarantees negligible backreaction even after the dynamo saturates, if $\tau_\mathrm{gen}$ also sets the time scale for the magnetic field's deviations from the saturation value to decay. However since the field amplification lives on a finite supply of energy of the galaxy, one may instead require $\tau_\mathrm{dis} > \tau_\mathrm{sat}$, giving a stronger bound.

The first (second) line sets the bound when $m$ is larger (smaller) than the threshold value,

$$\hat{m} \sim 10^{17}\,\text{GeV} \left(\frac{g}{g_{\text{D}}}\right) \left(\frac{B}{10^{-6}\,\text{G}}\right) \left(\frac{\lambda_{\text{G}}}{1\,\text{kpc}}\right) \left(\frac{R}{\lambda_{\text{G}}}\right)^{1/2} \left(\frac{\gamma_i - 1}{10^{-6}}\right)^{-1}. \tag{4.14}$$

Monopoles with masses smaller than this exit the galaxy with a velocity much larger than their incident velocity $v_i$.

By using the expression (4.1) for $\Delta E_N$ in the above derivation, it was implicitly assumed that the monopoles each pass through at least one cell within the dissipation time $\tau_{\text{dis}}$. Moreover for small-mass monopoles which gain energy as $\Delta E_N \propto \sqrt{N}$ (cf. second line of (4.1)), we assumed that the time it takes for the monopoles to cross the entire magnetic region is shorter than $\tau_{\text{dis}}$. These two assumptions are automatically satisfied when the condition (4.12) holds along with

$$\tau_{\text{gen}} \gtrsim \frac{R}{v_i} \sim 10^7\,\text{yr} \left(\frac{R}{10\,\text{kpc}}\right) \left(\frac{v_i}{10^{-3}}\right)^{-1}. \tag{4.15}$$

In other words, the flux bound (4.13) applies without modification under (4.15).

It should also be noted that for the first line of (4.1) to well describe the mean behavior of monopoles, the monopole number needs to be large enough to satisfy Eq. (3.17). The total number of unclustered monopoles passing through the magnetic region before the field is dissipated is $p = 4\pi^2 R^2 F \tau_{\text{dis}}$. Using also the first term in the far right-hand side of (4.11) for $\tau_{\text{dis}}$, and $N = R/\lambda_{\text{G}}$ for the number of cells each monopole crosses, then (3.17) yields an upper bound on the monopole mass,

$$m \lesssim 10^{63}\,\text{GeV} \left(\frac{B}{10^{-6}\,\text{G}}\right)^2 \left(\frac{R}{10\,\text{kpc}}\right)^3 \left(\frac{\gamma_i - 1}{10^{-6}}\right)^{-1}. \tag{4.16}$$

The condition (3.17) is not necessary when $\tau_{\text{dis}}$ is given by the second term in (4.11), however even in this case the monopole number $p \sim BR^{5/2}/g\lambda_{\text{G}}^{1/2}$ should be larger than unity for the derivation of the flux bound to be valid. This requires

$$B \gtrsim 10^{-52}\,\text{G} \left(\frac{g}{g_{\text{D}}}\right) \left(\frac{\lambda_{\text{G}}}{1\,\text{kpc}}\right)^{1/2} \left(\frac{R}{10\,\text{kpc}}\right)^{-5/2}. \tag{4.17}$$

This condition is equivalent to requiring that $\hat{m}$ given in (4.14) is smaller than the upper mass limit of (4.16). The conditions (4.16) and (4.17) seem rather weak, however they can become important when considering systems with extremely weak $B$, or when constraining extremely massive monopoles such as magnetic black holes.

The magnetic field energy taken away by the monopoles can, in principle, later be returned to the field. Then $\tau_{\text{dis}}$ would only correspond to the half-period of the energy oscillation between the magnetic field and monopoles, and the flux bound would be invalidated. However it was pointed out in [48, 50] that for monopoles with charge of $g \sim g_{\text{D}}$, the galactic magnetic fields cannot be maintained in this way since the oscillations are subject to Landau damping, and also because the oscillations would give features of the field that do not match with observations. It would be important to analyze whether Landau damping is effective with minicharges, $g \ll g_{\text{D}}$. We leave this for future work. We also note that for unclustered monopoles, they may fly away from the galaxy before returning the energy to the field.

**Clustered monopoles**

Monopoles that are bound in a galaxy move with the virial velocity $v_{\rm vir}$, and hence each monopole crosses approximately $N = v_{\rm vir}/\lambda_{\rm G}$ cells per unit time. The energy the monopoles steal from the magnetic field per time per volume is thus

$$\dot{\rho}_B \sim -n\,\Delta E_{N=v_{\rm vir}/\lambda_{\rm G}}, \tag{4.18}$$

where $n$ is the number density of clustered monopoles. While a monopole is clustered, its energy follows $\Delta E_N \propto N$ as shown in the first line of (4.1), with $\gamma_i - 1 \simeq v_{\rm vir}^2/2$. Taking the ratio with the magnetic energy density $\rho_B = B^2/2$, and noting that the flux is written as $F = nv_{\rm vir}/4\pi$, the dissipation time scale is obtained as

$$\tau_{\rm dis} = \frac{\rho_B}{|\dot{\rho}_B|} \sim \frac{mv_{\rm vir}^2}{4\pi g^2 F \lambda_{\rm G}}. \tag{4.19}$$

This matches up to an order-unity factor with the first expression in (4.11) for unclustered monopoles,[6] after the replacement $v_i \to v_{\rm vir}$. Hence the requirement of negligible backreaction on the magnetic field, $\tau_{\rm dis} > \tau_{\rm gen}$, yields a flux bound that is similar to the first line of (4.13), but with $v_{\rm vir}^2/2$ instead of $\gamma_i - 1$.

The derivation assumes that the monopoles pass through at least one cell before their backreaction becomes relevant, i.e. $\tau_{\rm dis} > \lambda_{\rm G}/v_{\rm vir}$. This is automatically satisfied under $\tau_{\rm dis} > \tau_{\rm gen}$ and the condition (4.7). From (4.7) it also follows that the lower mass limit (4.8) for clustered monopoles is larger than the threshold mass (4.14) where the flux bound for unclustered monopoles switches its behavior, if $v_i = v_{\rm vir}$. The flux bound also requires a monopole number large enough to satisfy (3.17), which yields a mass limit similar to (4.16).

Here we ignored the possibility of the monopoles escaping from the galaxy before dissipating the magnetic field, while in Section 4.1.1 we ignored the monopoles' backreaction on the magnetic field. By combining the discussions, however, we can say that clustered monopoles need to satisfy both the flux bound and the mass bound (4.8). Otherwise, either the galactic magnetic field is dissipated, the monopoles are ejected from the galaxy, or both.[7]

### 4.1.3 Summary of bounds from galactic magnetic fields

We have seen that the bounds on the flux of clustered and unclustered monopoles inside galaxies are collectively described by (4.13), given that the dynamo time scale, monopole mass, and magnetic field respectively satisfy (4.15), (4.16), and (4.17). For unclustered monopoles $\gamma_i$ in these expressions denotes the initial Lorentz factor with respect to the galaxy, while for clustered monopoles it is given by the virial velocity as $\gamma_i - 1 = v_{\rm vir}^2/2$. Clustered monopoles further need to satisfy the lower bound on the mass (4.8) in order to stay clustered until today.

---

[6]This is because in both (4.19) and the first expression of (4.11), monopoles gain energy as $\Delta E_N \propto N$, and the number of cells crossed per unit time by all the monopoles in the magnetic region is $\sim 4\pi^2 F R^3/\lambda_{\rm G}$.

[7]We may guess what happens by comparing the energy required to eject all monopoles from the galaxy per volume, $\rho_{\rm ej} \sim nmv_{\rm vir}^2/2$, and the magnetic energy density today, $\rho_B = B_0^2/2$. The former is larger if $mF \gtrsim B_0^2/4\pi v_{\rm vir}$. This threshold matches with the value of $mF$ where the mass lower limit (4.8) and flux upper limit (4.13) becomes equal, up to a factor of $\sim \tau_{\rm sat}/\tau_{\rm gen}$.
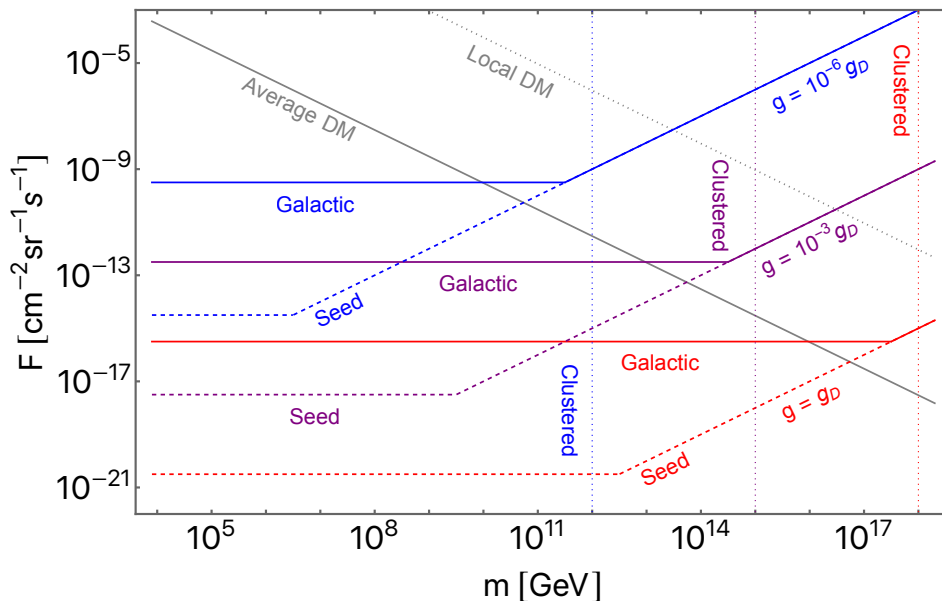
**Figure 4.1** Upper bound (4.13) on the monopole flux as a function of mass, from the survival of Galactic magnetic fields ($B = 10^{-6}$ G, solid lines) and seed fields ($B = 10^{-11}$ G, dashed). The magnetic charge is varied as $g = g_\mathrm{D}$ (red), $10^{-3}g_\mathrm{D}$ (purple), $10^{-6}g_\mathrm{D}$ (blue). The lower mass limit (4.8) for monopoles to stay clustered with the Galaxy is shown by the vertical dotted lines with different colors corresponding to different $g$. Other parameters are fixed to $\lambda_\mathrm{G} = 1$ kpc, $R = 10$ kpc, $\tau_\mathrm{gen} = 10^8$ yr, $\tau_\mathrm{sat} = 10^{10}$ yr, and $\gamma_i - 1 = 10^{-6}$. Also shown are bounds from requiring the density of monopoles not to exceed that of dark matter, for unclustered (gray solid) and clustered (gray dotted) monopoles.

The flux bound (4.13) at large $m$ increases with $m$ whereas it is independent of $B$, and vice versa at small $m$. Considering present-day magnetic fields, whose amplitude in spiral galaxies is typically of $B_0 \sim 10^{-6}$ G, one reproduces the results of [48] (see also [20, 23]). However, the bound applies throughout the history of a galaxy, and thus the bound at low masses can be improved by studying galaxies in the past when their magnetic fields were weaker. Strong bounds are obtained from the initial seed field for galactic dynamo [51],[8] although there is a huge uncertainty in the seed field ranging typically between $10^{-30}$ G $\lesssim B \lesssim 10^{-10}$ G [59, 111, 112]. We note that the seed Parker bound of the form (4.13) neglects the cosmic expansion since the initial time when the dynamo begins to operate. Hence, the bound can be modified for seed fields at high redshifts. We also note that increasing $\lambda_\mathrm{G}$ and/or $g$ improves the flux bound, as well as the lower mass limit for clustered monopoles.

In Figure 4.1 we show the flux upper bound (4.13) as a function of the monopole mass, with the magnetic charge varied as $g = g_\mathrm{D}$ (red), $10^{-3}g_\mathrm{D}$ (purple), $10^{-6}g_\mathrm{D}$ (blue). The solid lines denote bounds from the magnetic field in the present Milky Way, taken as $B = 10^{-6}$ G. The dashed lines show how the bound improves by

---

[8]The results in [48] and [51] are slightly different at the high mass end where the bound is independent of $B$; this is because the two works use different values for the other parameters such as $\lambda_\mathrm{G}$, and also different rounding methods.

considering a seed field of $B = 10^{-11}\,\text{G}$. The dotted vertical lines represent the lower mass limit (4.8) of clustered monopoles in the Milky Way. Here the other parameters are taken as $\lambda_{\text{G}} = 1\,\text{kpc}$, $R = 10\,\text{kpc}$, $\tau_{\text{gen}} = 10^8\,\text{yr}$, $\tau_{\text{sat}} = 10^{10}\,\text{yr}$, and $\gamma_i - 1 = 10^{-6}$.

In the plot we also show bounds from the requirement that the density of monopoles $\rho_{\text{M}}$ does not exceed the dark matter density $\rho_{\text{DM}}$. Using $\rho_{\text{M}} = mn$ for nonrelativistic monopoles with $n$ being the number density, the requirement translates into an upper bound on the monopole flux $F = nv_i/4\pi$ as,

$$
\begin{aligned}
F &\leq \frac{\rho_{\text{DM}} v_i}{4\pi m} \\
&\approx 3 \times 10^{-17}\,\text{cm}^{-2}\text{sec}^{-1}\text{sr}^{-1} \left(\frac{m}{10^{17}\,\text{GeV}}\right)^{-1} \left(\frac{v_i}{10^{-3}}\right) \left(\frac{\rho_{\text{DM}}}{1.3 \times 10^{-6}\,\text{GeV}\,\text{cm}^{-3}}\right).
\end{aligned}
\tag{4.20}
$$

The flux of unclustered monopoles is bound by setting the dark matter density to the average value in the universe, $\rho_{\text{DM}} \approx 1.3 \times 10^{-6}\,\text{GeV}\,\text{cm}^{-3}$ [113]; this is shown in the plot as the gray solid line. On the other hand, the abundance of clustered monopoles should be compared to the local dark matter density in galaxies; the gray dotted line shows the bound using the value in our Milky Way, $\rho_{\text{DM}} \approx 0.4\,\text{GeV}\,\text{cm}^{-3}$ [114].

One sees in the plot that for clustered monopoles, the bound from the local dark matter density (which scales as $\propto m^{-1}$) is stronger than that from the survival of galactic fields ($\propto m$) for most of the mass range where the monopoles can be clustered. This can be shown explicitly by comparing the mass $m_{\text{eq}}$ where the two upper bounds ((4.20) and the first line of (4.13)) become equal, to the lower limit on the mass $m_{\text{cl}}$ for clustered monopoles (cf. (4.8)); their ratio is

$$
\frac{m_{\text{eq}}}{m_{\text{cl}}} \sim 10 \left(\frac{B_0}{10^{-6}\,\text{G}}\right)^{-1} \left(\frac{\tau_{\text{gen}}}{10^8\,\text{yr}}\right)^{1/2} \left(\frac{\tau_{\text{sat}}}{10^{10}\,\text{yr}}\right)^{-1/2} \left(\frac{v_{\text{vir}}}{10^{-3}}\right) \left(\frac{\rho_{\text{DM}}}{0.4\,\text{GeV}\,\text{cm}^{-3}}\right)^{1/2}.
\tag{4.21}
$$

This shows that $m_{\text{eq}}$ and $m_{\text{cl}}$ are not too different in the Milky Way whose magnetic field and dark matter parameters are typically given by the reference values in the right-hand side. This means that if monopoles can cluster with our Galaxy and their density does not exceed that of dark matter, then they almost automatically satisfy the Parker bound from Galactic fields.[9] In the literature the Galactic Parker bound has often been analyzed for constraining monopoles as a dark matter candidate; however, most such studies focus on parameter regions where the monopoles actually cannot cluster with our Galaxy and hence obviously cannot serve as dark matter.

### 4.1.4 Magnetically charged extremal black holes

In this section we apply the bounds from the survival of Galactic magnetic fields to magnetically charged black holes. In particular, we focus on (nearly) extremal black holes for which Hawking radiation can be neglected. Assuming this, we do not loose generality since our primary focus is on a mass range where uncharged black holes would have already evaporated within the last Hubble time.

---

[9]It would be interesting to understand whether $m_{\text{eq}} \sim m_{\text{cl}}$ holds for generic galaxies hosting magnetic fields, by studying the relation between the dark matter density and the dynamo action.

At extremality the charge of a black hole is related to its mass through the relation:

$$m = \sqrt{2}\, g M_{\text{Pl}}. \tag{4.22}$$

Extremal magnetic black holes can be considered as monopoles with large mass and small charge-to-mass ratio. Thus, all the bounds we discussed in the previous sections can basically be applied to magnetically charged black holes. However, the direct relation between the charge $g$ and the mass $m$ of Eq. (4.22) changes the mass dependence of the bounds, as we will show in the following discussion.

The bound from galactic magnetic fields in Eq. (4.13) is rewritten for extremal magnetic black holes as:

$$
\begin{aligned}
F \lesssim \text{ max.} \Bigg\{ &10^{-27}\,\text{cm}^{-2}\text{sec}^{-1}\text{sr}^{-1} \left(\frac{m}{10^{10}\,\text{gm}}\right)^{-1} \left(\frac{\lambda_{\text{G}}}{1\,\text{kpc}}\right)^{-1} \left(\frac{\tau_{\text{gen}}}{10^{8}\,\text{yr}}\right)^{-1} \left(\frac{\gamma_i - 1}{10^{-6}}\right), \\
&10^{-30}\,\text{cm}^{-2}\text{sec}^{-1}\text{sr}^{-1} \left(\frac{m}{10^{10}\,\text{gm}}\right)^{-1} \left(\frac{B}{10^{-6}\,\text{G}}\right) \left(\frac{R}{\lambda_{\text{G}}}\right)^{1/2} \left(\frac{\tau_{\text{gen}}}{10^{8}\,\text{yr}}\right)^{-1} \Bigg\},
\end{aligned}
\tag{4.23}
$$

This bound is inversely proportional to the black hole mass. The first (second) line sets the bound when $B$ is weaker (stronger) than the threshold value:

$$\bar{B} \sim 10^{-3}\,\text{G} \left(\frac{\lambda_{\text{G}}}{1\,\text{kpc}}\right)^{-1} \left(\frac{\lambda_{\text{G}}}{R}\right)^{1/2} \left(\frac{\gamma_i - 1}{10^{-6}}\right). \tag{4.24}$$

Since galactic fields are typically weaker than this, the bound is given by the first line, which is independent of the field strength. This implies that the bound for extremal magnetic black holes does not improve by considering seed fields. We also remark that the conditions in Eqs. (4.16) and (4.17), which are necessary for the bound to apply, can be violated for massive magnetic black holes.[10]

For extremal magnetic black holes that are initially bound in a galaxy, their escape time is obtained using Eq. (4.5) as,

$$
\begin{aligned}
\tau_{\text{esc}} \sim \text{ max.} \Bigg\{ &10^{9}\,\text{yr} \left(\frac{B}{10^{-6}\,\text{G}}\right)^{-1} \left(\frac{v_{\text{vir}}}{10^{-3}}\right), \\
&10^{13}\,\text{yr} \left(\frac{B}{10^{-6}\,\text{G}}\right)^{-2} \left(\frac{\lambda_{\text{G}}}{1\,\text{kpc}}\right)^{-1} \left(\frac{v_{\text{vir}}}{10^{-3}}\right)^{3} \Bigg\}.
\end{aligned}
\tag{4.25}
$$

Note that the escape time of extremal magnetic black holes is independent of the mass, and is determined only by the galactic field properties and the virial velocity. For galaxies similar to the Milky Way, the second line sets the escape time, which depends rather sensitively on the galactic parameters.

The work [23] derived a constraint on the fraction of extremal magnetic black holes as dark matter by studying the Andromeda Galaxy, whose parameters were inferred from [115] and taken as $\lambda_{\text{G}} \sim 10\,\text{kpc}$, $\tau_{\text{gen}} \sim 10^{10}\,\text{yr}$, and $v_{\text{vir}} \sim 10^{-3}$. It was claimed that the large values of $\lambda_{\text{G}}$ and $\tau_{\text{gen}}$ improve the bound (4.23)

---

[10]If $B$ is below the threshold value (4.24), then (4.16) gives a stronger condition than (4.17).

compared to the Milky Way. However, these combined with the Andromeda's field strength $B \approx 5 \times 10^{-6}\,\mathrm{G}$ [115] yield $\tau_{\mathrm{esc}} \sim 10^{10}\,\mathrm{yr}$, which is comparable to the age of Andromeda itself. With the uncertainties in the parameters, we cannot yet give a definite answer on whether magnetic black holes can remain clustered with Andromeda until today. However, the general lesson here is that if some galaxy appears to give a significantly stronger Parker bound on extremal magnetic black holes than the Milky Way, then it is improbable that this galaxy can currently host magnetic black holes. The Parker bound from such a galaxy thus applies to unclustered black holes.

In the above discussions we have treated extremal magnetic black holes simply as very massive monopoles with charges much larger than the Dirac charge, and ignored black hole-specific features. However if accretion disks form around the black holes in galaxies, the interaction between the disks and the interstellar medium may affect the acceleration of black holes along the galactic fields. Extremal magnetic black holes can also be surrounded by an electroweak corona, where the value of the Higgs field varies [22, 23]. The presence of electroweak coronas can also change the interaction between the black holes and the interstellar medium, modifying the Parker-type bounds. We leave detailed studies of these effects for the future.

## 4.2 Modification of Parker bound from intergalactic acceleration

The Parker bound applies to both magnetic monopoles that are clustered with the Galaxy, and unclustered magnetic monopoles which only pass through the Galaxy. However, with the typical parameters of the Galactic field shown as the reference values in the above equation, Magnetic monopoles with a Dirac charge can stay clustered until today only if they are ultraheavy as $m \gtrsim 10^{18}\,\mathrm{GeV}$. As in this section we are primarily interested in intermediate to low mass monopoles which are significantly accelerated in IGMFs, in the following we focus on unclustered monopoles.

The Parker bound uses the entire Galaxy as a monopole detector, and consequently the bound depends on the monopoles' incident velocity on the Galaxy. The first line of (4.13) actually depends on $\gamma_{\mathrm{MW}}$, and in particular, the Parker bound becomes weaker for larger $\gamma_{\mathrm{MW}}$. This is because fast-moving monopoles pass through the Galaxy while being minimally deflected by the Galactic field, hence do not effectively dissipate the magnetic energy. In the literature, the incident velocity has always been assumed to be $v_{\mathrm{MW}} \sim 10^{-3}$ (i.e. $\gamma_{\mathrm{MW}} - 1 \sim 10^{-6}$), as both the Milky Way's peculiar velocity and the monopoles' gravitational infall velocity are of this order.[11] However, we have seen in the previous chapter that magnetic monopoles can be accelerated to much larger velocities in the IGMFs. In the following, we study how the presence of IGMFs affect the Parker bound.

In Figure 4.2 we plot the Parker bound in Eq. (4.13), with the monopole Lorentz factor $\gamma_{\mathrm{MW}}$ evaluated through Eq. (3.37). The monopole charge is fixed to $g = g_{\mathrm{D}}$. The gray solid line shows the bound from the survival of Galactic fields with

---

[11]The same value is used for clustered monopoles since the virial velocity of the Milky Way is also of this order.
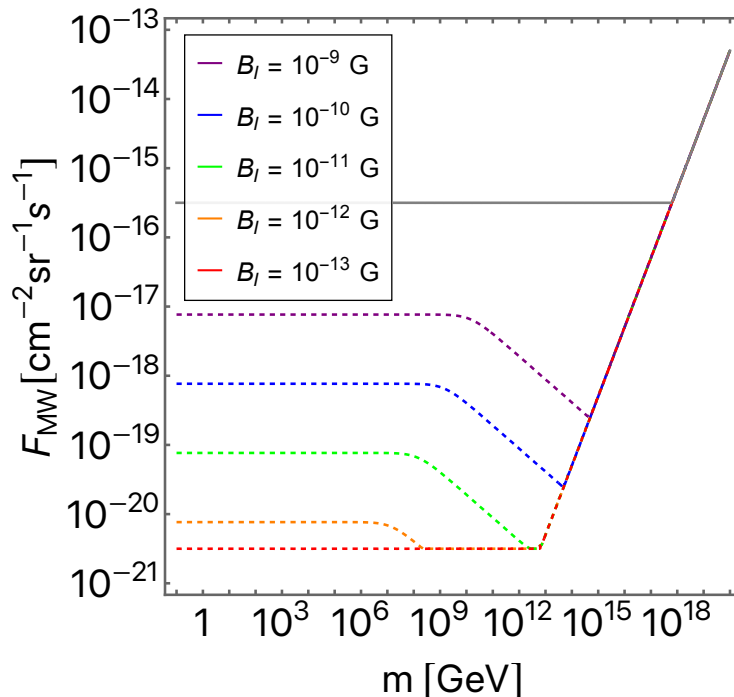
**Figure 4.2** Galactic Parker bound and seed Galactic Parker bound in the presence of IGMFs with strength $B_I \leq 10^{-9}$ G. The monopole charge is fixed to $g = g_D$. The Galactic Parker bound is not affected by the IGMFs and thus is shown by a single gray solid line. The seed Galactic Parker bound is affected, which is shown by dashed curves with different colors corresponding to different IGMF strengths. The Galactic field strength is taken as $B_G = 10^{-6}$ G, and the seed field as $B_G = 10^{-11}$ G, with the other parameters taken as $\lambda_G = 1$ kpc, $R = 10$ kpc, $\tau_{gen} = 10^8$ yr. The curves overlap in the right part of the plot.

$B_G = 10^{-6}$ G, while the dashed curves are from seed fields with an assumed strength of $B_G = 10^{-11}$ G. The other Galactic parameters are fixed to $\lambda_G = 1$ kpc, $R = 10$ kpc, $\tau_{gen} = 10^8$ yr, and $v_p = 10^{-3}$. The IGMF strength is varied between $B_I = 10^{-9}$ G and $B_I = 10^{-13}$ G. IGMFs within this range do not affect the Galactic bound, which hence is shown by a single solid line. On the other hand, the seed bound is strongly affected by the presence of IGMFs; dashed lines of different colors correspond to different IGMF strengths as shown in the plot legend. The Parker bounds for a fixed monopole velocity of $v_{MW} = 10^{-3}$, as have been assumed in the literature, are reproduced for sufficiently weak IGMFs. The Galactic and seed bounds in the weak IGMF limit are shown respectively by the gray solid and red dashed curves. All the curves join at large masses, in other words, IGMFs modify the seed bound at intermediate to low masses. We also note that with the choice of parameters, the flux bounds are independent of the IGMF correlation length, as long as it is as large as $\lambda_I \gtrsim 10^{-5}$ Mpc. This is because for values of $F_{MW}$ that saturate the bound, $v_{MW}$ is set either by $v_p$ or $v_{max}$, both of which do not depend on $\lambda_I$. This can also be seen from Figures 4.2 and 3.1 showing that the upper bounds of $F_{MW}$ are larger than the threshold value $F_{BR}$ for the backreaction to the IGMFs to become relevant.

For magnetic monopoles with large kinetic energies, the expression (4.13) for the Parker bound is set by the first line which explicitly depends on the kinetic energy. On the other hand for small kinetic energies, the bound is set by the second line which depends neither on the monopole mass nor on the velocity. The presence of IGMFs thus modify the Parker bound if the monopoles are accelerated to velocities larger than the Milky Way's peculiar velocity, and further if the monopole kinetic energy is sufficiently large such that the first line of the Parker bound applies.

For the choice of parameters in the plot, the upper bound on the flux from Galactic fields ($B_G = 10^{-6}$ G) in the weak IGMF limit is of $F_{\mathrm{MW}} \sim 10^{-16}\,\mathrm{cm}^{-2}\mathrm{sec}^{-1}\mathrm{sr}^{-1}$ or larger. The threshold kinetic energy between the two expressions for the Parker bound is $m(\gamma_{\mathrm{MW}} - 1) \sim 10^{11}$ GeV. For flux values saturating the bound, the energy that monopoles acquire from IGMFs with $B_I \leq 10^{-9}$ G is smaller than the threshold, which is why the Galactic bound is not altered by IGMFs. On the other hand, seed fields ($B_G = 10^{-11}$ G) give an upper bound in the weak IGMF limit of $F_{\mathrm{MW}} \sim 10^{-21}\,\mathrm{cm}^{-2}\mathrm{sec}^{-1}\mathrm{sr}^{-1}$ or larger, with the threshold energy between the two expressions being $m(\gamma_{\mathrm{MW}} - 1) \sim 10^{6}$ GeV. For these flux values, the energy can exceed the threshold with IGMFs of $B_I \gtrsim 10^{-12}$ G, hence the seed Parker bound is modified.

In order to understand the behavior of the modified Parker bound, note that substituting Eq. (3.37) for $\gamma_{\mathrm{MW}}$ into the first line of Eq. (4.13) yields an upper limit which itself depends on the monopole flux. In particular when $v_{\mathrm{MW}} = v_{\mathrm{max}}$ (i.e. $v_{\mathrm{p}} < v_{\mathrm{max}} < v_0$), one sees from Eq. (3.34) that $(\gamma v)_{\mathrm{MW}} \propto 1/(m F_{\mathrm{MW}})$. For sufficiently small masses such that $v_{\mathrm{MW}}$ is relativistic, the kinetic energy scales as $m\gamma_{\mathrm{MW}} \propto 1/F_{\mathrm{MW}}$. Thus the first line of Eq. (4.13) yields an inequality of the form $F_{\mathrm{MW}} < \kappa/F_{\mathrm{MW}}$ where $\kappa$ is a factor that is independent of the monopole mass and abundance. Solving this gives a flux bound $F_{\mathrm{MW}} < \kappa^{1/2}$, which is independent of the monopole mass, as shown in the plot for the modified seed Parker bound at small masses. On the other hand for larger masses with nonrelativistic $v_{\mathrm{MW}}$, the kinetic energy scales as $m v_{\mathrm{MW}}^2/2 \propto 1/m F_{\mathrm{MW}}^2$, and hence the first line of Eq. (4.13) takes a form $F_{\mathrm{MW}} < \kappa/m F_{\mathrm{MW}}^2$. This gives a bound $F_{\mathrm{MW}} < (\kappa/m)^{1/3}$, which is stronger for larger masses, as is seen for the middle parts of the modified seed bounds in the plot.

Before ending this section, we should remark that if a sufficiently strong IGMF existed at the time of Galaxy formation, this could have grown during a protogalactic collapse into the currently observed Galactic field. In this scenario, the necessity for a seed Galactic field and the dynamo amplification is obviated, and hence the Parker bounds are modified; in particular, the seed Parker bound is nullified. Our findings indicate that even if a seed field coexisted with a strong IGMF and hence the seed Parker bound holds, it would be significantly relaxed due to the acceleration effect.

# Chapter 5

# Modification of bounds from terrestrial experiments

Experimental bounds on the monopole flux are usually given in terms of the monopole velocity at the detector. In this chapter, we describe how to use the results for the acceleration of cosmic magnetic monopoles obtained in Chapter 3 to recast such bounds in terms of the monopole mass. The mechanism of monopole acceleration discussed in Chapter 3 provides the monopole velocity on the surface of the Earth. Therefore, the main goal of this chapter is to determine the relationship between the speed at the Earth surface and at the detector for each experiment. The result of the revisitation are reported in Fig. 5.3.

Hereafter, in this chapter we assume that monopoles do not cluster with the Milky Way. For the assumed typical parameters of the GMFs, monopoles with a Dirac charge can stay clustered with the Milky Way until today only if they have a mass $m \gtrsim 10^{18}$ GeV [2, 48]. As we are primarily interested on monopoles that are accelerated to relativistic velocities, the results of this chapter are unchanged by such an assumption.

When magnetic monopoles cross a medium, the varying magnetic field induces a strong electric field. As we discussed in Section 2.2, this opens the way to a classical interpretation of the interactions where the monopoles are treated as electrically charged particles with an equivalent speed-dependent electric charge of $g\beta$. The search for magnetic monopoles is naturally based on their speed at the detector. For $\beta \gtrsim 10^{-3}$ the energy loss is mostly through elastic collisions. For non-relativistic monopoles with $10^{-3} \lesssim \beta \lesssim 10^{-2}$, the medium is seen as a free degenerate gas of electrons [119], and the energy loss comes from the interaction with energy level crossings. Relativistic monopoles with $\beta \geq 0.1$ ionize and excite atoms. The ionization yield of a relativistic unit charge monopole is $\sim 4700$ times that of a minimum ionizing particle [120]. Ultra-relativistic monopoles, with $\gamma > 10^4$, lose energy mostly by pair production and photo-nuclear radiative processes, while bremsstrahlung is suppressed because of the large monopole mass. As we already mentioned, GUT monopoles can also catalyze nucleon decays [39]. However, this is not true for all the possible models of magnetic monopoles and therefore we do not consider this effect in our analysis.

If the medium is transparent, such as the Earth atmosphere or water or ice, also
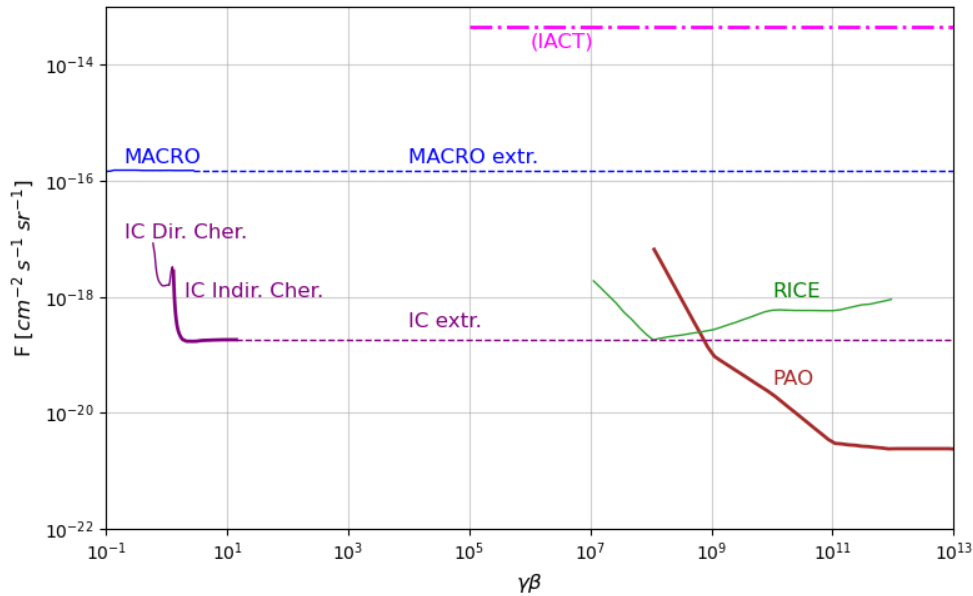
**Figure 5.1** Some of the most constraining upper limits on monopole flux (90% CL) expressed in term of monopole speed at the detector. We show limits from the IceCube [32] and RICE [116] neutrino experiments in the South pole, the MACRO detector at LNGS (now dismissed) [30], by the Pierre Auger Observatory for cosmic rays in Argentina [117] and by a preliminary study [118] for the High Energy Stereoscopic System (H.E.S.S.), an imaging atmospheric Cherenkov telescope (IACT) for high energy gamma-ray astronomy in Namibia. Conservative extrapolations of some limits are also reported.

Cherenkov radiation can be generated either directly from the magnetic monopoles or from secondary ionized electrons. The threshold for Cherenkov emission is $\beta > 1/n$, where $n$ is the refraction index of the medium. As modeled in [36, 121], the Cherenkov photon yield of a monopole would be $(g_D\, n/e)^2 \simeq 4700$ times more than that of a muon with the same speed. The condition for Cherenkov radiation emission by magnetic monopoles is $\gamma\beta \gtrsim 1.17$ ($\beta \gtrsim 0.76$) in ice or water (index of refraction $n = 1.33$) and $\gamma\beta \gtrsim 70$ in the atmosphere at the ground level (index of refraction $n \sim 1 + 10^{-4}$). Similarly, ultra-relativistic monopoles emit fluorescence light. The emission occurs radially from the monopole direction and can be sampled with large field of view optical detectors at ground or from space.

The experimental search for magnetic monopoles began soon after the original Dirac proposal [5]. A complete recent compilation of all experimental constraints can be found in [122, 123]. In the following, we limit ourselves to some of the most constraining limits produced so far. In Fig. 5.1, we report some of the most relevant experimental limits expressed in term of monopole speed. They encompass results from the IceCube and the Radio Ice Cherenkov Experiment (RICE) neutrino experiment in the South Pole [32, 116], the MACRO detector at the Italian National Laboratories of Gran Sasso (now dismissed) [30], the Pierre Auger Observatory (Auger) for cosmic rays in Argentina and a preliminary study [118] of the High Energy Stereoscopic System (H.E.S.S.), an imaging atmospheric Cherenkov telescope (IACT) for high energy gamma-ray astronomy in Namibia. Some of the published

limits were extrapolated with the conservative assumptions generally considered in the literature. We now describe separately the details of each experiment relevant for our discussion.

## 5.1 IceCube

Located at the South Pole in Antarctica, the IceCube detector is an array of 5160 photomultiplier tube-based optical modules arranged in 86 vertical strings deployed into the ice between 1500 m and 2500 m below the surface, with a total volume of 1 km$^3$. Its main scope is the detection of astrophysical and cosmological neutrinos in the ultra-high energy (PeV–UeV) range through the collection of Cherenkov light in the clean Antarctic ice, emitted after the decay into leptons. Magnetic monopoles would be directly detectable by the luminescence and Cherenkov light generated at their passage in ice. As mentioned above, the monopole signature would appear as a similar signal but extremely brighter and straighter than neutrino-induced events. As mentioned, considering the refraction index of ice $n = 1.33$, the threshold for direct Cherenkov emission is $\beta \gtrsim 0.76$ (horizontal black dotted line with IceCube label in Fig. 3.5). Cherenkov light from secondary electrons produced by ionization can instead occur if $\beta \gtrsim 0.51$. Therefore, taking into account also secondary Cherenkov emission, it is possible to slightly extend the bound to smaller monopole speeds.

IceCube reported limits on monopole flux over several years [31, 32, 33, 34]. The 2012 work [32] reports the first IceCube limits on mildly relativistic monopoles in the range $0.51 \leq \beta \leq 0.85$ using the first year of IceCube data. The monopole detection technique of IceCube is described at length in that seminal work and in [124]. The latest limits (2022) on relativistic monopoles are reported in [31] between $0.51 \leq \beta \leq 0.995$ using 8 years of data, updating previous limits [32, 33]. We show in Fig. 5.1 the limits reported in [31] with a thin purple curve for $0.51 \lesssim \beta \lesssim 0.76$ (Cherenkov light from secondary electrons) and a thick purple curve for $0.76 \lesssim \beta \lesssim 0.995$ (direct Cherenkov light). IceCube mentions that those limits can be conservatively extrapolated above $\beta > 0.995$ under the assumption that no significant further energy loss occurs above this value. Following this hypothesis, in Fig. 5.1 we show in a dashed purple line the conservative extrapolation of the IceCube limits to a higher monopole speed.

IceCube is sensitive to monopoles coming from all directions, but only those coming from below the detector can be easily discriminated from the ample background of atmospheric neutrinos. For monopoles crossing the Earth, the monopole energy loss, as discussed in [125], happens through collisional loss for $\gamma \lesssim 10^4$, while through pair production and photo-nuclear losses for larger Lorentz factors. Considering the density of Earth, monopoles lose a maximum energy of $10^{11}$ GeV by crossing the full length [125], while a smaller energy loss is expected from slanted directions. In order to be detected, the monopoles shall remain relativistic at the detector. Thus, the acceptance of the detector depends on whether the kinetic energy of the monopoles at the Earth surface is bigger than the energy loss in the Earth for a given direction of the monopoles at the detector. Therefore, a full computation of the detector acceptance depends on both the monopole mass and its incoming direction, once assumed a mechanism for the monopole acceleration.

Ref. [31] collects all previous results from IceCube and provides the strongest limits over all the sensitivity range. However, the limits are shown only in terms of the velocity of the monopoles at the detector. Thus, there is no updated computation of the acceptance of the detector in terms of the kinetic energy of the incoming monopoles in function of the distance traveled inside the Earth, as done only earlier in [34, 124]. We then now proceed with an estimate of the effects of the IceCube acceptance for the latest results, assuming the models described in [34, 124]. In particular, we use Tab. F2 of [124] where the acceptance was explicitly calculated. The table shows for a given monopole mass and kinetic energy at the Earth surface the fraction of solid angle under which IceCube can see the monopoles, and consequently the correspondent acceptance.

Fig. 5.2 displays the method used for our re-computation and the impact on the results shown in [31]. In the left plot, we synthesize the results in Tab. F2 of [124] for the monopole acceptance. The region above the solid line represents the combination of monopole mass-kinetic energy at the Earth surface in which monopoles remain relativistic from any direction with respect to the detector ($4\pi$ sr acceptance). On the other hand, monopole mass-kinetic energy combinations below the solid line show a detection efficiency $\epsilon < 1$. This means that the limits in this mass-energy range are weakened by a factor $\epsilon$. In these cases, monopoles that cannot reach the detector are those that cross the largest amount of Earth. Those monopoles are also the easiest to be discriminated from the background. Therefore, the $\epsilon$ factor is not only taking into account the reduced solid angle but also the reduced discriminating power of IC. monopole mass-kinetic energy combinations along the dashed line can be accepted only with an acceptance of $3\pi$ sr; using the results in Tab. F2 of [124], this translates into an efficiency $\epsilon(3\pi) = 0.6$. Similarly, monopole mass-kinetic energy combinations along the dot-dashed line can be accepted only with an acceptance of $2\pi$ sr. This translates into an efficiency $\epsilon(2\pi) = 0.09$. In the shadowed area below the diagonal line, which corresponds to $\beta = 0.76$, monopoles do not reach the detector above the minimum speed to generate Cherenkov light, and thus they cannot be detected. Curves of constant acceptance show two different behaviours, depending on the dominant mechanism of energy loss of the monopoles. When the curves are in the area of the plot where the mass-kinetic energy combinations correspond to values of $\gamma \lesssim 10^4$, monopoles lose energy through collisional loss and the curves show only a mild dependence on the monopole mass. On the other hand, in the region where the mass-kinetic energy combinations correspond to $\gamma \gtrsim 10^4$, the monopoles lose energy more efficiently through pair production and photo-nuclear losses and the mass dependence of the curves is significantly more pronounced.

The flux constraints by IceCube are of the order of $10^{-18}$ cm$^{-2}$m$^{-1}$, and therefore the speed-mass relation corresponds to the solid red line of Fig. 3.5, where the monopole velocity is set by acceleration in GMFs. From the intersection between the solid red line and the dotted black IceCube Cherenkov threshold line of Fig. 3.5, we read from the plots that IceCube is sensitive to magnetic monopoles with masses smaller than $\sim 10^{11}$ GeV. Additionally, IceCube cannot constrain monopoles lighter than $10^4$ GeV [32] because they would be absorbed in the Earth before reaching the detector from any direction. From the discussion in the previous section, we know that the reference kinetic energy gained through monopole acceleration in the GMFs is of the order $10^{11}$ GeV. In the left plot of Fig. 5.2, we show with a red dashed

horizontal line such a reference value for the kinetic energy. The range of monopole mass covered by the red line is the range of mass for which IceCube is capable of detecting magnetic monopoles, that hence is for $m \in [10^4, 10^{11}]$ GeV.

Using Tab. F2 of [124], we found that for a kinetic energy of $10^{11}$ GeV the constraints for monopoles with $0.51 \lesssim \beta \lesssim 0.76$ (thin solid purple line in Fig. 5.1) correspond to monopole masses for which IceCube does not have acceptance for the monopoles. Therefore, those limits are not valid in our framework, and are not reported further. On the other hand, in the region with $\beta \gtrsim 0.76$ (thick solid purple line in Fig. 5.1) we retrieve the mass range between $10^4$ GeV and $10^{11}$ GeV for which IceCube has acceptance for the monopoles, as we get from Fig. 5.2a. However, we cannot directly convert these limits without considering the differential kinetic energy loss due to the different monopole path in the Earth. We therefore take the acceptance values tabulated in Tab. F2 of [124] every 0.5 dex in log-scale and recast IceCube limits. This method is described by IceCube for the generation of Fig. 11 of [32].

The right plot of Fig. 5.2 shows the effect of the recomputation (purple dashed line with markers in steps of 0.5 of the logarithm of the monopole mass, as extracted from Tab. F2 of [124]) of the original limits (solid violet line) considering the efficiencies described above, and for a kinetic energy of $10^{11}$ GeV (red horizontal line in the left plot). One can see that for monopole masses $10^8 - 10^{10}$ GeV the limits are only slightly affected by the recomputation. For lower masses, down to $10^4$ GeV, up to an order of magnitude sensitivity is lost due to the reduced efficiency of the detector. Above $10^{10}$ GeV a similar effect is seen. As already mentioned, IceCube cannot constrain monopoles lighter than $10^4$ GeV. Therefore, also the 'extrapolated' IceCube limits are not considered further in Fig. 5.2b.

## 5.2 Pierre Auger Observatory

Ultra-relativistic magnetic monopoles deposit a large amount of energy when they cross the Earth atmosphere. For $\gamma < 10^4$, the dominant contribution is through elastic collisions, which deposit around 10 GeV/(g/cm$^2$). The Bremmstrahlung is suppressed due to the large monopole mass. For $\gamma > 10^4$, the energy deposit occurs through photonuclear effects and pair productions, increasing the cross section with $\gamma$. At $\gamma = 10^{11}$ the energy loss is 700 PeV/(g/cm$^2$). This results in the generation of secondary electromagnetic showers initiated by ionized ultra-relativistic electrons along the full path of the monopoles in the atmosphere. This is substantially different from the showers initiated by ultra-high energy ($>$ PeV) cosmic rays, which die off after some interaction lengths. A magnetic monopole would therefore be equivalent to a highly energetic long-lived charged particle, observable in the atmosphere through extended atmospheric particle showers as well as fluorescence light. Instruments searching for these signals consist of extensive arrays of particle detectors spread across several hundred square kilometers, provided with fluorescence detectors with a large field-of-view. Examples of such instruments are the Pierre Auger Observatory (hereafter simply called "Auger") in Argentina and the Telescope Array in the U.S.A. Telescope Array has never provided a dedicated analysis for magnetic monopoles, and therefore in the following we focus only on the Auger experiment.

**(a)**                                                                  **(b)**
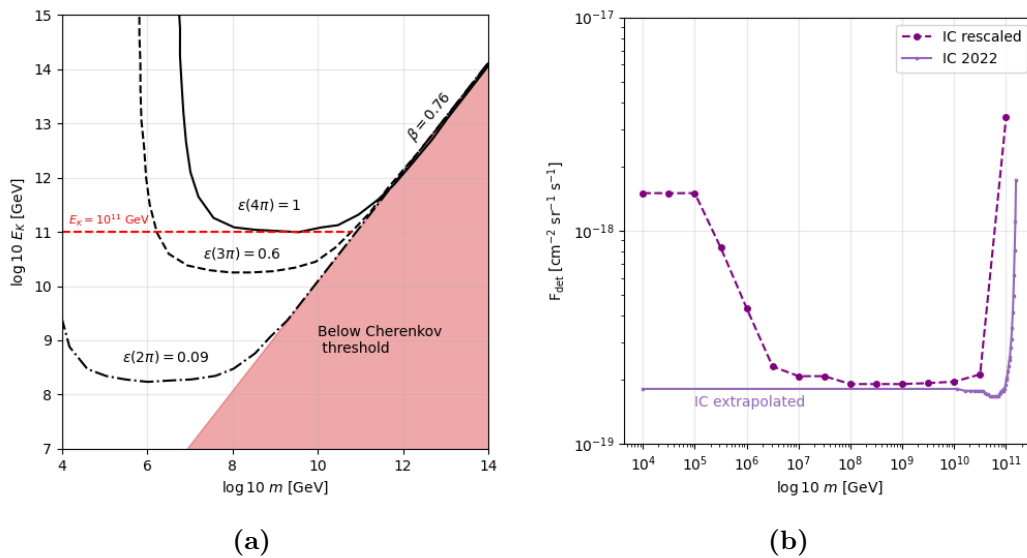
**Figure 5.2**    Left: Conversion factors between implicit limits obtained with IceCube [31] and mass-energy dependent limits obtained with full computation of the IceCube acceptance as described in [32, 124]. The red dashed line shows the monopole mass range accessible to IceCube for kinetic energy at the Earth of $10^{11}$ G. Right: Comparison between IceCube data in [31] (violet solid curve) and the bound after the use of the conversion factors (purple dashed curve).

Auger is the largest ultra-high-energy cosmic-ray detector currently in operation. It is located in Argentina and covers an area of $3,000$ km$^2$. It is provided with a surface-detector array that directly samples the charged particles of atmospheric showers, and 24 fluorescence detectors, each of them with a field-of-view of $30 \times 30$ deg$^2$. The surface detector array is made of large-area water tanks equipped with photomultipliers, while the fluorescence detectors search for the UV fluorescence light emitted by nitrogen molecules excited by CRs or magnetic monopoles along their trajectory in the atmosphere.

The latest search for magnetic monopoles in Auger is reported in [117]. For this search, Auger requires the operation of both the fluorescence and the surface detectors. This allows for a sensitivity to monopole velocities in the range $\gamma > 10^8$ (horizontal black dotted line labeled "Auger" in Fig. 3.5). This threshold derives from the fact that for $\gamma < 10^8$ a monopole would produce too little fluorescence or Cherenkov light to trigger the detectors. Although an energy of $10^{16}$ GeV is assumed in [117] for the Monte Carlo simulations of the monopole energy loss in the Earth atmosphere, the energy loss in the ultra-relativistic regime does not depend on the monopole energy, but only on the relativistic factor $\gamma$. Therefore, we can assume the results to be valid for generic monopole energy. The current Auger limits (solid brown curve in Fig. 5.1) constrain monopole fluxes in the interval $10^{-21} - 10^{-17}$ cm$^{-2}$sr$^{-1}$s$^{-1}$.

In Figure 3.5 we show that monopoles with masses $m \lesssim 10^4$ GeV are accelerated by the GMFs to $\gamma \gtrsim 10^8$. Therefore, monopoles with $m \lesssim 10^4$ GeV fall within the sensitivity range of Auger. Depending on the monopole flux and the characteristics of

the IGMFs, if the contribution of the IGMFs to the acceleration is large enough, even monopoles with mass as large as $10^6$ GeV (see Fig. 3.5d with $F \lesssim 10^{-22}$ cm$^{-2}$sr$^{-1}$s$^{-1}$) can be accelerated to $\gamma \gtrsim 10^8$ and might be energetic enough to be detected by Auger.

Considering the mechanism of acceleration described in Chapter 3, we express the speed dependence of the Auger bounds in terms of the monopole mass. Unlike IceCube, the Auger analysis considers only trajectories that come from within a $60°$ cone around the zenith. Therefore, the analysis does not consider magnetic monopoles that cross the Earth. Hence, no effects from energy loss must be taken into account and there is no need for additional considerations on the detector acceptance. We show the results of our analysis in Fig. 5.3. The solid brown line of Fig. 5.3 corresponds to the Auger results recomputed in function of the monopole mass, assuming contributions to the monopole velocity from GMFs only. For the range of monopole flux constrained by Auger, this assumption describes almost all IGMF scenarios within the experimental constraints. The only case where the IGMF contribution is non-negligible is for the extreme scenario of IGMFs with amplitude $B_I = 10^{-9}$ G and coherence length $\lambda_I \gtrsim 1/H_0$. This case corresponds to the largest possible contribution to the monopole velocity of IGMFs, which is the dominant one for monopole fluxes $F \lesssim 10^{-20}$ cm$^{-2}$sr$^{-1}$s$^{-1}$ (see Figure 3.5d). As a consequence of this additional contribution to the monopole velocity, the Auger velocity-dependent limit translates in even more constraining bounds on the monopole flux for a given monopole mass. These results are reported in Figure 5.3 as a dotted brown line. As one can see from the figure, at the current flux sensibility, even in such an extreme case Auger constraints only monopoles with mass $m \lesssim 10^4$ GeV. This is because the Auger limit is less constraining for values of $\gamma$ close to the lower threshold of $\gamma = 10^8$, and therefore the experiment is still not sensible to fluxes for which the IGMF contribution is dominant when approaching the end of the sensibility range. Higher masses will be constrained only when Auger enhances its sensitivity to the monopole flux, achieving $F \lesssim 10^{-20}$ cm$^{-2}$sr$^{-1}$s$^{-1}$ even for $\gamma \sim 10^8$.

## 5.3 Imaging Atmospheric Cherenkov Telescopes

Imaging Atmospheric Cherenkov Telescopes (IACTs) are large parabolas built to detect Cherenkov light induced by primary gamma ray and cosmic rays in the Earth atmosphere. They are sensitive to the Cherenkov light emitted by the passage of a magnetic monopole in the atmosphere, while they are not sensitive to the signals of secondary charged particles. The number of Cherenkov photons by monopoles in the atmosphere was computed by [126] to be 4700 times that of a unit-charge particle.

The search for monopole Cherenkov emission in the atmosphere was investigated in [127] by the H.E.S.S. experiment and presented in [118] for a total lifetime of about 5 years of data. Although at ground the refraction index is $n \sim 1 + 10^{-4}$, and therefore the Cherenkov threshold translates into $\gamma\beta > 70$ (horizontal black dotted line with "IACTs" label in Fig. 3.5), at a height of 30 km, where $n \sim 1 + 10^{-6}$, the threshold translates into $\gamma\beta > 700$ because of the smaller density of the atmosphere. Therefore, faster monopoles emit Cherenkov light starting at higher altitudes than slower monopoles and the Cherenkov emission angle $\cos\theta = 1/(n\beta)$ increases with

the depth reaching a semi-aperture of 1.2° at ground. The increasing Cherenkov angle has a peculiar effect on the image recorded by the IACT. For fast monopoles impinging close to the telescopes, a double image would be observed: a first one by Cherenkov photons emitted at small angles in the high atmosphere, followed by a second one from Cherenkov photons emitted much closer to the ground. At intermediate depths the Cherenkov light would be focused outside the telescope camera. In case of monopoles impinging far from the telescopes, only the Cherenkov light emitted at intermediate altitude would be observed, providing a single image. In the first case, the monopoles would be hardly mistaken with a primary gamma ray because of the peculiarity of the image, constituted by a bright compact first spot and a bright secondary extended image (ellipse like or ring-like). The second case is not investigated by [118] but we expect that the image would also be hardly mistaken with primary gamma rays due to the much larger Cherenkov photon yield of magnetic monopoles.

The main limitation of IACTs is connected to their small field of view of a few squared degrees, which strongly reduces the acceptance with respect, for instance, to Auger. The H.E.S.S. collaboration in [118] reports limits of of $4.5 \times 10^{-14}$ cm$^{-2}$s$^{-1}$sr$^{-1}$, as shown in Fig. 5.1 (dotdashed magenta line). A future generation of IACTs is under development for the Cherenkov Telescope Array Observatory (CTAO). While H.E.S.S. has only 5 telescopes (among which, only 4 have been considered in [118]), CTAO will be comprised of two arrays of telescopes (one in the North and one in the Southern hemisphere), endowed with 13 and 70 telescopes respectively. This would grant a larger energy range, better sensitivity and energy resolution, but also, because of instrument improvements, a larger field of view. In fact, CTAO will be assembled with telescopes of different sizes. Among them, the Small Size Telescopes (SSTs) while having a primary mirror size of 6 m, thanks to a Schwarzchild-Couder optics, will allow for a field of view of 10 degrees.

In Fig. 5.3 we show a forecast for monopole searches with CTAO (dotdashed magenta line), obtained by upscaling the H.E.S.S. results of [118] considering the following factors: a) H.E.S.S. has a field of view of 6° (at least this was assumed in [127]), while CTAO will host SSTs of 10°, thus entailing a factor 3 larger field of view; b) CTAO will display a factor of $10 - 100$ larger effective area than H.E.S.S. [128]; c) CTAO is planned to observe for 30 years, a time of exposure 6 times longer than H.E.S.S. in [127]. Hence, globally we may expect a factor $3 \times 10 \times 6 \sim 200$ of improvement. We have therefore estimated a sensitivity of CTAO at about $2 \times 10^{-16}$ cm$^{-2}$s$^{-1}$sr$^{-1}$, as shown in Fig. 5.3. Furthermore, [127] applies a speed threshold at $\gamma > 10^5$ to not account for the effects of the Earth magnetic field. We believe that by modeling this further effect, the speed threshold can be reduced to that required to generate Cherenkov photons close to the ground, that is $\gamma \gtrsim 100$.

Assuming the model of monopole acceleration described in Chapter 3 and considering the results shown in Figure 3.5a, for values of the monopole flux within the sensibility of CTAO, the main contribution to the monopole velocity comes from the acceleration in GMFs. Thus, using Eq. (3.18) to compute the the kinetic energy of the monopoles accelerated in GMFs, we can interpret the speed threshold of $\gamma \gtrsim 100$ as an upper limit on the monopole mass,

$$m \lesssim E_{\text{k,G}} \times (100 - 1)^{-1} \sim 10^9 \text{ GeV}, \tag{5.1}$$

which means that monopoles lighter than $m = 10^9$ GeV are accelerated to relativistic velocities above the speed threshold of CTAO. This value of the monopole mass corresponds to the endpoint of the magenta dotdashed line in Fig. 5.3.

Despite being generically less sensitive than Auger or IceCube, CTAO will allow independent measurement for magnetic monopole, bridging Auger and IceCube results.

## 5.4   MACRO

The Monopole, Astrophysics and Cosmic Ray Observatory (MACRO) was a dedicated instrument to search for magnetic monopoles [30]. It was operated at Gran Sasso INFN National Laboratories (LNGS), at water equivalent depth of 3,800 m, for a decade, until 2000. MACRO was composed of three sub-detectors operated in combination: scintillation counters that measured the particle position, energy deposition and time of flight of monopoles; limited streamer tubes that exploited the Penning effect and measured the monopole energy release in excited gas molecules; and nuclear track detectors that measured etchable tracks in stacks of layers of dense materials. Each sub-detector was sensitive to different monopole speeds with an overall sensitivity between $4 \times 10^{-5} \leq \beta < 1$ [30]. The latest global limits based on 4.2 to 9.5 years of data were reported in Fig. 9 of [129] in the range $4 \times 10^{-5} \leq \beta \leq 0.99$. The analysis in [129] shows an upper bound on the monopole flux moving at $\beta > 10^{-4}$ at an average of $1.4 \times 10^{-16}$ cm$^{-2}$s$^{-1}$sr$^{-1}$ for masses $\gtrsim 10^{16}$ GeV. We show this result in Figure 5.1 with a solid blue line. MACRO analysis did not consider monopole with velocities $\beta > 0.99$ because for higher velocities monopole could induce showers in the detector, reducing the efficiency of the analysis. However, in the literature this limit is usually improperly extrapolated to arbitrarily fast monopoles (blue dashed line in Figure 5.1).

As in the case of IceCube, the acceptance of the MACRO detectors depends on the direction of the magnetic monopoles, which cross different portions of the Earth before reaching the detector, losing different amount of energy. MACRO analysis distinguishes between monopoles that have enough kinetic energy to reach the detector both from below and above or only from above, for which the limit is twice less constraining. This translates into a monopole mass dependence of the acceptance. As an example, for a velocity $\beta > 0.1$, monopoles with mass in the interval $10^{10} - 10^{16}$ GeV reach the detector both from below and above and the flux limit is at $1.4 \times 10^{-16}$ cm$^{-2}$s$^{-1}$sr$^{-1}$, while for masses between $10^6 - 10^{10}$ GeV monopoles reach the detector only from above and the limit is at $2.8 \times 10^{-16}$ cm$^{-2}$s$^{-1}$sr$^{-1}$ (see Tab. 2 of [129]). For $\beta > 0.1$, monopoles with masses $< 10^6$ GeV do not reach the detector even from above and therefore are not constrained by MACRO. This result is explained by the fact that monopoles with lower mass require higher velocities to cross the Earth and reach the detector: if the monopoles can reach the detector only from above, the expected monopole flux is half the total and the bound is weakened. The complete analysis of the energy-mass dependence of the MACRO acceptance is reported in [39] and [130], and we refer to those works in this paper. Once the kinetic energy of the monopoles is enough to reach the detector and the monopole velocity is $\beta < 0.99$, the bound is independent of the monopole speed.

As we show in Figure 3.5, for the monopole flux constrained by MACRO (which is, never below $10^{-16}$ cm$^{-2}$s$^{-1}$sr$^{-1}$), monopole acceleration is dominated by the Galactic contribution. Therefore, we use Eq. (3.18) to estimate the kinetic energy of monopoles on the Earth's surface. In Fig. 6.18 of [130] the values of the monopole mass for which the MACRO acceptance is only from above the experiment or also from below are shown in function of the monopole velocity at the Earth's surface. Referring to those results, we can then compute whether monopoles have enough kinetic energy to reach the detector from below, or only from above, as a function of the monopole mass. We find that the kinetic energy in Eq. (3.18) is in the range for which the monopoles can reach the detector only from above the experiment. Therefore, we reproduce with a blue solid line in Fig. 5.3 the limit as $F \lesssim 2.8 \times 10^{-16}$ cm$^{-2}$s$^{-1}$sr$^{-1}$.

As already mentioned, MACRO cannot constrain magnetic monopoles with velocity $\beta > 0.99$. Considering the kinetic energy of the monopoles accelerated in GMFs in Eq. (3.18), we can interpret such an upper limit on the velocity as a lower limit on the monopole mass, below which the MACRO limits are not applicable. We find that such a limit is

$$m > E_{\text{k,G}} \times \left( \left( 1 - 0.99^2 \right)^{-1/2} - 1 \right)^{-1} \sim 10^{10} \text{ GeV}. \tag{5.2}$$

This value of the monopole mass corresponds to the endpoint of the blue solid line in Fig. 5.3.

## 5.5 MoEDAL

The Monopole and Exotics Detector at the LHC (MoEDAL) [41] is the first LHC experiment dedicated to the search for new physics through the detection of highly ionizing particles, and in particular magnetic monopoles and dyons. The experiment is also the only sensitive to high monopole magnetic charges and performed the first dedicated collider search for dyons. It is a largely passive detector, which provides a permanent physical register of the monopole passage through microscopic damages along the trajectory in the nuclear track detector. MoEDAL is also provided with monopole trappers, which capture particles with magnetic charge. The aluminum absorbers are therefore analyzed in the superconducting quantum interference device magnetometer, searching for differences in the persistent current through the superconducting loop [131]. A significant difference between the current before and after several transits of the same sample would be interpreted as a clear signal of a trapped magnetic monopole in the aluminum volume.

Heavy-ion collisions at the LHC produce the strongest known magnetic fields in the universe. These fields are about four orders of magnitude stronger than the magnetic fields on the surfaces of magnetars [132], which are the strongest known astrophysical magnetic fields. Such strong magnetic fields allow MoEDAL to search for pairs of monopoles produced by the magnetic dual of the Schwinger effect [12, 13, 14]. As we mentioned, the Schwinger pair production rate is calculated through semi-classical techniques, which overcomes the non-perturbativity of the monopole–photon coupling. This is not the case for the analysis of monopole production in proton-proton collision [90, 91, 92].
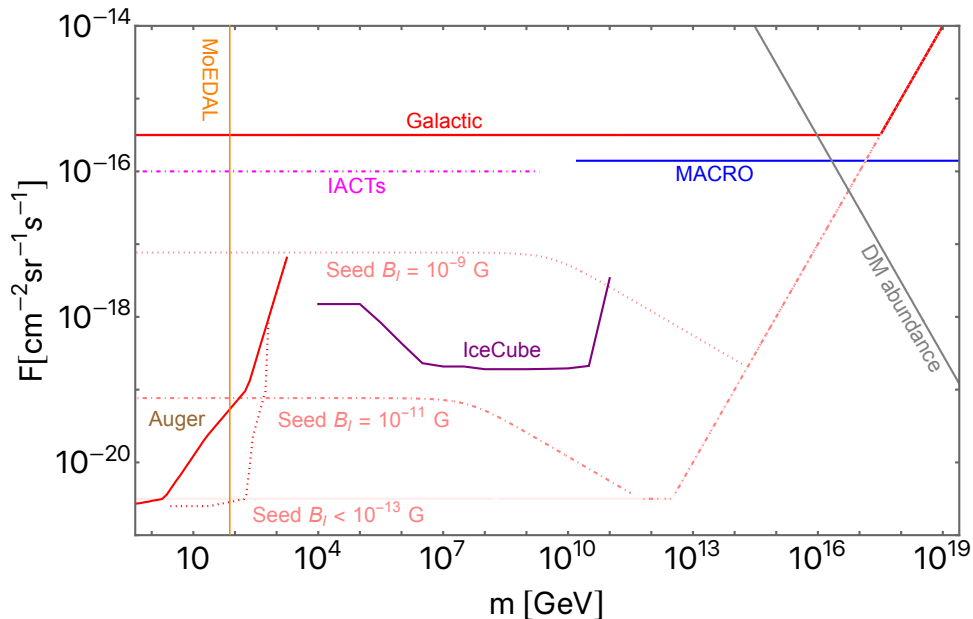
**Figure 5.3** Bounds on the monopole flux. Gray: cosmological bound from comparison with the average dark matter density in the universe, red: Galactic Parker bound, pink: seed Galactic Parker bound (light: $B_I < 10^{-13}$ G, dotdashed: $B_I = 10^{-11}$ G, dotted: $B_I = 10^{-9}$ G), blue: limits from the MACRO experiment, purple: limits from the IC experiment, brown: limits from the Auger collaboration (solid: Galactic acceleration only, dotted: intergalactic acceleration with $B_I = 10^{-9}$ G and $\lambda_I \gtrsim 1/H_0$), orange: lower limits on the monopole mass from Schwinger production given by the MoEDAL experiment [42], dotdashed magenta: expected sensibility for CTAO (next generation of IACTs detectors).

The analysis is based on the monopole trappers exposure to heavy-ion LHC collisions and yields the first theoretically robust lower mass limit on monopoles up to $n = 3$ Dirac charges. The results are compatible with the absence of monopoles, and therefore singly charged monopoles with mass smaller or equal to 75 GeV have been excluded [42]. The experiment is based on the detection of magnetic monopoles produced within the detector and therefore is independent of the cosmic mechanisms of monopole acceleration.

In Fig. 5.3 we report the lower limit on the monopole mass for the results obtained by MoEDAL [42] from the study of monopole pair production from the Schwinger effect in strong magnetic fields [12, 13]. The limit is independent of the monopole flux.

## 5.6 Discussion of the results

In this section, we discuss the results shown in Figure 5.3, which represents the main result of this chapter. We now address in detail the large amount of information contained in the figure.

For the first time, the accounting of the cosmic monopole acceleration is con-

sidered, and we show how the experimental limits are differently sensitive to that: the most constraining limits come from different experiments in different ranges according to the actual scenario. This should drive experiments to include the modeling of the monopole acceleration in their limits, as we discuss in detail below. Here we report the results for the specific model of monopole acceleration described in Chapter 3.

In Figure 5.3 we show also the indirect bounds on the monopole flux in Eq. (4.13) (Galactic and seed Galactic Parker bounds, with $\lambda_\mathrm{G} = 1\,\mathrm{kpc}$, $R = 10\,\mathrm{kpc}$, $\tau_\mathrm{gen} = 10^8\,\mathrm{yr}$ and for the Galactic field strength $B_\mathrm{G} = 10^{-6}\,\mathrm{G}$, and the seed field $B_\mathrm{G} = 10^{-11}\,\mathrm{G}$) and in Eq. (4.20) (cosmological abundance bound, with $\rho_\mathrm{DM} \approx 1.3 \times 10^{-6}\,\mathrm{GeV\,cm^{-3}}$ and $v_i = 10^{-3}$). The Galactic Parker bound (solid red curve) appears to be the weakest of all bounds, but it remains a very important limit as long as the Galactic magnetic field history is known with improved accuracy. In fact, the seed Galactic Parker bound (pink curves) would be the most constraining in several scenarios, especially at low IGMF amplitude or large monopole masses (case $B_\mathrm{I} < 10^{-13}$ G or for $m \gtrsim 10^{12}$ GeV). We show also how strongly seed Galactic Parker bound is modified once taken into account monopole acceleration from IGMFs [3] (dotted: $B_\mathrm{I} = 10^{-9}$ G, dotdashed: $B_\mathrm{I} = 10^{-11}$ G, light solid: $B_\mathrm{I} \lesssim 10^{-13}$ G). Monopoles with overplanckian masses remains mostly constrained by cosmological abundance (solid gray curve).

The MACRO limits (solid blue line) are the strongest of those from direct searches for large monopole masses. The reason is that large-mass magnetic monopoles are more and more difficult to accelerate to the relativistic velocities required to enable indirect observation of Cherenkov or fluorescence light with the other detectors. Non-relativistic monopoles can be probed only directly through interactions in matter such as those investigated in MACRO.

IceCube limits (solid purple curve) start to be competitive at small $\beta$, below the Cherenkov threshold in ice. After an initial regime in which the limits are strongly dependent on the mass/speed of the monopole, the instrument reaches full acceptance and the limits are almost flat for a large mass range. As already mentioned, IceCube is not sensitive to monopoles with masses smaller than $10^4$ GeV due to energy loss to the Earth. Therefore, approaching $m = 10^4$ GeV, the constrain power of IceCube decreases again. For the fluxes tested by IceCube the acceleration mechanism is dominated by the GMFs. However, as shown in Fig. 3.5, once the IceCube constraints will improve below $10^{-19}$ cm$^{-2}$sr$^{-1}$s$^{-1}$, they will become sensible to the acceleration in IGMFs for the extremal values of the IGMF parameters compatible with the experimental data.

The bounds from Auger (brown curves) are the strongest at the very large Lorentz factors required to generate a sufficient signal in the atmosphere. Although the masses sensible to the Auger limits are currently almost completely excluded by the MoEDAL lower mass limit, increasing the sensibility of Auger to the monopole fluorescence track would easily give access to larger monopole masses. The current flux limits of Auger are sensitive to intergalactic acceleration only for an amplitude of $B_\mathrm{I} = 10^{-9}$ G (dotted curve for dominant IGMF acceleration, solid curve in the other cases). However, once the limit will improve with larger statistic, intergalactic acceleration will be dominant also for smaller IGMF amplitude. When the acceleration mechanism is dominated by IGMFs, moving to smaller fluxes also means an increase of the

monopole velocity. Consequently, Auger would become sensible to larger masses with more statistics, even with the current sensibility.

Finally, our estimates for the sensitivity of future IACTs are interesting for low mass monopoles in the intermediate region between the sensitivity range of Auger and IceCube (for $m \sim 10^4 - 10^5$ GeV). A precursor of CTAO, the ASTRI Mini-Array [133], comprised of 9 standalone SSTs, can also be a valid IACT to search for monopoles, before the advent of CTAO. Also, the Trinity wide-field of view ground-based Cherenkov telescopes [134], principally meant for tau-neutrinos searches, may be optimal for monopole searches. Considering that the search for mangetic monopoles at IACTs is in its infancy, we strongly recommend to consider pursuing this research.

In this study, we have illustrated that accounting for the acceleration of magnetic monopoles in cosmic magnetic fields can fundamentally alter the framework of direct monopole searches, especially in the lower mass range. We have indicated that as a result of this acceleration, monopoles with masses under $10^{12}$ GeV travel at relativistic speeds. Consequently, experiments targeting high and ultra-high energy cosmic rays, such as IceCube, Auger, and IACTs, are best positioned to enhance the constraints on monopole flux in the near future. Upon achieving sensitivity to fluxes below $10^{-18}$ cm$^{-2}$ sr$^{-1}$ s$^{-1}$, these detectors will also become sensitive to IGMF physics, offering a novel approach to examining the IGMF structure through monopole detection. Given the crucial role of analyzing monopole energy loss within the Earth to correlate monopole velocity at the detector with monopole mass, we encourage the experimental collaborations to publish their future results on monopole flux with analysis similar to those of this chapter.

Our model for the cosmic magnetic field strength and correlation length does not aim to be a complete model for monopole acceleration. More sophisticated cosmological or astrophysical scenarios may certainly be the actual case. As an example, we remark that the real structure of the GMFs is still not completely understood. Furthermore, in order to get a correct estimate of the energy gain one should also take into account the effects of the turbulence of the magnetic fields. However, we expect the contribution to be negligible because of the large mass of the monopoles. We highlight also that here we assume a single speed for the current population of monopoles, while depending on the direction of the monopoles at the entrance of the Milky Way a velocity distribution is expected in the case of acceleration in GMFs. We assume that this does not change significantly our results, given that the number of crossed cells for unclustered monopoles cannot change of more than one order of magnitude. We also neglect any contribution due to possible anisotropies of the monopole velocity dispersion. In the current absence of numerical simulations of the monopole dynamics in the Milky Way, we leave this to future studies.

# Chapter 6

# Arbitrarily charged monopole dynamics in the early universe

Although the cosmological expansion history from Big Bang Nucleosynthesis onward is constrained by various observations [46, 113], we have very few information on what happened before. In this chapter, we assume that at the time of the end of inflation, $t_{\text{end}}$, the universe is initially dominated by an oscillating inflaton field, which decays perturbatively into radiation. At time $t_{\text{dom}}$ the radiation component starts to dominate the universe, until matter domination begins at matter-radiation equality, at time $t_{\text{eq}}$. During reheating, the cosmological plasma sourced by the inflaton decay is not necessary in thermal equilibrium, and then it is not possible to define a cosmic temperature. In any case, we assume the plasma to be in thermal equilibrium during both the reheating and radiation-dominated epochs. Imposing this assumption leads to a conservative bound, as we will explain later. In Appendix C we review the evolution of the Hubble rate and of the cosmic temperature during the reheating epoch and the subsequent radiation-dominated epoch.

As we discussed in the previous chapters, gamma-ray observations suggest the existence of an intergalactic magnetic field $B_0 \gtrsim 10^{-15}$ G coherent on Mpc scales or larger [53, 54, 55] (the subscript "0" here denotes quantities in the present universe). Throughout this chapter, we assume that this large-scale intergalactic magnetic field was produced in the early universe. We expect that large-scale magnetic fields redshift as $B \propto a^{-2}$ in the absence of significant back-reaction from the monopoles or of any external source for the fields [135], where $a(t)$ is the scale factor. Magnetic fields coherent on scales of Mpc have always been outside the Hubble horizon during the period that we are going to analyze. Thus, the distance crossed by the monopoles during the period of interest is smaller than the correlation length of the magnetic fields. This allows us to consider the magnetic field to be effectively homogeneous.

We now describe the motion of monopoles in a homogeneous magnetic field with a friction force due to the primordial relativistic plasma. Under these conditions, the general covariant form for the equation of motion of the monopoles is:

$$m \text{v}^\nu \nabla_\nu \text{v}^\mu = m \left( \frac{d\text{v}^\mu}{d\tau} + \Gamma^\mu_{\alpha\beta} \text{v}^\alpha \text{v}^\beta \right) = \mathcal{F}^\mu_{\text{mag}} + \mathcal{F}^\mu_{\text{p}}, \tag{6.1}$$

where $\nabla_\nu$ is the covariant derivative, $\mathcal{F}^\mu_{\text{mag}}$ is the magnetic force responsible for the acceleration of the monopoles, $\mathcal{F}^\mu_{\text{p}}$ is the drag force from the interaction with the

primordial plasma, $\Gamma^\mu_{\alpha\beta}$ are the Christoffel symbols of the metric, $m$ is the monopole mass, $v^\mu$ is the four-velocity of the monopole, with $v_\mu v^\mu = 1$, and $\tau$ its proper time. The magnetic force can be expressed through the four-vector [136]:

$$\mathcal{F}^\mu_{\mathrm{mag}} = g\tilde{F}^{\mu\nu}v_\nu, \tag{6.2}$$

where $\tilde{F}^{\mu\nu} = \frac{1}{2}\epsilon^{\mu\nu\alpha\beta}F_{\alpha\beta}$ is the dual electromagnetic tensor and $\epsilon^{\mu\nu\alpha\beta}$ is a totally antisymmetric pseudotensor normalized as $|\epsilon^{\mu\nu\alpha\beta}| = 1/\sqrt{-\det(g_{\rho\sigma})}$, if $\mu$, $\nu$, $\alpha$ and $\beta$ are all distinct. Without loss of generality, we take the magnetic charge of the monopole $g$ to be positive.

We limit our analysis to times before $e^+e^-$ annihilation, i.e. $T \gtrsim 1$ MeV, when the cosmological plasma consists of relativistic charged particles. Monopoles interact with the plasma through elastic scattering $M + x^\pm \to M + x^\pm$, where $x^\pm$ is a generic charged particle of the Standard Model and beyond[1]. The result is an effective drag force acting on the monopoles. We adopt the covariant form of the drag force shown in [10]:

$$\mathcal{F}^\mu_{\mathrm{p}} = f_{\mathrm{p}}\ \mathrm{h}(v_{\mathrm{rel}})\ (u \cdot v)^{-1}\ [u^\mu - (u \cdot v)v^\mu], \tag{6.3}$$

where $u^\mu$ is the mean four-velocity of the particles in the plasma and $v_{\mathrm{rel}} = (1 - (u \cdot v)^{-2})^{1/2}$ is the velocity of the monopole in the rest frame of the plasma. Here $\mathrm{h}(w)$ is a slowly-varying function with $\mathrm{h}(0) = 1$ and $\mathrm{h}(1) = 3/2$:

$$\mathrm{h}(w) = \frac{3}{2w^2}\left[1 + \frac{1 - w^2}{2w}\ln\left(\frac{1 - w}{1 + w}\right)\right]. \tag{6.4}$$

For simplicity we fix $\mathrm{h}(v_{\mathrm{rel}})$ to unity in the following analyses. For relativistic scatterers that are in thermal equilibrium, $f_{\mathrm{p}}$ can be expressed as[2]:

$$f_{\mathrm{p}} \sim \frac{e^2 g^2 \mathcal{N}_c}{16\pi^2}T^2. \tag{6.5}$$

Here $T$ is the temperature of the plasma and $\mathcal{N}_c$ the number of relativistic and electrically charged degrees of freedom in thermal equilibrium including also the contributions of the spin and the charge of the scatterers. In this work, we always assume for the electric charge a value $e = 0.30$.[3] Due to the drag force, the energy in the magnetic fields that is used to accelerate the monopoles eventually gets dissipated into the thermal plasma[4].

We now consider a Friedmann-Robertson-Walker (FRW) background spacetime $ds^2 = dt^2 - a^2 dx^i dx^i$, assuming sum over repeated spatial indices irrespective of

---

[1]The details of the calculation and phenomenological aspects of the effective operator of the interaction can be found in [81, 137].

[2]The expression of $f_{\mathrm{p}}$ is different by a factor $16\pi^2$ from that in [58], which used CGS units instead of Heaviside-Lorentz.

[3]Before the electroweak phase transition, the monopoles and primordial magnetic fields are those of the hypercharge U(1), and thus quantities such as the charge are modified by a number of order unity that depends on the Weinberg angle. We ignore this effect, as well as the running of the parameters; this treatment should be good enough for the order-of-magnitude calculations in this work.

[4]Depending on the amount of the magnetic field energy that is dissipated, the plasma experiences an additional reheating that can have non-negligible effects on the evolution of the universe.

their positions, and suppose the plasma to be at rest in the coordinate system $(t, x^i)$, i.e. $u^\mu = (1, 0, 0, 0)$. In this reference frame, the velocity of the monopoles can be expressed as $v^\mu = (\gamma, \gamma v^i/a)$, with $\gamma = \frac{1}{\sqrt{1-v^2}}$, $v^i = a(dx^i/dt)$, and $v = (v^i v^i)^{1/2}$ the modulus of the three-velocity.

In the absence of magnetic fields, the motion of the monopoles can be described as a Brownian motion within the plasma [10]. Consequently, the monopoles present thermal velocities $v_T \sim (T/m)^{1/2}$, with zero mean velocity after taking an average over the three directions. In the early universe, the thermal velocity can be larger than the mean velocity induced by a primordial magnetic field. However, in this work we ignore the thermal velocity, assuming that it does not leave any coherent effects on large scales. The mechanisms of monopole production that we assume for our analysis are not able to give the monopoles a significant mean velocity upon production. In addition, any initial mean velocity of the monopoles decays away due to the drag forces. This allows us to assume for the monopoles a zero mean velocity when the magnetic fields are generated, simplifying the analysis.

The magnetic field vector is $B^\mu = \tilde{F}^{\mu 0}$, with $B^\mu B_\mu = -B^2$ and $B$ the amplitude of the magnetic field. Choosing the $x^3$-axis along the direction of the magnetic field (namely, $B^3 = B/a$ and $B^1 = B^2 = 0$), we can ignore the monopole velocity along the other directions, i.e. $v^3 = v$ and $v^1 = v^2 = 0$. Under these assumptions, the motion of the monopoles can be described by the equation for the average velocity:

$$m\frac{d}{dt}(\gamma v) = gB - (f_{\mathrm{p}} + mH\gamma)\, v, \tag{6.6}$$

where $H(t) = \dot{a}/a$ is the Hubble rate, and an overdot denotes a time derivative. The contribution of the universe expansion can be seen as an additional frictional term proportional to the Hubble rate. In [1] the solution of the equation of motion has been studied for magnetic monopoles with Dirac charge $g_{\mathrm{D}} = 2\pi/e$, while in [2] we were interested in generalizing the results to generic magnetic charges.

We do not specify the detailed mechanism for the generation of the primordial magnetic fields. According to the models proposed in the literature, the magnetic fields can be generated during inflation [71, 72], after inflation when the universe is dominated by an oscillating inflaton [73], or at cosmological phase transitions [74, 75].

We define $t_{\mathrm{end}}$ as the moment when the generation of the magnetic fields has concluded and the fields start to redshift freely with the expansion of the universe (the subscript "end" denotes quantities at the end of magnetic field generation[5]). In this work we assume the primordial magnetic field to be suddenly switched on at time $t_{\mathrm{end}}$. This corresponds to considering only times after the end of the process of the magnetic field generation. Although it is possible to obtain further constraints by taking into account also the time interval during the production of the magnetic fields, we leave this for future analysis. For this work we assume that $t_{\mathrm{end}}$ is at the end of inflation or in the subsequent epochs. In other words, we consider the Hubble rate during inflation to be no smaller than that at the magnetic field generation, i.e.

---

[5]Notice that in [1] we referred to the time at the end of magnetogenesis as $t_i$, instead of $t_{\mathrm{end}}$. Moreover, we used $n$ to denote the number density of monopole-antimonopole pairs, while in this paper we will use it for the total number density of monopoles and antimonopoles, i.e. $n \to n/2$.

$H_{\text{inf}} \geq H_{\text{end}}$. Moreover, we define $T_{\text{dom}}$ as the temperature at the end of reheating when the universe becomes dominated by radiation (the subscript "dom" denotes quantities computed at this time, i.e. $t_{\text{dom}}$).

At time $t_{\text{end}}$, the monopoles have a mean velocity equal to zero. (Here we are tacitly assuming that the monopoles are present when the magnetic fields are switched on. For monopoles produced afterward the 'initial time' should be taken as the time when the monopoles are produced.) Considering time intervals $t - t_{\text{end}}$ shorter than the time scales of the frictional forces (which will be specified below), the effects of the universe expansion and of the plasma can be ignored and the product of the velocity and gamma factor can be expressed as:

$$\gamma v \simeq \frac{g B_{\text{end}}}{m}(t - t_{\text{end}}). \tag{6.7}$$

Thus, monopoles can be freely accelerated to relativistic or non-relativistic velocities depending on the intensity of the fields and on their mass. At later times, the frictional terms become important, and the velocity of the monopoles starts to decrease. Depending on the temperature, one of the frictional terms eventually dominates over the other, giving rise to different behaviors of the velocity. We analyze the velocity evolution for two different regimes: during radiation domination ($t > t_{\text{dom}}$), and during the reheating epoch ($t < t_{\text{dom}}$).

## 6.1   Velocity of magnetic monopoles with Dirac charge

In this section, we compute the evolution of the magnetic monopoles, assuming a magnetic charge comparable to the Dirac charge. We will comment on the dynamics of arbitrarily charged magnetic monopoles in the next section. We discuss separately the dynamics during radiation domination and during reheating.

### 6.1.1   Radiation-dominated epoch

During radiation domination, the Hubble rate and the cosmic temperature redshift as $H \propto a^{-2}$ and $T \propto a^{-1}$, up to the time variation of the number of relativistic degrees of freedom, $g_{*(s)}$. For $t > t_{\text{dom}}$, let us for the moment assume that the Hubble friction on the monopoles is negligible. We also assume that the monopoles move at non-relativistic velocities because of the interaction with the plasma. Under these assumptions, the equation of motion of the monopoles can be rewritten as:

$$m\dot{v} = gB - f_{\text{p}}v. \tag{6.8}$$

Neglecting the time variation of $B$, $f_{\text{p}}$ and $H$, the general solution of the equation is $v = C \exp\left(-(f_{\text{p}}/m)t\right) + v_{\text{p}}$, where $C$ is a constant that depends on the initial conditions and $v_{\text{p}}$ is the terminal velocity:

$$v_{\text{p}} = \frac{gB}{f_{\text{p}}} \sim \frac{16\pi^2 B}{e^2 g \mathcal{N}_c T^2}. \tag{6.9}$$

The characteristic time necessary for the monopoles to feel the effects of the interaction with the particles of the plasma can then be defined as $\Delta t_{\text{p}} \sim m/f_{\text{p}} \simeq$

$(16\pi^2 m) / (e^2 g^2 \mathcal{N}_c T^2)$ [58]. After a time $\Delta t_{\rm p}$, the monopoles approach the terminal velocity $v_{\rm p}$.

As long as we consider magnetic fields of order $10^{-15}$ G today, they cannot have dominated the energy density of the universe during radiation domination, i.e. $B \ll T^2$. Thus, for $g \sim 2\pi/e$ the expression in Eq. (6.9) gives $v_{\rm p} \ll 1$. This justifies our use of non-relativistic equations.

Comparing the timescale $\Delta t_{\rm p}$ with the Hubble time $\Delta t_H \sim 1/H \sim M_{\rm Pl}/(g_*^{1/2}T^2)$, we observe that for a magnetic charge of $g = 2\pi/e$ the effect of the expansion of the universe can be neglected for masses:

$$m < \frac{M_{\rm Pl}\mathcal{N}_c}{g_*^{1/2}}. \tag{6.10}$$

Limiting our analysis to sub-planckian values for the masses of the monopoles, this condition is always satisfied. Therefore, this justifies our assumption of neglecting the Hubble friction during radiation domination.

Using $T_0 \sim 10^{-4}$ eV and $B_0 \sim 10^{-15}$ G $\simeq 2 \cdot 10^{-17}$ eV$^2$, the terminal velocity at $T \sim 1$ MeV (at which time $\mathcal{N}_c \sim g_{*s} \simeq 10.75$) is estimated as $v_{\rm p} \sim 10^{-8}$ for $g \sim 2\pi/e$.

### 6.1.2 Reheating epoch

Within this work, for simplicity we assume the total number of relativistic degrees of freedom $g_{*(s)}$, as well as the number of charged relativistic degrees of freedom $\mathcal{N}_c$, to stay constant for $t < t_{\rm dom}$. During the reheating epoch, assuming that the plasma is in thermal equilibrium, then $H \propto a^{-3/2}$ and $T \propto a^{-3/8}$ (see Appendix C for the computation). Consequently, the Hubble friction can play an important role in the monopole dynamics, and moreover the monopoles can move with relativistic velocities.

Thus, let us compare $f_{\rm p}$ and $mH\gamma$ in the equation of motion in Eq. (6.6), to see which of the friction terms dominates during the reheating epoch. We introduce the ratio $r(t) = \rho_{\rm rad}(t)/\rho_{\rm tot}(t)$, where $\rho_{\rm tot}$ is the total energy density of the universe and $\rho_{\rm rad}$ the energy density in radiation, with $r \leq 1/2$. The value of $r$ decreases going back in time. The Hubble rate then can be expressed as:

$$H \sim \frac{g_*^{1/2}T^2}{r^{1/2}M_{\rm Pl}} \gtrsim \frac{g_*^{1/2}T^2}{M_{\rm Pl}}. \tag{6.11}$$

If the monopoles move at non-relativistic velocities and assuming $g \sim 2\pi/e$, in order for $mH\gamma$ to be smaller than $f_{\rm p}$, the radiation fraction needs to satisfy:

$$r \gtrsim \left(\frac{g_*^{1/2}m}{\mathcal{N}_c M_{\rm Pl}}\right)^2. \tag{6.12}$$

For example, with a mass $m \simeq 10^{16}$ GeV and with $g_* \sim \mathcal{N}_c \simeq 100$, the condition in Eq. (6.12) can be read as $r \gtrsim 10^{-7}$. If the magnetic fields are generated sufficiently in the past, going back in time eventually the condition in Eq. (6.12) breaks down.

This signals $f_p < mH\gamma$, namely, the Hubble friction dominates, and the equation of motion of the monopoles can be approximately written as:

$$m\frac{d}{dt}(\gamma v) = gB - mH\gamma v. \qquad (6.13)$$

The terminal velocity can be estimated by equating the terms in the right-hand side as,[6]

$$(\gamma v)_{\mathrm{H}} \sim \frac{gB}{mH}. \qquad (6.14)$$

This can also take relativistic values, unlike the terminal velocity in Eq. (6.9) due to the plasma friction.

In Figure 6.1 we show the time evolution for $\gamma v$, by numerically solving the equation of motion Eq. (6.6). The results are shown for $H(t) < H_{\mathrm{end}}$, and for different values of the monopole mass. For $H(t) > H_{\mathrm{dom}}$, each value of the mass is associated to a differently colored solid curve (from bottom to top, brown: $m = 10^{19}$ GeV; red: $m = 10^{17}$ GeV; orange: $m = 10^{15}$ GeV; green: $m = 10^{14}$ GeV; blue: $m = 10^{13}$ GeV; purple: $m = 10^{11}$ GeV). The dashed line in the regime $H(t) > H_{\mathrm{dom}}$ shows $v_{\mathrm{p}}$ given in Eq. (6.9), which corresponds to the terminal velocity set by the plasma when $v_{\mathrm{p}} \ll 1$. For $H(t) < H_{\mathrm{dom}}$ the velocity is constant and independent of the mass of the monopoles, hence it is represented by a single solid horizontal grey line. For the computation we assume $g = 2\pi/e$, $B_0 = 10^{-15}$ G and $g_* = \mathcal{N}_c = 100$ throughout. We use the results presented in Appendix C for setting the time dependence of $a$, $T$ and $B$. We start the computation at $H_{\mathrm{end}} = 10^{11}$ GeV, with an initial condition $v(t_i) = 0$. Moreover, we choose the cosmic temperature when radiation domination takes over as $T_{\mathrm{dom}} = 10^6$ GeV, which corresponds to the Hubble rate $H_{\mathrm{dom}} \simeq 10^{-6}$ GeV.

Independently from the initial condition, the monopole velocity rapidly falls into one of the attractor solutions, $v_{\mathrm{p}}$ in Eq. (6.9) and $v_{\mathrm{H}}$ in Eq. (6.14). The evolution of the velocity for $H(t) < H_{\mathrm{end}}$ is hence independent of the value of $H_{\mathrm{end}}$. However, the choice of $H_{\mathrm{end}}$ determines how far back in time can one go with the attractor solutions. With a sufficiently large $H_{\mathrm{end}}$, the Hubble friction initially dominates over the friction from the plasma, yielding $(\gamma v)_{\mathrm{H}}$ which redshifts as $H^{1/3}$. During reheating the fraction of energy density in the radiation component increases with time and at some point Eq. (6.12) starts to be satisfied. This is the signal that the velocity begins to be controlled by the friction from the plasma, cf. Eq. (6.9), and then the velocity decreases as $H^{5/6}$. For masses satisfying the condition in Eq. (6.10), monopoles achieve $v_{\mathrm{p}}$ before radiation domination and the value of the velocity at $T = T_{\mathrm{dom}}$ is independent of the mass.

Of crucial relevance is the time $t_*$ of the transition between the domination of the Hubble friction term and that of the friction term by the primordial plasma:

$$f_{\mathrm{p},*} = mH_*\gamma_* , \qquad (6.15)$$

where the subscript "$*$" stands for quantities computed at time $t_*$. For $t < t_*$ the monopoles move at the terminal velocity set by the expansion of the universe shown

---

[6]The time scales for $v$ to achieve $v_{\mathrm{H}}$, and for the redshifting of $B$ and $H$, are all of order the Hubble time. Hence $d(\gamma v)/dt$ actually does not vanish and the terminal velocity is $(\gamma v)_{\mathrm{H}} = 2gB/mH$ (see Eq. (A7) in [45] for the derivation). However we will omit the factor 2 since we are interested in order-of-magnitude estimates.

in Eq. (6.14). For $t > t_*$ the frictional term due to the interaction with the plasma dominates the evolution and the velocity of the monopoles can be expressed through Eq. (6.9). Rewriting Eq. (6.15) as an expression for the velocity of the monopoles $v_*$, we get:

$$v_*^2 = 1 - \left( \frac{mH_*}{f_{p,*}} \right)^2.$$ (6.16)

When $v > v_*$ the motion of the monopole is set by the Hubble friction term, while for $v < v_*$ it is dominated by the friction force of the plasma. We can obtain the Hubble rate at the transition by using Eq. (6.14) and setting $v_* \simeq v_{H,*}$ as:

$$\frac{m^2 H_*^2}{f_{p,*}^2} + \frac{g^2 B_*^2}{f_{p,*}^2} \simeq 1.$$ (6.17)

Considering that $f_p \propto H^{1/2}$ and $B \propto H^{4/3}$ during reheating, we can rewrite Eq. (6.17) in terms of quantitites at $t_{\text{dom}}$ as:

$$\alpha \left( \frac{H_*}{H_{\text{dom}}} \right)^{5/3} + \beta(m) \left( \frac{H_*}{H_{\text{dom}}} \right) \simeq 1,$$ (6.18)

where we define:

$$\alpha = \left( \frac{gB_{\text{dom}}}{f_{p,\text{dom}}} \right)^2,$$ (6.19a)

$$\beta(m) = \left( \frac{mH_{\text{dom}}}{f_{p,\text{dom}}} \right)^2.$$ (6.19b)

Depending on the value of the monopole mass, one of the two terms on the left-hand side of Eq. (6.18) is larger than the other. The two terms are always positive and they are of the same order only if both of them are of order unity, i.e. $\alpha(H_*/H_{\text{dom}})^{5/3} \sim \beta(\bar{m})(H_*/H_{\text{dom}}) \sim 1$, where we define $\bar{m}$ as the mass for which the two terms are comparable. From these considerations we obtain the relation for $\bar{m}$:

$$\alpha\beta(\bar{m})^{-5/3} \sim 1.$$ (6.20)

Substituting the definition for $\alpha$ and $\beta$, we get the explicit expression for $\bar{m}$:

$$\bar{m} \sim \frac{\left( g^3 B_{\text{dom}}^3 f_{p,\text{dom}}^2 \right)^{1/5}}{H_{\text{dom}}}.$$ (6.21)

Notice that the combination $B^3 f_p^2 / H^5$ is actually time-independent during the reheating epoch, up to mild variations from changes in the numbers of relativistic degrees of freedom. Hence $\bar{m}$ is constant in time. Using Eq. (C.5) in Appendix C to rewrite the expressions for $f_{p,\text{dom}}$, $B_{\text{dom}}$ and $H_{\text{dom}}$ in terms of their values at the present time, we obtain:

$$\bar{m} \simeq 10^{14} \text{ GeV} \left( \frac{B_0}{10^{-15} \text{ G}} \right)^{3/5} \left( \frac{g}{10} \right)^{7/5} \left( \frac{\mathcal{N}_{c,\text{dom}}}{100} \right)^{2/5}.$$ (6.22)

Assuming $B_0 \sim 10^{-15}$ G, $\mathcal{N}_c \sim 100$ and $g \sim 2\pi/e \sim 10$, we get $\bar{m} \simeq 10^{14}$ GeV. Thus, in Figure 6.1 the green curve corresponds to the evolution of the velocity of monopoles with a mass $m = \bar{m}$.

For $m \ll \bar{m}$ the left-hand side of Eq. (6.18) is dominated by the first term and the expression for $H_*$ is independent of the monopole mass:

$$\frac{H_*}{H_{\rm dom}} \simeq \frac{1}{\alpha^{3/5}} = \left(\frac{f_{\rm p,dom}}{gB_{\rm dom}}\right)^{6/5}, \tag{6.23}$$

while for $m \gg \bar{m}$ the second term dominates and:

$$\frac{H_*}{H_{\rm dom}} \simeq \frac{1}{\beta(m)} = \left(\frac{f_{\rm p,dom}}{mH_{\rm dom}}\right)^2. \tag{6.24}$$

Using Eq. (C.5), the expressions for $H_*$ can be further rewritten as:

$$H_* \simeq \begin{cases} 10^4 \text{ GeV} \left(\dfrac{g}{10}\right)^{6/5} \left(\dfrac{\mathcal{N}_{c,\rm dom}}{100}\right)^{6/5} \left(\dfrac{T_{\rm dom}}{10^6 \text{ GeV}}\right)^2 \left(\dfrac{10^{-15} \text{ G}}{B_0}\right)^{6/5} & , \ m \ll \bar{m}, \\[3ex] 10^4 \text{ GeV} \left(\dfrac{g}{10}\right)^4 \left(\dfrac{\mathcal{N}_{c,\rm dom}}{100}\right)^2 \left(\dfrac{T_{\rm dom}}{10^6 \text{ GeV}}\right)^2 \left(\dfrac{10^{14} \text{ GeV}}{m}\right)^2 & , \ m \gg \bar{m}. \end{cases} \tag{6.25}$$

In Figure 6.1 we plot in vertical line the value of $H_*$ in the limit $m \ll \bar{m}$, i.e. the first line of Eq. (6.25).

For $m \ll \bar{m}$, the monopole velocity is always relativistic while it is on the Hubble-friction branch, $v = v_{\rm H}$; this is seen for the purple and blue curves in the plot. On the other hand, for $m \gg \bar{m}$, the monopoles become non-relativistic before switching to the plasma-friction branch, $v = v_{\rm p}$, as it is seen for the brown, red, and orange curves. In other words, if $m \ll \bar{m}$, the balancing of the frictional forces happens while the monopoles are relativistic, and the monopole velocity jumps from an ultrarelativistic $v_{\rm H}$ to a mildly relativistic $v_{\rm p}$. On the other hand if $m \gg \bar{m}$, the balancing happens while the monopoles are nonrelativistic, and the velocity transition is smooth.

Let us better estimate the time it takes for monopoles with $m \ll \bar{m}$ to jump from a relativistic $v_{\rm H}$ branch to a non-relativistic $v_{\rm p}$ branch. For times $t \lesssim t_*$ we can consider $v \simeq 1$ and the equation of motion for the monopoles can be rewritten in terms of the relativistic factor $\gamma$:

$$\dot{\gamma} = \frac{gB - f_{\rm p}}{m} - H\gamma. \tag{6.26}$$

Using $B \propto a^{-2}$, $f_{\rm p} \propto a^{-3/4}$, and $H \propto a^{-3/2}$, one can check that this equation has a solution,

$$\gamma = 2\frac{gB}{mH} - \frac{4}{7}\frac{f_{\rm p}}{mH} = \gamma_* \left[\frac{11}{7}\left(\frac{a}{a_*}\right)^{-1/2} - \frac{4}{7}\left(\frac{a}{a_*}\right)^{3/4}\right], \tag{6.27}$$

which asymptotes to $\gamma \simeq 2gB/mH$ in the past. Upon moving to the far right-hand side, we used Eq. (6.15). For $\gamma_* \gg 1$, the $\gamma$ factor approaches unity at $a = (11/4)^{4/5}a_* \simeq 2.2a_*$, which is obtained by equating the terms in the square
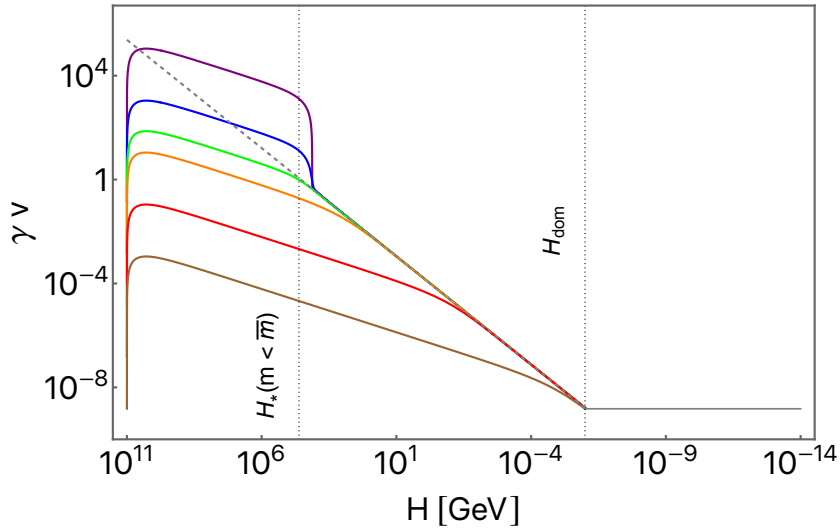
**Figure 6.1** Evolution of the monopole velocity in primordial magnetic fields for different values of the monopole mass (from bottom to top, brown: $m = 10^{19}$ GeV; red: $m = 10^{17}$ GeV; orange: $m = 10^{15}$ GeV; green: $m = 10^{14}$ GeV; blue: $m = 10^{13}$ GeV; purple: $m = 10^{11}$ GeV) and for magnetic charge $g = 2\pi/e$. The expression in Eq. (6.9) for the terminal velocity set by the friction with the thermal plasma is also shown in dashed line. Here $H_{\rm dom} = 10^{-6}$ GeV, $B_0 = 10^{-15}$ G, $g_* = \mathcal{N}_c = 100$ and we use $H_{\rm end} = 10^{11}$ GeV as the starting point of the evolution. The value of $H_* \sim 10^5$ GeV for monopole masses smaller than $\bar{m}$ is also shown in the plots (see the text for details).

brackets in Eq. (6.27). Thus, the jump from an ultra-relativistic $v_{\rm H}$ to a non-relativisitc $v_{\rm p}$ happens with a time scale of $1/H_*$, as shown in the figure for the purple and blue curves.

Before closing this section, we should also remark that, as one goes back in time in the reheating epoch, the energy density in primordial magnetic fields grows relative to the total density as $\rho_B/\rho_{\rm tot} \propto a^{-1}$. Hence for primordial magnetic fields generated at the end of inflation or during reheating, i.e. $t_{\rm inf} \le t_{\rm end} < t_{\rm dom}$, requiring that they have never dominated the universe constrains the time when magnetic field generation happened. The constraint is written using (C.5) and (C.6) as,

$$H_{\rm end} \lesssim 10^{22} \, {\rm GeV} \left( \frac{T_{\rm dom}}{10^6 \, {\rm GeV}} \right)^2 \left( \frac{10^{-15} \, {\rm G}}{B_0} \right)^3 . \tag{6.28}$$

With a reasonable choice of parameters (such as $g \sim 10$, $B_0 \sim 10^{-15}$ G, and $\mathcal{N}_{c,{\rm dom}} \sim 100$), one sees that $H_*$ in Eq. (6.25) is well below this limit on $H_{\rm end}$, independently of $T_{\rm dom}$ and $m$.

## 6.2 Generalization to arbitrarily charged monopoles

We now move to the generalization of the analysis in the previous section to arbitrarily charged monopoles. In particular, we comment on how the results are affected by small values of the magnetic charge.

As we have already explained, depending on the parameters of the model, one of the two frictional terms in the equation of motion of Eq. (6.6) becomes dominant and eventually the monopoles achieve a terminal velocity. We recall that if the Hubble friction is the dominant term, i.e. $mH\gamma \gg f_\mathrm{p}$, the terminal velocity is set approximately by:

$$(\gamma v)_\mathrm{H} \sim \frac{gB}{mH}. \qquad (6.29)$$

The expression is directly proportional to the magnetic charge of the monopoles. Thus, smaller magnetic charge corresponds to smaller $v_\mathrm{H}$.

On the other hand, when the drag force by the interaction with the plasma is dominant, i.e. $mH\gamma \ll f_\mathrm{p}$, and the monopoles move at nonrelativistic velocities, the terminal velocity corresponds to:

$$v_\mathrm{p} = \frac{gB}{f_\mathrm{p}} \sim \frac{16\pi^2 B}{e^2 g \mathcal{N}_c T^2}. \qquad (6.30)$$

Since the interaction rate with the particles of the plasma is proportional to $g^2$ and the monopole acceleration by the magnetic field to $g$, the velocity $v_\mathrm{p}$ scales as $v_\mathrm{p} \propto g^{-1}$.

Even for generic magnetic charge, due to the $\gamma$ factor in front of the Hubble friction term, for relativistic monopoles ($\gamma \gg 1$) the drag force due to the expansion of the universe tends to become dominant. In this case the terminal velocity of the monopoles corresponds to the value of $v_\mathrm{H}$ shown in Eq. (6.29). However, in the case when the monopoles move at relativistic velocities and $mH\gamma \ll f_\mathrm{p}$, the monopole velocity rapidly decreases to nonrelativistic values and eventually starts to follow the terminal velocity $v_\mathrm{p}$.

In Figure 6.2 we plot the time evolution of $\gamma v$ for small values of the magnetic charge. The time evolution of $\gamma v$ is obtained by numerically solving the equation of motion Eq. (6.6) with an initial condition of $v_\mathrm{end} = 0$. For the plots we assume $H_\mathrm{end} = 10^{11}$ GeV, $H_\mathrm{dom} = 10^{-6}$ GeV (i.e. $T_\mathrm{dom} \sim 10^6$ GeV, see Appendix C), and fix the number of relativistic (charged) degrees of freedom as $g_* = \mathcal{N}_c = 100$ throughout the displayed epochs. The magnetic field strength is taken such that it approaches a present-day strength of $B_0 = 10^{-15}$ G.

In Figure 6.2a, the results are shown for a magnetic charge $g = 10^{-3} g_\mathrm{D}$ and for different values of the monopole mass. The value of the magnetic charge has been chosen in order to cover a wide range of possible behaviors of the monopole velocity which we will explain in the following sections. Each value of the mass is associated to a differently colored solid curve; from bottom to top, red: $m = 10^{19}$ GeV, orange: $m = 10^{16}$ GeV, green: $m = 10^{13}$ GeV, blue: $m = 10^{10}$ GeV, purple: $m = 10^7$ GeV. The purple curve disappears when it is behind the blue curve. In Figure 6.2a, the dashed gray line shows $\gamma v$ with $v$ substituted by $v_\mathrm{p}$ given in Eq. (6.30). This corresponds to the terminal velocity set by the plasma when $v_\mathrm{p} \ll 1$, and it overlaps with the blue and purple lines in the right part of the figure.

In Figure 6.2b, the results are shown for a mass $m = 10^{11}$ GeV and for different values of the magnetic charge. As in the previous case, the value of the mass has been chosen in order to show the various behaviors of the monopole velocity. Each value of the charge is associated to a differently colored solid curve; from top to

bottom, red: $g = g_{\mathrm{D}}$, orange: $g = 10^{-3} g_{\mathrm{D}}$, green: $g = 10^{-6} g_{\mathrm{D}}$, blue: $g = 10^{-9} g_{\mathrm{D}}$, purple: $g = 10^{-12} g_{\mathrm{D}}$. The dashed curves show $(\gamma v)_{\mathrm{p}}$ for different charges, indicated by the colors. The red and orange dashed curves overlap with the corresponding solid curves in the right part of the plot. The blue and purple dashed curves are not shown because a terminal velocity set by the friction with the plasma cannot be defined in those cases, being $v_{\mathrm{p}} \gg 1$.

In the figures, the monopole velocity follows $v_{\mathrm{p}}$ in Eq. (6.30) shown as the dashed lines, otherwise it follows $v_{\mathrm{H}}$ in Eq. (6.29) (except for at the left edges of the plots where $H \sim H_{\mathrm{end}}$[7]). This indicates that one of the two terminal velocities always gives an attractor solution for the monopole velocity. One also sees from the figures that the velocity can make a transition from $v_{\mathrm{H}}$ to $v_{\mathrm{p}}$ as the universe expands, but not vice versa. The transition can be smooth as for the blue curve in Figure 6.2a, but can also take the form of a sudden jump as for the purple curve in Figure 6.2a.

Whether the monopole velocity during radiation domination follows $v_{\mathrm{p}}$ or $v_{\mathrm{H}}$ depends on the monopole properties and the magnetic field strength. This is illustrated in Figure 6.3 in the $m$-$g$ plane, where we took the field strength such that it becomes $B_0 = 10^{-15}$ G today. The numbers of relativistic (charged) degrees of freedom are fixed to $g_* = \mathcal{N}_c = 10.75$. The purple curve shows where the plasma and Hubble frictions in the monopole's equation of motion in Eq. (6.6) are comparable, i.e. $f_{\mathrm{p}} = mH\gamma_{\mathrm{H}}$. In the red region the plasma friction is dominant ($f_{\mathrm{p}} \gg mH\gamma_{\mathrm{H}}$) and the monopole velocity is given by $v_{\mathrm{p}}$. On the other hand, in the blue region the Hubble friction is dominant ($f_{\mathrm{p}} \ll mH\gamma_{\mathrm{H}}$) and the velocity is given by $v_{\mathrm{H}}$.

The balance condition $f_{\mathrm{p}} = mH\gamma_{\mathrm{H}}$ is rewritten using Eqs. (6.30) and (6.29) as

$$\left( \frac{e^2 g^2 \mathcal{N}_c T^2}{16\pi^2} \right)^2 \sim (gB)^2 + (mH)^2. \tag{6.31}$$

This can be solved for the magnetic charge, and the solution $g = g_{\mathrm{min}}$ is approximated by:

$$g_{\mathrm{min}} \sim \begin{cases} \dfrac{16\pi^2}{e^2 \mathcal{N}_c} \dfrac{B}{T^2} & \text{for } m \ll \dfrac{16\pi^2}{e^2 \mathcal{N}_c} \dfrac{B^2}{HT^2}, \\[3mm] \left( \dfrac{16\pi^2}{e^2 \mathcal{N}_c} \dfrac{mH}{T^2} \right)^{1/2} & \text{for } m \gg \dfrac{16\pi^2}{e^2 \mathcal{N}_c} \dfrac{B^2}{HT^2}. \end{cases} \tag{6.32}$$

For $g > g_{\mathrm{min}}$ the monopole velocity approaches $v_{\mathrm{p}}$, and for $g < g_{\mathrm{min}}$ it approaches $v_{\mathrm{H}}$. In other words, $g_{\mathrm{min}}$ sets the minimum charge for a monopole during radiation domination to lose its kinetic energy mainly through its interaction with the plasma. The expressions of Eq. (6.32) describe the two asymptotic behaviors of the purple curve in the figure. In the first line the balance condition is realized for relativistic velocities ($(\gamma v)_{\mathrm{H}} \gg 1$), while the second line is for nonrelativistic velocities ($(\gamma v)_{\mathrm{H}} \ll 1$). In the figure, the dashed gray line shows where $(\gamma v)_{\mathrm{H}} = 1$, with $(\gamma v)_{\mathrm{H}} < 1$ on its right side. One actually sees that the dashed gray and purple lines intersect at the point where the purple line bends. We also note that the first line of Eq. (6.32) corresponds to the charge that gives $v_{\mathrm{p}} = 1$; this is depicted in the figure by the

---

[7]Radiative emission may affect the monopole dynamics before one of the terminal velocities is reached. However this also depends on how the magnetic field is initially switched on.

**(a)** $g = 10^{-3}g_{\mathrm{D}}$ with varying $m$.



**(b)** $m = 10^{11}\,\mathrm{GeV}$ with varying $g$.
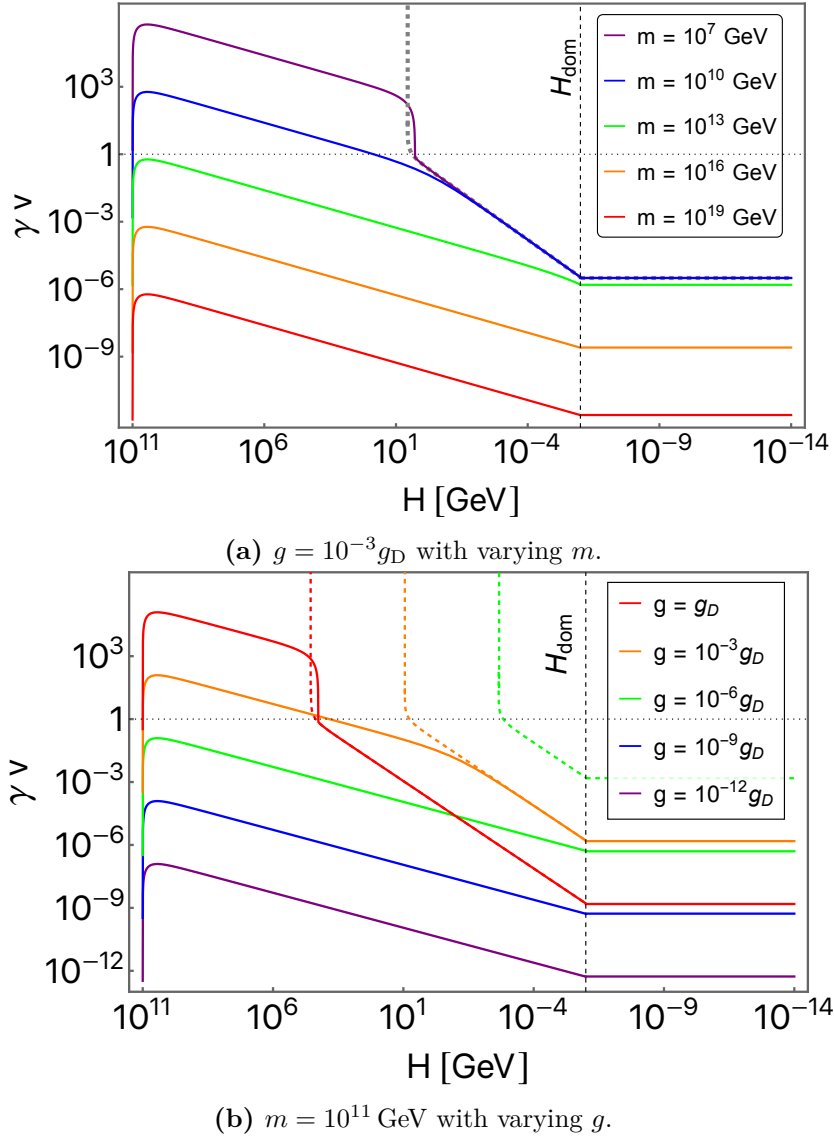
**Figure 6.2** Time evolution of the monopole velocity in primordial magnetic fields. The Hubble scales at the end of magnetogenesis and at the onset of radiation domination are taken respectively as $H_{\mathrm{end}} = 10^{11}\,\mathrm{GeV}$ and $H_{\mathrm{dom}} = 10^{-6}\,\mathrm{GeV}$. The present-day magnetic field strength is taken as $B_0 = 10^{-15}\,\mathrm{G}$. The numbers of relativistic (charged) degrees of freedom are fixed to $g_* = \mathcal{N}_c = 100$. In the upper panel, the charge of the monopole is fixed to $g = 10^{-3}g_{\mathrm{D}}$ while the mass is varied as $m = 10^{19}\,\mathrm{GeV}$ (red), $10^{16}\,\mathrm{GeV}$ (orange), $10^{13}\,\mathrm{GeV}$ (green), $10^{10}\,\mathrm{GeV}$ (blue), $10^{7}\,\mathrm{GeV}$ (purple), from bottom to top. In the bottom panel, the mass is fixed to $m = 10^{11}\,\mathrm{GeV}$ while the charge is varied as $g = g_{\mathrm{D}}$ (red), $10^{-3}g_{\mathrm{D}}$ (orange), $10^{-6}g_{\mathrm{D}}$ (green), $10^{-9}g_{\mathrm{D}}$ (blue), $10^{-12}g_{\mathrm{D}}$ (purple), from top to bottom. The dashed colored curves in the upper panels show the terminal velocity set by the friction from the cosmological plasma.

dashed black line. In the region below this line the expression Eq. (6.30) yields $v_{\mathrm{p}} > 1$, indicating that the plasma friction does not yield a terminal velocity for monopoles.
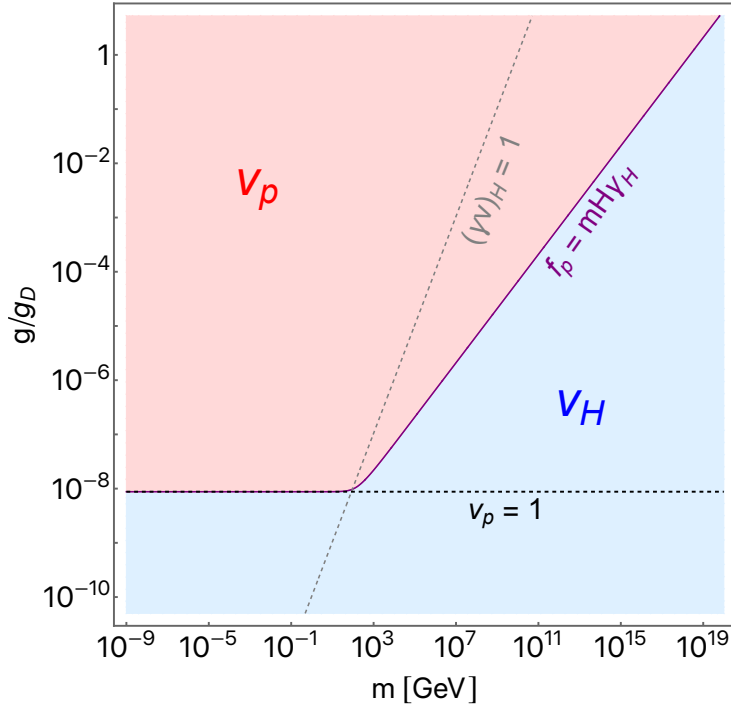
**Figure 6.3**   Velocity of monopoles accelerated by primordial magnetic fields during radia-
tion domination. The solid purple curve shows the combination of the monopole mass
and charge for which the friction term due to the interaction with the primordial plasma,
$f_{\rm p}$, is comparable to the friction term due to the expansion of the universe, $mH\gamma_{\rm H}$.
In the red region above the curve the monopole velocity is controlled by the plasma
friction, $f_{\rm p} \gg mH\gamma_{\rm H}$. In the blue region below the curve the velocity is controlled by
the Hubble friction, $f_{\rm p} \ll mH\gamma_{\rm H}$. The dashed gray line shows where $(\gamma v)_{\rm H} = 1$. The
dashed black horizontal line shows where $v_{\rm p} = 1$. Here we assume $B_0 = 10^{-15}$ G and
$g_* = \mathcal{N}_c = 10.75$.

The expressions in Eq. (6.32) are time independent during radiation, up to mild
variations due to the change in the numbers of relativistic degrees of freedom. The
cosmic temperature and the Hubble rate during the radiation-dominated epoch are
related to the redshift as

$$T \sim 1\,\mathrm{MeV} \left( \frac{10^{-10}}{a/a_0} \right), \quad H \sim 10^{-15}\,\mathrm{eV} \left( \frac{10^{-10}}{a/a_0} \right)^2, \qquad (6.33)$$

where we ignored their mild dependence on $g_{*(s)}$. For the number of relativistic
charged degrees of freedom, hereafter we use $\mathcal{N}_c \sim 10$ as a reference value. Combining
these with the magnetic scaling $B = B_0(a_0/a)^2$, one can rewrite Eq. (6.32) as

$$g_{\rm min} \sim \begin{cases} 10^{-8} g_{\rm D} \left( \dfrac{B_0}{10^{-15}\,\mathrm{G}} \right) & \text{for } m \ll 10^2\,\mathrm{GeV} \left( \dfrac{B_0}{10^{-15}\,\mathrm{G}} \right)^2, \\[3ex] 10^{-1} g_{\rm D} \left( \dfrac{m}{10^{17}\,\mathrm{GeV}} \right)^{1/2} & \text{for } m \gg 10^2\,\mathrm{GeV} \left( \dfrac{B_0}{10^{-15}\,\mathrm{G}} \right)^2. \end{cases} \qquad (6.34)$$

The terminal velocities of Eqs. (6.30) and (6.29) can also be rewritten during radiation

domination as,

$$v_{\mathrm{p}} \sim 10^{-8} \left( \frac{g}{g_{\mathrm{D}}} \right)^{-1} \left( \frac{B_0}{10^{-15}\,\mathrm{G}} \right), \tag{6.35}$$

$$(\gamma v)_{\mathrm{H}} \sim 10^{-7} \left( \frac{m}{10^{17}\,\mathrm{GeV}} \right)^{-1} \left( \frac{g}{g_{\mathrm{D}}} \right) \left( \frac{B_0}{10^{-15}\,\mathrm{G}} \right). \tag{6.36}$$

The monopole velocity during radiation domination shown in the right parts of Figure 6.2 can be understood from Figure 6.3, and by noting that the terminal velocities scale with the monopole mass and charge as $v_{\mathrm{p}} \propto g^{-1}$, $(\gamma v)_{\mathrm{H}} \propto gm^{-1}$. The variation of the velocities in Figure 6.2a is understood by moving horizontally in Figure 6.3 along $g = 10^{-3} g_{\mathrm{D}}$; for small $m$ the velocity is set to $v_{\mathrm{p}}$ which is independent of $m$ (cf. purple and blue lines in Figure 6.2a), while for large $m$ the velocity is $v_{\mathrm{H}}$ which decreases with $m$ (cf. green, orange, and red lines). On the other hand, Figure 6.2b corresponds to moving vertically in Figure 6.3 along $m = 10^{11}\,\mathrm{GeV}$; for small $g$ the velocity $v_{\mathrm{H}}$ increases with $g$ (cf. purple, blue, and green lines in Figure 6.2b), while for large $g$ the velocity $v_{\mathrm{p}}$ decreases with $g$ (cf. orange and red lines).

# Chapter 7

# Bounds from the survival of primordial magnetic fields

In the previous chapter, we treated the primordial magnetic field as a background, however the magnetic fields themselves lose energy as they accelerate the monopoles. Here we study the energy depletion of the magnetic field, and derive conditions for the primordial magnetic field to survive until today. The kind of bounds analyzed in this section are analogous to the Parker bounds but with respect to large-scale magnetic fields in the early universe, instead of galactic magnetic fields in the recent universe[1]. The bound during radiation domination has already been proposed in [58]. In this chapter we review the bound for times $t > t_{\text{dom}}$ and we extend the analysis for $t < t_{\text{dom}}$. We first describe the evolution of the primordial magnetic fields in the presence of magnetic monopoles from the end of magnetogenesis to the epoch of $e^+e^-$ annihilation, when the number of charged particles in the universe becomes drastically reduced. Then, we derive bounds on the monopole abundance from the survival of the primordial magnetic fields. Finally, we generalize the results to arbitrarily charged monopoles.

As in the previous chapter, in our analysis we suppose that the process of magnetogenesis terminates at the end of inflation or during the reheating phase. Thus, we study the dynamics of the primordial magnetic fields during the reheating epoch when the energy density of the universe is dominated by an oscillating inflaton field, and the subsequent epoch of radiation domination.

The magnetic fluid is described by the barotropic equation of state $P_{\text{B}}/\rho_{\text{B}} = 1/3$, where $P_B$ is the pressure of the magnetic fluid and $\rho_{\text{B}} = B^2/2$ is the physical energy density. This corresponds to assuming that there are no external sources for the magnetic field for $t > t_{\text{end}}$. Under the hypothesis of a spatially homogeneous magnetic field, the evolution of the energy density $\rho_B$ within a FRW background, taking into account the effects of the monopole acceleration, is described by:

$$d\left[\rho_{\text{B}}(t)a(t)^3\right] = -P_{\text{B}}(t)d\left[a(t)^3\right] - 2gB(t)dt\int_{-\infty}^{t} dt' a\left(t'\right)^3 \Gamma\left(t'\right) v\left(t',t\right), \quad (7.1)$$

where $\Gamma(t)$ is the production rate for either monopoles or antimonopoles at time $t$. The second term on the right-hand side of the equation denotes the loss of energy

---

[1]See also [23] for an extension of the Parker bound using Andromeda galaxy.

due to accelerating the population of monopoles and antimonopoles produced from the infinite past to time $t$. All the possible production mechanisms that we take into account, i.e. monopole pairs produced by the magnetic fields, thermal production and production during phase transitions, cannot produce an asymmetry on the number of monopoles with respect to that of antimonopoles. Therefore, we always consider the monopole and antimonopole number densities to be equal and there is a factor 2 in the second term of Eq. (7.1). Here $a(t')^3 \Gamma(t')dt'$ represents the comoving number density of monopoles produced between $t'$ and $t' + dt'$, $v(t', t)$ corresponds to the velocity in the direction of the magnetic field at time $t$ of monopoles produced at $t'$ (with $t \geq t'$). For the antimonopoles, we choose a charge of $-g$ and a velocity $-v(t', t)$.[2]

The monopoles can be produced at a phase transition [8, 80], through a thermal process [138, 139], or by the magnetic field itself via the Schwinger effect. In this section we keep the discussion general and do not specify the production mechanism. The particular case of the Schwinger pair production will be the topic of the next chapter.

It has been shown that the monopole-antimonopole annihilation is relevant only if the monopole abundance is large enough to overdominate the universe [8, 9]. Thus, we assume monopole-antimonopole annihilation to be negligible.

Eq. (7.1) can be then rewritten as:

$$\frac{\dot{\rho}_{\mathrm{B}}}{\rho_{\mathrm{B}}} = -\Pi_{\mathrm{red}} - \Pi_{\mathrm{acc}}, \tag{7.2}$$

where $\Pi_{\mathrm{red}}$ and $\Pi_{\mathrm{acc}}$ are the dissipation rates of the magnetic field energy due to redshifting and monopole acceleration:

$$\Pi_{\mathrm{red}}(t) = 4H(t), \tag{7.3a}$$

$$\Pi_{\mathrm{acc}}(t) = \frac{4g}{a(t)^3 B(t)} \int_{-\infty}^{t} dt' a\left(t'\right)^3 \Gamma\left(t'\right) v\left(t', t\right). \tag{7.3b}$$

Once the expression for the monopole velocity and for the total production rate is given, the evolution of the magnetic field energy density can be derived by solving Eq. (7.2).

In the previous chapter we have shown that the memory of the monopole velocity at the time when the magnetic field is switched on is quickly lost. Hence, we assume that the monopoles have a uniform velocity independent of when they were produced, i.e. $v(t', t) = v(t)$. Under this assumption, it is possible to rewrite the expression for $\Pi_{\mathrm{acc}}$ in the following way:

$$\Pi_{\mathrm{acc}}(t) = \frac{4g}{B(t)} v(t) n(t), \tag{7.4}$$

---

[2]Primordial magnetic fields can lose their energy also by pair-producing monopoles through the Schwinger effect. This effect can be taken into account by adding a term $-2m\Gamma_{\mathrm{sw}}(t)a(t)^3 dt$ on the right-hand side of Eq. (7.1), where $\Gamma_{\mathrm{sw}}$ is the rate of monopole pair production through the Schwinger effect. However, we neglect such a contribution in our analysis. Back-reaction of pair production on the magnetic field energy density has been studied in [45].

where $n(t)$ is the physical number density of the monopole pairs,

$$n(t) = \frac{1}{a(t)^3} \int_{-\infty}^{t} dt' a(t')^3 \Gamma(t'). \tag{7.5}$$

Hereafter we assume $n \propto a^{-3}$ at times $t > t_{\text{end}}$, namely, that there is no further monopole production after the magnetic fields have switched on. This is a good approximation also for monopoles produced by the magnetic field, since in such a case the monopole population is dominated by those produced at $t \sim t_{\text{end}}$, as we will discuss in the next section.

Using for $\Pi_{\text{red}}$ the definition in Eq. (7.3a), we can express the ratio $\Pi_{\text{acc}}/\Pi_{\text{red}}$ as:

$$\frac{\Pi_{\text{acc}}(t)}{\Pi_{\text{red}}(t)} = \frac{g}{B(t)H(t)} v(t)n(t). \tag{7.6}$$

In the case $\Pi_{\text{acc}}/\Pi_{\text{red}} \ll 1$ the solution of Eq. (7.2) gives simply $\rho_B \propto a^{-4}$, i.e. the energy density of the magnetic field redshifts as radiation. In the opposite case $\Pi_{\text{acc}}/\Pi_{\text{red}} \gg 1$, the back-reaction on the magnetic fields due to the monopole acceleration is non-negligible and the energy of the fields is transferred to the monopoles at a time scale shorter than the Hubble time.

While the monopoles interact with the plasma, the energy given to the monopoles by the magnetic fields is further passed on to the plasma. If the interactions are efficient and in the absence of mechanisms for the regeneration, the magnetic fields would quickly decay away. In this case, the condition $\Pi_{\text{acc}}/\Pi_{\text{red}} \gg 1$, corresponds to a rapid dispersion of the energy of the magnetic fields into the plasma and the disappearance of the fields. On the other hand, as discussed in [48, 58], if the interaction with the plasma is negligible, the kinetic energy of the monopoles is eventually transferred back to the magnetic fields, giving rise to oscillatory behaviors. Such oscillations can happen at late times, i.e. $T < 1$ MeV, after the cosmological $e^+e^-$ annihilation drastically reduces the number density of the scatterers, and possibly at early times when $v \simeq v_{\text{H}}$ and the interaction rate is negligible compared to the Hubble rate.

Without the necessity of specifying the production mechanism for the monopoles, it is then possible to give bounds on their number density from the persistence of the primordial magnetic fields still today. This can be done requiring that the condition $\Pi_{\text{acc}}/\Pi_{\text{red}} \ll 1$ holds when the interaction with the particles of the plasma is non-negligible[3].

As in the previous chapter, we first discuss the results for magnetic monopoles with order the Dirac charge. Then, we generalize the discussion to arbitrarily charged monopoles in the next section.

## 7.1 Bounds on magnetic monopoles with Dirac charge

We now describe the computations for the derivation of the bounds from the survival of the primordial magnetic fields for magnetic monopoles with Dirac charge.

---

[3]If the initial magnetic field is extremely strong, then the leftover after the damping by the monopoles may serve as the present-day cosmological magnetic fields. However we do not investigate such a possibility in this paper.
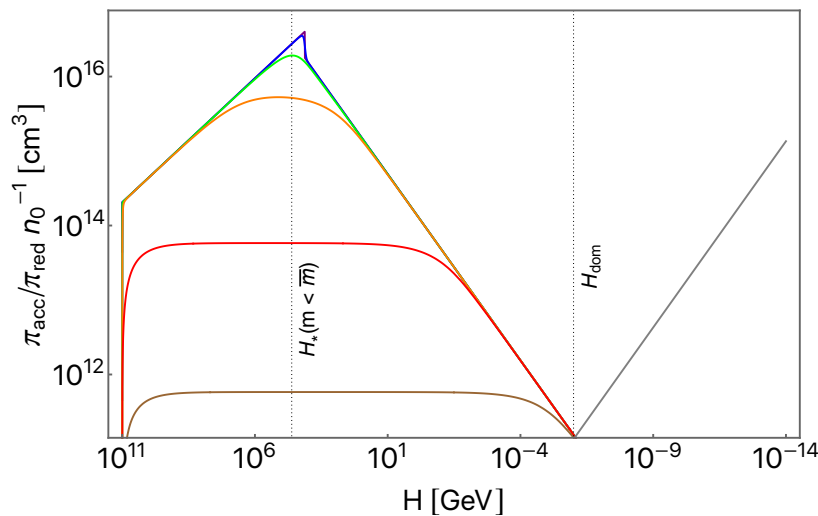
**Figure 7.1** Evolution of the monopole velocity in primordial magnetic fields (top) and of the normalized damping rate of the magnetic fields (bottom) for different values of the monopole mass (from bottom to top, brown: $m = 10^{19}$ GeV; red: $m = 10^{17}$ GeV; orange: $m = 10^{15}$ GeV; green: $m = 10^{14}$ GeV; blue: $m = 10^{13}$ GeV; purple: $m = 10^{11}$ GeV) and for magnetic charge $g = 2\pi/e$. The expression in Eq. (6.9) for the terminal velocity set by the friction with the thermal plasma is also shown in dashed line in the top plot. Here $H_{\mathrm{dom}} = 10^{-6}$ GeV, $B_0 = 10^{-15}$ G, $g_* = \mathcal{N}_c = 100$ and we use $H_{\mathrm{end}} = 10^{11}$ GeV as the starting point of the evolution. The value of $H_* \sim 10^5$ GeV for monopole masses smaller than $\bar{m}$ is also shown in the plots (see the text for details).

We show in Figure 7.1 the evolution of the ratio $\Pi_{\mathrm{acc}}/\Pi_{\mathrm{red}}$ from time $t_{\mathrm{end}}$ for different values of the mass. The monopole velocity necessary for computing $\Pi_{\mathrm{acc}}/\Pi_{\mathrm{red}}$ is taken from Figure 6.1, which was obtained by solving the equation of motion Eq. (6.6). We ignore back-reaction on the $B$ field and we apply the relations in Eq. (C.4) and Eq. (C.5) to rewrite all the quantities that present a time dependence in terms of $H(t)$. Since $\Pi_{\mathrm{acc}}/\Pi_{\mathrm{red}} \propto n$, we have normalized the value of $\Pi_{\mathrm{acc}}/\Pi_{\mathrm{red}}$ in the plot by $n_0$ so that its value is independent of the monopole number density today. The parameter choice and the mass for each colored curve are the same as for Figure 6.1. Notice that the blue and purple curves overlap with each other almost everywhere in the plot.

For $t > t_{\mathrm{dom}}$ the monopoles move at the terminal velocity set by the interactions with the plasma shown in Eq. (6.9). In this case the expression for the ratio is:

$$\frac{\Pi_{\mathrm{acc}}}{\Pi_{\mathrm{red}}} \simeq \frac{g^2}{f_{\mathrm{p}} H} n. \tag{7.7}$$

During radiation domination, the ratio constantly grows as $\Pi_{\mathrm{acc}}/\Pi_{\mathrm{red}} \propto a \propto H^{-1/2}$. Such behavior is shown in the right part of Figure 7.1 as the grey line and it is independent of the monopole mass.

For $t < t_{\mathrm{dom}}$, the time evolution can be more complicated and exhibits mainly three kinds of behaviors. The first case is realized for monopoles light enough to be initially accelerated to relativistic velocities, i.e. $v \simeq 1$. In this case the Hubble friction dominates over the friction from the plasma. As long as the monopoles

maintain a relativistic velocity, the expression for the ratio is:

$$\frac{\Pi_{\text{acc}}}{\Pi_{\text{red}}} \simeq \frac{g}{BH} n. \tag{7.8}$$

This ratio scales as $\Pi_{\text{acc}}/\Pi_{\text{red}} \propto a^{1/2} \propto H^{-1/3}$ and increases with time. Eq. (7.8) corresponds to the growing segments of the purple, blue, green, and orange curves in the left part of Figure 7.1. For the parameter choice in the plot, the velocity is relativistic soon after $t_{\text{end}}$ for $m \lesssim 10^{16}$ GeV.

The second case is when the Hubble friction is dominant over the plasma friction and the monopoles present non-relativistic velocities. In this case, the velocity is given by $v \sim gB/(mH)$ and the ratio is constant in time:

$$\frac{\Pi_{\text{acc}}}{\Pi_{\text{red}}} \simeq \frac{g^2}{mH^2} n. \tag{7.9}$$

This case corresponds to the horizontal segments of the brown, red, and orange curves of Figure 7.1.

The last case is realized when the monopoles achieve the terminal velocity set by the interaction with the plasma. The expression for the ratio in this case is the same as that in Eq. (7.7), but during reheating this scales as $\Pi_{\text{acc}}/\Pi_{\text{red}} \propto a^{-3/4} \propto H^{1/2}$, decreasing in time. This case is shown in Figure 7.1 as the decreasing segments of the colored curves.

During the reheating epoch, the $\Pi_{\text{acc}}/\Pi_{\text{red}}$ ratio given by monopoles with masses $m < \bar{m}$ is maximized at the time when the monopoles turn non-relativistic. On the other hand, for $m > \bar{m}$, the ratio $\Pi_{\text{acc}}/\Pi_{\text{red}}$ exhibits a plateau-like behavior while the monopole velocity follows $v_H$ and is non-relativistic.

In correspondence to the jump from a relativistic velocity to a non-relativistic velocity shown in Figure 6.1 for $m < \bar{m}$, a jump in the value of the ratio is seen in Figure 7.1 for the purple and blue curves. Such a jump corresponds to a sudden transition during reheating from the value of the ratio shown in Eq. (7.8) to that of Eq. (7.7).

Below we obtain bounds on the cosmic abundance of monopoles by requiring that $\Pi_{\text{acc}}/\Pi_{\text{red}}$ stays smaller than unity during radiation domination and reheating.

### 7.1.1 Radiation-dominated epoch

The analysis that we present for the bound during radiation domination follows the work in [58]. For times $t > t_{\text{dom}}$, we express the value of $\Pi_{\text{acc}}/\Pi_{\text{red}}$ through the result shown in Eq. (7.7). Using the expression for $f_{\text{p}}$ given in Eq. (6.5), we can rewrite the ratio $\Pi_{\text{acc}}/\Pi_{\text{red}}$ as:

$$\frac{\Pi_{\text{acc}}}{\Pi_{\text{red}}} \simeq \frac{16\pi^2}{e^2 \mathcal{N}_c T^2 H} n. \tag{7.10}$$

Using $H \simeq (\pi/\sqrt{90}) g_*^{1/2} T^2 / M_{\text{Pl}}$, $n \propto a^{-3}$ and the relation between the scale factor and the temperature in Eq. (C.2), the expression for $\Pi_{\text{acc}}/\Pi_{\text{red}}$ becomes:

$$\frac{\Pi_{\text{acc}}}{\Pi_{\text{red}}} \simeq \frac{48\sqrt{10}\pi g_{*s} M_{\text{Pl}}}{e^2 \mathcal{N}_c g_*^{1/2} g_{*s,0}} \frac{n_0}{T_0^3} \frac{1}{T}, \tag{7.11}$$

where $g_{*s,0} \simeq 3.9$. As shown in Figure 7.1, the ratio increases with time during radiation domination. The expression in Eq. (6.5) for the friction assumes relativistic plasma particles, and hence our analysis is valid up to the time of $e^+ e^-$ annihilation, namely, when $T \sim 1$ MeV. After the annihilation, the number of charged particles in the plasma decreases by a factor $10^{-10}$ [140] and thus the monopoles cannot give away their energy effectively to the plasma. For this value of the temperature we have $\mathcal{N}_c \sim g_* \simeq g_{*s} \simeq 10.75$. Therefore, the maximum value of the ratio during radiation domination is:

$$\frac{\Pi_{\text{acc}}}{\Pi_{\text{red}}}(T = 1 \text{ MeV}) \simeq \frac{n_0}{10^{-21} \text{ cm}^{-3}}. \tag{7.12}$$

The survival of the primordial magnetic field then requires $\Pi_{\text{acc}}/\Pi_{\text{red}}(T = 1 \text{ MeV}) \lesssim 1$. This yields the Primordial Parker Bound of [58]:

$$n_0 \lesssim 10^{-21} \text{ cm}^{-3}. \tag{7.13}$$

The bound does not depend on $B_0$, $g$, or $m$. It should also be noted that this is a bound on the average monopole number density in the universe.

Introducing the flux of monopoles at time $t$ as $F(t) = n(t)v(t)/4\pi$, we can express the above bound in terms of the present-day monopole flux $F_0$:

$$F_0 \lesssim 10^{-15} \text{ cm}^{-2}\text{sr}^{-1}\text{s}^{-1} \left( \frac{v_0}{10^{-3}} \right). \tag{7.14}$$

Here, we use the virial velocity in the Galaxy $10^{-3}$ as a reference value [47], although as we mentioned above this result applies to the average monopole flux in the universe. Let us also notice that we define the flux as that of only monopoles (or antimonopoles) and thus our results differ by a factor 2 from those for the flux of both monopoles and antimonopoles. However, such a difference is negligible for the order-of-magnitude bounds we derive in this work.

Strictly speaking, the above analysis is valid only for monopoles with sub-Planckian masses, cf. Eq. (6.10). For monopoles that present masses $m > M_{\text{Pl}}\mathcal{N}_c/g_*^{1/2}$, the Hubble friction term of the equation of motion is dominant over the drag force of the plasma even during radiation domination. Such monopoles never achieve the terminal velocity set by the plasma, and hence the bound in Eq. (7.14) must be modified.

### 7.1.2 Reheating epoch

Bounds on the monopole number density can also be derived based on the survival of primordial magnetic fields during the reheating epoch. Here we assume the cosmological plasma during reheating to be in thermal equilibrium, however let us remark that this assumption leads to a conservative bound on the monopole abundance. Without the assumption of thermal equilibrium, the number density of the particles of the plasma is not related to the mean energy of the particles. Inflaton decay results in an initially dilute plasma that contains a small number of very energetic particles that are not in thermal equilibrium [141]. Under these conditions the monopoles are more easily accelerated by the magnetic fields than in

the case of thermal equilibrium.[4] Thus, the drag force is smaller and the monopole velocity larger. Hence, the damping rate of the magnetic field, $\Pi_{\mathrm{acc}} \propto v$, turns out to be larger than in the case of thermal equilibrium, and the resulting bound on the monopole abundance can become stronger. We leave the case of a non-thermal plasma for future analysis.

As discussed below Eq. (7.6), the survival of the primordial magnetic fields requires the condition $\Pi_{\mathrm{acc}}/\Pi_{\mathrm{red}} \ll 1$ to be satisfied while the monopoles frequently interact with the plasma particles. Hence we can restrict ourselves to times when the monopole velocity is controlled by the plasma friction, instead of the Hubble friction[5]. And since we are interested in times after the magnetic fields have been generated, we focus on the regime $\max\{t_*, t_{\mathrm{end}}\} \le t \le t_{\mathrm{dom}}$, where $t_*$ is defined in Eq. (6.15). The expression for $\Pi_{\mathrm{acc}}/\Pi_{\mathrm{red}}$ during this regime is given in Eq. (7.7), which decreases with the Hubble scale as $\propto H^{1/2}$. Therefore, in order to derive the strongest bound from the reheating epoch, we should evaluate $\Pi_{\mathrm{acc}}/\Pi_{\mathrm{red}}$ at $t = \max\{t_*, t_{\mathrm{end}}\}$.[6]

Considering that $n \propto a^{-3}$, the expression for the value of the ratio at $t = \max\{t_*, t_{\mathrm{end}}\}$ is:

$$\frac{\Pi_{\mathrm{acc}}}{\Pi_{\mathrm{red}}}(t = \max\{t_*, t_{\mathrm{end}}\}) \simeq \frac{16\pi^2}{e^2 \mathcal{N}_{c,\mathrm{dom}} H_{\mathrm{dom}}^{3/2} T_{\mathrm{dom}}^2} \left(\frac{a_0}{a_{\mathrm{dom}}}\right)^3 (\min\{H_*, H_{\mathrm{end}}\})^{1/2} n_0. \tag{7.15}$$

Now we derive the bounds on the monopole abundance in both the cases $H_{\mathrm{end}} < H_*$ and $H_{\mathrm{end}} > H_*$. Once the value of $H_*$ is fixed, the bound in the case $H_{\mathrm{end}} < H_*$ is always weaker than the bound for $H_{\mathrm{end}} > H_*$.

**Case with $\mathbf{H_{end} < H_*}$**

For $H_{\mathrm{end}} < H_*$, we rewrite the condition $\Pi_{\mathrm{acc}}/\Pi_{\mathrm{red}} \lesssim 1$ on Eq. (7.15) as a bound on the average monopole number density in the present universe using the relations in Eq. (C.5):

$$n_0 \lesssim 10^{-16} \text{ cm}^{-3} \left(\frac{\mathcal{N}_{c,\mathrm{dom}}}{100}\right) \left(\frac{T_{\mathrm{dom}}}{10^6 \text{ GeV}}\right)^2 \left(\frac{10^4 \text{ GeV}}{H_{\mathrm{end}}}\right)^{1/2}. \tag{7.16}$$

As a reference value for $H_{\mathrm{end}}$, here we chose $10^4$ GeV which is the reference value for $H_*$ in Eq. (6.25). We express the result also in terms of the monopole flux today:

$$F_0 \lesssim 10^{-10} \text{ cm}^{-2}\mathrm{sr}^{-1}\mathrm{s}^{-1} \left(\frac{v_0}{10^{-3}}\right) \left(\frac{\mathcal{N}_{c,\mathrm{dom}}}{100}\right) \left(\frac{T_{\mathrm{dom}}}{10^6 \text{ GeV}}\right)^2 \left(\frac{10^4 \text{ GeV}}{H_{\mathrm{end}}}\right)^{1/2}. \tag{7.17}$$

---

[4]The rough estimate of the drag force is $f_{\mathrm{p}} \sim n\sigma\Delta p$, where $\sigma \sim e^2 g^2 E^{-2}$ is the cross section of the interaction with the particles of the plasma with mean energy $E$ and $\Delta p \sim E$ is the exchanged momentum. Since the number density $n$ is smaller and $\sigma\Delta p \propto E^{-1}$, the drag force is also smaller in the absence of thermal equilibrium.

[5]If $\Pi_{\mathrm{acc}}/\Pi_{\mathrm{red}} > 1$ during $t < t_*$, the energy rapidly oscillates between the magnetic field and monopoles, whose effect is to modify the redshifting of the magnetic energy density from the usual $\rho_{\mathrm{B}} \propto a^{-4}$ [58].

[6]For $m < \bar{m}$, the ratio $\Pi_{\mathrm{acc}}/\Pi_{\mathrm{red}}$ actually continues to increase after $t = t_*$ for about a Hubble time. However, we use simply Eq. (7.7) to derive our bound because the value of the ratio does not change substantially within a Hubble time. This leads to a conservative bound on the monopole abundance.

**Case with $H_{end} > H_*$**

We get a bound for the average monopole number density in the present universe applying the condition $\Pi_{acc}/\Pi_{red} \lesssim 1$ on Eq. (7.15) to the case $H_{end} > H_*$ and using the expression for $H_*$ shown in Eq. (6.25):

$$
n_0 \lesssim
\begin{cases}
10^{-16} \text{ cm}^{-3} \left( \dfrac{B_0}{10^{-15} \text{ G}} \right)^{3/5} \left( \dfrac{T_{dom}}{10^6 \text{ GeV}} \right) \left( \dfrac{10}{g} \right)^{3/5} & , \quad m \ll \bar{m}, \\[3mm]
10^{-16} \text{ cm}^{-3} \left( \dfrac{m}{10^{14} \text{ GeV}} \right) \left( \dfrac{T_{dom}}{10^6 \text{ GeV}} \right) \left( \dfrac{10}{g} \right)^{2} & , \quad m \gg \bar{m}.
\end{cases}
\tag{7.18}
$$

Here we drop the dependence on $\mathcal{N}_{c,dom}$, because the final results depend weakly on its value. The bound for the monopole flux today is:

$$
F_0 \lesssim
\begin{cases}
10^{-10} \text{ cm}^{-2}\text{sr}^{-1}\text{s}^{-1} \left( \dfrac{v_0}{10^{-3}} \right) \left( \dfrac{B_0}{10^{-15} \text{ G}} \right)^{3/5} \left( \dfrac{T_{dom}}{10^6 \text{ GeV}} \right) \left( \dfrac{10}{g} \right)^{3/5} & , \quad m \ll \bar{m}, \\[3mm]
10^{-10} \text{ cm}^{-2}\text{sr}^{-1}\text{s}^{-1} \left( \dfrac{v_0}{10^{-3}} \right) \left( \dfrac{m}{10^{14} \text{ GeV}} \right) \left( \dfrac{T_{dom}}{10^6 \text{ GeV}} \right) \left( \dfrac{10}{g} \right)^{2} & , \quad m \gg \bar{m}.
\end{cases}
\tag{7.19}
$$

Recall that $\bar{m}$ divides monopoles that are relativistic ($m \ll \bar{m}$) or non-relativistic ($m \gg \bar{m}$) when the interactions with the plasma become important. For $m \ll \bar{m}$ the bound depends on the value of the magnetic field today, while it is independent of the monopole mass. On the contrary, for $m \gg \bar{m}$ the result is independent of $B_0$, while it is proportional to the mass of the monopoles.

In Figure 7.2 we compare various upper bounds on the monopole flux today as functions of the monopole mass. The blue curves show the bounds that we derived in Eq. (7.19) from the survival of the primordial magnetic fields during reheating for three different values of $T_{dom} = 100$ MeV (solid curve), 100 GeV (dashed curve), $10^5$ GeV (dotted curve). The red line shows the bound in Eq. (7.14) from the survival of primordial magnetic fields during radiation domination, which was first obtained in [58]. The orange line corresponds to the original Parker bound from the survival of the Galactic magnetic field [48]. The pink line corresponds to the "extended Parker bound" that has been derived from the survival of the Galactic seed field by [51].[7] The black line shows the limit obtained by the MACRO experiment [30], which corresponds to the strongest bound from the direct search of non-relativistic monopoles. The dashed grey line shows the cosmological abundance bound from the requirement that the monopole energy density is smaller than the total energy density of the universe [8, 47]. In the plot we assume $g = 2\pi/e$, $B_0 = 10^{-15}$ G and the reference value of the monopole velocity today $v_0 = 10^{-3}$.

In the plot we have displayed the various bounds for comparison purpose, however we should remark that their targets are different: the bounds based on primordial magnetic fields and the relic abundance constrain the average monopole number density in the universe, while the bounds from Galactic fields (the original and

---

[7]The original and extended Parker bounds in the large $m$ region (where the bounds grow with $m$) are independent of the magnetic field strength, and thus should be equivalent if the other parameters are the same. The lines in the plot do not coincide because they exhibit the results presented in [48] and [51], which use slightly different values for the parameters, as well as different rounding methods.
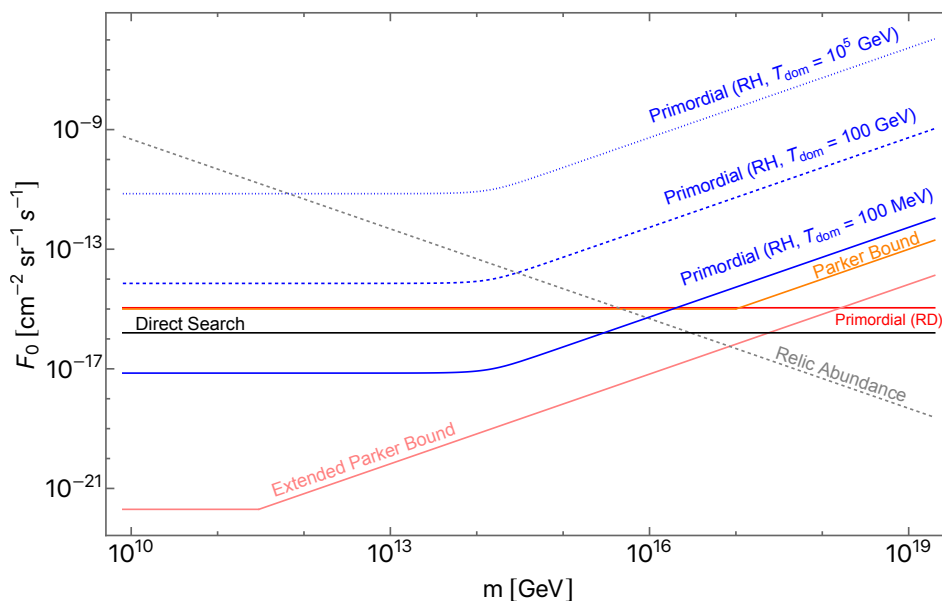
**Figure 7.2** Upper bounds on the magnetic monopole flux today. Here $g = 2\pi/e$, $B_0 = 10^{-15}$ G and $v_0 = 10^{-3}$. Blue: bounds from primordial magnetic fields during the reheating epoch shown in Eq. (7.19), for reheating temperatures $T_{\rm dom} = 100$ MeV (solid curve), 100 GeV (dashed curve), $10^5$ GeV (dotted curve). Red: the bound from primordial magnetic fields during radiation domination shown in Eq. (7.14). Orange: the original Parker bound. Pink: the extended Parker bound. Black: direct search limit from the MACRO experiment. Dashed grey: the cosmological abundance bound.

extended Parker bounds) and direct searches constrain the monopole density inside the Galaxy. If the monopoles are clustered with the Galaxy, their local density in the Galaxy can be significantly larger than the average density in the universe; in such a case the bounds on the local density translate into much stronger bounds on the average density.

As shown in the plot, for a sufficiently small $T_{\rm dom}$, our bound in Eq. (7.19) from the analysis during reheating becomes stronger than the original Parker bound and the limits from direct searches. For a GUT scale monopole, our bound is comparable to the original Parker bound for $T_{\rm dom} \sim 1$ GeV. The bound during reheating can also be stronger than that during radiation domination, Eq. (7.14), for $T_{\rm dom} \lesssim 10$ GeV and in the low-mass range.

## 7.2 Generalization to arbitrarily charged monopoles

In this section, we extend the computations for the bounds from primordial magnetic fields to allow for the monopoles to carry an arbitrarily magnetic charge.

As in the previous section, we require that the condition $\Pi_{\rm acc}/\Pi_{\rm red} \ll 1$ holds during the period from the end of magnetogenesis, $t = t_{\rm end}$, to $e^+e^-$ annihilation. This condition corresponds to having negligible backreaction on the primordial magnetic fields from the monopole acceleration. In order to rewrite such a condition as a bound on the monopole abundance, we use the results for the evolution of the

monopole velocity in the early universe as described in Section 6.2. We show in Figure 7.3 the time evolution of the ratio $\Pi_{\mathrm{acc}}/\Pi_{\mathrm{red}}$ from the end of magnetogenesis to the time of $e^+ e^-$ annihilation. In Figure 7.3a we fix the monopole charge to $g = 10^{-3} g_{\mathrm{D}}$, while the mass is varied as $m = 10^{19}\,\mathrm{GeV}$ (red), $10^{16}\,\mathrm{GeV}$ (orange), $10^{13}\,\mathrm{GeV}$ (green), $10^{10}\,\mathrm{GeV}$ (blue), $10^{7}\,\mathrm{GeV}$ (purple). In Figure 7.3b we fix the monopole mass to $m = 10^{11}\,\mathrm{GeV}$ while the charge is varied as $g = g_{\mathrm{D}}$ (red), $10^{-3} g_{\mathrm{D}}$ (orange), $10^{-6} g_{\mathrm{D}}$ (green), $10^{-9} g_{\mathrm{D}}$ (blue), $10^{-12} g_{\mathrm{D}}$ (purple). The monopole velocity necessary for computing $\Pi_{\mathrm{acc}}/\Pi_{\mathrm{red}}$ is taken from Figure 6.2, which was obtained by solving the equation of motion Eq. (6.6). Since $\Pi_{\mathrm{acc}}/\Pi_{\mathrm{red}} \propto n$, we have normalized the value of $\Pi_{\mathrm{acc}}/\Pi_{\mathrm{red}}$ in the plot by $n_0$ so that its value is independent of the monopole number density today. The parameter choice and the mass for each colored curve are the same as for Figure 6.2. Notice that the blue and purple curves overlap with each other almost everywhere in the upper plot, and the red and orange in the right part of the lower plot.

As in the previous section, below we obtain bounds on the cosmic abundance of arbitrarily charged monopoles by requiring that $\Pi_{\mathrm{acc}}/\Pi_{\mathrm{red}}$ stays smaller than unity during radiation domination and reheating.

### 7.2.1 Radiation-dominated epoch

We start by analyzing the backreaction of monopoles on primordial magnetic fields during the radiation-dominated epoch. Neglecting the time dependence of $g_{*(s)}$ and $\mathcal{N}_c$, then during radiation domination the Hubble rate redshifts as $H \propto a^{-2}$, and the temperature of the plasma as $T \propto a^{-1}$. These, together with $B \propto a^{-2}$, render both $v_{\mathrm{p}}$ and $v_{\mathrm{H}}$ constant in time. The monopoles during radiation domination thus move with a constant velocity.

With constant velocities the dissipation rate ratio grows as $\Pi_{\mathrm{acc}}/\Pi_{\mathrm{red}} \propto a$. Thus, as for monopoles with a Dirac charge, requiring negligible monopole backreaction while there are abundant charged particles in the universe amounts to demanding that this ratio is smaller than unity at $e^+ e^-$ annihilation, i.e.,

$$\left( \frac{\Pi_{\mathrm{acc}}}{\Pi_{\mathrm{red}}} \right)_{T \sim 1\,\mathrm{MeV}} < 1. \tag{7.20}$$

This also means that the bounds we derive in this section apply as long as the primordial magnetic fields have been generated before $e^+ e^-$ annihilation.

In the case of $g > g_{\mathrm{min}}$, the ratio $\Pi_{\mathrm{acc}}/\Pi_{\mathrm{red}}$ is evaluated by substituting $v = v_{\mathrm{p}}$ into Eq. (7.6) and the result is the same than that for Dirac charged monopoles. Hence, the condition in Eq. (7.20) can be rewritten as,

$$n_0 \lesssim 10^{-21}\,\mathrm{cm}^{-3}, \tag{7.21}$$

or in terms of the present-day monopole flux $F = n_0 v_0 / 4\pi$:

$$F \lesssim 10^{-14}\,\mathrm{cm}^{-2}\mathrm{sr}^{-1}\mathrm{s}^{-1} \left( \frac{v_0}{10^{-3}} \right). \tag{7.22}$$

The bound is mainly determined by the temperature and redshift at $e^+ e^-$ annihilation, and thus is independent of the amplitude of the magnetic fields and of the

**(a)** $g = 10^{-3}g_D$ with varying $m$.



**(b)** $m = 10^{11}$ GeV with varying $g$.
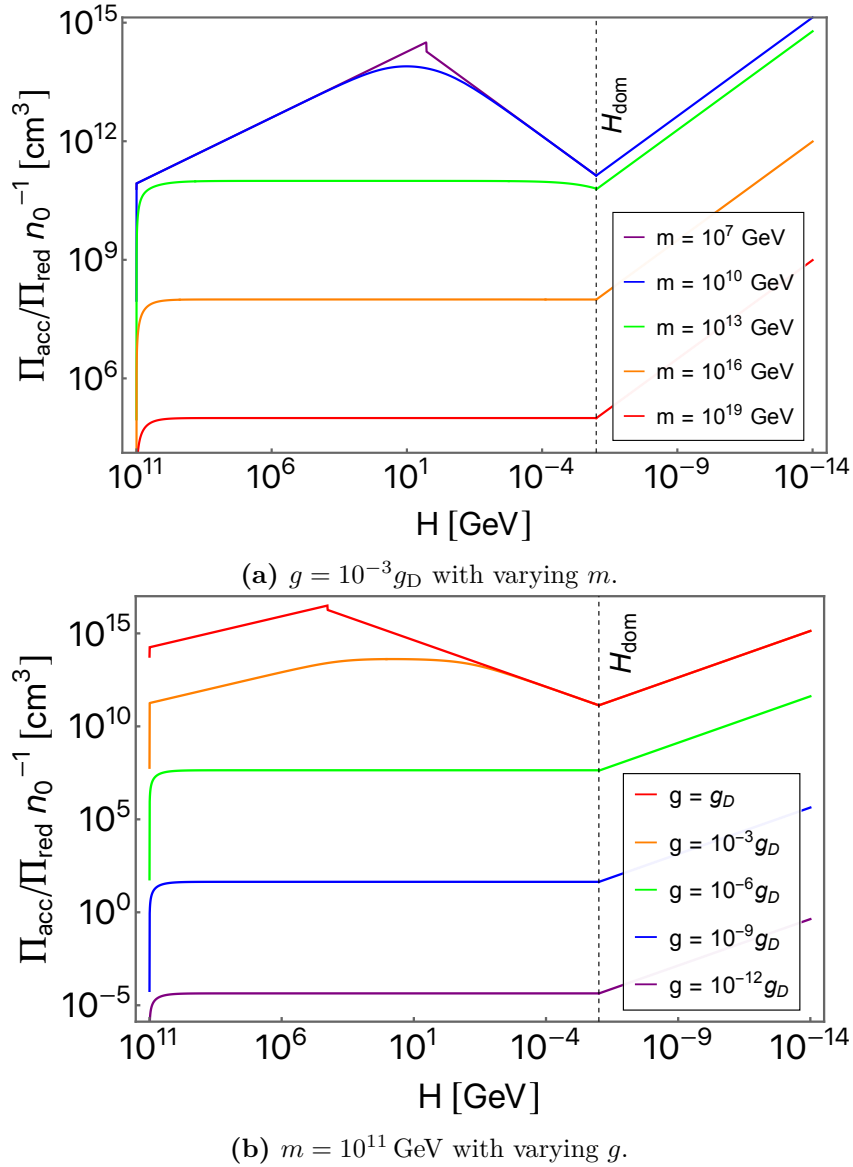
**Figure 7.3** Time evolution of the normalized dissipation rate of the magnetic fields due to monopole acceleration. The Hubble scales at the end of magnetogenesis and at the onset of radiation domination are taken respectively as $H_{\mathrm{end}} = 10^{11}$ GeV and $H_{\mathrm{dom}} = 10^{-6}$ GeV. The present-day magnetic field strength is taken as $B_0 = 10^{-15}$ G. The numbers of relativistic (charged) degrees of freedom are fixed to $g_* = \mathcal{N}_c = 100$. In the upper panel, the charge of the monopole is fixed to $g = 10^{-3}g_D$ while the mass is varied as $m = 10^{19}$ GeV (red), $10^{16}$ GeV (orange), $10^{13}$ GeV (green), $10^{10}$ GeV (blue), $10^7$ GeV (purple), from bottom to top. In the bottom panel the mass is fixed to $m = 10^{11}$ GeV while the charge is varied as $g = g_D$ (red), $10^{-3}g_D$ (orange), $10^{-6}g_D$ (green), $10^{-9}g_D$ (blue), $10^{-12}g_D$ (purple), from top to bottom.

mass and the charge of the monopoles. However, the red region in Figure 6.3 where the bound can be applied ($g > g_{\min}$) becomes smaller for stronger magnetic fields.

In the case of $g < g_{\min}$, the monopoles do not efficiently transfer the magnetic

energy to the plasma. Hence their presence does not lead to the dissipation of primordial magnetic fields, but can only induce oscillations of the fields and affect their redshift evolution. In order for the fields' redshifting to be unaltered by monopoles, the condition $\Pi_{\mathrm{acc}}/\Pi_{\mathrm{red}} < 1$ should hold all the way until today. However, in order to connect with the bounds we derived for $g > g_{\mathrm{min}}$, here let us only require the redshifting to be unaltered at temperatures $T > 1\,\mathrm{MeV}$ and impose Eq. (7.20). We further limit our analysis to nonrelativistic monopoles, i.e. $(\gamma v)_{\mathrm{H}} \lesssim 1$, which from Eq. (6.36) is equivalent to considering masses of:

$$ m \gtrsim 10^{10}\,\mathrm{GeV} \left( \frac{g}{g_{\mathrm{D}}} \right) \left( \frac{B_0}{10^{-15}\,\mathrm{G}} \right). \tag{7.23} $$

(We are thus focusing on the region in Figure 6.3 on the right of both the purple and gray dashed lines.) Then the dissipation rate ratio can be evaluated by substituting $v = v_{\mathrm{H}} \sim gB/mH$ into Eq. (7.6), and the condition of Eq. (7.20) translates into:

$$ n_0 \lesssim 10^{-22}\,\mathrm{cm}^{-3} \left( \frac{m}{10^{17}\,\mathrm{GeV}} \right) \left( \frac{g}{g_{\mathrm{D}}} \right)^{-2}. \tag{7.24} $$

The condition in terms of the present-day monopole flux is:

$$ F \lesssim 10^{-16}\,\mathrm{cm}^{-2}\mathrm{sr}^{-1}\mathrm{s}^{-1} \left( \frac{m}{10^{17}\,\mathrm{GeV}} \right) \left( \frac{g}{g_{\mathrm{D}}} \right)^{-2} \left( \frac{v_0}{10^{-3}} \right). \tag{7.25} $$

## 7.2.2 Reheating epoch

We now discuss the bounds from the reheating epoch generalizing the results of Section 7.1.2 to arbitrarily charged monopoles. For simplicity, here we discuss only the case $H_{\mathrm{end}} > H_*$.

During reheating the universe is effectively matter-dominated, and the Hubble rate redshifts as $H \propto a^{-3/2}$. The final results of this section depend only mildly on the numbers of relativistic degrees of freedom. Thus, for simplicity we ignore their time dependences and use $g_{*(s)} \sim \mathcal{N}_c \sim 100$ in the following analyses. We also assume the plasma particles to be in thermal equilibrium during reheating. Under these assumptions, the temperature of the primordial plasma redshifts as $T \propto a^{-3/8}$ [47]. Consequently, the plasma-induced terminal velocity scales as $v_{\mathrm{p}} \propto a^{-5/4}$, and the Hubble-induced terminal velocity scales as $(\gamma v)_{\mathrm{H}} \propto a^{-1/2}$; the redshifting of the former being faster is related to the fact that the monopole velocity during reheating can make a transition from $v_{\mathrm{H}}$ to $v_{\mathrm{p}}$ but not vice versa [1], as was shown in Figure 6.2. Combining this with the discussion in the previous chapter, we see that monopoles make the transition to the $v_{\mathrm{p}}$-branch before reheating completes if the charge satisfies $g > g_{\mathrm{min}}$, with $g_{\mathrm{min}}$ given in Eq. (6.34).

For the case of $g > g_{\mathrm{min}}$, we refer to the computation in Sections 6.1.2 and 7.1.2, where we have defined $t_*$ as the time when the plasma friction takes over the Hubble friction, i.e. $f_{\mathrm{p}*} = mH_*\gamma_{\mathrm{H}*}$. For $t < t_*$ the monopoles move at the terminal velocity $v_{\mathrm{H}}$, while for $t > t_*$ the monopoles follow $v_{\mathrm{p}}$. The balance of the frictional forces is written as Eq. (6.31), which transform into an equation for $H_*$ as in Eq. (6.18) by considering that $f_{\mathrm{p}} \propto H^{1/2}$ and $B \propto H^{4/3}$.

The relation $H_* > H_{\text{dom}}$ holds if $g > g_{\text{min}}$ and therefore it is always possible to derive a bound during the reheating epoch. While monopoles carrying such a charge move at the velocity $v_{\text{p}}$ and transfer the magnetic field energy into the plasma, the dissipation ratio decreases in time as $\Pi_{\text{acc}}/\Pi_{\text{red}} \propto a^{-3/4}$ (this behavior is shown in Figure 7.3a by the middle parts of the blue and purple lines). Hence requiring that the fields survive during reheating amounts to imposing

$$\left(\frac{\Pi_{\text{acc}}}{\Pi_{\text{red}}}\right)_* < 1. \tag{7.26}$$

Combining this with $v = v_{\text{p}}$ and Eq. (6.25) yields a bound on the monopole abundance that has the same expression than the one in Eq. (6.22), which we report here for simplicity[8]

$$n_0 \lesssim \max.\left\{10^{-16}\,\text{cm}^{-3}\left(\frac{g}{g_{\text{D}}}\right)^{-3/5}\left(\frac{B_0}{10^{-15}\,\text{G}}\right)^{3/5}\left(\frac{T_{\text{dom}}}{10^6\,\text{GeV}}\right),\right.$$
$$\left. 10^{-13}\,\text{cm}^{-3}\left(\frac{m}{10^{17}\,\text{GeV}}\right)\left(\frac{g}{g_{\text{D}}}\right)^{-2}\left(\frac{T_{\text{dom}}}{10^6\,\text{GeV}}\right)\right\}. \tag{7.27}$$

The first (second) line sets the condition when $m$ is smaller (larger) than $\bar{m}$ given in Eq. (6.22). We show also the condition in terms of the present monopole flux:

$$F \lesssim \max.\left\{10^{-10}\,\text{cm}^{-2}\text{sr}^{-1}\text{s}^{-1}\left(\frac{g}{g_{\text{D}}}\right)^{-3/5}\left(\frac{B_0}{10^{-15}\,\text{G}}\right)^{3/5}\left(\frac{T_{\text{dom}}}{10^6\,\text{GeV}}\right)\left(\frac{v_0}{10^{-3}}\right),\right.$$
$$\left. 10^{-7}\,\text{cm}^{-2}\text{sr}^{-1}\text{s}^{-1}\left(\frac{g}{g_{\text{D}}}\right)^{-2}\left(\frac{m}{10^{17}\,\text{GeV}}\right)\left(\frac{T_{\text{dom}}}{10^6\,\text{GeV}}\right)\left(\frac{v_0}{10^{-3}}\right)\right\}. \tag{7.28}$$

As already discussed, the bounds in Eqs. (7.27) and (7.28) assume that the velocity transition happens during the reheating epoch, and in particular after the primordial magnetic fields are generated, hence

$$H_* < H_{\text{end}}, H_{\text{inf}}. \tag{7.29}$$

Here $H_{\text{inf}}$ is the inflationary Hubble rate, which is constrained by current observational limits on primordial gravitational waves as [142]

$$H_{\text{inf}} \lesssim 10^{14}\,\text{GeV}. \tag{7.30}$$

Thus the condition of Eq. (7.29) would be violated if $H_*$ becomes very large, for instance due to a large $T_{\text{dom}}$. We also remember that for magnetic fields generated at the end of inflation or during reheating, requiring that they have never dominated the universe yields a constraint on the scale of magnetogenesis as in Eq. (6.28). For $B_0 \sim 10^{-15}\,\text{G}$ and $g \lesssim g_{\text{D}}$, there is a wide range for $H_{\text{end}}$ where both this and (7.29) are satisfied. However, this constraint can become relevant for magnetic black holes,

---

[8]For $m \ll \bar{m}$, the ratio $\Pi_{\text{acc}}/\Pi_{\text{red}}$ undergoes a jump shortly after $t_*$ (cf. purple line in Figure 7.3a). By plugging $v = v_{\text{p}}$, here we are approximately evaluating the value of $\Pi_{\text{acc}}/\Pi_{\text{red}}$ after the jump.

as we will later see. As we have analyzed in Section 7.1.2, if the fields are generated after $t_*$, i.e. $H_{\text{end}} < H_*$ then the monopole bound becomes weaker. However, we do not discuss again this possibility for arbitrarily charged monopoles.

If the charge is as small as $g < g_{\text{min}}$, the monopole velocity never approaches $v_{\text{p}}$. We can also derive the condition for such monopoles not to affect the redshifting of the magnetic fields during the reheating epoch. In this case the dissipation rate ratio is non-decreasing during reheating: It increases as $\Pi_{\text{acc}}/\Pi_{\text{red}} \propto a^{1/2}$ while the monopoles move at relativistic $v_{\text{H}}$, then stays constant after $v_{\text{H}}$ becomes nonrelativistic. Hence we impose the condition at the onset of radiation domination,

$$\left(\frac{\Pi_{\text{acc}}}{\Pi_{\text{red}}}\right)_{\text{dom}} < 1. \tag{7.31}$$

This condition assumes that the magnetic fields were produced before the radiation-dominated epoch begins. We further focus on monopoles that become nonrelativistic before $t_{\text{dom}}$, which amounts to considering masses satisfying the condition of Eq. (7.23). This allows us to plug $v_{\text{dom}} \sim (gB/mH)_{\text{dom}}$ into Eq. (7.31). One can check that the upper bound on the present-day monopole number density thus obtained is the same as the second line of Eq. (7.27), and the flux bound is the same as the second line of Eq. (7.28).

### 7.2.3 Summary of bounds from primordial magnetic fields

We have seen that the bounds on the monopole flux from the survival of primordial magnetic fields are described by Eq. (7.22) during radiation domination, and by Eq. (7.28) during reheating. The bounds are valid under the condition $g > g_{\text{min}}$, where the minimum magnetic charge $g_{\text{min}}$ is given in Eq. (6.34). The bound from radiation domination assumes that primordial magnetic fields are generated before $e^+e^-$ annihilation. For the bound from reheating it is further assumed that the scales of magnetogenesis $H_{\text{end}}$, inflation $H_{\text{inf}}$, and $H_*$ given in Eq. (6.25) satisfy the condition of Eq. (7.29); here $H_{\text{end}}$ is also constrained by Eq. (6.28), and $H_{\text{inf}}$ by Eq. (7.30).

The flux bound from radiation domination is independent of the amplitude of the magnetic fields and of the mass and the charge of the monopoles, although the minimum charge $g_{\text{min}}$ depends on the field strength and mass. The bound from reheating depends on a number of parameters, and in particular it becomes stronger for larger charges and lower reheating temperatures.

For monopoles with $g < g_{\text{min}}$, we derived conditions for them not to alter the redshifting of primordial magnetic fields.[9] Focusing on masses satisfying Eq. (7.23), the condition during radiation domination gives the flux bound in Eq. (7.25) (assuming magnetogenesis before $e^+e^-$ annihilation), and from reheating arises the bound which takes the same expression as the second line of Eq. (7.28) (assuming magnetogenesis before the radiation-dominated epoch begins). For these bounds, we stress that primordial magnetic fields can survive even if they are violated, however in such cases one needs to take into account the monopoles in order to assess the cosmological evolution of primordial magnetic fields.

---

[9]Monopoles with $g > g_{\text{min}}$ can also affect the magnetic redshifting, however we did not analyze this case.
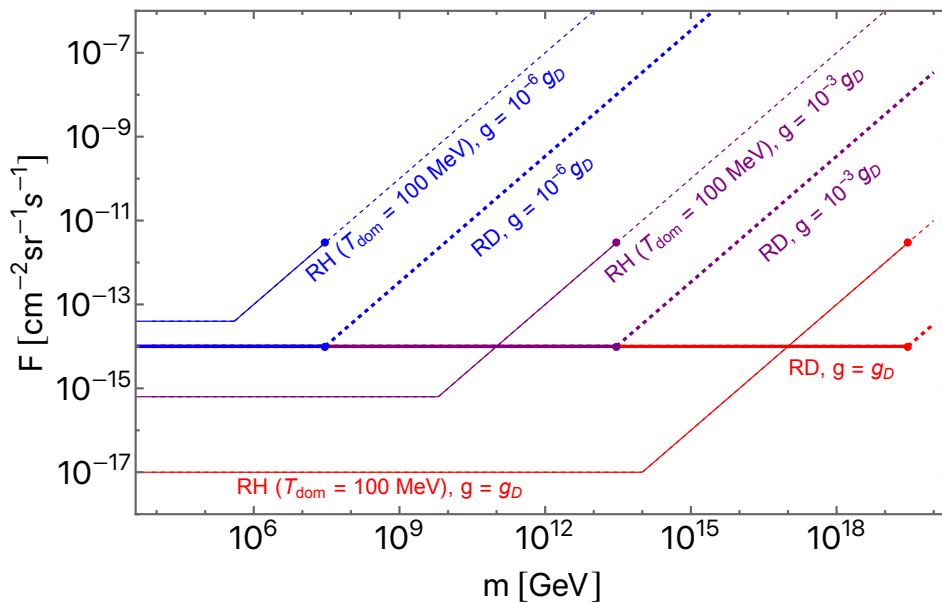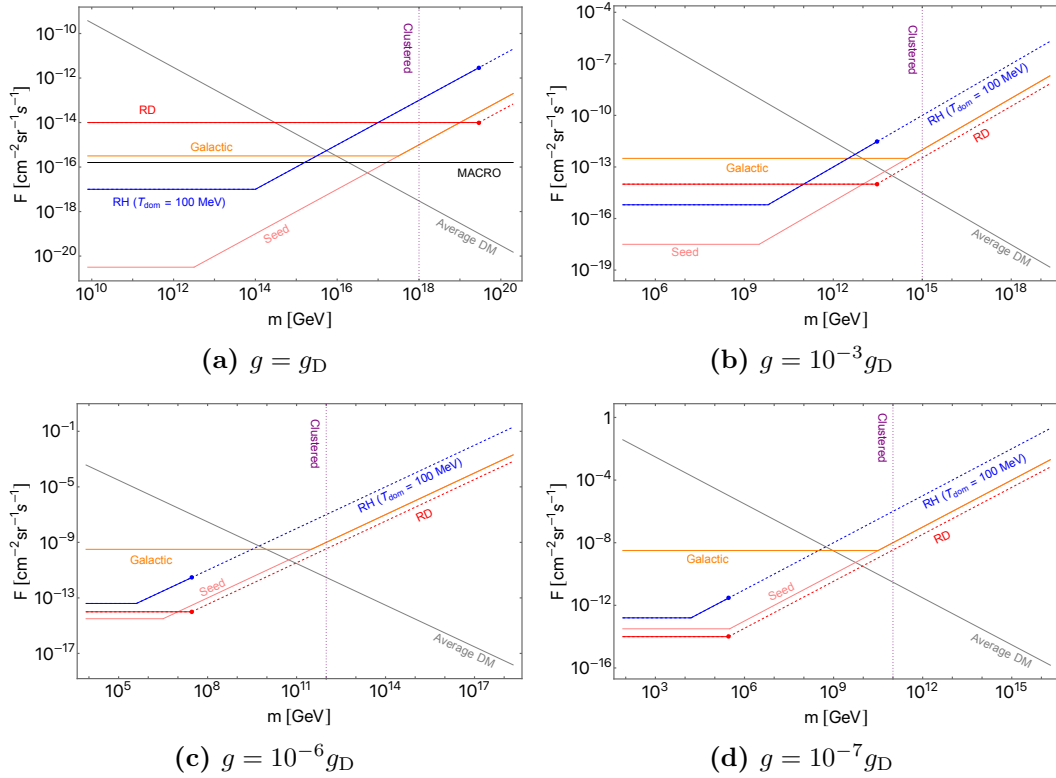
**Figure 7.4**  Upper bounds on the monopole flux as a function of mass, from the survival of primordial magnetic fields during radiation domination (thick lines) and reheating era (thin lines). The magnetic charge is varied as $g = g_{\mathrm{D}}$ (red), $10^{-3}g_{\mathrm{D}}$ (purple), $10^{-6}g_{\mathrm{D}}$ (blue). The dotted parts of the lines show where the fields exhibit modified redshifting behaviors, instead of being dissipated. The magnetic field strength is taken such that it realizes a present-day value of $B_0 = 10^{-15}\,\mathrm{G}$, and the monopole velocity today is fixed to $v_0 = 10^{-3}$. The reheating bounds assume a reheating temperature of $T_{\mathrm{dom}} = 100\,\mathrm{MeV}$.

In Figure 7.4 we show the upper bounds on the monopole flux from radiation domination (thick lines), and from reheating with $T_{\mathrm{dom}} = 100\,\mathrm{MeV}$ (thin lines). The magnetic charge is varied as $g = g_{\mathrm{D}}$ (red), $g = 10^{-3}g_{\mathrm{D}}$ (purple), and $g = 10^{-6}g_{\mathrm{D}}$ (blue). We have chosen a rather low reheating temperature just a few orders of magnitude above the scale of Big Bang Nucleosynthesis, as an optimal value for the reheating bound. The purple, blue, and red thick lines overlap in the left part of the plot. Here we assume $v_0 = 10^{-3}$, and $B_0 = 10^{-15}\,\mathrm{G}$. The solid parts of the lines are based on the survival of primordial fields ($g > g_{\mathrm{min}}$), while the dashed parts are from the requirement that the redshifting of the primordial fields is unaltered ($g < g_{\mathrm{min}}$). For the masses shown in the plot, $g_{\mathrm{min}}$ is given by the second line of (6.34), and thus the condition $g > g_{\mathrm{min}}$ can be rewritten as:

$$m \lesssim 10^{19}\,\mathrm{GeV}\left(\frac{g}{g_{\mathrm{D}}}\right)^2. \tag{7.32}$$

The points in the plot show where this bound is saturated. We also note that the parameters used for the plot allow for ranges of values for $H_{\mathrm{end}}$ and $H_{\mathrm{inf}}$ that satisfy the assumptions in Eqs. (7.29), (7.30), and (6.28). Moreover, the condition in Eq. (7.23) is satisfied on the dashed lines.

As shown in the plot, for $T_{\mathrm{dom}} = 100\,\mathrm{MeV}$ the bound from reheating is stronger than the bound from radiation domination at low masses, for $g \gtrsim 10^{-5}g_{\mathrm{D}}$. However for $T_{\mathrm{dom}} \gtrsim 10^2\,\mathrm{GeV}$, the bound from radiation domination becomes stronger than the bound from reheating even at $g = g_{\mathrm{D}}$. We stress again that the bound from

**Figure 7.5**   Upper bounds on the monopole flux as functions of mass, for different values of magnetic charge.  Gray: cosmological bound from comparison with the average dark matter density in the universe. Orange: bound from Galactic magnetic fields of $B = 10^{-6}$ G; the lower mass limit for monopoles to stay clustered with the Galaxy is shown by the vertical dotted line. Pink: bound from Galactic seed magnetic fields of $B = 10^{-11}$ G. Red: bound from primordial magnetic fields during radiation domination, with present-day strength $B_0 = 10^{-15}$ G. Blue: bound from primordial magnetic fields during reheating era, with present-day strength $B_0 = 10^{-15}$ G and reheating temperature $T_{\text{dom}} = 100$ MeV. For the primordial bounds, the dashed parts of the lines show where the fields exhibit modified redshifting behaviors, instead of being dissipated. The panel for $g = g_{\text{D}}$ also shows the limit from direct searches by the MACRO collaboration [30] in black. We assume $v_0 = 10^{-3}$ and for the Galactic parameters $l_{\text{c}} = 1$ kpc, $R = 10$ kpc, $\tau_{\text{gen}} = 10^8$ yr, and $\gamma_i - 1 = 10^{-6}$. See the text for details.

the survival of primordial fields during radiation domination does not weaken for smaller charges (although its range of applicability shrinks to smaller masses); this feature makes the radiation domination bound particularly useful for constraining minicharged monopoles.

## 7.2.4   Comparison of different types of Parker bounds

Let us now compare the various bounds presented in this chapter and in Chapter 4 for arbitrarily charged monopoles. In Figure 7.5 we show the upper bounds on the flux of magnetic monopoles as functions of the mass, for different values of the magnetic charge. The solid gray line shows the cosmological abundance bound in

Eq. (4.20) where $\rho_{DM}$ is taken as the average dark matter density in the universe, i.e. $\rho_{DM} = 1.3 \times 10^{-6}$ GeV cm$^{-3}$, along with $v_i = 10^{-3}$. The orange line shows the bound based on the survival of Galactic magnetic fields, using Eq. (4.13) and Galactic field strength $B = 10^{-6}$ G, along with the other parameters as $l_c = 1$ kpc, $R = 10$ kpc, $\tau_{gen} = 10^8$ yr, and $\gamma_i - 1 = 10^{-6}$. Using the same set of parameters, the dotted vertical line shows the lower mass limit in Eq. (4.8) for monopoles to be clustered with our Galaxy. The pink line shows the bound from seed Galactic fields, using again Eq. (4.13) but with the seed field assumed to be $B = 10^{-11}$ G; the other parameters are the same as the orange line. The pink and orange lines overlap on the right side of the plots. The red line shows the bounds in Eqs. (7.22) and (7.25)) from primordial magnetic fields during radiation domination. The blue line shows the bound in Eq. (7.28) from primordial magnetic fields during reheating, for $T_{dom} = 100$ MeV. For the primordial bounds we assume the present-day amplitude of the primordial magnetic fields to be $B_0 = 10^{-15}$ G, and monopole velocity $v_0 = 10^{-3}$; moreover the solid parts of the lines are based on the survival of the fields, while the dashed parts are from the requirement that the redshifting of the fields is unaltered. With $B_0 = 10^{-15}$ G, the smallest charge with which monopoles can dissipate primordial magnetic fields is of $10^{-8}g_D$, cf. Figure 6.3. As a value slightly above this, $g = 10^{-7}g_D$ is shown in panel 7.5d. In panel 7.5a for $g = g_D$, we also show in black the limit from direct searches by the MACRO collaboration [30].[10]

We see that monopoles with large masses are most strongly constrained by the cosmological abundance bound, while those with intermediate to low masses are mainly constrained by the Parker bounds. Which of the Parker bounds is most stringent for light monopoles depends on the charge. In particular, the bound from seed Galactic magnetic fields is by far the strongest for monopoles with a Dirac charge, while the primordial bounds become comparable or even stronger for monopoles with small magnetic charges. However, we also note that the seed field bound further improves at very small masses if the field strength is smaller than $B = 10^{-11}$ G used in the plots.[11]

In Figure 7.5 we have displayed the various bounds for comparison purpose. However, we should note that the target of each bound is not necessarily the same. The cosmological abundance bound and the primordial bounds constrain the average monopole density in the universe, while the Galactic bounds and the MACRO bound constrain the local monopole density inside the Galaxy. If monopoles are clustered with the Galaxy (although this can happen only in regions on the right of the dotted lines), their local density can be much higher than the average density; then the bounds on the local density translate into much stronger bounds on the average density.

For monopoles that can cluster with the Galaxy, namely, for masses larger than that indicated by the dotted lines, the cosmological abundance bound gives the strongest constraint. The situation is similar even when comparing with the local dark matter density; see Figure 4.1 and the discussion at the end of Section 4.1.3.

---

[10]We show here the MACRO limits extrapolated to arbitrarily light monopoles, without considering the discussion on the MACRO results presented in Chapter 5.

[11]We do not consider here the relaxation of the seed Parker bound due to monopole acceleration in IGMFs, as shown in Chapter 4.

In other words, monopoles that cluster with our Galaxy and whose density does not exceed that of dark matter almost automatically satisfy the Parker bounds. Hence monopoles in this mass region, if they can be produced, are a valid candidate of dark matter.

## 7.3 Magnetically charged extremal black holes

We now describe how the primordial bounds derived in this chapter can be applied to magnetically charged extremal primordial black holes. We then compare the bounds to those obtain from the survival of galactic magnetic fields, and discuss the implication on magnetic black holes as dark matter candidates.

Using the relation in Eq. (4.22), the terminal velocity set by the Hubble friction in Eq. (6.29) can be rewritten for extremal magnetic black holes as:

$$(\gamma v)_{\mathrm{H}} \sim \frac{B}{\sqrt{2} M_{\mathrm{pl}} H}.$$ (7.33)

Thus, under the condition that the magnetic fields do not dominate the universe, i.e. $\rho_{\mathrm{B}}/\rho_{\mathrm{tot}} \sim (B/(M_{\mathrm{pl}} H))^2 \ll 1$, the velocity $v_{\mathrm{H}}$ is always nonrelativistic, $(\gamma v)_{\mathrm{H}} \ll 1$. From this it also follows that extremal magnetic black holes satisfy the mass bound in Eq. (7.23). Notice that $(\gamma v)_{\mathrm{H}}$ does not depend on the black hole mass.

With $v_{\mathrm{H}}$ being nonrelativistic, the value of $g_{\mathrm{min}}$ is given by the second line of Eq. (6.34). Consequently, using the relation in Eq. (4.22) the condition $g > g_{\mathrm{min}}$ can be rewritten as:

$$m \gtrsim 10^{-3}\,\mathrm{gm}.$$ (7.34)

Extremal magnetic black holes with such masses are subject to the flux bound of Eq. (7.22) which is based on the survival of primordial fields during radiation domination.

Regarding the bound from the reheating epoch, we saw for generic monopoles that the second line of Eq. (7.28) applies at larger masses for which the monopoles are nonrelativistic upon making the transition from $v_{\mathrm{H}}$ to $v_{\mathrm{p}}$. However for extremal black holes, this instead applies at smaller masses, $m < \bar{m}_{\mathrm{BH}}$, with the threshold being

$$\bar{m}_{\mathrm{BH}} \sim 10^{10}\,\mathrm{gm} \left( \frac{B_0}{10^{-15}\,\mathrm{G}} \right)^{-3/2}.$$ (7.35)

One can also check that for $m > \bar{m}_{\mathrm{BH}}$, the scale $H_*$ which is given by the first line of Eq. (6.25), is comparable to or larger than the upper limit for $H_{\mathrm{end}}$ given in Eq. (6.28); hence the assumption in Eq. (7.29) breaks down. Therefore only the second line of the reheating bound in Eq. (7.28) applies for extremal black holes, which is rewritten as

$$F \lesssim 10^{-18}\,\mathrm{cm}^{-2}\mathrm{sr}^{-1}\mathrm{s}^{-1} \left( \frac{m}{10^{10}\,\mathrm{gm}} \right)^{-1} \left( \frac{T_{\mathrm{dom}}}{10^6\,\mathrm{GeV}} \right) \left( \frac{v_0}{10^{-3}} \right).$$ (7.36)

This bound applies to the mass range $10^{-3}\,\mathrm{gm} \lesssim m < \bar{m}_{\mathrm{BH}}$, given that the magnetogenesis and inflation scales satisfy the conditions in Eqs. (7.29), (7.30), and (6.28).
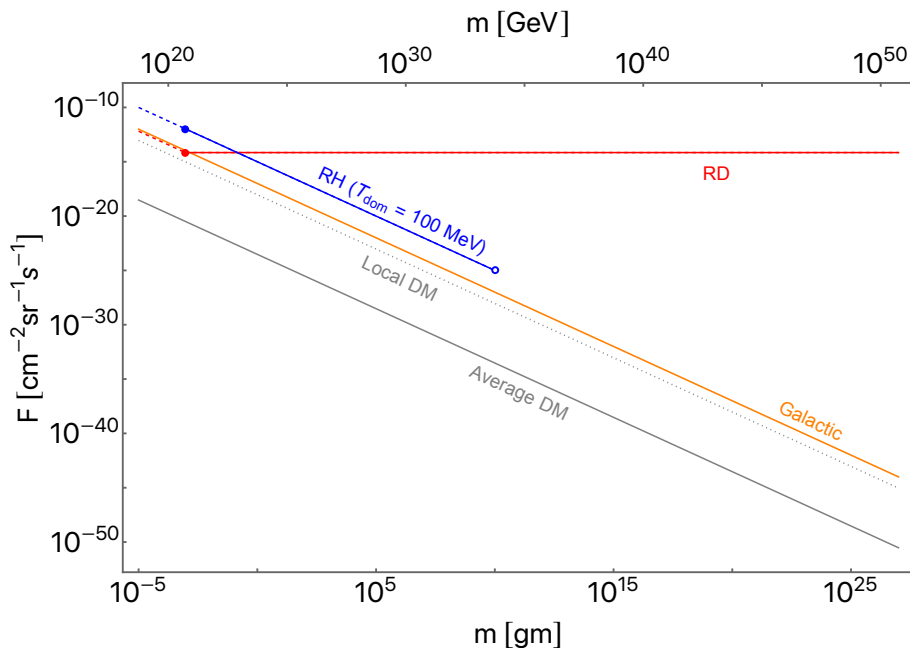
**Figure 7.6** Upper bounds on the flux of extremal magnetic black holes. Gray solid: abundance bound from comparison with the average dark matter density in the universe. Gray dotted: abundance bound from comparison with the local dark matter density in our Galaxy. Orange: bound from Galactic magnetic fields. Red: bound from primordial magnetic fields during radiation domination, with present-day strength $B_0 = 10^{-15}$ G. Blue: bound from primordial magnetic fields during reheating, with present-day strength $B_0 = 10^{-15}$ G and reheating temperature $T_{\text{dom}} = 100$ MeV. For the primordial bounds, the dotted parts of the lines show where the fields exhibit modified redshifting behaviors, instead of being dissipated. Here we assume $v_0 = 10^{-3}$ and for the Galactic parameters $l_c = 1$ kpc, $R = 10$ kpc, $\tau_{\text{gen}} = 10^8$ yr, and $\gamma_i - 1 = 10^{-6}$. See the text for details.

At $m > \bar{m}_{\text{BH}}$, the bound is weaker than in the first line of Eq. (7.28) as discussed in [1], however we will not analyze this in detail.

Extremal magnetic black holes as light as $m \lesssim 10^{-3}$ gm (i.e. $g < g_{\text{min}}$) move at nonrelativistic $v_{\text{H}}$ throughout the early cosmic history. The condition for such black holes not to alter the redshifting of the magnetic fields during radiation domination is Eq. (7.25), which is now rewritten as

$$F \lesssim 10^{-14} \text{ cm}^{-2}\text{sr}^{-1}\text{s}^{-1} \left( \frac{m}{10^{-3} \text{ gm}} \right)^{-1} \left( \frac{v_0}{10^{-3}} \right). \tag{7.37}$$

The condition from the reheating epoch has the same expression as Eq. (7.36).

### 7.3.1 Comparison of bounds

In Figure 7.6 we show different upper bounds on the flux of extremal magnetic black holes. The solid gray line shows the cosmological abundance bound in Eq. (4.20) with $\rho_{\text{DM}}$ taken as the average dark matter density in the universe, i.e. $\rho_{\text{DM}} \approx 1.3 \times 10^{-6}$ GeVcm$^{-3}$. The dotted gray line shows the abundance bound with $\rho_{\text{DM}}$ set to the local dark matter density in the Milky Way, i.e. $\rho_{\text{DM}} \approx 0.4$ GeV cm$^{-3}$.

In both of the abundance bounds we also used $v_i = 10^{-3}$. The orange line shows the bound in Eq. (4.23) from the survival of Galactic magnetic fields, with the parameters taken as $l_c = 1$ kpc, $R = 10$ kpc, $\tau_{\mathrm{gen}} = 10^8$ yr, and $\gamma_i - 1 = 10^{-6}$; this bound is independent of the Galactic field strength (as long as $B \lesssim 10^{-3}\,\mathrm{G}$), hence the present-day and seed Galactic fields give similar bounds. We note that the condition in Eq. (4.16) holds for all the values of the mass of the black holes shown in the plot, as long as $B \gtrsim 10^{-11}\,\mathrm{G}$. The red line shows the bounds in Eqs. (7.22) and (7.37) from primordial fields during radiation domination. The blue line shows the bound in Eq. (7.36) from primordial fields during reheating for $T_{\mathrm{dom}} = 100\,\mathrm{MeV}$. For the primordial bounds we assume a present-day field strength $B_0 = 10^{-15}\,\mathrm{G}$, and velocity $v_0 = 10^{-3}$. The filled points on the primordial bounds show where the mass limit of Eq. (7.34) is saturated, and the dashed parts of the lines show where the fields exhibit modified redshifting behaviors, instead of being dissipated. Differently from Figure 7.4, the dashed parts of the bounds are now on the lower mass end. The blue open circle shows the threshold mass $\bar{m}_{\mathrm{BH}}$ given in Eq. (7.35). A reheating bound also exists at $m > \bar{m}_{\mathrm{BH}}$, however we did not analyze this case and hence the blue line is truncated at $\bar{m}_{\mathrm{BH}}$. Let us also note that an extremal magnetic black hole with a Dirac charge $g = g_{\mathrm{D}}$ has a mass of $7.1 \times 10^{19}$ GeV. However, lighter extremal black holes can in principle exist by absorbing minicharged monopoles.

The bound from primordial fields during radiation domination does not depend on the mass of the black holes, while the other Parker bounds become stronger for larger masses. Consequently, the radiation domination bound is much less constraining. The reheating bound, even with the rather low reheating temperature chosen in the plot, is weaker than the Galactic bound; this is also seen in Figure 7.5 for the mass-dependent segments of the reheating and Galactic bounds.

We also see that the abundance bound is stronger than the Galactic Parker bound, even when considering the local dark matter density. The Parker bound can in principle be significantly improved by considering galaxies hosting magnetic fields with coherence lengths much larger than the Milky Way; however it is unlikely that magnetic black holes can be clustered with such galaxies, as was discussed at the end of Section 4.1.4. And if magnetic black holes cannot cluster with some galaxies, then they cannot make up all the dark matter.

As we have already mentioned in Section 4.1.4, in the above discussions we have treated extremal magnetic black holes simply as very massive monopoles with charges much larger than the Dirac charge, and ignored black hole-specific features. There has not been enough time for accretion disks to form in the early universe [143], hence this should not affect the bounds from primordial magnetic fields. On the other hand, the presence of electroweak coronas around the extremal magnetic black holes can also change the interaction between the black holes and the primordial plasma, modifying the Parker-type bounds. We leave detailed studies of this effect for the future.

# Chapter 8

# Schwinger effect in the early universe: production and acceleration

## 8.1 Monopoles produced by primordial magnetic fields

In the previous chapter, we derived bounds on the abundance of magnetic monopoles without specifying their origin. Here we focus on monopoles that are Schwinger-produced by the primordial magnetic field itself, and study whether the magnetic field is dissipated by the monopole acceleration. Here we note that even in the absence of any initial monopole population, strong magnetic fields in the early universe can trigger the monopole pair production. By studying this process, we derive further constraints on monopoles, which also serve as the most conservative condition for the survival of primordial magnetic fields.

The implications of monopole pair production in primordial magnetic fields were recently investigated in [45], however, that work used a simplified treatment of the magnetic field dissipation by monopole acceleration. In particular, it focused on the acceleration right after the monopoles are pair-produced, but did not take into account the integrated effect of monopole acceleration over the entire cosmological history.

The Schwinger effect describes the production of particle-antiparticle pairs in an external field. The analysis by Schwinger [12] assumed weak couplings; however, this is not the case for magnetic monopoles which, due to the Dirac quantization condition, have strong magnetic couplings. As we have already mentioned in Chapter 2, the rate of monopole-antimonopole pair production at arbitrary coupling in a static magnetic field has been derived in [13, 14] through an instanton method:

$$\Gamma = \frac{(gB)^2}{(2\pi)^3} \exp\left[ -\frac{\pi m^2}{gB} + \frac{g^2}{4} \right]. \tag{8.1}$$

This result is valid under the following weak field conditions:

$$B \lesssim \frac{m^2}{g}, \tag{8.2a}$$

$$B \lesssim \frac{4\pi m^2}{g^3}. \tag{8.2b}$$

The second condition is stricter than the first one if $g \gg 1$, and suggests that the instanton computation is valid when the exponent of the expression in Eq. (8.1) is negative. The second condition can be understood as the requirement that, in order for the semi-classical instanton techniques to be valid, the loop radius of the classical instanton solution [13, 14],

$$R = \frac{m}{gB}, \tag{8.3}$$

must be larger than the typical size of a monopole,

$$r = \frac{g^2}{4\pi m}. \tag{8.4}$$

Under this condition, the instanton computation sees the monopoles as point-like objects. Therefore, the result of Eq. (8.1) holds for both Dirac point-like monopoles and 't Hooft-Polyakov extended objects. We also notice here that it has been suggested that basic Dirac monopoles might possess a comparable spatial size [144, 145] to that of 't Hooft-Polyakov monopoles; a straightforward reasoning is that the classical point-particle model should fail at distances smaller than Eq. (8.4), because otherwise the combined rest energy and potential energy of a monopole-antimonopole pair could turn negative, destabilizing the vacuum. As explained, the computation for the Schwinger effect should hold also in this case.

After the process of magnetogenesis, the primordial magnetic fields redshift as $B \propto a^{-2}$. Thus, it suffices to assume that the weak field condition Eq. (8.2b) is verified at time $t_{\rm end}$. Defining:

$$\mathscr{I} = \frac{4\pi m^2}{g^3 B_{\rm end}}, \tag{8.5}$$

we rewrite the weak field condition Eq. (8.2b) as:

$$\mathscr{I} \gtrsim 1. \tag{8.6}$$

Using Eqs. (C.5) and (C.6), the initial amplitude of the primordial magnetic field can be written in terms of the field strength today as:

$$B_{\rm end} = B_0 \left(\frac{a_0}{a_i}\right)^2 \simeq 10^{43} \text{ G} \left(\frac{B_0}{10^{-15} \text{ G}}\right) \left(\frac{H_{\rm end}}{10^{14} \text{ GeV}}\right) \max\left\{\left(\frac{H_{\rm end}}{H_{\rm dom}}\right)^{1/3}, 1\right\}. \tag{8.7}$$

Here, the first expression within the curly brackets corresponds to the case with $t_{\rm end} < t_{\rm dom}$ and the second to $t_{\rm end} > t_{\rm dom}$. Substituting the expression for $B_{\rm end}$ into the definition of $\mathscr{I}$, we get:

$$\mathscr{I} \simeq \left(\frac{10}{g}\right)^3 \left(\frac{10^{-15} \text{ G}}{B_0}\right) \left(\frac{10^{14} \text{ GeV}}{H_{\rm end}}\right) \left(\frac{m}{10^{12} \text{ GeV}}\right)^2 \min\left\{\left(\frac{H_{\rm dom}}{H_{\rm end}}\right)^{1/3}, 1\right\}, \tag{8.8}$$

and we can express the weak field condition in Eq. (8.2b) as a lower limit on the mass of the monopoles in terms of the Hubble rate at magnetogenesis:

$$m \gtrsim 10^{12} \text{ GeV} \left( \frac{g}{10} \right)^{3/2} \left( \frac{B_0}{10^{-15} \text{ G}} \right)^{1/2} \left( \frac{H_{\text{end}}}{10^{14} \text{ GeV}} \right)^{1/2} \max \left\{ \left( \frac{H_{\text{end}}}{H_{\text{dom}}} \right)^{1/6}, 1 \right\}.$$

$$(8.9)$$

The number density of monopoles pair-produced by the magnetic fields can be obtained using the expression in Eq. (7.5) and substituting the production rate shown in Eq. (8.1). Because the production rate presents an exponential dependence on the magnetic fields, the monopoles are produced predominantly within an interval $\Delta t_{\Gamma_{\text{end}}} \sim |\Gamma_{\text{end}}/\dot{\Gamma}_{\text{end}}| \simeq (gB_{\text{end}})/(2\pi m^2 H_{\text{end}})$ after $t_{\text{end}}$ [45]. Therefore, we can approximately express the number density at times around $t_{\text{end}}$ as:

$$n_{\text{end}} \simeq \frac{g\Gamma_{\text{end}}B_{\text{end}}}{2\pi m^2 H_{\text{end}}}.$$

$$(8.10)$$

Using $n \propto a^{-3}$, the monopole number density today is thus written as:

$$n_0 \simeq \left( \frac{a_{\text{end}}}{a_0} \right)^3 \frac{g\Gamma_{\text{end}}B_{\text{end}}}{2\pi m^2 H_{\text{end}}}.$$

$$(8.11)$$

It was pointed out in [45] that Eq. (8.2b) also gives an absolute upper bound on the initial amplitude of primordial magnetic fields: saturating this bound leads to either an overproduction of monopoles in the universe, or a self-screening of the magnetic field. Below we revisit the magnetic field bounds in light of the energy dissipation due to the production of monopole pairs and of the constraints derived in the previous chapter. We show that for the monopoles produced by the primordial magnetic fields, the bounds on the monopole flux approximately reduce to the weak field condition in Eq. (8.2b).

## 8.2  Magnetic field dissipation by monopole production

We first take into account the energy dissipation due to the production of monopole-antimonopole pairs. This analysis is taken from the work in [45].

In terms of the energy density of the magnetic field $\rho_B = B^2/2$, the redshifting of the magnetic fields due to the cosmic expansion can be written as

$$(\dot{\rho}_B)_{\text{red}} = -4H\rho_B.$$

$$(8.12)$$

One can estimate the time scale of redshifting as $\Delta t_{\text{red}} \sim \rho_B/(\dot{\rho}_B)_{\text{red}} = 1/(4H)$, which is of order the Hubble time.

Furthermore, each time the magnetic fields produce a pair of monopole and antimonopole the fields lose energy corresponding to the rest energy of the pairs $\Delta E_B = -2m$. Therefore, we can estimate the energy dissipation due to pair production per unit of time and volume as

$$(\dot{\rho}_B)_{\text{prod}} = -2m\Gamma,$$

$$(8.13)$$

where $\Gamma$ is the pair production rate in Eq. (8.1). From requiring that the dissipation rate is smaller thant the rate of redshifting, we get an upper bound on the amplitude

of the primordial magnetic fields necessary to have negligible back-reaction due to pair production:

$$B < B_{\text{prod}} = \frac{4\pi m^2}{g^3} \left( 1 + \frac{4}{g^2} \log \left( \frac{g^2}{8\pi^3} \frac{m}{H} \right) \right)^{-1} . \tag{8.14}$$

If the magnetic fields were stronger than the right hand side, they would have decayed through pair production in less than a Hubble time, until the fields fall below $B_{\text{prod}}$. Thus, Eq. (8.14) is an upper bound on the amplitude of the primordial magnetic fields.

When the expression for $B_{\text{prod}}$ becomes negative, i.e. if $(4/g^2) \log(g^2 m/(8\pi^3 H))$, the dissipation of the fields is significant only at the very strong fields for which the computation for the pair production rate in Eq. (8.1) breaks down. However, this is not usually the case for $g \ll 1$. In fact, considering the lower bound on the monopole mass from heavy-ion collisions [42, 43] $m \gtrsim 70$ GeV, and the upper bound on the Hubble rate from the inflation scale [142] $H \lesssim 10^{14}$ GeV, we get that $(4/g^2) \log(m/H) \gtrsim -0.5$ for $g \gtrsim 15$. Normally the monopole charge is $g \gg 1$ and therefore $B_{\text{prod}}$ is smaller than the field that saturates the weak field condition, i.e. the weak field condition $\mathscr{I} \gtrsim 1$ is still valid for $B = B_{\text{prod}}$.

Considering that the ratio $B/B_{\text{prod}}$ decreases with time, energy dissipation by monopole pair production is more important in the past. Therefore, by taking $B = B_{\text{end}}$ it is possible to rewrite the upper limit for the primordial magnetic fields from pair production as a lower limit for the monopole mass in terms of the Hubble rate at magnetogenesis as:

$$\mathscr{I} \gtrsim 1 + \frac{4}{g^2} \log \left( \frac{g^2}{8\pi^3} \frac{m}{H_{\text{end}}} \right) , \tag{8.15}$$

which differs from the mass bound from the weak field condition in Eq. (8.9) only by the negligible logarithmic term.

## 8.3   Magnetic field dissipation by monopole acceleration

We now discuss the bounds on the primordial magnetic fields from the energy dissipation due to the acceleration of the monopoles pair-produced by the magnetic fields themselves. We first discuss the bounds from the acceleration during the radiation domination, up to the time of $e^+ e^-$ annihilation, and then the bounds from the acceleration during the reheating epoch after the end of the process of magnetogenesis, before radiation domination.

### 8.3.1   Radiation-dominated epoch

We substitute the expression for the number density of monopoles produced by the Schwinger effect in Eq. (8.11) into the expression for the maximum of $\Pi_{\text{acc}}/\Pi_{\text{red}}$ during radiation domination shown in Eq. (7.12). Making use of the relations in Eqs. (8.7), (C.5), (C.6), we can rewrite the expression for the ratio as:

$$\frac{\Pi_{\text{acc}}}{\Pi_{\text{red}}} (T = 1 \text{ MeV}) \simeq \tilde{x}_D \exp \left( -\frac{g^2}{4} (\mathscr{I} - 1) \right) , \tag{8.16}$$

where we define:

$$\tilde{x}_D = \left(\frac{g}{10}\right)^3 \left(\frac{B_0}{10^{-15}\text{ G}}\right)^3 \left(\frac{10^{16}\text{ GeV}}{m}\right)^2 \left(\frac{H_{\text{end}}}{10^{14}\text{ GeV}}\right)^{1/2} \max\left\{\left(\frac{H_{\text{end}}}{H_{\text{dom}}}\right)^{1/2}, 1\right\}.$$

(8.17)

Under the requirement of negligible back-reaction on the primordial magnetic fields, $\Pi_{\text{acc}}/\Pi_{\text{red}}(T = 1\text{ MeV}) \lesssim 1$, we get:

$$\tilde{x}_D \exp\left(-\frac{g^2}{4}(\mathscr{I} - 1)\right) \lesssim 1.$$

(8.18)

In Figure 8.1 we show in solid curves the bound in Eq. (8.18). We also plot the weak field condition in Eq. (8.9) in dashed curves. The region below the curves is not compatible with the survival of the primordial magnetic fields, namely, the curves give lower bounds on the monopole mass. For the computation we assume $g = 2\pi/e$ and $B_0 = 10^{-15}$ G. The bound is shown for different values of $T_{\text{dom}}$ (from bottom to top, red: $10^{15}$ GeV, which corresponds to $H_{\text{dom}} = 10^{12}$ GeV; orange: $10^9$ GeV, which corresponds to $H_{\text{dom}} = 1$ GeV; pink: $10^3$ GeV, which corresponds to $H_{\text{dom}} = 10^{-12}$ GeV). In cases where the magnetic fields are produced after reheating, i.e. $t_{\text{end}} > t_{\text{dom}}$, the bound is independent of $T_{\text{dom}}$; this is seen in the plot as the red and orange curves overlapping on the low-$H_{\text{end}}$ end.

Due to the exponential dependence on $\mathscr{I}$ in Eq. (8.18), this condition reduces approximately to the weak field condition Eq. (8.9), as seen in the plot. This can be easily shown by computing the natural logarithm of the expression and rewriting it as:

$$\mathscr{I} \gtrsim 1 + \frac{4}{g^2}\ln\tilde{x}_D.$$

(8.19)

The expression now takes a form similar to that for the weak field condition in Eq. (8.6) with an additional logarithmic factor. For values of $H_{\text{end}}$ that saturates the upper bound on the inflation scale $H \lesssim 10^{14}$ GeV [113] and assuming for $B_0$ the reference value of $10^{-15}$ G, the logarithmic term can become comparable to 1 only for very low monopole masses and very small values of $T_{\text{dom}}$. In any case, the corrections are generically less than order unity and negligible for an estimate at the level of the order of magnitude. In summary, the bounds on the monopole abundance obtained for $t > t_{\text{dom}}$ approximately reduce to the weak field condition in Eq. (8.9).

### 8.3.2 Reheating epoch

We now study the back-reaction of pair-produced monopoles on the primordial magnetic field during the reheating epoch. Hence, in this subsection we only focus on cases where the magnetic field generation takes place prior to radiation domination.

As explained in Section 7.1.2, the monopole bound is obtained by evaluating the ratio $\Pi_{\text{acc}}/\Pi_{\text{red}}$ at the time $t_{\text{end}}$ or $t_*$, whichever is later (see Eq. (6.25) for the definition of $H_*$). We compute the ratio by substituting Eq. (8.11) into Eq. (7.15). Taking into account the relations in Eqs. (8.7), (C.5), (C.6), we obtain:

$$\frac{\Pi_{\text{acc}}}{\Pi_{\text{red}}}(t = \max\{t_{\text{end}}, t_*\}) \simeq \tilde{x}_B \exp\left(-\frac{g^2}{4}(\mathscr{I} - 1)\right),$$

(8.20)
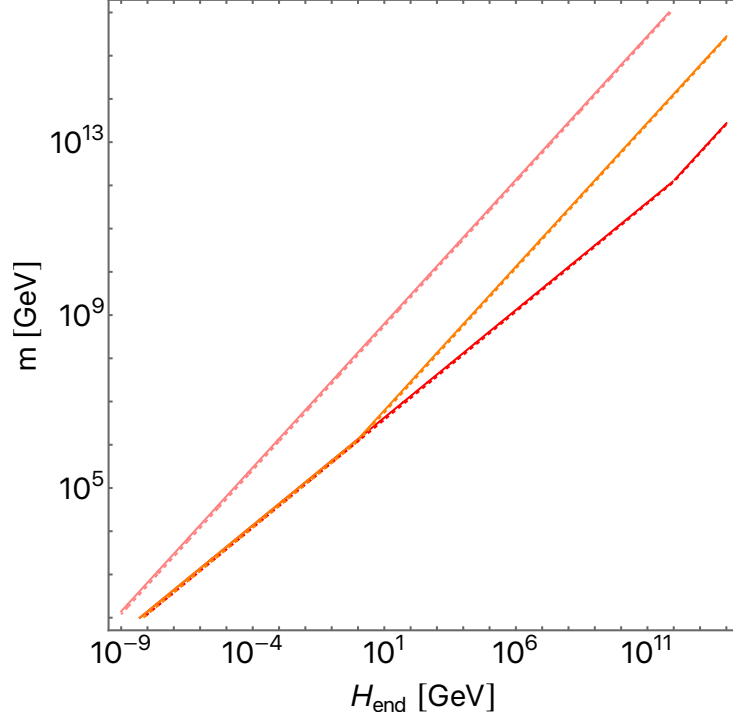
**Figure 8.1** Lower bounds for the monopole mass as a function of the Hubble scale at magnetic field generation $H_{\rm end}$. The plot shows the comparison between the weak field condition in (8.9) (dashed curves) and the bound from requiring negligible back-reaction on the primordial magnetic fields during radiation domination, shown in (8.18) (solid curves). Here $g = 2\pi/e$ and $B_0 = 10^{-15}$ G. The results are shown for three different values of the reheating temperature $T_{\rm dom}$; from bottom to top, red: $10^{15}$ GeV, orange: $10^9$ GeV, pink: $10^3$ GeV. For $H_{\rm end} < H_{\rm dom}$, the results are independent from $T_{\rm dom}$.

where we define:

$$
\begin{aligned}
\tilde{x}_B = {} & \left(\frac{g}{10}\right)^3 \left(\frac{100}{\mathcal{N}_{c,{\rm dom}}}\right) \left(\frac{B_0}{10^{-15}\ {\rm G}}\right)^3 \left(\frac{10^{11}\ {\rm GeV}}{T_{\rm dom}}\right)^3 \left(\frac{10^{13}\ {\rm GeV}}{m}\right)^2 \\
& \cdot \left(\frac{H_{\rm end}}{10^{14}\ {\rm GeV}}\right)^{3/2} \min\left\{\left(\frac{H_*}{H_{\rm end}}\right)^{1/2}, 1\right\}.
\end{aligned}
\tag{8.21}
$$

We remind the reader that the form of $H_*$ in Eq. (6.25) depends on whether the mass of the monopoles is smaller or larger than $\bar{m}$.

Negligible back-reaction on the magnetic fields implies $\Pi_{\rm acc}/\Pi_{\rm red}\left(t = \max\{t_{\rm end}, t_*\}\right) \lesssim 1$. From this condition, we get a bound in the $(H_{\rm end}, m)$ plane similar to that obtained during radiation domination:

$$
\tilde{x}_B \exp\left(-\frac{g^2}{4}\left(\mathscr{I} - 1\right)\right) \lesssim 1.
\tag{8.22}
$$

In Figure 8.2 we show in solid curves the condition in Eq. (8.22) and in dashed curves the weak field condition given in Eq. (8.9) for different values of $T_{\rm dom}$ (from
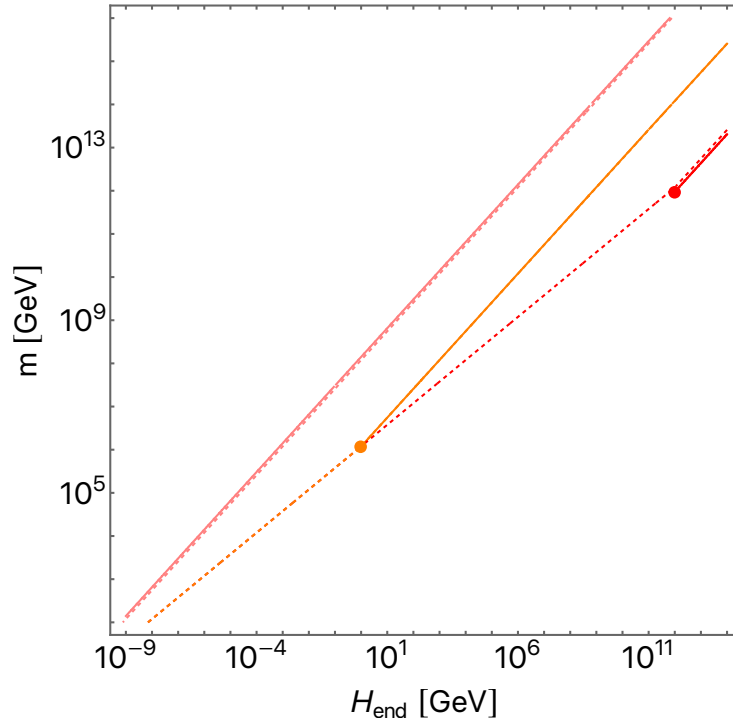
**Figure 8.2** Lower bounds for the monopole mass as a function of the Hubble scale at magnetic field generation $H_{\text{end}}$. The plot shows the comparison between the weak field condition in (8.9) (dashed curves) and the bound from requiring negligible back-reaction on the primordial magnetic fields during reheating, shown in (8.22) (solid curves). Here $g = 2\pi/e$, $\mathcal{N}_{c,\text{dom}} = 100$ and $B_0 = 10^{-15}$ G. The results are shown for three different values of the reheating temperature $T_{\text{dom}}$; from bottom to top, red: $10^{15}$ GeV, orange: $10^9$ GeV, pink: $10^3$ GeV. The bound of Eq. (8.22) applies only for $H_{\text{end}} \geq H_{\text{dom}}$. The endpoints of the solid curves correspond to where $H_{\text{end}} = H_{\text{dom}}$.

bottom to top, red: $10^{15}$ GeV, which corresponds to $H_{\text{dom}} = 10^{12}$ GeV; orange: $10^9$ GeV, which corresponds to $H_{\text{dom}} = 1$ GeV; pink: $10^3$ GeV, which corresponds to $H_{\text{dom}} = 10^{-12}$ GeV). For the computation we assume $g = 2\pi/e$, $\mathcal{N}_{c,\text{dom}} = 100$ and $B_0 = 10^{-15}$ G. Since now we are focusing on the case where the magnetic fields are generated before radiation domination, the bound of Eq. (8.22) applies only for $H_{\text{end}} \geq H_{\text{dom}}$. In the plot, the endpoints of the red and orange curves correspond to where $H_{\text{end}} = H_{\text{dom}}$.

Also in this case, the exponential factor mainly sets the left-hand side of Eq. (8.22). Consequently, the bound reduces to the weak field condition up to an order-unity factor, as seen in the plot. This is also seen by rewriting Eq. (8.22) as,

$$\mathscr{I} \gtrsim 1 + \frac{4}{g^2} \ln \tilde{x}_B. \tag{8.23}$$

The logarithmic factor can be generically neglected for an order-of-magnitude estimate of the bounds.

The work [45] obtained a similar condition by only considering the acceleration of monopoles soon after they are pair-produced. This indicates that the bound

on the initial magnetic field strength does not improve significantly even when the integrated effect of the monopole acceleration is taken into account over the entire cosmological history. This insensitivity to the detailed dynamics of the monopoles is due to the exponential dependence of the monopole production rate on the magnetic field strength.

## 8.4 Symmetry breaking scale and weak field condition

We now describe some specific features [45] that applies to this discussion when we consider topological solitonic monopoles, as in the t' Hooft-Polyakov model.

For solitonic monopoles in spontaneously broken gauge theories, the symmetry-breaking scale is typically of the order of $M = m/g$. If the cosmic temperature or the Hubble rate upon magnetic field generation exceeds this scale, the symmetry is unbroken; then the monopole solution does not exist and the monopole mass limit of Eq. (8.9) can be evaded. The magnetic field itself can also restore the symmetry if it exceeds the weak field limit of Eq. (8.2b) [146, 147, 148]. For topological solitons the preceding discussions are not applicable if the symmetry is unbroken, as the monopole solution does not exist in such a case. Consequently, strong magnetic fields can be generated without the production of monopole pair when the cosmic temperature or the Hubble rate is higher than the symmetry breaking scale, that is $\sigma < \max\{T, H\}$, or if the value of $B_{\text{end}}$ saturates the weak field condition.

If the symmetry is unbroken at some time during the post-inflation period, monopoles are copiously produced at the symmetry breaking phase transition and eventually dominate the universe, if the symmetry breaking scale is not sufficiently low. It is important to note that the monopole problem is particularly grave if the phase transition occurs before radiation domination. Therefore, while theoretically magnetic field constraints could be bypassed by maintaining the symmetry unbroken, this approach might cause the monopole problem and is not doable. As a result, we can conclude that primordial magnetic fields beyond the stated upper limits could not have existed post-inflation even in the case of solitonic monopoles.

We also observe that in a phase of broken symmetry, the magnetic field strength in a radiation-dominated universe is limited above by the symmetry breaking scale, thus is typically well below the threshold of the weak field condition. Conversely, stronger fields are possible before radiation domination, when solitonic monopoles can be abundantly produced by the fields [45].

In parts of the region displayed in Figures 8.1 and 8.2, the temperatures $T_i$ and/or $T_{\text{dom}}$ are larger than M. However in such regions, the symmetry breaking after inflation can induce a monopole problem, which leads to further constraints on the monopole mass. We refer the reader to [45] for a detailed discussion on this point.

In Figures 6.1 and 7.1, with the choice of parameters there, the weak field condition implies $m \gtrsim 10^{14}\,\text{GeV}$, and the condition of broken symmetry ($T_{\text{end}}, H_{\text{end}} <$ M) gives $m \gtrsim 10^{12}\,\text{GeV}$. These conditions are violated in the plot by some of the curves with low masses. Such curves, hence, should be taken only as a qualitative indication of how light monopoles respond to primordial magnetic fields.

In Figure 7.2 we showed monopole bounds based on primordial magnetic fields

during reheating, which were derived by evaluating the ratio $\Pi_{\mathrm{acc}}/\Pi_{\mathrm{red}}$ at the time $t_*$. (Recall that we do not need to specify the value of $H_{\mathrm{end}}$ for these bounds, as long as $H_{\mathrm{end}} > H_*$ is satisfied.) The magnetic field strength at $t_*$, i.e. $B_*$, satisfies the weak field condition in the entire range of $m$ and $T_{\mathrm{dom}}$ displayed in the plot. The condition $T_*, H_* < \mathrm{M}$ is also satisfied in the entire range, and thus the symmetry is broken at $t_*$.

We also remark that the constraint on the Hubble rate in Eq. (6.28) from the requirement that the magnetic field energy does not dominate the early universe is satisfied by the values of $H_{\mathrm{end}}$ shown in Figures 6.1,7.1, 8.1, 8.2, and also by $H_*$ shown in Figure 7.2.

# Chapter 9

# Global solution to the cosmological monopole problem

In this chapter, we propose a solution to the monopole problem (see the discussion in Section 2.3.1) based on a modification of the kinetic term of the gauge field that breaks the conformal symmetry of the gauge sector. Similar models have been proposed for the implications on the processes of primordial magnetogenesis [72, 73, 149], however here we are interested in the consequences for monopole production during primoridal phase transitions.

## 9.1 The global monopole solution

In the case of the spontaneous breaking of a global symmetry of the lagrangian, a monopole solution can still be defined. Such monopoles do not have a magnetic charge, but they have a global charge in the unbroken global group. They are usually called "global monopoles", in constrast with the standard gauge monopoles, which we address here also as "local". Global monopoles present some peculiar and exotic characteristics that we review here in some detail.

As for the 't Hooft-Polyakov monopoles, global monopoles are produced during the spontaneous symmetry breaking of a global symmetry $G$ into a smaller group $H$ such that the second homotopy group of the vacuum manifold $G/H$ is nontrivial, i.e. $\Pi_2(G/H) \neq I$. The simplest model where a global monopole solution can be defined is the global version of the Georgi-Glashow model discussed in Section 2.1.2:

$$\frac{\mathcal{L}}{\sqrt{-g}} = -\frac{1}{2}(\partial_\mu \phi)^a (\partial_\mu \phi)^a - \frac{\lambda}{4}(\phi^a \phi^a - v^2)^2. \tag{9.1}$$

Here $\phi^a$ is a triplet of $SO(3)$ and the vacuum expectation value $v$ breaks the $SO(3)$ global symmetry into a $SO(2)$ global symmetry.

The global monopole solution is characterized by the topological charge

$$N = \frac{1}{8\pi} \oint dS^{ij} |\phi|^{-3} \epsilon_{abc} \phi^a \partial_i \phi^b \partial_j \phi^c, \tag{9.2}$$

which corresponds to the global charge of the monopole. In the fundamental case

$N = 1$ the solution is the spherically-symmetric configuration:

$$\phi^a = vh(r)\frac{x^a}{r}, \tag{9.3}$$

where the function $h(r)$ vanishes for $r = 0$ and approaches 1 in the limit $r \to \infty$.[1]

As in the gauge case, one can compute the mass of the global monopole by integrating the time-time component of the stress-energy tensor outside the monopole core of size $\delta \sim (\sqrt{\lambda}v)^{-1}$ [10],

$$m \sim 4\pi \int_\delta^R T_t^t r^2 dr \sim 4\pi v^2 R, \tag{9.4}$$

where $R$ is a cut-off radius. This integral is clearly divergent for $R \to \infty$. However, for practical realizations, a cutoff radius can be approximately fixed to the distance of the closest antimonopole. So, although one isolated global monopole would have infinite mass, the problem is solved in a physical realization of the symmetry breaking, where the coherence length of the Higgs field is finite.

As a consequence of the peculiar structure of the stress-energy tensor of global monopoles, the energy of a monopole-antimonopole pair separated by a distance $R$ is $E \sim 4\pi v^2 R$ and the attractive force is independent of the distance:

$$F = \frac{\partial E}{\partial R} \sim 4\pi v^2. \tag{9.5}$$

Such a large attractive force between global monopole-antimonopole pairs make the pair annihilation process very efficient. Simulations [150] suggest that the global evolution rapidly reach a scale-invariant regime with a monopole number density

$$n_{\mathrm{M}} = (4 \pm 1.5) R_{\mathrm{H}}^{-3}, \tag{9.6}$$

where $R_{\mathrm{H}}$ is the horizon length. This result has been shown to hold in both radiation and matter eras. As a consequence of the very efficient mechanism of annihilation, the monopole problem from over-production during the phase transition in the early universe does not exist for global monopoles.

## 9.2   I²FF theories

Let us consider now gauge theories of the type [72] which break the conformal symmetry of the gauge sector through a modification of the kinetic sector of the vector boson field,

$$\frac{\mathcal{L}}{\sqrt{-g}} \supset -\frac{I^2}{4} F_{\mu\nu} F^{\mu\nu}, \tag{9.7}$$

where $F_{\mu\nu}$ is the field strength of the $U(1)$ (hypercharge or electromagnetism, depending on the energy scale) gauge field, and $I(> 0)$ represents a generic coupling between the gauge field and some other fields. Supposing that $I$ is constant in space, then it can be absorbed by the redefinitions

$$\tilde{A}_\mu^a = I A_\mu^a, \quad \tilde{e} = e/I. \tag{9.8}$$

---

[1]Notice that here the symmetry is global and therefore there is no monopole solution for a vector boson field as in the gauge case.

Then, the effect of $I$ is merely to shift the gauge coupling $e$, and in particular it is clear that a small $I$ would lead to strong couplings [149]. In order to avoid the problem we assume $I \geq 1$. We also assume $I$ to be time-dependent and constantly decreasing until it becomes equal to 1. We then define $t_{\mathrm{con}}$ as the time when we recover the conformal invariance of the gauge sector, i.e. $I(t_{\mathrm{con}}) = I_{\mathrm{con}} = 1$ (the subscript "con" denotes quantities computed at $t_{\mathrm{con}}$). We assume the temperature $T_{\mathrm{con}}$ to be larger than 1 MeV to avoid the constraints from BBN. As a toy model, we assume that the time evolution of the function $I$ can be expressed as

$$I = \begin{cases} \left(\dfrac{a_{\mathrm{con}}}{a}\right)^s & \text{for } a \leq a_{\mathrm{con}}, \\ 1 & \text{for } a \geq a_{\mathrm{con}}, \end{cases} \tag{9.9}$$

where $s$ is a positive integer.

We now want to embed the conformal-violating term into the toy model of a $G = \mathrm{SO}(3)$ gauge theory with a triplet Higgs [6, 7]. We discuss here only the case of minimal coupling with $I$. In this case, the Weyl symmetry-violating coupling $I$ exists only in front of the gauge kinetic term:

$$\frac{\mathcal{L}}{\sqrt{-g}} = -\frac{I^2}{4}F^a_{\mu\nu}F^{a\mu\nu} - \frac{1}{2}(D_\mu\phi)^a(D_\mu\phi)^a - \frac{\lambda}{8}(\phi^a\phi^a - v^2)^2, \tag{9.10}$$

where $a = 1, 2, 3$, $F^a_{\mu\nu} = \partial_\mu A^a_\nu - \partial_\nu A^a_\mu + e\varepsilon^{abc}A^b_\mu A^c_\nu$, $(D_\mu\phi)^a = \partial_\mu\phi^a + e\varepsilon^{abc}A^b_\mu\phi^c$, $\varepsilon^{abc}$ is the Levi-Civita symbol, and $\lambda, v > 0$. We therefore canonically redefine the gauge field and the gauge coupling as in Eq. (9.8).

After the symmetry breaks at the critical temperature $T_c$, which is typically $T_c \sim v$,[2] the particle spectrum consists of a Higgs particle with mass $M_{\mathrm{H}} = \sqrt{\lambda}v$, one massless gauge boson, and two massive gauge bosons with mass $M_{\mathrm{V}} = |\tilde{e}|v$. There also exist topological monopoles with fundamental magnetic charge $\tilde{g} = \pm 4\pi/\tilde{e}$, mass $M_{\mathrm{M}} \sim |\tilde{g}|v = 4\pi v/|\tilde{e}|$, and size $r_{\mathrm{M}} \sim 1/M_{\mathrm{V}} = 1/(|\tilde{e}|v)$. The shift in the gauge coupling $e$ further leads to the following $I$-dependence of the the mass of the the gauge boson and the charge, mass and radius of the monopole,

$$M_{\mathrm{V}} \propto I^{-1}, \, g \propto I, \, M_{\mathrm{M}} \propto I, \, r_{\mathrm{M}} \propto I. \tag{9.12}$$

Given that $I$ decreases in time, one sees that a large $I$ in the asymptotic past gives rise to a strong coupling for the monopoles, i.e. large $\tilde{g}$. However, one also sees that $M_{\mathrm{V}}/v$ decreases towards the past. Hence, in the asymptotic past, the condition $M_{\mathrm{V}} < H_{\mathrm{inf}} < T_c \sim v$ might hold; in this regime, the monopoles in the theory are expected to be effectively global, i.e. chargeless under the gauge group, as only the global part of the symmetry is effectively spontaneously broken and the monopole radius extend beyond the Hubble horizon.[3] Then, when $I$ approach

---

[2]The critical temperature where the effective mass of the Higgs field at symmetry-preserving vacuum is [10]

$$T_{\mathrm{c}} = \left(\frac{\frac{12}{5}}{1 + \frac{12}{5}\frac{e^2}{\lambda}}\right)^{1/2} v. \tag{9.11}$$

[3]Hence there should also be two electrically charged Nambu-Goldstone bosons. These, along with other electrically charged particles like electrons, would be pair produced by the electric fields and may back-react to the gauge fields.

unity, one eventually enters the regime $H_{\text{inf}} < M_{\text{V}} < T_c \sim v$, and the monopoles get dressed by the gauge fields becoming magnetically charged.[4] We explain the implication of this for monopole production in the next section.

## 9.3 Solution of the monopole problem without inflation

Let us assume that during the early universe before BBN the function $I$ is much larger than 1. We consider for simplicity that radiation domination holds for all the period we consider for the analysis.

When the temperature of the universe goes down below the critical temperature of the phase transition, i.e. $T \lesssim v$, if the Hubble rate is larger than the vector boson mass, i.e. $H \gg \tilde{e}v = ev/I$, the gauge sector is decoupled from the scalar sector and the monopoles are produced as global. We define $T_{\text{global}} = v$ as the temperature at the time of the global monopole production. When the Hubble rate becomes comparable to the vector boson mass, also the local gauge part of the symmetry is broken and the monopoles become magnetically charged. We define

$$H_{\text{local}} = \frac{e}{I_{\text{local}}}v, \tag{9.13}$$

$$T_{\text{local}}^2 = \frac{e}{I_{\text{local}}}M_{\text{pl}}v, \tag{9.14}$$

as the Hubble rate and the temperature at the time of the breaking of the local symmetry.

In the time period when $T_{\text{local}} < T < T_{\text{global}}$, the number density of monopoles is fixed to the value in (9.6) and the number of monopoles per Hubble volume is time invariant. When the temperature drops below the temperature at which even local symmetry breaking occurs, the monopoles recover their standard evolution.

The energy density of non-relativistic monopoles is define as

$$\rho_{\text{M}} = n_{\text{M}}\tilde{m}_{\text{M}}, \tag{9.15}$$

where $\tilde{m}_{\text{M}}$ is defined as the time-dependent mass of the monopoles. Considering that the monopole masses for which a monopole problem subsist are very heavy, we do not lose generality by assuming nonrelativistic monopoles. Assuming $n_{\text{M}}(t_{\text{local}}) \approx 4 \times H_{\text{local}}^3$ and considering that non-relativistic monopoles redshift as matter, we can rewrite the energy density today as

$$\rho_{\text{M,glo}} = n_{\text{M,local}}\, m_{\text{M}} \left(\frac{a_{\text{local}}}{a_0}\right) \sim \rho_{\text{crit}} \left(\frac{v}{10^{14}\text{ GeV}}\right) \left(\frac{T_{\text{local}}}{10^3\text{ GeV}}\right)^3, \tag{9.16}$$

where $m_{\text{M}} = 4\pi v/e$ is the mass of the monopoles after the restoring of the conformal symmetry and we assume $g_{*(s)}$ constant over time. Let us compare this with the standard estimate for the monopole energy density through the Kibble mechanism in the local case,

$$\rho_{\text{M,loc}} = \rho_{\text{crit}} \times \Omega_M h^2 \sim \rho_{\text{crit}} \left(\frac{v}{10^{11}\text{ GeV}}\right)^4, \tag{9.17}$$

---

[4]If when the monopoles become local, the magnetic charge $\tilde{g}$ is still sufficiently large, strong primordial magnetic fields would give rise to very efficient monopole pair production. This would serve as an obstacle for magnetogenesis, or a new production mechanism for monopoles.

where $\Omega_M$ is defined in Eq. (2.33). For low values of $T_{\text{local}}$, much higher symmetry-breaking scales (even higher than the GUT scale) are admitted by the model without incurring into the monopole problem.

We now want to discuss the effective range of applicability of our model. The model has three degrees of freedom; we choose as free parameters the vacuum expectation value, $v$, the temperature at which the conformal symmetry is restored, $T_{\text{con}}$, and the exponent for the time dependence of $I$ defined in Eq. (9.9), $s$. We can express $T_{\text{local}}$ in terms of the chosen parameters as

$$T_{\text{local}} = (evM_{\text{Pl}}T_{\text{con}}^s)^{-2-s}. \tag{9.18}$$

Our new estimate of the relic monopole energy density in Eq. (9.16) is valid under the assumptions: $T_{\text{con}} \gtrsim T_{\text{BBN}} \sim 1$ MeV (the conformal symmetry must be recovered before BBN to not affect standard cosmology), $T_{\text{local}} \gtrsim T_{\text{con}}$ (the local phase transition must occur before the restoring of the conformal symmetry), and $T_{\text{global}} > T_{\text{local}}$ (the global symmetry breaking must occur before the local one). From the last two conditions, we get relations between the free parameters of the model $(v, T_{\text{con}}, s)$. In particular, from the second condition we get

$$T_{\text{con}}^2 \gtrsim eM_{\text{pl}}v, \tag{9.19}$$

and from the third one

$$v^{s+1} \gtrsim eM_{\text{Pl}}T_{\text{con}}^n. \tag{9.20}$$

If the condition in Eq. (9.20) is not verified, the symmetry breaking follows the usual pattern and occurs at the temperature $T_c \sim v$. Hence, the monopoles are produced as local and the energy density follows the expression in Eq. (9.17). For realistic values of the paramenters, the condition in Eq. (9.19) is usually weaker than that in Eq. (9.20), and therefore in the following we focus mainly on the condition in Eq. (9.20).

In Figure 9.1 we show the values of the symmetry breaking scale of the theory $v$ and the temperature at the restoration of the conformal symmetr $T_{\text{con}}$ for which the monopole energy density is lower than the critical energy density of the universe and therefore there is no monopole problem. We show the results for two different values of the integer $s$ (Figure 9.1a: $s = 3$, Figure 9.1b: $s = 6$). We show in the plots values of $T_{\text{con}}$ that satisfy the condition $T_{\text{con}} \gtrsim T_{\text{BBN}}$, and of $v$ larger than the electroweak symmetry breaking scale and smaller than the Planck mass.

The purple line corresponds to the values of the parameters for which the temperature at the local symmetry breaking, i.e. $T_{\text{local}}$, is equal to the temperature at the global symmetry breaking, that is, when the two phase transitions occur at the same time and in Eq. (9.20) the equality holds. On the right of the purple line the global symmetry breaking occurs before the local one and the monopoles are first produced as global. On the left of the purple line the symmetry breaking affects at the same time both the gauge and the Higgs sector, and therefore the monopoles are produced directly as the standard gauge monopoles through the standard Kibble mechanism. The brown line signals the combination of the parameters for which the monopole energy density in Eq. (9.16) is equal to the critical energy density of the universe $\rho_{\text{crit}} \approx 10^{-46}\text{GeV}^4$. In the region above the brown line the abundance

**(a)** $s = 3$.  **(b)** $s = 6$.
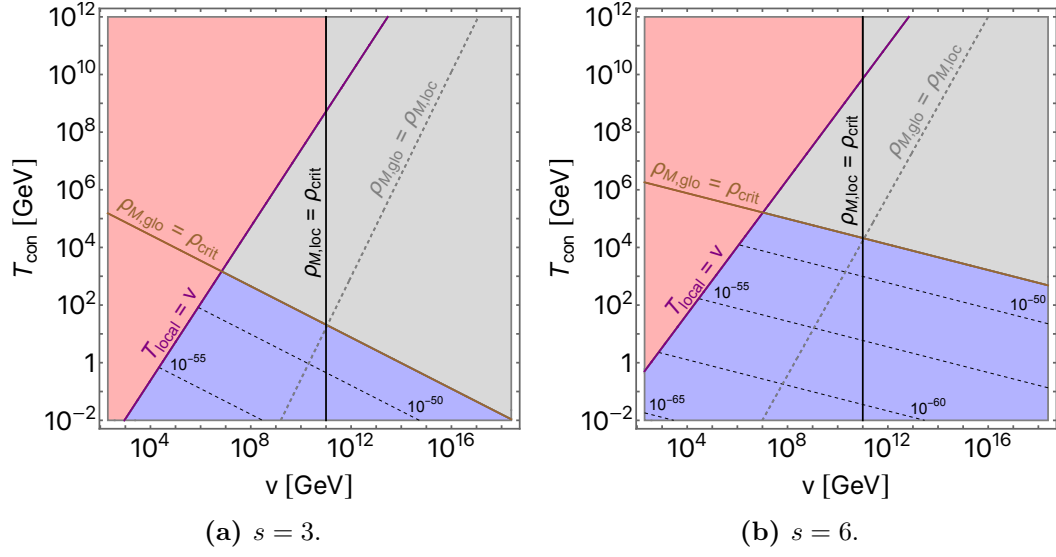
**Figure 9.1** Parameter space for the relic monopole energy density as a function of the vacuum expectation value of the theory $v$ and the temperature at which the conformal symmetry of the gauge kinetic sector is restored $T_{\rm con}$. We show the results for two different values of $s$, as defined in Eq. (9.9). The gray area is excluded because the monopole energy density is larger than the critical energy density of the universe. In the red area the monopoles are produced directly as local, the energy density is fixed by Eq. (9.17) and they are not excluded by the critical energy density of the universe. In the blue area the monopoles are first produced as global, and only later acquired a magnetic charge. In this case the energy density is set by Eq. (9.16) and they are not excluded by the critical energy density of the universe. The dashed contours in the blue area show the value of the monopole energy density in units of GeV$^4$. The solid brown line shows the combination of $m$ and $T_{\rm con}$ for which the expression in Eq. (9.16) is equal to the critical energy density of the universe, while the solid black line when the latter is equal to the expression in Eq. (9.17). The dashed gray line shows the combination of the parameters for which Eq. (9.16) and Eq. (9.17) are equal. The solid purple line shows the parameters for which $T_{\rm local} = v$. Here we assume $g_{*(s)}$ constant in time.

of monopoles in our new setup overcloses the universe, while below is compatible with the cosmological parameters. The solid vertical black line corresponds to the value of $v$ for which the standard calculation for the monopole energy density in Eq. (9.17) corresponds to the critical energy density. On the left of that line the monopole problem does not exist in the standard scenario, while on the right the standard calculation excludes monopole production after inflation. The dashed gray line shows the values of the parameters for which the monopole energy density in the standard scenario from Eq. (9.17) and in our model from Eq. (9.16) are the same. Above that line the value of $T_{\rm local}$ is large enough to have $\rho_{\rm M,glo} > \rho_{\rm M,loc}$, while the opposite is true below the line.

The gray area of the plots is excluded because the monopole energy density in our model is larger than the critical energy density of the universe. Notice that there is a gray region on the left of the vertical solid black line. In that region, the number of monopoles produced in our model overcloses the universe, while this is

not the case in the standard scenario. On the other hand, in the red and blue areas the monopole energy density is less than the critical energy density of the universe. In the red area the monopoles are produced directly as local and the energy density is fixed by Eq. (9.17). In the blue area the monopoles are first produced as global, and only later acquired a magnetic charge. In this case the energy density is set by Eq. (9.16). The dashed contours in the blue area show the value of the monopole energy density in units of $GeV^4$.

We have demonstrated that the modification of the kinetic term of the gauge sector in Eq. (9.7) might enlarge the interval of allowed symmetry breaking scales to admit higher values of the vacuum expectation value. In particular, in our simplified model we have shown that for a quick enough redshifting of the $I$ function (for $s \geq 3$), it is possible to solve the monopole problem up to scale close to the Planck mass without the necessity of an inflationary epoch. Hence, once embedded in this model, even GUT-scale monopoles can be produced during phase transitions after inflation without any problem for the cosmology, solving the monopole problem.

# Chapter 10

# Conclusion

In this thesis, we have highlighted the importance of the studies on the dynamics of magnetic monopoles accelerated by cosmic magnetic fields within a cosmic setting, exploring various potential applications of analyzing the monopole-cosmic magnetic field interaction. In this conclusion, we review the main results of the work and discuss future directions.

The first half of this thesis has been dedicated to the study of the monopole system in the late universe. In particular, we have comprehensively analyzed the acceleration of magnetic monopoles in intergalactic and galactic space, in light of the modern understanding of galactic and intergalactic magnetic fields. We found that monopoles with intermediate to low masses are accelerated to relativistic velocities. We have also shown that if the cosmic flux of magnetic monopoles is larger enough, their backreaction on IGMFs is non-negligible. In this case, the energy oscillates between the IGMFs and the monopoles, and the oscillation-averaged monopole velocity depends on the monopole density. Future developments in studies of IGMFs may be able to constrain such IGMF-monopole oscillations, which will allow us to improve bounds on the monopole flux. Although this will not happen presumably in the near future, this is the first time that a cosmological probe for a monopole abundance well below the dark matter abundance or the terrestrial experiment sensitivity has been proposed for the detection of magnetic monopoles. Finally, we also note that a cosmic population of relativistic monopoles from IGMF acceleration can serve as dark radiation, which may be further constrained by cosmological studies. Given the monopole acceleration mechanism in intergalactic voids that we have described, this might be an independent test to constrain the cosmic monopole abundance.

We have then shown some applications of the monopole acceleration study, as a deeper understanding of the monopole acceleration in cosmic magnetic fields is crucial for both indirect and direct bounds on the monopole abundance. In particular, we first studied the mechanism at the basis of the galactic Parker bounds, generalizing the bounds for arbitrarily charged monopoles. We noticed that while monopoles with a Dirac charge have to be heavier than $10^{18}$ GeV to cluster with our Galaxy, minicharged monopoles can cluster with much lighter masses. For monopoles that can cluster with our Galaxy, the Parker bounds are generically less constraining than the bound from the dark matter density. Such monopoles can thus make up

the entire dark matter. Subsequently, we studied how the Galactic Parker bounds are modified for fast-moving monopoles accelerated in the IGMFs. Although it has been assumed in the literature that the initial monopole velocity with respect to the Milky Way Galaxy is of the order of the peculiar velocity or the virial velocity of the Galaxy, this is not necessarily the case in the presence of IGMFs. Therefore, we have shown that large monopole velocities weaken the so-called extended Parker bound based on the survival of seed Galactic magnetic fields. On the other hand, the Parker bound from the present-day Galactic field is unaffected by IGMFs that are compatible with observations. Any additional magnetic fields around the Milky Way, such as those transported by galactic winds, can also accelerate the monopoles and further weaken the Parker bound. An accurate study of the effects of such fields requires numerical analyses, which we leave for future works.

Monopole acceleration in cosmic magnetic fields is also crucial for terrestrial experiments that seek magnetic monopoles. From our model of monopole acceleration in cosmic magnetic fields, we were able to rewrite the limits on the monopole flux in terrestrial experiments, usually presented in terms of the monopole velocity at the detector, in terms of the monopole mass. We have shown the updated monopole limits in Figure 5.3. We obtained that light monopoles $m < 10^4$ GeV are mostly constrained by the results from the Pierre Auger Observatory, while intermediate mass monopoles with $10^4$ GeV $< m < 10^{11}$ GeV are mostly constrained by the IceCube results. Monopoles with masses $10^{11}$ GeV $< m < 10^{16}$ GeV are still mostly constrained by the MACRO results, and more massive monopoles only by the cosmological abundance of dark matter. We encourage the experimental collaborations to present their future results following the same logic of this chapter. These results show that ultra-high energetic cosmic ray experiments can put very stringent bounds on the abundance of light to intermediate monopoles. We encourage other experimental collaborations to work on similar analysis.

The analysis in this thesis serves as a first step toward a complete understanding of monopole acceleration in cosmic environments. An accurate knowledge of the velocity of magnetic monopoles entering the Earth is crucial for interpreting the constraints from terrestrial detectors in terms of the monopole mass, as well as for strengthening the galactic Parker bounds. It would also be interesting to study relativistic monopoles as a possible explanation of the recently claimed detection of an extremely high-energy cosmic ray [151][1]. It will then be really important in the future to compute numerical simulations of monopole propagation in cosmic magnetic fields, and we encourage new studies on this topic.

In the second part of the thesis, under the assumption that the IGMFs we observe in intergalactic voids have a primordial origin, we have presented new results from the study of the monopole system in the early universe. We carried out a comprehensive study of the monopole dynamics in the early universe and its back-reaction to the primordial magnetic fields from the time when the primordial magnetic fields were generated to the epoch of $e^+e^-$ annihilation. Hence, we derived new bounds on the average abundance of magnetic monopoles in the universe by extending the Parker bound to the survival of the primordial magnetic fields during the radiation-dominated epoch and reheating.

---

[1]See also the earlier papers [76, 77, 152, 153, 154] that studied similar ideas.

In the case of magnetic monopoles with Dirac charges, for a sufficiently low reheating temperature, the bound from reheating is stronger than the original Parker bound and the limits from direct searches, even for GUT-scale monopoles. At low masses, the bound from reheating is stronger than that during radiation domination for a reheating temperature $T_{\rm dom} \lesssim 10$ GeV. In our analyses we assumed the plasma particles during the reheating epoch to always be in thermal equilibrium, however removing this assumption may further strengthen the bound on monopoles. We leave this for future studies.

We have then carried out a comprehensive study of the Parker-type bounds on magnetic monopoles with arbitrary charges, comparing the various bounds. Heavy monopoles are mainly constrained by the dark matter density limit, while intermediate to low mass monopoles are mainly constrained by the Parker bounds. Among the Parker bounds, the seed galactic field bound strongly constrains monopoles with a Dirac charge,[2] while the primordial bound from radiation domination can be the strongest for monopoles with small magnetic charges. This is because the bound from radiation domination in the low-mass regime is independent of the monopole charge, while the other Parker bounds become weaker for smaller charges. Minicharged monopoles are typically connected by dark strings, whose tension is set by the mass $\mu$ of dark photons; in addition, they appear as minicharged monopoles only at distances greater than $1/\mu$ (see, e.g., [18, 19]). In our analyses we ignored these effects, supposing that the force from the background magnetic field is stronger than the string tension, and that the field's coherence length is larger than $1/\mu$. These assumptions can break down depending on the dark photon mass, in which case our bounds can be modified.

We also studied extremal magnetic black holes, finding that they are mainly constrained by comparison with the dark matter density. However, even stronger constraints can in principle be obtained if there exist galaxies whose magnetic fields have coherence lengths much larger than those of the Milky Way. The large coherence lengths also lead to the acceleration of black holes up to the escape velocity within a rather short time period, and hence it is improbable that black holes remain clustered with such galaxies until today. The existence of galaxies not being able to host magnetic black holes, if confirmed, would rule out the possibility of magnetic black holes as a dark matter candidate. Although not yet certain, this might be the case for the characteristics of the Andromeda galaxy's magnetic fields. Therefore, it is very unlikely that extremal magnetic black holes might be dark matter. For extremal black holes, some of the Parker bounds could be modified by the presence of accretion disks and/or the electroweak corona [22, 23]. We leave detailed considerations of these effects for future analysis.

The monopole-primordial magnetic field system is also interesting for Schwinger production of monopole pairs in the early universe. Although not investigated in this thesis, this might provide a workable process for the production of magnetic monopoles after inflation. Hence, monopole pair production must be taken into account in the different mechanisms of primordial magnetogenesis presented in the literature because the produced pairs might induce a self-screening of the field

---

[2]We note however that, as we have shown in Chapter 4, in the presence of strong IGMFs the seed Galactic Parker bound might be significantly relaxed.

amplitude. Monopole pair production during primordial magnetogenesis is an important topic that should be investigated in the future. As a first contribution to the topic, we applied our new primordial bounds to the monopole pairs produced in primordial magnetic fields after the end of magnetogenesis to obtain the most conservative condition for the survival of the fields. We found that the bounds on the monopole density reduce to a weak field condition on the initial strength of the primordial magnetic fields, which can also be translated into a lower bound on the monopole mass. The work [45] obtained a similar bound by only considering the energy extraction by the production of the monopole pairs. We then concluded that as long as the initial amplitude of the primordial magnetic field is sufficiently below such a weak field condition, the back-reaction from Schwinger-produced monopoles can be safely ignored.

Finally, we have proposed a new solution to the problem of the over-abundance of monopoles produced during primordial phase transitions after inflation. Our model involves a modification of the kinetic term of the gauge sector of the lagrangian that breaks the conformal invariance on the same line of many models of magnetogenesis proposed in the literature. We demonstrated that in this model the monopoles are first produced as global and this involves a drastic reduction of the monopole abundance after monopole-antimonopole annihilation. This allows for symmetry-breaking scales as large as the Planck mass, reviving the possibility for even GUT-scale magnetic monopoles to be produced in sensible quantities after inflation, without any monopole problem.

At the end of this thesis, we remark that the physics of magnetic monopoles in the universe is far from being completely understood. We have shown that by a rigorous analysis of their dynamics in the late and early universe, it is possible to test high-energy fundamental physics, as well as models of primordial magnetogenesis, phase transitions in the early universe, the structure of cosmic magnetic fields and even models of dark matter. We hope that this work, which showed some applications of the analysis of the monopoles-cosmic magnetic fields system, may renew the interest of the community in the centenary, but more relevant than ever, quest for magnetic monopoles.

# Appendix A

# Primordial contribution to the monopole velocity

In Chapter 3, we did not specify the origin of the IGMFs. In particular in Section 3.2, we evaluated the velocity of magnetic monopoles that have been accelerated in IGMFs for a Hubble time. However it is often claimed in the literature that IGMFs have a primordial origin.[1] Based on this premise, one might inquire about the relevance of monopole acceleration in primordial magnetic fields after the epoch of $e^+e^-$ annihilation, since primordial fields would have been much stronger at higher redshifts. In this appendix, we demonstrate that the acceleration in primordial fields only give an order-unity correction to the results derived in Section 3.2.

Let us consider for simplicity a homogeneous primordial magnetic field. As shown in Chapter 6, the equation of motion of a magnetic monopole in an expanding universe filled with a homogeneous magnetic field with strength $B$ is

$$ m\frac{d}{dt}(\gamma v) = gB - f_\mathrm{p}v - mH\gamma v, \tag{A.1} $$

where we ignored velocity components perpendicular to the direction of the magnetic field. The last two terms in the right-hand side denote frictional forces from the monopole scattering on charged particles in the primordial plasma, and from the cosmological expansion, with $H$ being the Hubble rate.

Before electron-positron annihilation, one can write the friction coefficient $f_\mathrm{p}$ as [1, 58]

$$ f_p \sim \frac{e^2 g^2 \mathcal{N}_c}{16\pi^2}T^2, \tag{A.2} $$

where $\mathcal{N}_c$ is the number of relativistic and electrically charged degrees of freedom in thermal equilibrium, and $T$ is the temperature of the plasma. Considering magnetic monopoles with charges not too far from the Dirac charge, the Hubble friction is negligible compared to the friction from the plasma [1, 2]. The monopoles thus approach a terminal velocity which results from equating the first two terms in the right-hand side of Eq. (A.1) as

$$ v_\mathrm{p} = \frac{gB}{f_\mathrm{p}} \sim 10^{-8} \left(\frac{g_D}{g}\right)\left(\frac{B_\mathrm{I}}{10^{-15}G}\right). \tag{A.3} $$

---

[1] See, e.g., [155] for an alternative explanation.

We note that the terminal velocity before the electron-positron annihilation is constant, since the homogeneous magnetic field $B$ and the friction coefficient $f_\mathrm{p} \propto T^2$ both redshift[2] as $(1+z)^2$. In the far right-hand side of Eq. (A.3), $B_\mathrm{I}$ represents the present-day magnetic field strength.

After electron-positron annihilation, the number of the free charged particles drops by 10 orders of magnitude, so one can neglect the plasma friction, i.e. the second term in the right-hand side of Eq. (A.1). Then the present-day monopole velocity can be obtained by integrating Eq. (A.1) as

$$(\gamma v)_0 = \frac{(\gamma v)_\mathrm{p}}{1 + z_\mathrm{an}} + \int_0^{z_\mathrm{an}} \frac{gB(z)}{mH(z)(1+z)^2} dz \approx \frac{(\gamma v)_\mathrm{p}}{1 + z_\mathrm{an}} + 3 \times \frac{gB_\mathrm{I}}{mH_0}, \qquad (A.4)$$

where $z_\mathrm{an} \sim 10^9$ is the redshift at electron-positron annihilation. Since the homogeneous magnetic field redshifts as $B(z) \propto (1+z)^2$, the only redshift dependence in the integrand comes from the Hubble rate $H(z)$. Upon moving to the far right-hand side, we have used the cosmological parameters for $\Lambda$CDM cosmology [113] and numerically integrated the second term. Using Eq. (A.3), the ratio between the two terms in Eq. (A.4) is written as

$$\frac{(\gamma v)_\mathrm{p}}{1 + z_\mathrm{an}} \left( \frac{gB_\mathrm{I}}{mH_0} \right)^{-1} \sim 10^{-8} \left( \frac{g_\mathrm{D}}{g} \right)^2 \left( \frac{m}{10^{18}\,\mathrm{GeV}} \right), \qquad (A.5)$$

which shows that the first term is negligible for monopole masses considered in this paper. Hence we obtain the velocity of magnetic monopoles accelerated in a homogeneous primordial magnetic field as

$$(\gamma v)_0 \approx 3 \times \frac{gB_\mathrm{I}}{mH_0}. \qquad (A.6)$$

This matches with the result given in Eq. (3.28) at the order-of-magnitude level. We therefore conclude that the order-of-magnitude results of this paper remain unaffected, even if the IGMFs have a primordial origin.

---

[2]Magnetic fields with small coherence lengths can evolve differently, when the wave mode is inside the Hubble horizon [70].

# Appendix B

# Monopole-magnetic field oscillation

If magnetic monopoles accelerated in magnetic fields do not dissipate their kinetic energy into the ambient plasma, they eventually return the energy to the magnetic fields. In this way the energy can move back and forth between the magnetic field and monopoles. However one would expect such oscillations to be subject to Landau damping, if the phase velocity of the magnetic field were smaller than the random velocity of the individual monopoles [48].

In order to estimate the phase velocity, we start by considering a homogeneous one-dimensional system where the magnetic field has a component $B$ along a certain direction, and the monopoles with charge $g$ ($> 0$) have a velocity component $v$ along the same direction. (In this appendix, $B$ and $v$ are not the amplitudes and thus can be negative.) Then by combining the monopoles' equation of motion, $m\,d(\gamma v)/dt = gB$, with the conservation of total energy density $\rho_{\rm tot} = nm\gamma + B^2/2$ where $n$ is the monopole number density, one obtains an evolution equation for the magnetic field,

$$\frac{d^2 B}{dt^2} + \Omega^2 B = 0. \tag{B.1}$$

Here $\Omega$ is the effective frequency taking the form:

$$\Omega = \frac{g}{\gamma^{3/2}} \left(\frac{n}{m}\right)^{1/2}. \tag{B.2}$$

This becomes time-independent for nonrelativistic monopoles ($\gamma \simeq 1$), hence let us focus on this case for simplicity. Further supposing that inhomogeneous fields with a finite coherence length $\lambda$ also oscillate with this frequency, then the magnetic field's phase velocity is obtained as $v_{\rm ph} = \lambda\Omega/2\pi$.

*Galactic magnetic fields.* The phase velocity of Galactic fields with coherence length $\lambda_{\rm G}$ is of

$$v_{\rm ph} \sim 10^{-5} \left(\frac{v_{\rm MW}}{10^{-3}}\right)^{-1/2} \left(\frac{F_{\rm MW}}{10^{-15}\,{\rm cm}^{-2}{\rm sec}^{-1}{\rm sr}^{-1}}\right)^{1/2} \left(\frac{g}{g_{\rm D}}\right) \left(\frac{m}{10^{18}\,{\rm GeV}}\right)^{-1/2} \left(\frac{\lambda_{\rm G}}{1\,{\rm kpc}}\right). \tag{B.3}$$

We have rewritten $n$ in terms of the monopole flux in the rest frame of the Milky Way Galaxy (cf. below (3.37); however here we consider both clustered and unclustered

monopoles). The reference value for the flux is set to the Galactic Parker limit at $m = 10^{18}\,\mathrm{GeV}$ (cf. Figure 4.1). Note that magnetic monopoles with a Dirac charge and mass $m \gtrsim 10^{18}\,\mathrm{GeV}$ can cluster with the Galaxy [2, 48]. Such clustered monopoles obtain a virial velocity of $10^{-3}$, which is larger than the magnetic field's phase velocity; hence the oscillation is expected to rapidly evaporate. The phase velocity can in principle become larger for smaller masses, however light monopoles do not cluster and hence should pass through the Galaxy before (completely) returning the energy to the Galactic fields. A flux much larger than the Parker limit can also increase the phase velocity beyond the virial velocity, however [50] claimed that oscillating Galactic fields do not match with observations, and also that the inhomogeneity in the monopole distribution further leads to the damping of the oscillations. For these reasons, one can trust the Parker bound without worrying about the possibility that the Galactic fields survive as oscillating fields.

*Intergalactic magnetic fields.* The phase velocity of IGMFs is of

$$v_{\mathrm{ph}} \sim 10^{-5}\, v_{\mathrm{CMB}}^{-1/2} \left( \frac{F_{\mathrm{CMB}}}{10^{-27}\,\mathrm{cm}^{-2}\mathrm{sec}^{-1}\mathrm{sr}^{-1}} \right)^{1/2} \left( \frac{g}{g_{\mathrm{D}}} \right) \left( \frac{m}{10^{10}\,\mathrm{GeV}} \right)^{-1/2} \left( \frac{\lambda_{\mathrm{I}}}{1\,\mathrm{Mpc}} \right).$$

(B.4)

Here we rewrote $n$ in terms of the flux in the CMB rest frame (cf. below (3.32)), and for its reference value used the flux threshold where the monopole backreaction becomes relevant for IGMFs with $B_{\mathrm{I}} = 10^{-15}\,\mathrm{G}$ at $m = 10^{10}\,\mathrm{GeV}$ (cf. Figure 3.1). Note that the phase velocity increases for smaller $m$ and $v_{\mathrm{CMB}}$. Magnetic monopoles in the intergalactic space can obtain random velocities from scattering with the IGM and/or from gravitational potentials. However we expect these to be much smaller than the IGMF's phase velocity, and hence in this paper we consider the IGMF-monopole oscillations to survive.

# Appendix C

# The universe from the end of inflation to the matter-radiation equality

In this appendix, we derive the relations between the Hubble rate, the cosmic temperature and the scale factor both during reheating and in the following radiation-dominated epoch. We define $t_{\text{end}}$ as the time of the end of inflation, when the universe begins to be dominated by an oscillating inflaton field. The inflaton eventually decays into radiaton, and at time $t_{\text{dom}}$ the radiation component starts to dominate the universe. Then at time $t_{\text{eq}}$, the time of matter-radiation equality, matter domination begins. Setting $t_{\text{end}} = t_{\text{dom}}$ corresponds to the case of an instantaneous reheating.

During radiation domination, for times $t_{\text{dom}} \ll t \ll t_{\text{eq}}$, the Friedmann equation gives $3M_{\text{Pl}}^2 H^2 \simeq \rho_{\text{rad}}$, with $\rho_{\text{rad}} = (\pi^2/30)g_* T^4$ the radiation energy density and $T$ the radiation temperature. Considering the expression for the entropy density $s = (2\pi^2/45)g_{*s}T^3$, we get (the subscript "0" denotes quantities in the present universe):

$$H \simeq \left(\frac{45}{128\pi^2}\right)^{1/6} \frac{g_*^{1/2}}{g_{*s}^{2/3}} \frac{s_0^{2/3}}{M_{\text{Pl}}} \left(\frac{a_0}{a}\right)^2, \quad T \simeq \left(\frac{45}{2\pi^2} \frac{s_0}{g_{*s}}\right)^{1/3} \frac{a_0}{a}. \tag{C.1}$$

Here we have assumed the conservation of entropy until today, i.e. $s \propto a^{-3}$. The relation between the scale factor and the temperature during radiation domination is as follows:

$$\left(\frac{a_0}{a}\right)^3 = \frac{g_{*s}T^3}{g_{*s,0}T_0^3}. \tag{C.2}$$

During reheating, for times $t_{\text{end}} \ll t \ll t_{\text{dom}}$, the oscillating inflaton field decays perturbatively into relativistic particles. During this period the universe is effectively matter-dominated, with $H \propto a^{-3/2}$. Let us assume that the relativistic particles are in thermal equilibrium also during this period, so that $\rho_{\text{rad}} = (\pi^2/30)g_* T^4$ holds. For simplicity, we ignore the time dependence of $g_{*(s)}$ before radiation domination. This amounts to assuming that no additional relativistic degrees of freedom appear as one goes back in time from $t = t_{\text{dom}}$. Then the radiation density, which is sourced by the inflaton decay, evolves as $\rho_{\text{rad}} \propto a^{-3/2}$. The scaling behavior of $\rho_{\text{rad}}$ can be

verified by solving the continuity equation $\dot{\rho}_{\rm rad} + 4H\rho_{\rm rad} = \Gamma_\phi \rho_\phi$, where $\Gamma_\phi$ is the inflaton decay rate and $\rho_\phi = \rho_{\phi\,\rm inf}(a_{\rm inf}/a)^3 e^{-\Gamma_\phi(t-t_{\rm inf})}$ is the energy density of the inflaton field [47]. The radiation temperature thus redshifts as $T \propto a^{-3/8}$. We can also write the relation between the scale factor and the temperature before radiation domination as:

$$\frac{a_0}{a} = \frac{a_{\rm dom}}{a}\frac{a_0}{a_{\rm dom}} = \left(\frac{T}{T_{\rm dom}}\right)^{8/3}\left(\frac{g_{*s,\rm dom}}{g_{*s,0}}\right)^{1/3}\left(\frac{T_{\rm dom}}{T_0}\right). \tag{C.3}$$

We summarize the dependence on the scale factor of the Hubble rate and of the temperature in the following expressions:

$$H \simeq H_{\rm dom} \min\left\{\left(\frac{a_{\rm dom}}{a}\right)^{3/2}, \left(\frac{g_*}{g_{*,\rm dom}}\right)^{1/2}\left(\frac{g_{*s,\rm dom}}{g_{*s}}\right)^{2/3}\left(\frac{a_{\rm dom}}{a}\right)^2\right\},$$
$$T \simeq T_{\rm dom} \min\left\{\left(\frac{a_{\rm dom}}{a}\right)^{3/8}, \left(\frac{g_{*s,\rm dom}}{g_{*s}}\right)^{1/3}\left(\frac{a_{\rm dom}}{a}\right)\right\}. \tag{C.4}$$

The first expression in the curly brackets holds for $t_{\rm end} < t < t_{\rm dom}$ and the second for $t_{\rm dom} < t < t_{\rm eq}$.

By extrapolating Eq. (C.1) to the time when radiation domination begins, we can obtain the relations between $H_{\rm dom}$, $T_{\rm dom}$, and $a_{\rm dom}$. After substituting numerical values for the reduced Planck mass $M_{\rm Pl}$ and for the cosmological parameters we get:

$$\frac{a_0}{a_{\rm dom}} \simeq 10^{29}\left(\frac{H_{\rm dom}}{10^{14}{\rm GeV}}\right)^{1/2}, \quad T_{\rm dom} \simeq 10^{16}{\rm GeV}\left(\frac{H_{\rm dom}}{10^{14}{\rm GeV}}\right)^{1/2}. \tag{C.5}$$

We also underline that these expressions present only a weak dependence on $g_{*(s)}$ and then the order-of-magnitude estimates are not affected by its precise value. Reversing the first line in Eq. (C.4) and ignoring the contributions of $g_{*(s)}$, we express the scale factor as a function of the Hubble rate:

$$\frac{a_{\rm dom}}{a} \simeq \left(\frac{H}{H_{\rm dom}}\right)^{1/2}\max\left\{\left(\frac{H}{H_{\rm dom}}\right)^{1/6}, 1\right\}. \tag{C.6}$$

The first term inside the curly brackets holds for $t_{\rm inf} < t < t_{\rm dom}$ and the second for $t_{\rm dom} < t < t_{\rm eq}$.

# Bibliography

[1] Takeshi Kobayashi and Daniele Perri. Parker bound and monopole pair production from primordial magnetic fields. Phys. Rev. D, 106(6):063016, 2022.

[2] Takeshi Kobayashi and Daniele Perri. Parker bounds on monopoles with arbitrary charge from galactic and primordial magnetic fields. Phys. Rev. D, 108(8):083005, 2023.

[3] Daniele Perri, Kyrilo Bondarenko, Michele Doro, and Takeshi Kobayashi. Monopole acceleration in intergalactic magnetic fields. 12 2023.

[4] Daniele Perri, Kyrylo Bondarenko, Michele Doro, and Takeshi Kobayashi. in preparation.

[5] Paul Adrien Maurice Dirac. Quantised singularities in the electromagnetic field,. Proc. Roy. Soc. Lond. A, 133(821):60–72, 1931.

[6] Gerard 't Hooft. Magnetic Monopoles in Unified Gauge Theories. Nucl. Phys. B, 79:276–284, 1974.

[7] Alexander M. Polyakov. Particle Spectrum in Quantum Field Theory. JETP Lett., 20:194–195, 1974.

[8] John Preskill. Cosmological Production of Superheavy Magnetic Monopoles. Phys. Rev. Lett., 43:1365, 1979.

[9] Ya. B. Zeldovich and M. Yu. Khlopov. On the Concentration of Relic Magnetic Monopoles in the Universe. Phys. Lett. B, 79:239–241, 1978.

[10] A. Vilenkin and E. P. S. Shellard. Cosmic Strings and Other Topological Defects. Cambridge University Press, 7 2000.

[11] A. Kogut et al. Dipole anisotropy in the COBE DMR first year sky maps. Astrophys. J., 419:1, 1993.

[12] Julian S. Schwinger. On gauge invariance and vacuum polarization. Phys. Rev., 82:664–679, 1951.

[13] Ian K. Affleck and Nicholas S. Manton. Monopole Pair Production in a Magnetic Field. Nucl. Phys. B, 194:38–64, 1982.

[14] Ian K. Affleck, Orlando Alvarez, and Nicholas S. Manton. Pair Production at Strong Coupling in Weak External Fields. Nucl. Phys. B, 197:509–519, 1982.

[15] Felix Brummer and Joerg Jaeckel. Minicharges and Magnetic Monopoles. Phys. Lett. B, 675:360–364, 2009.

[16] Michele Del Zotto, Jonathan J. Heckman, Piyush Kumar, Arada Malekian, and Brian Wecht. Kinetic Mixing at Strong Coupling. Phys. Rev. D, 95(1):016007, 2017.

[17] Catalina Gomez Sanchez and Bob Holdom. Monopoles, strings and dark matter. Phys. Rev. D, 83:123524, 2011.

[18] Anson Hook and Junwu Huang. Bounding millimagnetically charged particles with magnetars. Phys. Rev. D, 96(5):055010, 2017.

[19] Takashi Hiramatsu, Masahiro Ibe, Motoo Suzuki, and Soma Yamaguchi. Gauge kinetic mixing and dark topological defects. JHEP, 12:122, 2021.

[20] Michael L. Graesser, Ian M. Shoemaker, and Natalia Tapia Arellano. Millimagnetic monopole dark matter and the survival of galactic magnetic fields. JHEP, 03:105, 2022.

[21] Ignacio J. Araya, Nelson D. Padilla, Marcelo E. Rubio, Joaquín Sureda, Juan Magaña, and Loreto Osorio. Dark matter from primordial black holes would hold charge. JCAP, 02:030, 2023.

[22] Juan Maldacena. Comments on magnetic black holes. JHEP, 04:079, 2021.

[23] Yang Bai, Joshua Berger, Mrunal Korwar, and Nicholas Orlofsky. Phenomenology of magnetic black holes with electroweak-symmetric coronas. JHEP, 10:210, 2020.

[24] Chen Zhang and Xin Zhang. Gravitational capture of magnetic monopoles by primordial black holes in the early universe. JHEP, 10:037, 2023.

[25] Diptimoy Ghosh, Arun Thalapillil, and Farman Ullah. Astrophysical hints for magnetic black holes. Phys. Rev. D, 103(2):023006, 2021.

[26] Digvijay Wadekar and Zihui Wang. Constraining axion and compact dark matter with interstellar medium heating. Phys. Rev. D, 107(8):083011, 2023.

[27] Melissa D. Diamond and David E. Kaplan. Constraints on relic magnetic black holes. JHEP, 03:157, 2022.

[28] I. J. Araya, M. E. Rubio, Marco San Martin, F. A. Stasyszyn, N. D. Padilla, J. Magaña, and J. Sureda. Magnetic field generation from PBH distributions. Mon. Not. Roy. Astron. Soc., 503(3):4387–4399, 2021.

[29] Blas Cabrera. First Results from a Superconductive Detector for Moving Magnetic Monopoles. Phys. Rev. Lett., 48:1378–1380, 1982.

[30] M. Ambrosio et al. The MACRO detector at Gran Sasso. Nucl. Instrum. Meth. A, 486:663–707, 2002.

[31] R. Abbasi et al. Search for Relativistic Magnetic Monopoles with Eight Years of IceCube Data. Phys. Rev. Lett., 128(5):051101, 2022.

[32] R. Abbasi et al. Search for Relativistic Magnetic Monopoles with IceCube. Phys. Rev. D, 87(2):022001, 2013.

[33] M. G. Aartsen et al. Search for non-relativistic Magnetic Monopoles with IceCube. Eur. Phys. J. C, 74(7):2938, 2014. [Erratum: Eur.Phys.J.C 79, 124 (2019)].

[34] M. G. Aartsen et al. Searches for Relativistic Magnetic Monopoles in IceCube. Eur. Phys. J. C, 76(3):133, 2016.

[35] A. Albert et al. Search for magnetic monopoles with ten years of the ANTARES neutrino telescope. JHEAp, 34:1–8, 2022.

[36] Martin Frank, Alex Antoshkin, Craig Dukes, Ralf Ehrlich, and Enhao Song. Subluminal Magnetic Monopole Search with NOvA. PoS, ICRC2019:888, 2020.

[37] V. A. Rubakov. Superheavy Magnetic Monopoles and Proton Decay. JETP Lett., 33:644–646, 1981.

[38] Curtis G. Callan, Jr. Monopole Catalysis of Baryon Decay. Nucl. Phys. B, 212:391–400, 1983.

[39] J. Derkaoui, G. Giacomelli, T. Lari, A. Margiotta, M. Ouchrif, L. Patrizii, V. Popa, and V. Togo. Energy losses of magnetic monopoles and of dyons in the earth. Astropart. Phys., 9:173–183, 1998.

[40] K. Ueno et al. Search for GUT monopoles at Super–Kamiokande. Astropart. Phys., 36:131–136, 2012.

[41] James Pinfold et al. Technical Design Report of the MoEDAL Experiment. 6 2009.

[42] B. Acharya et al. Search for magnetic monopoles produced via the Schwinger mechanism. Nature, 602(7895):63–67, 2022.

[43] Search for magnetic monopole pair production in ultraperipheral Pb+Pb collisions at $\sqrt{s_{\mathrm{NN}}} = 5.36$ TeV with the ATLAS detector at the LHC. 2024.

[44] Oliver Gould and Arttu Rajantie. Magnetic monopole mass bounds from heavy ion collisions and neutron stars. Phys. Rev. Lett., 119(24):241601, 2017.

[45] Takeshi Kobayashi. Monopole-antimonopole pair production in primordial magnetic fields. Phys. Rev. D, 104(4):043501, 2021.

[46] P. A. Zyla et al. Review of Particle Physics. PTEP, 2020(8):083C01, 2020.

[47] Edward W. Kolb. The Early Universe, volume 69. Taylor and Francis, 5 2019.

[48] Michael S. Turner, Eugene N. Parker, and T. J. Bogdan. Magnetic Monopoles and the Survival of Galactic Magnetic Fields. Phys. Rev. D, 26:1296, 1982.

[49] Eugene N. Parker. The Origin of Magnetic Fields. Astrophys. J., 160:383, 1970.

[50] Eugene N. Parker. Magnetic Monopole Plasma Oscillations and the Survival of Galactic Magnetic Fields. Astrophys. J., 321:349, 1987.

[51] Fred C. Adams, Marco Fatuzzo, Katherine Freese, Gregory Tarle, Richard Watkins, and Michael S. Turner. Extension of the Parker bound on the flux of magnetic monopoles. Phys. Rev. Lett., 70:2511–2514, 1993.

[52] Yoel Rephaeli and Michael S. Turner. The Magnetic Monopole Flux and the Survival of Intracluster Magnetic Fields. Phys. Lett. B, 121:115–118, 1983.

[53] F. Tavecchio, G. Ghisellini, L. Foschini, G. Bonnoli, G. Ghirlanda, and P. Coppi. The intergalactic magnetic field constrained by Fermi/LAT observations of the TeV blazar 1ES 0229+200. Mon. Not. Roy. Astron. Soc., 406:L70–L74, 2010.

[54] A. Neronov and I. Vovk. Evidence for strong extragalactic magnetic fields from Fermi observations of TeV blazars. Science, 328:73–75, 2010.

[55] Charles D. Dermer, Massimo Cavadini, Soebur Razzaque, Justin D. Finke, James Chiang, and Benoit Lott. Time Delay of Cascade Radiation for TeV Blazars and the Measurement of the Intergalactic Magnetic Field. Astrophys. J. Lett., 733:L21, 2011.

[56] V. A. Acciari et al. A lower bound on intergalactic magnetic fields from time variability of 1ES 0229+200 from MAGIC and Fermi/LAT observations. Astron. Astrophys.

[57] Kandaswamy Subramanian. The origin, evolution and signatures of primordial magnetic fields. Rept. Prog. Phys., 79(7):076901, 2016.

[58] Andrew J. Long and Tanmay Vachaspati. Implications of a Primordial Magnetic Field for Magnetic Monopoles, Axions, and Dirac Neutrinos. Phys. Rev. D, 91:103522, 2015.

[59] Lawrence M. Widrow. Origin of galactic and extragalactic magnetic fields. Rev. Mod. Phys., 74:775–823, 2002.

[60] Michael Unger and Glennys R. Farrar. The Coherent Magnetic Field of the Milky Way. 11 2023.

[61] John D. Barrow, Pedro G. Ferreira, and Joseph Silk. Constraints on a primordial magnetic field. Phys. Rev. Lett., 78:3610–3613, May 1997.

[62] Andrii Neronov, Dmitri Semikoz, and Oleg Kalashev. Limit on intergalactic magnetic field from ultra-high-energy cosmic ray hotspot in Perseus-Pisces region. 12 2021.

[63] Rafael Alves Batista and Andrey Saveliev. The Gamma-ray Window to Intergalactic Magnetism. Universe, 7(7):223, 2021.

[64] M. Ackermann et al. The Search for Spatial Extension in High-latitude Sources Detected by the Fermi Large Area Telescope. , 237(2):32, August 2018.

[65] D. Miceli, P. Da Vela, and E. Prandini. Prospects for detection of the pair-echo emission from TeV gamma-ray bursts. 5 2024.

[66] Zi-Qing Xia, Yun Wang, Qiang Yuan, and Yi-Zhong Fan. A delayed 400 GeV photon from GRB 221009A and implication on the intergalactic magnetic field. Nature Commun., 15(1):4280, 2024.

[67] Avery E. Broderick, Philip Chang, and Christoph Pfrommer. The Cosmological Impact of Luminous TeV Blazars I: Implications of Plasma Instabilities for the Intergalactic Magnetic Field and Extragalactic Gamma-Ray Background. Astrophys. J., 752:22, 2012.

[68] Francesco Miniati and Andrii Elyiv. Relaxation of Blazar Induced Pair Beams in Cosmic Voids: Measurement of Magnetic Field in Voids and Thermal History of the IGM. Astrophys. J., 770:54, 2013.

[69] Andrii Neronov and Ievgen Vovk. Evidence for Strong Extragalactic Magnetic Fields from Fermi Observations of TeV Blazars. Science, 328(5974):73, April 2010.

[70] Ruth Durrer and Andrii Neronov. Cosmological Magnetic Fields: Their Generation, Evolution and Observation. Astron. Astrophys. Rev., 21:62, 2013.

[71] Michael S. Turner and Lawrence M. Widrow. Inflation Produced, Large Scale Magnetic Fields. Phys. Rev. D, 37:2743, 1988.

[72] Bharat Ratra. Cosmological 'seed' magnetic field from inflation. Astrophys. J. Lett., 391:L1–L4, 1992.

[73] Takeshi Kobayashi. Primordial Magnetic Fields from the Post-Inflationary Universe. JCAP, 05:040, 2014.

[74] T. Vachaspati. Magnetic fields from cosmological phase transitions. Phys. Lett. B, 265:258–261, 1991.

[75] John M. Cornwall. Speculations on primordial magnetic helicity. Phys. Rev. D, 56:6146–6154, 1997.

[76] Thomas W. Kephart and Thomas J. Weiler. Magnetic monopoles as the highest energy cosmic ray primaries. Astropart. Phys., 4:271–279, 1996.

[77] C. O. Escobar and R. A. Vazquez. Are high-energy cosmic rays magnetic monopoles? Astropart. Phys., 10:197–202, 1999.

[78] Stuart D. Wick, Thomas W. Kephart, Thomas J. Weiler, and Peter L. Biermann. Signatures for a cosmic flux of magnetic monopoles. Astropart. Phys., 18:663–687, 2003.

[79] J.J. Thomson. Xxxiv. on momentum in the electric field. The London, Edinburgh, and Dublin Philosophical Magazine and Journal of Science, 8(45):331–356, 1904.

[80] John Preskill. Magnetic Monopoles. Ann. Rev. Nucl. Part. Sci., 34:461–530, 1984.

[81] Nick E. Mavromatos and Vasiliki A. Mitsou. Magnetic monopoles revisited: Models and searches at colliders and in the Cosmos. Int. J. Mod. Phys. A, 35(23):2030012, 2020.

[82] N. Cabibbo and E. Ferrari. Quantum electrodynamics with Dirac monopoles. Nuovo Cim., 23:1147–1154, 1962.

[83] A. Salam. Magnetic monopole and two photon theories of c-violation. Physics Letters, 22(5):683–684, 1966.

[84] Daniel Zwanziger. Local-lagrangian quantum field theory of electric and magnetic charges. Phys. Rev. D, 3:880–891, Feb 1971.

[85] M. K. Prasad and Charles M. Sommerfield. Exact classical solution for the 't hooft monopole and the julia-zee dyon. Phys. Rev. Lett., 35:760–762, Sep 1975.

[86] Th. Kaluza. Zum Unitätsproblem der Physik. Sitzungsber. Preuss. Akad. Wiss. Berlin (Math. Phys. ), 1921:966–972, 1921.

[87] Oskar Klein. Quantum Theory and Five-Dimensional Theory of Relativity. (In German and English). Z. Phys., 37:895–906, 1926.

[88] David J. Gross and Malcolm J. Perry. Magnetic monopoles in kaluza-klein theories. Nuclear Physics B, 226(1):29–48, 1983.

[89] C. Nash and S. Sen. Topology and Geometry for Physicists. 1983.

[90] Armen Tumasyan et al. Search for strongly interacting massive particles generating trackless jets in proton–proton collisions at $\sqrt{s} = 13\,\text{TeV}$. Eur. Phys. J. C, 82(3):213, 2022.

[91] Georges Aad et al. Search for magnetic monopoles and stable particles with high electric charges in $\sqrt{s} = 13$ TeV pp collisions with the ATLAS detector. JHEP, 11:112, 2023.

[92] B. Acharya et al. Search for highly-ionizing particles in *pp* collisions at the LHC's Run-1 using the prototype MoEDAL detector. Eur. Phys. J. C, 82(8):694, 2022.

[93] Kimball A. Milton. Theoretical and experimental status of magnetic monopoles. Rept. Prog. Phys., 69:1637–1712, 2006.

[94] T. W. B. Kibble. Topology of Cosmic Domains and Strings. J. Phys. A, 9:1387–1398, 1976.

[95] Alan H. Guth and Erick J. Weinberg. Could the Universe Have Recovered from a Slow First Order Phase Transition? Nucl. Phys. B, 212:321–364, 1983.

[96] Paul Langacker and So-Young Pi. Magnetic Monopoles in Grand Unified Theories. Phys. Rev. Lett., 45:1, 1980.

[97] Michael S. Turner. Thermal production of superheavy magnetic monopoles in the early universe. Physics Letters B, 115(2):95–98, 1982.

[98] Oliver Gould and Arttu Rajantie. Thermal Schwinger pair production at arbitrary coupling. Phys. Rev. D, 96(7):076002, 2017.

[99] Oliver Gould, Arttu Rajantie, and Cheng Xie. Worldline sphaleron for thermal Schwinger pair production. Phys. Rev. D, 98(5):056022, 2018.

[100] Takuya Akahori et al. Cosmic Magnetism in Centimeter and Meter Wavelength Radio Astronomy. Publ. Astron. Soc. Jap., 70(1):R2, 2018.

[101] Ana Erceg, Vibor Jelić, Marijke Haverkorn, Andrea Bracco, Timothy W. Shimwell, Cyril Tasse, John M. Dickey, Lana Ceraj, Alexander Drabent, Martin J. Hardcastle, and Luka Turić. Faraday tomography of lotss-dr2 data: I. faraday moments in the high-latitude outer galaxy and revealing loop iii in polarisation. Astronomy and Astrophysics, 663:A7, 2022.

[102] E. Carretti, S. P. O'Sullivan, V. Vacca, F. Vazza, C. Gheller, T. Vernstrom, and A. Bonafede. Magnetic field evolution in cosmic filaments with LOFAR data. Mon. Not. Roy. Astron. Soc., 518(2):2273–2286, 2022.

[103] S. P. O'Sullivan et al. The Faraday Rotation Measure Grid of the LOFAR Two-metre Sky Survey: Data Release 2. Mon. Not. Roy. Astron. Soc., 519(4):5723–5742, 2023.

[104] V. Heesen, S. P. O'Sullivan, M. Brüggen, A. Basu, R. Beck, A. Seta, E. Carretti, M. G. H. Krause, M. Haverkorn, S. Hutschenreuter, A. Bracco, M. Stein, D. J. Bomans, R. J. Dettmar, K. T. Chyży, G. H. Heald, R. Paladino, and C. Horellou. Detection of magnetic fields in the circumgalactic medium of nearby galaxies using Faraday rotation. Astronomy and Astrophysics, 670:L23, 2023.

[105] Serena Bertone, Corina Vogt, and Torsten Ensslin. Magnetic Field Seeding by Galactic Winds. Mon. Not. Roy. Astron. Soc., 370:319–330, 2006.

[106] Karsten Jedamzik and Andrey Saveliev. Stringent Limit on Primordial Magnetic Fields from the Cosmic Microwave Background Radiation. Phys. Rev. Lett., 123(2):021301, 2019.

[107] A. J. S. Hamilton and C. L. Sarazin. Deceleration of Grand Unified Theory monopoles in a plasma. Astrophys. J., 274:399–407, 1983.

[108] N. Meyer-Vernet. Energy loss by slow magnetic monopoles in a thermal plasma. Astrophys. J., 290:21–23, 1985.

[109] S. P. Ahlen. Theoretical and Experimental Aspects of the Energy Loss of Relativistic Heavily Ionizing Particles. Rev. Mod. Phys., 52:121–173, 1980. [Erratum: Rev.Mod.Phys. 52, 653–653 (1980)].

[110] Malcolm S. Longair. High Energy Astrophysics. Cambridge University Press, 3 edition, 2011.

[111] Tigran G. Arshakian, Rainer Beck, Marita Krause, and Dmitry Sokoloff. Evolution of magnetic fields in galaxies and future observational tests with the Square Kilometre Array. Astron. Astrophys., 494:21, 2009.

[112] A. M. Beck, H. Lesch, K. Dolag, H. Kotarba, A. Geng, and F. A. Stasyszyn. Origin of strong magnetic fields in Milky Way-like galactic haloes. , 422(3):2152–2163, May 2012.

[113] N. Aghanim et al. Planck 2018 results. VI. Cosmological parameters. Astron. Astrophys., 641:A6, 2020. [Erratum: Astron.Astrophys. 652, C4 (2021)].

[114] J. I. Read. The Local Dark Matter Density. J. Phys. G, 41:063101, 2014.

[115] Andrew Fletcher, E. M. Berkhuijsen, R. Beck, and A. Shukurov. The Magnetic field of M 31 from multi-wavelength radio polarization observations. Astron. Astrophys., 414:53–67, 2004.

[116] D. P. Hogan, D. Z. Besson, J. P. Ralston, I. Kravchenko, and D. Seckel. Relativistic Magnetic Monopole Flux Constraints from RICE. Phys. Rev. D, 78:075031, 2008.

[117] Alexander Aab et al. Search for ultrarelativistic magnetic monopoles with the Pierre Auger Observatory. Phys. Rev. D, 94(8):082002, 2016.

[118] G. Spengler and U. Schwanke. Signatures of ultrarelativistic magnetic monopoles in imaging atmorpheric cherenkov telescopes. In Proceedings to the 32nd ICRC, October 2011.

[119] S. P. Ahlen and K. Kinoshita. Calculation of the stopping power of very-low-velocity magnetic monopoles. Phys. Rev. D, 26:2347–2363, Nov 1982.

[120] S. P. Ahlen. Stopping-power formula for magnetic monopoles. Phys. Rev. D, 17:229–233, Jan 1978.

[121] Donald R. Tompkins. Total energy loss and Čerenkov emission from monopoles. Phys. Rev., 138:B248–B250, Apr 1965.

[122] G. Giacomelli, M. Giorgini, T. Lari, M. Ouchrif, L. Patrizii, V. Popa, P. Spada, and V. Togo. Magnetic monopole bibliography. 5 2000.

[123] S. Balestra, G. Giacomelli, M. Giorgini, L. Patrizii, V. Popa, Z. Sahnoun, and V. Togo. Magnetic Monopole Bibliography-II. 5 2011.

[124] Brian John Christy. PhD thesis, Maryland U., College Park, 2011.

[125] S. P. Ahlen. Stopping Power Formula for Magnetic Monopoles. Phys. Rev. D, 17:229–233, 1978.

[126] E. Tamm and M. Frank. Dokl. Akad. Nauk SSSR (Akad. of Science of the USSR), 14:107, 1937.

[127] G Spengler. Master's thesis, Humboldt-University of Berlin, 2009.

[128] Axel Donath et al. Gammapy: A Python package for gamma-ray astronomy. Astron. Astrophys., 678:A157, 2023.

[129] M. Ambrosio et al. Final results of magnetic monopole searches with the MACRO experiment. Eur. Phys. J. C, 25:511–522, 2002.

[130] De Mitri Ivan. Ricerca di Monopoli Magnetici supermassivi nella radiazione cosmica. PhD thesis, Università degli Studi di L'Aquila, 1996.

[131] A. De Roeck, H. P. Hächler, A. M. Hirt, M. D. Joergensen, A. Katre, P. Mermod, D. Milstead, and T. Sloan. Development of a magnetometer-based search strategy for stopped monopoles at the Large Hadron Collider. Eur. Phys. J. C, 72:2212, 2012.

[132] Victoria M. Kaspi and Andrei Beloborodov. Magnetars. Ann. Rev. Astron. Astrophys., 55:261–301, 2017.

[133] S. Vercellone et al. ASTRI Mini-Array core science at the Observatorio del Teide. JHEAp, 35:1–42, 2022.

[134] A. Nepomuk Otte et al. Trinity: The PeV Neutrino Observatory. PoS, ICRC2023:1170, 2023.

[135] Takeshi Kobayashi and Martin S. Sloth. Early Cosmological Evolution of Primordial Electromagnetic Fields. Phys. Rev. D, 100(2):023524, 2019.

[136] John David Jackson. Classical Electrodynamics. Wiley, 1998.

[137] Jean Alexandre and Nick E. Mavromatos. Weak-U(1) × strong-U(1) effective gauge field theories and electron-monopole scattering. Phys. Rev. D, 100(9):096005, 2019.

[138] Michael S. Turner. Thermal Production of Superheavy Magnetic Monopoles in the Early Universe. Phys. Lett. B, 115:95–98, 1982.

[139] W. Collins and Michael S. Turner. Thermal Production of Superheavy Magnetic Monopoles in the New Inflationary Universe Scenario. Phys. Rev. D, 29:2158–2161, 1984.

[140] Luke C. Thomas, Ted Dezen, Evan B. Grohs, and Chad T. Kishimoto. Electron-Positron Annihilation Freeze-Out in the Early Universe. Phys. Rev. D, 101(6):063507, 2020.

[141] Rouzbeh Allahverdi, Robert Brandenberger, Francis-Yan Cyr-Racine, and Anupam Mazumdar. Reheating in Inflationary Cosmology: Theory and Applications. Ann. Rev. Nucl. Part. Sci., 60:27–51, 2010.

[142] P. A. R. Ade et al. Improved Constraints on Primordial Gravitational Waves using Planck, WMAP, and BICEP/Keck Observations through the 2018 Observing Season. Phys. Rev. Lett., 127(15):151301, 2021.

[143] Massimo Ricotti, Jeremiah P. Ostriker, and Katherine J. Mack. Effect of Primordial Black Holes on the Cosmic Microwave Background and Cosmological Parameter Estimates. Astrophys. J., 680:829, 2008.

[144] L. I. Schiff. Quarks and magnetic poles. Phys. Rev. Lett., 17:714–716, Sep 1966.

[145] Alfred S. Goldhaber. Monopoles and Gauge Theories. 10 1982.

[146] Abdus Salam and J. A. Strathdee. Transition Electromagnetic Fields in Particle Physics. Nucl. Phys. B, 90:203–220, 1975.

[147] D. A. Kirzhnits and Andrei D. Linde. Symmetry Behavior in Gauge Theories. Annals Phys., 101:195–238, 1976.

[148] Graham M. Shore. Symmetry Restoration and the Background Field Method in Gauge Theories. Annals Phys., 137:262, 1981.

[149] Vittoria Demozzi, Viatcheslav Mukhanov, and Hector Rubinstein. Magnetic fields from inflation? JCAP, 08:025, 2009.

[150] David P. Bennett and Sun Hong Rhie. Cosmological evolution of global monopoles and the origin of large-scale structure. Phys. Rev. Lett., 65:1709–1712, Oct 1990.

[151] R. U. Abbasi et al. An extremely energetic cosmic ray observed by a surface detector array. Science, 382:903–907, 2023.

[152] N. A. Porter. The dirac monopole as a constituent of primary cosmic radiation. Nuovo Cimento, 16:958, 1960.

[153] Veniamin Berezinsky, Pasquale Blasi, and Alexander Vilenkin. Ultrahigh-energy gamma-rays as signature of topological defects. Phys. Rev. D, 58:103515, 1998.

[154] V. Berezinsky. Ultrahigh-energy cosmic rays from cosmological relics. Nucl. Phys. B Proc. Suppl., 87:387–396, 2000.

[155] Andrei Gruzinov. Grb phenomenology, shock dynamo, and the first magnetic fields. Astrophys. J. Lett., 563:L15, 2001.

# Acknowledgements